PATHOLOGICAL CONDITIONS - EDITOR'S PICK 2021

EDITED BY: Rainer Spanagel

PUBLISHED IN: Frontiers in Behavioral Neuroscience

frontiers Research Topics

ISSN 1664-8714
ISBN 978-2-88971-198-7
DOI 10.3389/978-2-88971-198-7

About Frontiers

Frontiers is more than just an open-access publisher of scholarly articles: it is a pioneering approach to the world of academia, radically improving the way scholarly research is managed. The grand vision of Frontiers is a world where all people have an equal opportunity to seek, share and generate knowledge. Frontiers provides immediate and permanent online open access to all its publications, but this alone is not enough to realize our grand goals.

Frontiers Journal Series

The Frontiers Journal Series is a multi-tier and interdisciplinary set of open-access, online journals, promising a paradigm shift from the current review, selection and dissemination processes in academic publishing. All Frontiers journals are driven by researchers for researchers; therefore, they constitute a service to the scholarly community. At the same time, the Frontiers Journal Series operates on a revolutionary invention, the tiered publishing system, initially addressing specific communities of scholars, and gradually climbing up to broader public understanding, thus serving the interests of the lay society, too.

Dedication to Quality

Each Frontiers article is a landmark of the highest quality, thanks to genuinely collaborative interactions between authors and review editors, who include some of the world's best academicians. Research must be certified by peers before entering a stream of knowledge that may eventually reach the public - and shape society; therefore, Frontiers only applies the most rigorous and unbiased reviews.
Frontiers revolutionizes research publishing by freely delivering the most outstanding research, evaluated with no bias from both the academic and social point of view. By applying the most advanced information technologies, Frontiers is catapulting scholarly publishing into a new generation.

What are Frontiers Research Topics?

Frontiers Research Topics are very popular trademarks of the Frontiers Journals Series: they are collections of at least ten articles, all centered on a particular subject. With their unique mix of varied contributions from Original Research to Review Articles, Frontiers Research Topics unify the most influential researchers, the latest key findings and historical advances in a hot research area! Find out more on how to host your own Frontiers Research Topic or contribute to one as an author by contacting the Frontiers Editorial Office: frontiersin.org/about/contact

PATHOLOGICAL CONDITIONS - EDITOR'S PICK 2021

Topic Editor:
Rainer Spanagel, University of Heidelberg, Germany

Citation: Spanagel, R., ed. (2021). Pathological Conditions - Editor's Pick 2021. Lausanne: Frontiers Media SA. doi: 10.3389/978-2-88971-198-7

Table of Contents

frontiers in Behavioral Neuroscience

ORIGINAL RESEARCH
published: 23 January 2019
doi: 10.3389/fnbeh.2019.00006

Long-Term Effects of Traumatic Brain Injury on Anxiety-Like Behaviors in Mice: Behavioral and Neural Correlates

Juliana Popovitz[1], *Shreesh P. Mysore*[1,2] *and Hita Adwanikar*[1]*

[1]Department of Psychological and Brain Sciences, Johns Hopkins University, Baltimore, MD, United States,
[2]Department of Neuroscience, Johns Hopkins University, Baltimore, MD, United States

Traumatic brain injury (TBI) has been frequently linked to affective disorders such as anxiety and depression. However, much remains to be understood about the underlying molecular and signaling mechanisms that mediate affective dysfunctions following injury. A lack of consensus in animal studies regarding what the affective sequelae of TBI are has been a major hurdle that has slowed progress, with studies reporting the full range of effects: increase, decrease, and no change in anxiety following injury. Here, we addressed this issue directly by investigating long-term anxiety outcomes in mice following a moderate to severe controlled cortical impact (CCI) injury using a battery of standard behavioral tests—the open field (OF), elevated zero maze (EZM), and elevated plus maze (EPM). Mice were tested on weeks 1, 3, 5 and 7 post-injury. Our results show that the effect of injury is time- and task-dependent. Early on—up to 3 weeks post-injury, there is an increase in anxiety-like behaviors in the elevated plus and zero mazes. However, after 5 weeks post-injury, anxiety-like behavior decreases, as measured in the OF and EZM. Immunostaining in the basolateral amygdala (BLA) for GAD, a marker for GABA, at the end of the behavioral testing showed the late decrease in anxiety behavior was correlated with upregulation of inhibition. The approach adopted in this study reveals a complex trajectory of affective outcomes following injury, and highlights the importance of comparing outcomes in different assays and time-points, to ensure that the affective consequences of injury are adequately assessed.

Keywords: traumatic brain injury, anxiety behaviors, basolateral amygdala, controlled cortical impact, GABA

OPEN ACCESS

Edited by:
Gregg Stanwood,
Florida State University, United States

Reviewed by:
Kelly M. Standifer,
University of Oklahoma Health Sciences Center, United States
Cathy W. Levenson,
Florida State University, United States

***Correspondence:**
Hita Adwanikar
hita@jhu.edu

Received: *23 October 2018*
Accepted: *08 January 2019*
Published: *23 January 2019*

Citation:
Popovitz J, Mysore SP and Adwanikar H (2019) Long-Term Effects of Traumatic Brain Injury on Anxiety-Like Behaviors in Mice: Behavioral and Neural Correlates. Front. Behav. Neurosci. 13:6. doi: 10.3389/fnbeh.2019.00006

INTRODUCTION

Traumatic brain injury (TBI), characterized as any damage to the brain caused by external acceleration or deceleration forces (Ingebrigtsen and Romner, 2003; Menon et al., 2010), is a complex health problem affecting millions of people worldwide (Hyder et al., 2007). TBI produces considerable and wide-ranging losses in cognitive, motor and affective functions (Draper and Ponsford, 2008; Ponsford et al., 2008). This is true even of injuries considered mild or moderate, which constitute 80% of all cases and can lead to debilitating long-term effects (Buck, 2011; Coronado et al., 2015). The high prevalence and substantial impact of TBI emphasize the importance of understanding the neural mechanisms underlying the outcomes of injury.

Animal models of TBI, and specifically rodent models, have been used to replicate the human symptomatology, examine neural mechanisms and test therapeutic interventions

(Xiong et al., 2013). The cognitive and motor outcomes of TBI have been well established and replicated among pre-clinical studies (Fujimoto et al., 2004; Morales et al., 2005; Shear et al., 2010). However, affective outcomes, and specifically, maladaptive anxiety outcomes, which can affect up to 70% of all TBI patients (Rao and Lyketsos, 2002; Moore et al., 2006; Osborn et al., 2016; Scholten et al., 2016), have been difficult to reproduce in animal models. Studies in rodents, which typically quantify anxiety as the proportion of time animals spend in a more exposed, anxiogenic portion of a behavioral apparatus, as opposed to an enclosed, less anxiogenic zone, have yielded inconsistent and, at times, contradictory results (Wagner et al., 2007; Wakade et al., 2010; Schultz et al., 2011; Ajao et al., 2012; Cope et al., 2012; Washington et al., 2012; Budinich et al., 2013; Almeida-Suhett et al., 2014; Amorós-Aguilar et al., 2015; Sierra-Mercado et al., 2015).

One group of pre-clinical studies found an increase in anxiety-like behaviors following TBI. Injured rats and mice spent less time than sham controls in the anxiogenic zones in the open field (OF) test, elevated plus maze (EPM), elevated zero maze (EZM) and in the dark-light chamber tests, and exhibited increased immobility in the tail suspension test for up to 8 weeks post-TBI (Wagner et al., 2007; Schultz et al., 2011; Ajao et al., 2012; Cope et al., 2012; Almeida-Suhett et al., 2014). Paradoxically, another group of studies found a decrease in anxiety-like behaviors, with injured animals spending more time than sham controls in the anxiogenic zones in the EPM and OF tests for up to 3 weeks post-TBI (Wakade et al., 2010; Washington et al., 2012; Budinich et al., 2013). Finally, a third group of studies found no difference between injured and sham animals in the EPM and OF tests for up to 6 weeks post-TBI (Schultz et al., 2011; Amorós-Aguilar et al., 2015; Sierra-Mercado et al., 2015). It is likely that the diversity in range of time-points tested—ranging from 3 to 8 weeks; and differences in the choice of behavioral tests administered to assess anxiety account for these variations. Together, they contribute to the idiosyncratic results reported in the literature. An additional factor that can add to variation is the degree of injury severity, which differs between studies. However, even for a similar injury level, variable results have been described. Wagner et al. (2007), Ajao et al. (2012) and Almeida-Suhett et al. (2014) and produced mild controlled cortical impact (CCI) in rats and found increased anxiety at 7 days (Almeida-Suhett et al., 2014), at 14 days (Wagner et al., 2007) and up to 60 days (Ajao et al., 2012). However, Amorós-Aguilar et al. (2015) produced a mild CCI in rats and found no effects on behavior. A moderate to severe CCI can lead to no anxiety early after injury (Sierra-Mercado et al., 2015), increased anxiety at 45 days (Thau-Zuchman et al., 2019), or variable effects depending on the test used (Tucker et al., 2017). Washington et al. (2012) explicitly tested this by using varying levels of injury severity. While severity impacted lesion volume differentially, behavioral effects at 3 weeks after injury were similar. Mild, moderate or severe injury leads to reduced anxiety in the EPM at 21 days post injury, and showed no effects in the OF test. However, moderate or severe injury showed greater lesion volumes and decreased ipsilateral hippocampal volumes, as compared to mild injury.

The primary goal of this study was to explicitly address the issues of variability in time-points and behavioral assays in mice. We hypothesize that there is a time and test dependance of anxiety-like behaviors measured following CCI. To achieve this goal, we used a well-established model of brain injury—the CCI model (Adwanikar et al., 2011; Xiong et al., 2013), employed a battery of commonly used tests to measure anxiety-like behaviors in mice, and measured anxiety over a long time-course. Anxiety behaviors were assessed every 2 weeks up to 7 weeks following moderate to severe injury, and all mice were subjected to a battery of OF, EPM, and EZM tests of anxiety at each time point. This experimental design permitted the direct comparison of different anxiety metrics within the same animals and over time, allowing for a systematic dissection of the behavioral affective sequelae of anxiety following injury. Repeated measures of anxiety tests, on one hand have been interpreted as leading to habituation in response. However, this is also associated with changes in assessment of threat in the anxiogenic zone and implies the development of a learned form of fear response (Bertoglio and Carobrez, 2000), which has implications for anxiety behavior. Additionally, following this behavioral characterization, we also measured a molecular marker of GABAergic function in the basolateral amygdala (BLA), one of the key hubs of anxiety processing, to gain a window into the molecular underpinnings of changes in anxiety-like behavior following injury.

Our results support the central hypothesis of this study, by demonstrating that early effects on affective behavior following injury can differ from late effects, and that the observed effects can vary depending on the behavior test used. Consequently, they reveal a complex picture regarding the affective consequences of injury, and argue for the need for a standardized and comprehensive approach to study affective outcomes of TBI in animal models.

MATERIALS AND METHODS

Subjects

A total of 42 adult male C57BL6J mice (Jackson Labs, Bar Harbor, ME, USA) were used in the experiments. Mice were split in two groups, CCI and sham. They were housed in colonies of four, with CCI and sham animals mixed in the same cage, in a 12 h light cycle (lights on from 7 am to 7 pm), with constant temperature and humidity (22°C and 40%). Food and water were available *ad libitum*. Animals' weight was monitored weekly, averaging 32 g. Mice were 6–8 weeks-old at the beginning of experiments and allowed 2 weeks of acclimation before experiments began. Behavioral testing was conducted between 10 am and 5 pm. This study was carried out in accordance with the recommendations of IACUC guidelines. All experimental procedures were approved by Johns Hopkins Animal Care and Use Committee.

Injury Procedures

Mice were anesthetized with Avertin (2,2,2 tribromoethanol-Sigma, St. Louis, MO, USA) diluted in isotonic saline (500 mg/kg, i.p.). After a midline skin incision, a circular craniotomy was

made midway between Bregma and lambda with the medial edge of the craniotomy 0.5 mm lateral to the midline. The mice were then subjected to a moderate to severe (Wakade et al., 2010; Tucker et al., 2017; Wang et al., 2018) CCI injury using a convex impactor tip of 3 mm in diameter. The injury was generated using the following parameters: 4.5 m/s velocity, 1.50 mm depth of penetration and a sustained depression for 150 ms. Mice were given 1 ml saline and 100 μl of 10% Meloxicam subcutaneously. Body temperature was maintained at 37°C with a warming blanket until full recovery from anesthesia (recovery of righting reflex). Sham-operated controls underwent the same surgical procedures with the exception of the traumatic injury. After surgery, mice were kept in individual cages for 72 h and monitored daily, then returned to their home-cages. Survival rate for the surgeries were about 90%. Righting times for both groups for recovery from anesthesia and surgery were similar (CCI: 101 ± 7.09 min; Sham: 103 ± 1 9.17 min). All surviving animals (25 CCI group, 17 sham control group) underwent further behavioral testing following recovery.

Behavioral Tests and Apparatus

Baseline and post-injury behavioral testing were performed with all mice—TBI and sham—together, in the same order each week. Testing proceeded as follows: animals were brought into the experimental room at least 30 min before the experiments began. They were first tested in the OF, and given at least 2 h to recover before testing on the EZM. Twenty-four hours later, they were brought back to the experimental room and tested in the EPM. Mazes were cleaned with 70% ethanol between each animal. Each mouse was tested twice in each maze before injury. Baseline testing was performed 5–7 days apart, and injury was induced 1 week after the last baseline test. Baseline values were averaged for each animal to calculate their individual baseline level of anxiety.

Open-Field Test (OF—Accuscan, Columbus, OH)

The apparatus consisted of a 40.6 cm × 40.6 cm sound-attenuating box, with sensors on the bottom that monitored the animals' movement. A computer connected to the device recorded time spent in the center and distance traveled. Mice were placed in the center of the field and allowed to freely explore for 20 min. There were two trials before injury and four biweekly trials after injury.

Elevated Plus Maze (EPM) Test

Apparatus consisted of two intersecting runways (50 cm × 50 cm × 5 cm), placed at 1 m from the ground. One runway had no walls (two open arms), while the other had 20 cm dark, high walls (two closed arms). Mice were placed in the center of the maze, facing one closed arm, and allowed to explore for 10 min. There were two trials before surgery and four biweekly trials after. A camera placed above the maze recorded the animal's movement, and trials were analyzed using Ethovision© software. Behavioral metrics monitored were total distance traveled, distance traveled, number of entrances and time spent in each arm.

Elevated Zero-Maze (EZM) Test

Apparatus consisted of a circular platform (width: 5 cm, inner diameter: 40 cm), placed at 1 m from the ground and divided in four quadrants. Two opposite quadrants had a 20 cm dark, high walls (closed arm), while the other two had no walls (open arms). Mice were placed facing the entrance of a closed arm, and allowed to explore for 10 min. There were two trials before and four biweekly trials after surgery. A camera placed above the maze recorded the animal's movement, and trials were analyzed using Ethovision© software. Behavioral metrics monitored were total distance traveled, distance traveled, number of entrances and time spent in each arm.

Anatomical Metrics and Immunohistochemistry

Fixation and Sectioning

Two weeks after behavioral testing was finished, mice were deeply anesthetized (2.5% Avertin, 250 mg/kg body weight, i.p., Sigma, St. Louis, MO, USA) and transcardially perfused with 1 M phosphate buffer saline (PBS, 50 ml) followed by 4% paraformaldehyde (PFA, 100 ml, Sigma, St. Louis, MO, USA). Brains were removed and post-fixed in 4% PFA (50 ml) for 72 h, then transferred to a solution of 30% sucrose in 4% PFA, where they were kept refrigerated until sectioning. Coronal sections (40 μm) of the whole brain were performed using a slide microtome (Leica Microsystems, model CM-1860).

Immunohistochemistry

Mounted sections were washed three times for 10 min each wash in 0.1 M PBS and then incubated in blocking solution containing 10% normal goat serum and 0.5% Triton X-100 in PBS for 2 h at room temperature. Slides were then incubated with 1:1,000 of mouse anti-GAD-65/67 (EMD Millipore), 10% normal goat serum, 0.5% Triton X-100, for 72 h at 4°C. The sections were then rinsed three times in PBS, and incubated with the secondary antibody, Alexa Fluor 488 (1:1,000, Abcam), with 5% normal goat serum, 0.5% Triton X-100, for 2 h in room temperature. Sections were washed 3× for 10 min with PBS, and incubated for 30 min with NeuroTrace 640/660 Deep-Red Fluorescent Nissl (Thermo Fisher) and mounted with Vectashield antifade mounting medium (Vector Labs).

Imaging for Volumetric Measure

Fluorescent images of the brain in the peri-injury region were taken with an Axiozoom v16 microscope (Carl Zeiss, Germany) using a 10× objective. Volume estimation was performed as described previously (Claus et al., 2010), adopting Cavalieri estimation (Gundersen and Jensen, 1987). Images from four sections were taken for each mouse in each area. We determined the position of each section by using Mouse Brain Atlas coordinates (Paxinos and Franklin, 2004). Sections were located between −0.70 and −2.46 mm Bregma, and they contained the lesioned area in the injured mice or equivalent position in sham controls. BLA images were taken between −1.22 and 2.18 mm Bregma. Images were pre-processed using Fiji software (Schindelin et al., 2012). The hemispheric and BLA areas were outlined using Fiji on the ipsilateral and contralateral sides of

the four brain sections, volume was calculated as the sum of the areas multiplied by the distance between sections (300 μm). The ipsilateral volume was normalized to the contralateral volume to estimate the extent of hemispheric volume loss (lesion) and change in BLA volume.

Imaging for Immunohistochemistry

Fluorescent images of the BLA were taken with a Zeiss LSM 700 microscope (Carl Zeiss, Germany) using 20× and 40× objectives. Four bilateral immunofluorescent labeled sections were taken in each mouse (eight images per animal), sections were approximately 200 μm apart. Images were pre-processed using Fiji (Schindelin et al., 2012). Number and intensity of GAD puncta were calculated using a custom MATLAB analysis package (IMFLAN3D; Tai et al., 2007). Here, a "punctum" was defined as a cluster of "connected" pixels identified in an unbiased manner using the MATLAB function *bwlabeln* with the "eight-connected neighborhood" criterion.

Statistical Analysis

For the behavioral tasks, a two-way unbalanced repeated measure ANOVA was performed after standard methods of outlier exclusion in MATLAB were applied. Data shown (at each time point in **Figures 1**, **2**, and in **Figures 3**, **4**) represent distributions obtained after removal of outliers following a standard procedure in MATLAB: samples that deviated from the median by more than fac*interquartile range were deemed outliers (average value of fac used = 1.5). *Post hoc t*-tests were performed whenever ANOVA indicated a significant effect, and *p*-values were corrected by a false discovery rate (FDR) test. For hemispheric volume, the normalized ipsilateral volumes (ipsilateral/contralateral) were compared among groups using *t*-tests and FDR correction. For GAD65/67 puncta analysis, the mean of each group was compared using *t*-test with FDR correction. Individual baseline data was averaged across the two pre-injury sessions to determine the mean value for each animal and assay. Post-injury behavioral data was plotted normalized to each animal's individual baseline: behavioral metrics at each time-point was divided by the animal's baseline value. Values greater than one indicate the mouse's anxiety level decreased in comparison to its baseline, whereas values smaller than one indicate increase in anxiety. This approach allows us to measure how anxiety changed for each individual animal because of the injury. Normalized values are presented as mean ± standard error (SEM). All statistical tests were performed using MATLAB (Mathworks Inc., Natick, MA, USA). Statistical analysis was considered significant for $p < 0.05$.

RESULTS

Effects of TBI on Anxiety-Like Behaviors Exhibit a Complex Trajectory

We determined the long-term effects of TBI on affective outcomes in a battery of innate anxiety behavioral tests following exposure to a CCI injury. Mice were tested in the OF, EZM and EPM tests. These tasks exploit the animals' natural conflict between seeking protection and exploring a novel environment. All mice were tested twice in the behavior tests before surgery, and these were averaged to determine each animal's baseline level of anxiety. Post-injury or sham surgery, they were then tested on weeks 1, 3, 5 and 7. Anxiety was measured by the change in proportion of time they spent in the anxiogenic zone in each assay, as well as number of entrances to the open arm (EZM and EPM). Values at each time point are normalized to each animal's baseline; this approach allowed us to determine how the anxiety level of each animal changed due to the injury. We controlled for possible locomotion deficits, by measuring total distance traveled in all three mazes.

Examples of heat maps representing the proportion of time TBI and sham mice spent in each zone in the OF arena on week 7 are illustrated in **Figure 1A**. In this test, we found an overall effect of injury across the population, tested by an unbalanced repeated two-way ANOVA ($F_{(1,3)} = 4.04$, $p < 0.01$, **Figure 1B**). Injured mice spent significantly more time in the center of the arena on week 7 (*post hoc t*-test with FDR correction, $p = 0.02$), but we did not observe difference between groups in the other time-points. These results indicate that the main effect of injury was driven by the strong decrease in anxiety TBI mice presented on week 7.

In order to compare the effect of injury across different behavioral assays, we measured anxiety-like behaviors in the EZM and EPM tests. Heat maps illustrating the proportion of time mice spent in each type of arm are shown in **Figures 1C,E**. In the EZM, there was no main effect of injury in the proportion of time spent in the open arm (unbalanced repeated two-way ANOVA, $F = 0.002$, $p = 0.96$, **Figure 1D**). However, we found a strong interaction effect between time and injury (unbalanced repeated two-way ANOVA, $F_{(1,3)} = 4.24$, $p < 0.01$). TBI mice display increased anxiety on week 1 (*post hoc t*-test with FDR, $p < 0.01$) and decreased anxiety on week 5 (*post hoc t*-test with FDR correction, $p = 0.01$), as measured by time spent in the open arms. Interestingly, in both the OF and EZM, we observed a decrease in anxiety-like behaviors as compared to sham controls, on week 7 and 5, respectively, which suggests a delayed effect of the injury. There were no differences between groups in baseline, prior to TBI (**Supplementary Figure 1**).

In addition to the OF and EZM tests, we measured anxiety in the EPM. **Figure 1F** shows the proportion of time mice spent in the open arm in this assay. We found a main effect of injury, tested by an unbalanced repeated two-way ANOVA ($F_{(1,3)} = 4.44$, $p = 0.03$), and a strong effect of time (unbalanced repeated two-way ANOVA, $F_{(1,3)} = 9.18$, $p < 0.01$). *Post hoc t*-test with FDR correction showed that TBI mice spent significantly less time in the open arm on week 3, indicating increased anxiety ($p < 0.05$). We observed that both in the EZM and EPM tests, there was an increase of anxiety-like behaviors on earlier time-points: on week 1 for the EZM and week 3 in the EPM. Across the 3 behavioral assays, our results indicate that the effects of TBI on anxiety-like behaviors are time- and task-dependent: generally, TBI led to an early increase and late decrease in anxiety-like behaviors.

As an additional metric of anxiety, we measured number of entrances to the open arm in the EZM and EPM tests. Injured mice did not differ from sham on number of entrances in

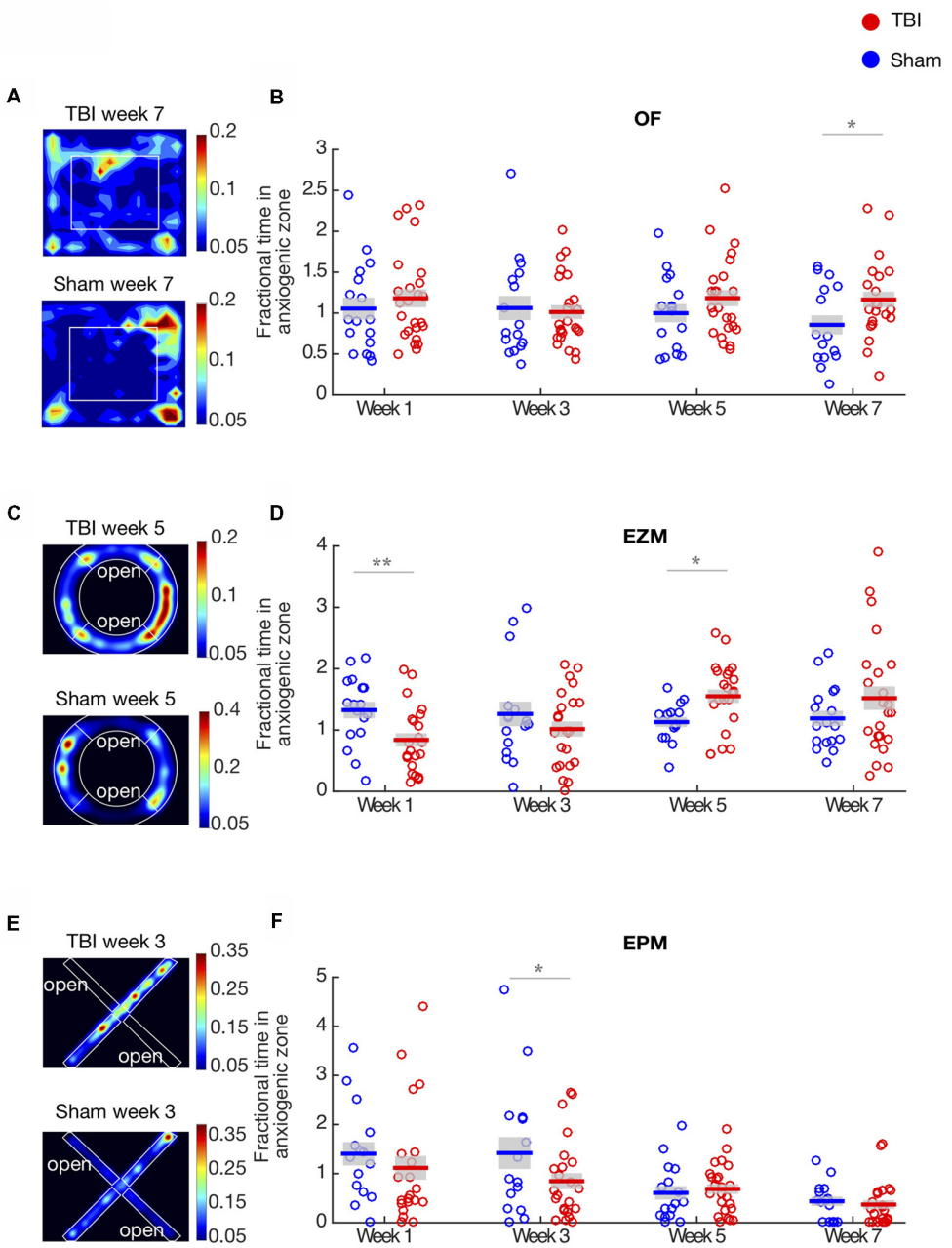

FIGURE 1 | Traumatic brain injury (TBI) causes long-term effects on affective behaviors. **(A,C,E)** Representative heat maps of TBI and Sham animals in the open field (OF), elevated zero maze (EZM) and elevated plus maze (EPM), respectively. Warmer colors represent that the animals spent more time on that zone. **(B)** Proportion of time in the center of the OF arena. Each circle represents one mouse. Horizontal bars denote means; shaded regions denote SEM. There is a main effect of injury (repeated two-way ANOVA, $p < 0.01$) and anxiety significantly decreases on week 7. **(D)** Proportion of time in the open arm of the EZM; conventions as in **(B)**. There is an interaction between time and injury (repeated two-way ANOVA, $p < 0.01$). Anxiety is significantly increased on week 1 and decreased on week 5. **(F)** Proportion of time in the open arm of the EPM; conventions as in **(B)**. There is a main effect of injury and time (repeated two-way ANOVA, $p < 0.01$). Anxiety significantly increases on week 3. Panels **(B,D,E)** show data are from $n = 25$ mice in TBI condition, and $n = 17$ mice in sham condition after removal of outliers at each time point ("Materials and Methods" section); the number of outliers at any time point for any condition did not exceed four mice; $^{*}p < 0.05$, $^{**}p < 0.01$ by *post hoc* *t*-test with false discovery rate (FDR) correction.

the EPM (unbalanced repeated two-way ANOVA, $F_{(1,3)} = 0.25$, $p = 0.61$, **Figure 2D**). In the EZM, we observed an effect of injury in the number of entrances to the open arm (unbalanced repeated two-way ANOVA, $F_{(1,3)} = 5.10$, $p = 0.02$, **Figure 2E**), and TBI mice presented significantly fewer entrances on week 1 (*post hoc* *t*-test with FDR correction, $p = 0.01$), which is consistent with the decreased anxiety observed in the proportion of time in the open arm on week 1 in this maze.

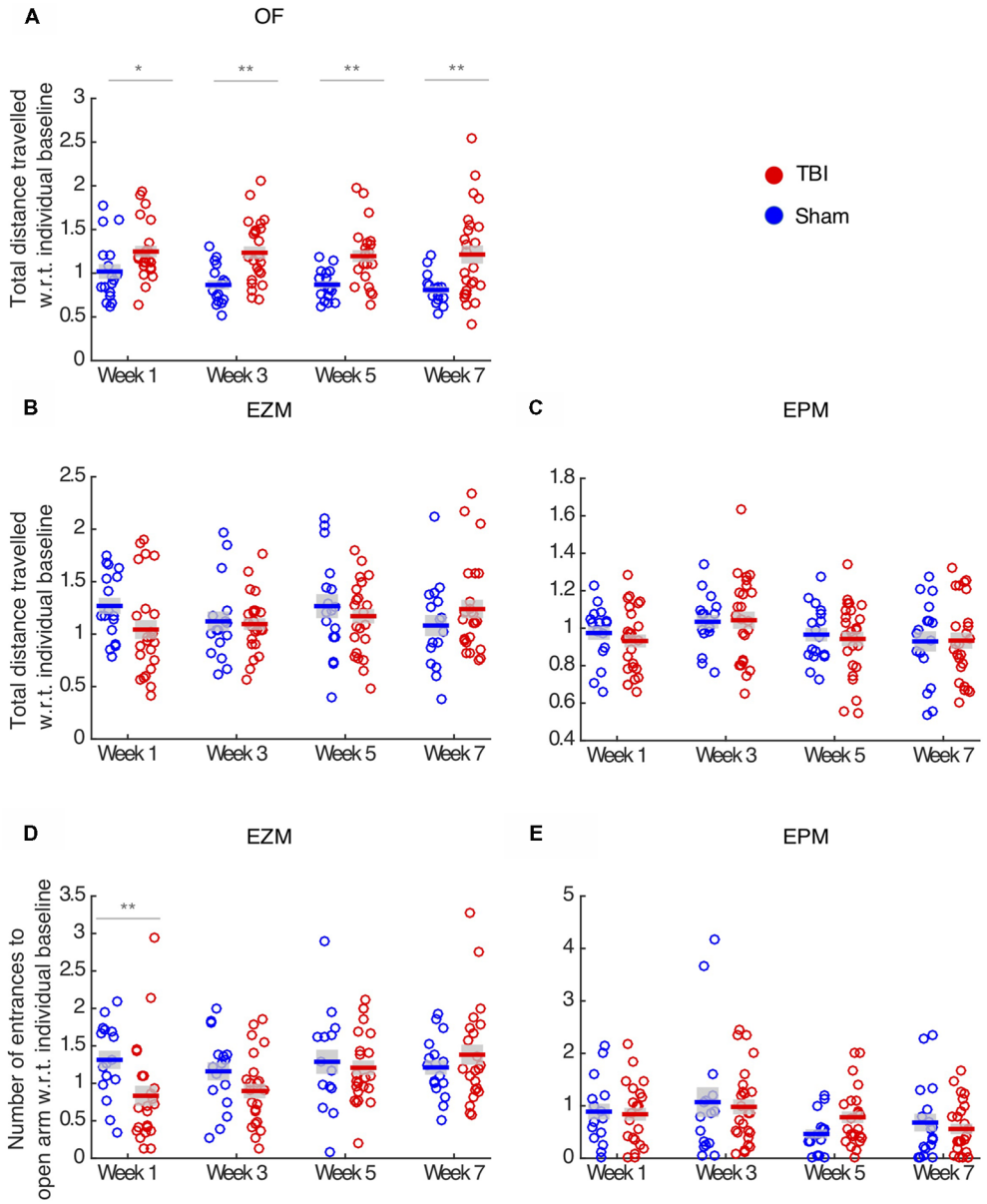

FIGURE 2 | TBI effects vary across behavioral assays and metrics. **(A)** Total distance traveled in the OF. There is a main effect of injury (repeated two-way ANOVA, $p < 0.01$), and TBI animals travel more at all time-points compared to sham controls. **(B,C)** Total distance traveled in the EZM and EPM, respectively. There is no effect of injury in locomotion in these assays. **(D)** Number of entrance to the open arm in the EZM. There is a main effect of injury (repeated two-way ANOVA, $p < 0.05$) and TBI animals present fewer entrance on week 1 than sham controls. **(E)** Number of entrances to the open arm in the EPM. There is no effect of injury. In all panels, each circle represents one mouse. Horizontal bars denote means; shaded regions denote SEM. Data from $n = 25$ mice in TBI condition, and $n = 17$ mice in sham condition are shown after removal of outliers at each time point ("Materials and Methods" section); the number of outliers at any time point for any condition did not exceed three mice; $^{*}p < 0.05$, $^{**}p < 0.01$.

To ensure that anxiety metrics were not affected by locomotion deficits, we measured total distance traveled in each maze. In the OF, TBI led to hyperactivity throughout all time points (unbalanced repeated two-way ANOVA, $F_{(1,3)} = 36.69$, $p < 0.01$, *post hoc* t-test with FDR correction, $p > 0.05$, **Figure 2A**). Injury had no locomotion effect on the EZM (unbalanced repeated two-way ANOVA, $F_{(1,3)} = 0.56$, $p = 0.45$, **Figure 2B**) and EPM tests (unbalanced repeated two-way ANOVA, $F_{(1,3)} = 1.23$, $p = 0.26$, **Figure 2C**). Since TBI and sham did not differ in terms of total distance traveled in the EZM, we concluded that the reduced number of entrances to the open arm in this maze reflects the increase in anxiety those mice presented on week 1. Finally, we concluded that the effects in anxiety-like behaviors were not confounded by locomotion deficits.

Our behavioral results indicated that the effects of TBI in anxiety-like behaviors are complex. Although injury did not

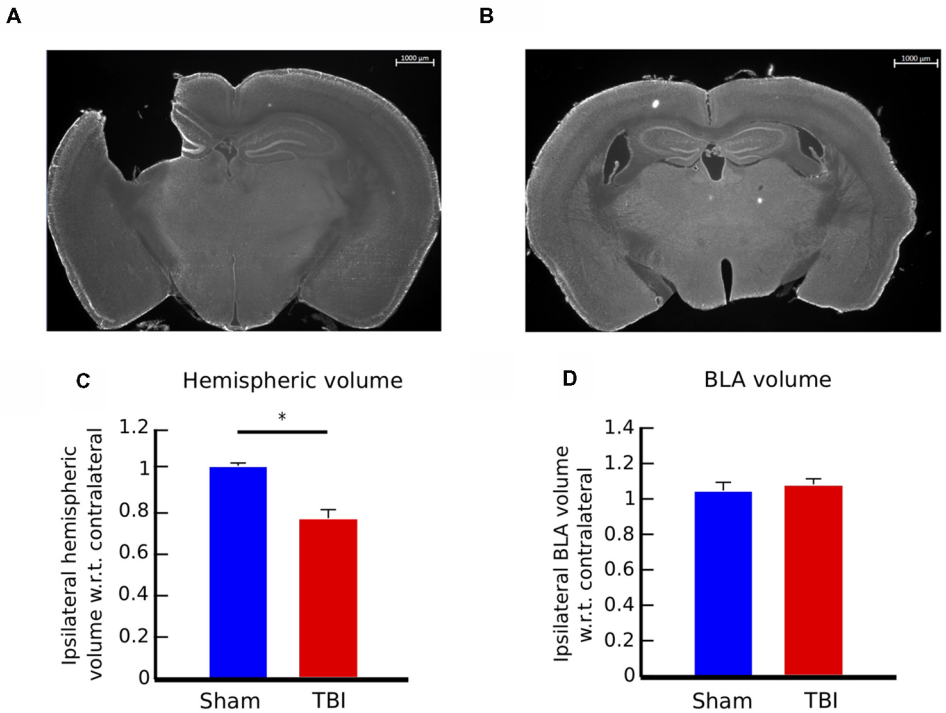

FIGURE 3 | Controlled cortical impact (CCI) causes consistent injury across animals and no volumetric change in the basolateral amygdala (BLA). **(A)** 12× panoramic coronal sections stained with Fluoro Nissl, representing the lesion in the cortex and hippocampus for TBI animals and **(B)** intact areas in sham controls. **(C)** Hemispheric volume in TBI and sham animals. There is a significant reduction in the ipsilateral hemisphere volume of injured animals, compared to sham controls (*t*-test, $p < 0.05$). **(D)** Volumetric measure of the BLA. Injury does not cause volumetric change in the BLA of TBI animals. Bar graphs in **(C,D)** show mean ± SEM of data from $n = 10$ mice in the TBI condition and $n = 10$ mice in the sham condition after removal of outliers ("Materials and Methods" section); the number of outliers did not exceed one mouse for any condition; $^*p < 0.05$.

affect locomotion in the EPM and EZM tests, the effect on anxiety metrics varied across time-points and assays. By comparing different assays, we identified that in the first few weeks after injury, mice had a significant increase in anxiety-like behaviors. This effect, however, inverted after about a month post-injury. After this point, TBI mice display decreased anxiety-like behaviors as compared to sham controls.

Injury Was Consistent Across Mice

Considering the complex effects of injury, we asked if differences in the extent of injury across mice could be a confounding factor. Because we were interested in the long-term effects of injury, we sacrificed the mice on week 9 post-injury or sham surgery, obtained brain sections and quantified hemispherical volumes as an anatomical metric of the extent of injury.

Coronal brain sections of an injured mouse illustrating the extent of the injury to the cortex and hippocampus, as well as a brain section in the same region of control mouse are presented in **Figures 3A,B**. We determined the extent of the injury by measuring the hemispheric area of the peri-injury site, on the ipsilateral and contralateral sides of four brain sections per mouse, located between −0.70 and −2.46 mm Bregma, and multiplied the sum of the areas for each side by the distance between sections (300 μm; $n = 10$ for each group). The ipsilateral hemispheric volume of each brain was then normalized to its contralateral side. There is no effect of injury on the contralateral side (data not shown). The injury caused a reduction of the ipsilateral hemispheric volume of approximately 20%, compared to control mice (**Figure 3C**, two-tailed *t*-test, $p < 0.01$). The extent of the injury was consistent among TBI mice, as shown by the standard error of the mean ($SEM_{TBI} = \pm 0.04$, $SEM_{sham} = \pm 0.01$).

Injury Did Not Cause a Volumetric Change in the BLA

We proceeded to identify potential neural correlates of the long-term behavioral outcomes. Past work has demonstrated that injury can cause volumetric changes in brain areas distal from the site of injury. Motivated by this, we hypothesized that the affective behavioral changes could correlate with anatomical changes in the BLA, a key brain area involved in the control of emotional responses. To test this hypothesis, we measured volumetric changes in the BLA on week 9.

Volume of the BLA was estimated by measuring area of four sections on each side per mouse, and multiplying the area of the BLA by the distance between sections (300 μm). BLA sections were located between −1.22 and −2.18 mm Bregma. The ipsilateral volume was then normalized to its contralateral side ($n = 10$ for each group). There is no effect

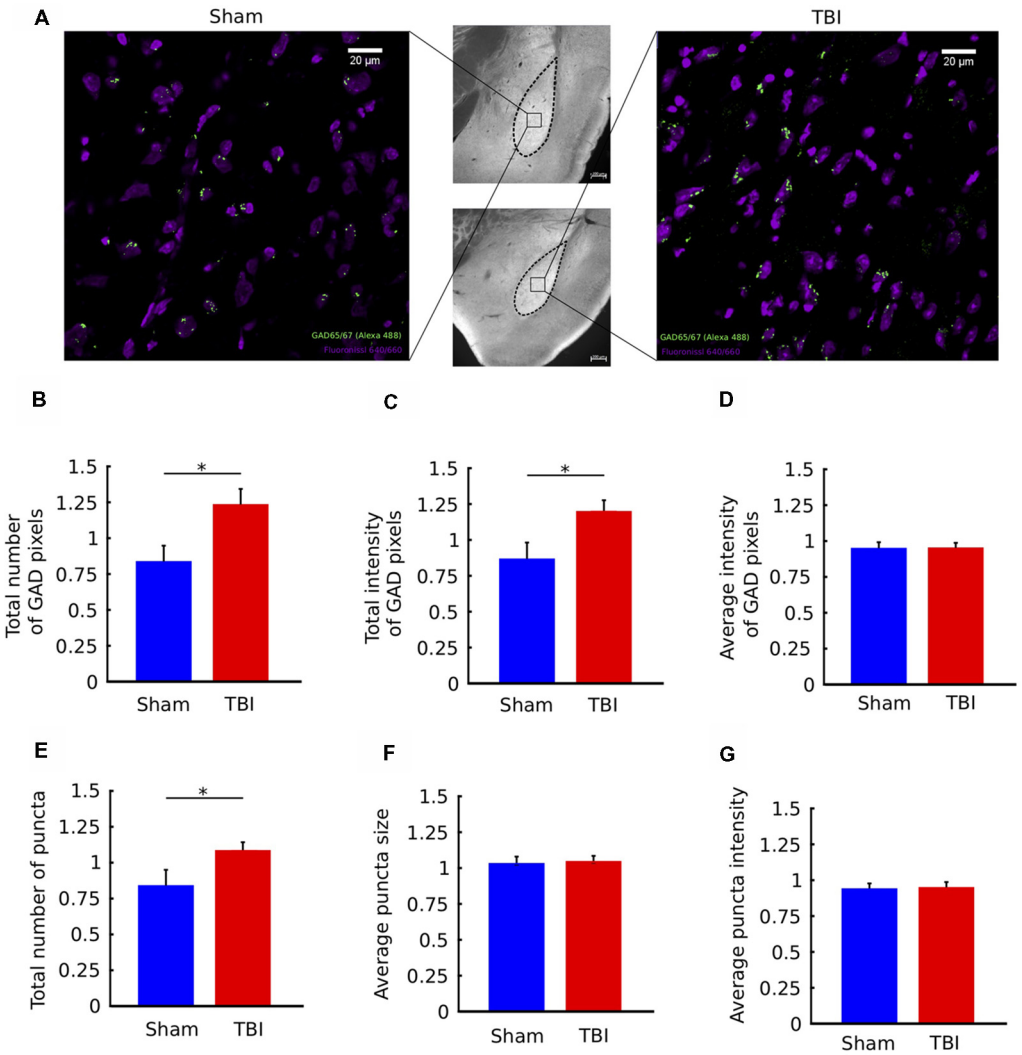

FIGURE 4 | TBI is associated with upregulation of GAD immunostaining in the ipsilateral amygdala. **(A)** Middle column: 10× images of histological sections from a sham animal (top) and TBI animal (bottom). Left/Right columns: 63× views of the indicated portions of the sections. Fluoro Nissl staining in purple and GAD65/67 staining in green. **(B–G)** Quantification of GAD65/67 expression in the ipsilateral and contralateral BLA in four sections per animal. Metrics in **(B–G)** are reported as ratios of ipsilateral to contralateral values for each animal. In injured animals, there was a significant increase in the total number of GAD pixels **(B)** and the total intensity of GAD pixels **(C)**, but not the average intensity of GAD pixels **(D)**. In addition, there was an increase in the total number of GAD "puncta" (clusters of contiguous GAD pixels **(E)**, but not in the average size of puncta **(F)** or average intensity of puncta **(G)**. All bar graphs show mean ± SEM of data from $n = 10$ mice in the TBI condition and $n = 10$ mice in the sham condition after removal of outliers ("Materials and Methods" section); the number of outliers did not exceed two mice for any; $^*p < 0.05$ (two-tailed t-test).

of injury on the contralateral side (data not shown). There was no significant difference in BLA volume between injured and sham mice, as shown in **Figure 3D** (two-tailed t-test, $p = 0.7$). These results indicate that the changes in anxiety-like behaviors were not correlated with changes in volume in the BLA.

Neural Marker: Immunostaining Indicates Upregulation of GAD Ipsilaterally

Next, we assessed functional neural correlates of the long-term affective outcomes of injury. To investigate whether the observed late decrease in anxiety had a molecular correlate, we examined the strength of inhibitory signaling in the BLA. To this end, we performed GAD immunostaining by targeting GAD65/67, which are two enzymes expressed in the brain and involved in the synthesis of GABA. GAD67 is expressed equally through the cell body, while GAD65 is mainly found in nerve terminals (Asada et al., 1996). We chose to target GAD because it has been demonstrated that GABA plays a crucial role in anxiety disorders (Kalueff and Nutt, 2007). We quantified several metrics of GAD expression, such as number and intensity of GAD puncta. Ipsilateral values were normalized to contralateral for each mouse.

Figure 4A shows coronal sections zoomed-in on the BLA, with labeling of cell bodies and GAD puncta for a sham and a TBI mouse. There was an overall increase in the total number of GAD-stained pixels in the ipsilateral BLA of injured mice, measured by a two-tailed *t*-test ($p = 0.03$, **Figure 4B**). There was also an overall increase in total GAD signal intensity ($p = 0.01$, **Figure 4C**). Notably, the average intensity of GAD-stained pixels was not different between groups ($p > 0.05$, **Figure 4D**). Together, these results indicate that injury causes an increase in the number of GAD-stained pixels, but not in the intensity (brightness) of individual pixels.

To understand if there were effects on spatial clustering of GAD-stained pixels, we next analyzed the properties of groups of contiguous (or connected) GAD-pixels, called "puncta" (see "Materials and Methods" section). Compared to individual pixels, which can be contaminated by noise, puncta are more likely to represent functional signal. We found that there was an increase in the number of GAD puncta following injury (**Figure 4E**, $p = 0.04$), but no change in the average size of puncta or the average intensity of puncta ($p > 0.05$, **Figures 4F,G**). In other words, consistent with the results from individual pixels, GAD puncta are not larger or brighter, they are greater in number following injury. Together, the immunostaining results show an upregulation of GAD immunostaining in the ipsilateral BLA of TBI mice.

DISCUSSION

Human TBI has a complex pathology, and studies show that, among the many outcomes of injury, patients are at a higher risk of suffering from anxiety disorders (Rao and Lyketsos, 2002; Moore et al., 2006; Scholten et al., 2016). Reports on the prevalence of anxiety following injury are variable: pooled long-term prevalence is reported at 36%, according to a recent review (Scholten et al., 2016), but some studies suggest prevalence between 11% and 70% (Rao and Lyketsos, 2002). One unsolved issue is our lack of understanding about the neural mechanisms of injury that may increase a patient's chance of developing an anxiety disorder. Animal models of TBI are valuable to address this problem, for their ability to control for injury parameters and to allow us to measure behavioral changes and neural markers in well-controlled experiments. However, a complex, and at times contradictory, picture has emerged from various animal studies. It is important to comprehensively study these models over long time frames, to develop an understanding of TBI pathophysiology and its impact on affective behavior.

In this study, we adopt a well-established and highly controlled mouse injury model (CCI), and test mice in three assays of innate anxiety over a 7-week time-course, to evaluate how the evolving consequences of TBI impacts affective behavioral function. We demonstrate that the effects of moderate to severe TBI on anxiety-like behaviors are complex and long lasting. Additionally, with this behavioral characterization as a basis, we also measured a molecular marker of GABAergic function in the BLA, one of the key hubs of anxiety processing, and we demonstrated that there is an upregulation of GAD staining at 9 weeks post-injury.

Early after TBI, injury caused a significant increase in anxiety-like behavior measured in the EPM and EZM tests, consistent with several studies that show increased anxiety acutely after injury to the murine brain (Meyer et al., 2012; Almeida-Suhett et al., 2014; Tucker et al., 2017). However, no such effect was observed in the OF test. This is consistent with Sierra-Mercado et al. (2015), who tested the effect of CCI in mice 1 week after injury, and found no change in anxiety as measured by the OF test. Interestingly, a few other studies are able to measure this early increase in anxiety in the OF test as well (Wagner et al., 2007; Almeida-Suhett et al., 2014; Tucker et al., 2017). This inconsistency could be explained by differences in severity of injury (Tucker et al., 2017) or rodent model (Wagner et al., 2007; Almeida-Suhett et al., 2014). However, the difference between effects observed among behavioral tests in our study—within the same group of mice at the same time points—underlines the complexity of measuring anxiety-like behavior in animal models. An important potential implication of this finding is that different assays of anxiety do not always measure the same aspect of anxiety-like behaviors. A comprehensive approach to behavioral testing following TBI is therefore imperative to draw useful conclusions. In order to study the progression of the anxiety response following injury, it is necessary to employ a repeated testing model. One concern with repeated measurement for behavioral tests of anxiety is that of potential habituation and learning. While repeated testing has been shown to have effects on anxiety tests in many studies (Griebel et al., 1993; Adamec et al., 2005; Walf and Frye, 2007), Bertoglio and Carobrez (2000) suggest that the decreased exploration of open arm in the EPM could be related to a qualitative shift from unconditioned to a learned form of fear response. Thus, what is generally considered habituation or learning in the testing arena, is likely a change in the acquired fear response underlying the expression of anxiety-like behavior. Changes in the sham group over time suggest that some of these factors do play a role in this study. Sham mice presented habituation to the OF and EPM, observed in the decrease in proportion of time spent in the anxiogenic zone over time post-surgery on the OF and EPM, as well as in decrease over time in the total distance traveled in the OF. These results are consistent with previous literature, which has demonstrated that repeated exposure to the OF and EZM lead to adaptation to the apparatus measured by decreased exploration of the anxiogenic zone and decreased overall locomotion (Rodgers and Shepherd, 1993; Treit et al., 1993; Logue et al., 1997; Bolivar et al., 2000).

While this study does not rule out these factors in the testing arena, that effect is consistent between both sham and injured groups, and differences observed between groups can be attributed to the TBI. Changes in the expression of anxiety behavior can therefore be interpreted as a deficit in the learned fear response due to re-exposure, a deficit in learning about the context of the anxiogenic zone, or as an increase in risk taking behavior. Direct assays measuring changes in fear learning, such as acoustic startle, might help to parse out these changes over time.

The affective response to TBI is not limited to the early time points, but evolves over time, reflecting the fact that neural mechanisms of injury evolve over time (Werner and Engelhard, 2007). Five weeks after TBI, injured mice show significantly less anxiety-like behaviors. At this stage, the mice showed an increase in exploration of the open arm in the EZM test, as compared to sham controls. The mice also display an increased tendency to explore the center anxiogenic zone in the OF test. Curiously, a similar increase in exploration of the open arm is not observed in the EPM test. Our findings are consistent with findings of decreased anxiety-like behavior in the EZM test at later time points after injury (Jones et al., 2008; Thau-Zuchman et al., 2019), as well as decreased anxiety in the OF test in rats exposed to lateral fluid percussion at 1 and 3 months post-injury (Jones et al., 2008). Interestingly, several studies have found decreased anxiety in the EPM as well, tested in mice following CCI at 20 days (Washington et al., 2012) and rats tested in a closed-head model at between 12 and 30 days (Pandey et al., 2009; Schwarzbold et al., 2010). This difference could also be explained by the fact that we use repeated measurements of behavior in the EPM. Similarly, Ajao et al. (2012) measured an initial increase in anxiety like behavior after juvenile rats were exposed to CCI, which appears to reverse at later time points.

Injury also caused increased locomotion in the OF throughout all time-points, consistent with other studies (Jones et al., 2008; Pandey et al., 2009; Tucker et al., 2017). This suggests that the observed hyperactivity is independent of the early increase and later decrease in anxiety-like behavior. These findings are consistent with human studies where hyperactivity has been reported following pediatric TBI (Max et al., 1998) and impulsivity has been reported following TBI in adults (James et al., 2014; Kocka and Gagnon, 2014).

Several neural mechanisms underlying anxiety changes following injury have been investigated (Schwarzbold et al., 2010; Ajao et al., 2012; Elder et al., 2012; Meyer et al., 2012; Reger et al., 2012; Almeida-Suhett et al., 2014; Sönmez et al., 2015; Tucker et al., 2017). Of particular interest is the BLA, which has been linked to changes in anxiety-like behaviors. Causal manipulations of projections from and to the BLA directly alter anxiety-like behaviors (Scott et al., 1997; Amano et al., 2011; Tye et al., 2011; Felix-Ortiz et al., 2013; Hong et al., 2014), indicating that this area is an important hub for emotional responses in the brain. In addition, signaling by GABA, the major inhibitory neurotransmitter in the nervous system, is greatly implicated in psychiatric disorders such as anxiety and depression (Lydiard, 2003; Nemeroff, 2003; Möehler, 2006; Kalueff and Nutt, 2007). Infusion of $GABA_A$ receptor antagonist into the amygdala increases anxiety (Sanders and Shekhar, 1995), whereas GABA agonist infusion into the BLA reduces anxiety (Bueno et al., 2005), indicating that the inhibitory balance within the amygdala drives changes in anxiety. In previous TBI studies, it has been shown that reduced GABAergic inhibition and increase in number of neurons in the BLA correlate with enhanced anxiety in rodents early after injury (Meyer et al., 2012; Almeida-Suhett et al., 2014).

In this study, while the volumetric measures of the peri-injury area indicate a reduction in ipsilateral hemispheric volume as expected (Bueno et al., 2005; Washington et al., 2012; Almeida-Suhett et al., 2014), there is no significant difference in volumetric measures of the BLA between injured mice and sham controls. However, GAD immunostaining is upregulated in the ipsilateral BLA at 9 weeks following injury, indicating increased GABAergic inhibition within this area. This increase is correlated with late decreases in anxiety-like behavior of the injured animals at later time points. Our results are consistent with causal, $GABA_A$ agonist infusion experiments in the BLA (Chen et al., 2003). Almeida-Suhett et al. (2014) observed TBI-induced decrease in GABAergic inhibition and an increase in anxiety-like behavior at early time points after injury, whereas this study shows the opposite effects at later time points. Thus, our results regarding GABA signaling are in line with previous work and extend our understanding about the longer-term effects of injury.

In summary, we demonstrate a time-dependent reversal in the course of affective behavioral response following traumatic injury to the mouse brain: an early increase followed by a late decrease in anxiety, with the latter being correlated with an increase in GABAergic inhibition in the BLA. In addition to revealing a complex affective trajectory, results support the hypothesis that the lack of consensus across past studies (Jones et al., 2008; Pandey et al., 2009; Washington et al., 2012) on the effects on anxiety outcomes following injury may be the result of the variability in injury models used, behavioral assays of anxiety chosen and time-points at which assessments were made. Consequently, they highlight the need for the use of a reproducible model of injury as well as the use of multiple assays and time-points within future studies. Such an approach can provide a consistent foundation for investigating the neural mechanisms underlying affective outcomes of TBI and the development of therapeutic strategies.

DATA AVAILABILITY

The datasets generated for this study are available on request to the corresponding author.

AUTHOR CONTRIBUTIONS

HA and SM designed the study. JP carried out experiments and analyzed the data. All authors contributed to the interpretation of the results and writing of the manuscript.

FUNDING

This research is funded by a start-up grant awarded to HA by Johns Hopkins University.

SUPPLEMENTARY MATERIAL

The Supplementary Material for this article can be found online at: https://www.frontiersin.org/articles/10.3389/fnbeh.2019.00006/full#supplementary-material

REFERENCES

Adamec, R., Shallow, T., and Burton, P. (2005). Anxiolytic and anxiogenic effects of kindling—role of baseline anxiety and anatomical location of the kindling electrode in response to kindling of the right and left basolateral amygdala. *Behav. Brain Res.* 159, 73–88. doi: 10.1016/j.bbr.2004.10.004

Adwanikar, H., Noble-Haeusslein, L., and Levin, H. S. (2011). "Traumatic brain injury in animal models and humans," in *Animal Models of Behavioral Analysis*, ed. J. Raber (Totawa, NJ: Springer), 237–265.

Ajao, D. O., Pop, V., Kamper, J. E., Adami, A., Rudobeck, E., Huang, L., et al. (2012). Traumatic brain injury in young rats leads to progressive behavioral deficits coincident with altered tissue properties in adulthood. *J. Neurotrauma* 29, 2060–2074. doi: 10.1089/neu.2011.1883

Almeida-Suhett, C. P., Prager, E. M., Pidoplichko, V., Figueiredo, T. H., Marini, A. M., Li, Z., et al. (2014). Reduced GABAergic inhibition in the basolateral amygdala and the development of anxiety-like behaviors after mild traumatic brain injury. *PLoS One* 9:e102627. doi: 10.1371/journal.pone.0102627

Amano, T., Duvarci, S., Popa, D., and Paré, D. (2011). The fear circuit revisited: contributions of the basal amygdala nuclei to conditioned fear. *J. Neurosci.* 31, 15481–15489. doi: 10.1523/JNEUROSCI.3410-11.2011

Amorós-Aguilar, L., Portell-Cortés, I., Costa-Miserachs, D., Torras-Garcia, M., and Coll-Andreu, M. (2015). Traumatic brain injury in late adolescent rats: effects on adulthood memory and anxiety. *Behav. Neurosci.* 129, 149–159. doi: 10.1037/bne0000046

Asada, H., Kawamura, Y., Maruyama, K., Kume, H., Ding, R.-G., Ji, F. Y., et al. (1996). Mice lacking the 65 kDa isoform of glutamic acid decarboxylase (GAD65) maintain normal levels of GAD67 and GABA in their brains but are susceptible to seizures. *Biochem. Biophys. Res. Commun.* 229, 891–895. doi: 10.1006/bbrc.1996.1898

Bertoglio, L. J., and Carobrez, A. P. (2000). Previous maze experience required to increase open arms avoidance in rats submitted to the elevated plus-maze model of anxiety. *Behav. Brain Res.* 108, 197–203. doi: 10.1016/s0166-4328(99)00148-5

Bolivar, V. J., Caldarone, B. J., Reilly, A. A., and Flaherty, L. (2000). Habituation of activity in an open field: a survey of inbred strains and F1 hybrids. *Behav. Genet.* 30, 285–293. doi: 10.1023/A:1026545316455

Buck, P. W. (2011). Mild traumatic brain injury: a silent epidemic in our practices. *Health Soc. Work* 36, 299–302. doi: 10.1093/hsw/36.4.299

Budinich, C. S., Tucker, L. B., Lowe, D., Rosenberger, J. G., and McCabe, J. T. (2013). Short and long-term motor and behavioral effects of diazoxide and dimethyl sulfoxide administration in the mouse after traumatic brain injury. *Pharmacol. Biochem. Behav.* 108, 66–73. doi: 10.1016/j.pbb.2013.04.001

Bueno, C. H., Zangrossi, H. Jr., and Viana, M. B. (2005). The inactivation of the basolateral nucleus of the rat amygdala has an anxiolytic effect in the elevated T-maze and light/dark transition tests. *Braz. J. Med. Biol. Res.* 38, 1697–1701. doi: 10.1590/s0100-879x2005001100019

Chen, S., Pickard, J. D., and Harris, N. G. (2003). Time course of cellular pathology after controlled cortical impact injury. *Exp. Neurol.* 182, 87–102. doi: 10.1016/s0014-4886(03)00002-5

Claus, C. P., Tsuru-Aoyagi, K., Adwanikar, H., Walker, B., Whetstone, W., and Noble-Haeusslein, L. J. (2010). Age is a determinant of leukocyte infiltration and loss of cortical volume after traumatic brain injury. *Dev. Neurosci.* 32, 454–465. doi: 10.1159/000316805

Cope, E. C., Morris, D. R., Scrimgeour, A. G., and Levenson, C. W. (2012). Use of zinc as a treatment for traumatic brain injury in the rat: effects on cognitive and behavioral outcomes. *Neurorehabil. Neural Repair* 26, 907–913. doi: 10.1177/1545968311435337

Coronado, V. G., Haileyesus, T., Cheng, T. A., Bell, J. M., Haarbauer-Krupa, J., Lionbarger, M. R., et al. (2015). Trends in sports-and recreation-related traumatic brain injuries treated in US emergency departments: the National Electronic Injury Surveillance System-All Injury Program (NEISS-AIP) 2001–2012. *J. Head Trauma Rehabil.* 30, 185–197. doi: 10.1097/HTR.0000000000000156

Draper, K., and Ponsford, J. (2008). Cognitive functioning ten years following traumatic brain injury and rehabilitation. *Neuropsychology* 22, 618–625. doi: 10.1037/0894-4105.22.5.618

Elder, G. A., Dorr, N. P., De Gasperi, R., Gama Sosa, M. A., Shaughness, M. C., Maudlin-Jeronimo, E., et al. (2012). Blast exposure induces post-traumatic stress disorder-related traits in a rat model of mild traumatic brain injury. *J. Neurotrauma* 29, 2564–2575. doi: 10.1089/neu.2012.2510

Felix-Ortiz, A. C., Beyeler, A., Seo, C., Leppla, C. A., Wildes, C. P., and Tye, K. M. (2013). BLA to vHPC inputs modulate anxiety-related behaviors. *Neuron* 79, 658–664. doi: 10.1016/j.neuron.2013.06.016

Fujimoto, S. T., Longhi, L., Saatman, K. E., Conte, V., Stocchetti, N., and McIntosh, T. K. (2004). Motor and cognitive function evaluation following experimental traumatic brain injury. *Neurosci. Biobehav. Rev.* 28, 365–378. doi: 10.1016/j.neubiorev.2004.06.002

Griebel, G., Moreau, J.-L., Jenck, F., Martin, J. R., and Misslin, R. (1993). Some critical determinants of the behaviour of rats in the elevated plus-maze. *Behav. Processes* 29, 37–47. doi: 10.1016/0376-6357(93)90026-n

Gundersen, H. J. G., and Jensen, E. B. (1987). The efficiency of systematic sampling in stereology and its prediction. *J. Microsc.* 147, 229–263. doi: 10.1111/j.1365-2818.1987.tb02837.x

Hong, W., Kim, D.-W., and Anderson, D. J. (2014). Antagonistic control of social versus repetitive self-grooming behaviors by separable amygdala neuronal subsets. *Cell* 158, 1348–1361. doi: 10.1016/j.cell.2014.07.049

Hyder, A. A., Wunderlich, C. A., Puvanachandra, P., Gururaj, G., and Kobusingye, O. C. (2007). The impact of traumatic brain injuries: a global perspective. *Neurorehabilitation* 22, 341–353.

Ingebrigtsen, T., and Romner, B. (2003). Biochemical serum markers for brain damage: a short review with emphasis on clinical utility in mild head injury. *Restor. Neurol. Neurosci.* 21, 171–176.

James, L. M., Strom, T. Q., and Leskela, J. (2014). Risk-taking behaviors and impulsivity among veterans with and without PTSD and mild TBI. *Mil. Med.* 179, 357–363. doi: 10.7205/milmed-d-13-00241

Jones, N. C., Cardamone, L., Williams, J. P., Salzberg, M. R., Myers, D., and O'Brien, T. J. (2008). Experimental traumatic brain injury induces a pervasive hyperanxious phenotype in rats. *J. Neurotrauma* 25, 1367–1374. doi: 10.1089/neu.2008.0641

Kalueff, A. V., and Nutt, D. J. (2007). Role of GABA in anxiety and depression. *Depress. Anxiety* 24, 495–517. doi: 10.1002/da.20262

Kocka, A., and Gagnon, J. (2014). Definition of impulsivity and related terms following traumatic brain injury: a review of the different concepts and measures used to assess impulsivity, disinhibition and other related concepts. *Behav. Sci.* 4, 352–370. doi: 10.3390/bs4040352

Logue, S. F., Owen, E. H., Rasmussen, D. L., and Wehner, J. M. (1997). Assessment of locomotor activity, acoustic and tactile startle, and prepulse inhibition of startle in inbred mouse strains and F1 hybrids: implications of genetic background for single gene and quantitative trait loci analyses. *Neuroscience* 80, 1075–1086. doi: 10.1016/s0306-4522(97)00164-4

Lydiard, R. B. (2003). The role of GABA in anxiety disorders. *J. Clin. Psychiatry* 64, 21–27.

Max, J. E., Arndt, S., Castillo, C. S., Bokura, H., Robin, D. A., Lindgren, S. D., et al. (1998). Attention-deficit hyperactivity symptomatology after traumatic brain injury: a prospective study. *J. Am. Acad. Child Adolesc. Psychiatry* 37, 841–847. doi: 10.1097/00004583-199808000-00014

Menon, D. K., Schwab, K., Wright, D. W., and Maas, A. I. (2010). Position statement: definition of traumatic brain injury. *Arch. Phys. Med. Rehabil.* 91, 1637–1640. doi: 10.1016/j.apmr.2010.05.017

Meyer, D. L., Davies, D. R., Barr, J. L., Manzerra, P., and Forster, G. L. (2012). Mild traumatic brain injury in the rat alters neuronal number in the limbic system and increases conditioned fear and anxiety-like behaviors. *Exp. Neurol.* 235, 574–587. doi: 10.1016/j.expneurol.2012.03.012

Möehler, H. (2006). $GABA_A$ receptors in central nervous system disease: anxiety, epilepsy, and insomnia. *J. Recept. Signal Transduct. Res.* 26, 731–740. doi: 10.1080/10799890600920035

Moore, E. L., Terryberry-Spohr, L., and Hope, D. A. (2006). Mild traumatic brain injury and anxiety sequelae: a review of the literature. *Brain Inj.* 20, 117–132. doi: 10.1080/02699050500443558

Morales, D. M., Marklund, N., Lebold, D., Thompson, H. J., Pitkanen, A., Maxwell, W. L., et al. (2005). Experimental models of traumatic brain injury: do we really need to build a better mousetrap? *Neuroscience* 136, 971–989. doi: 10.1016/j.neuroscience.2005.08.030

Nemeroff, C. B. (2003). The role of GABA in the pathophysiology and treatment of anxiety disorders. *Psychopharmacol. Bull.* 37, 133–146. doi: 10.1073/pnas.2336126100

Osborn, A. J., Mathias, J. L., and Fairweather-Schmidt, A. K. (2016). Prevalence of anxiety following adult traumatic brain injury: a meta-analysis comparing measures, samples and postinjury intervals. *Neuropsychology* 30, 247–261. doi: 10.1037/neu0000221

Pandey, D. K., Yadav, S. K., Mahesh, R., and Rajkumar, R. (2009). Depression-like and anxiety-like behavioural aftermaths of impact accelerated traumatic brain injury in rats: a model of comorbid depression and anxiety? *Behav. Brain Res.* 205, 436–442. doi: 10.1016/j.bbr.2009.07.027

Paxinos, G., and Franklin, K. (2004). *The Mouse Brain in Stereotaxic Coordinates.* Cambridge, MA: Gulf Professional Publishing.

Ponsford, J., Draper, K., and Schönberger, M. (2008). Functional outcome 10 years after traumatic brain injury: its relationship with demographic, injury severity, and cognitive and emotional status. *J. Int. Neuropsychol. Soc.* 14, 233–242. doi: 10.1017/s1355617708080272

Rao, V., and Lyketsos, C. G. (2002). Psychiatric aspects of traumatic brain injury. *Psychiatr. Clin. North Am.* 25, 43–69. doi: 10.1016/s0193-953x(03)00052-2

Reger, M. L., Poulos, A. M., Buen, F., Giza, C. C., Hovda, D. A., and Fanselow, M. S. (2012). Concussive brain injury enhances fear learning and excitatory processes in the amygdala. *Biol. Psychiatry* 71, 335–343. doi: 10.1016/j.biopsych.2011.11.007

Rodgers, R. J., and Shepherd, J. K. (1993). Influence of prior maze experience on behaviour and response to diazepam in the elevated plus-maze and light/dark tests of anxiety in mice. *Psychopharmacology* 113, 237–242. doi: 10.1007/bf02245704

Sanders, S. K., and Shekhar, A. (1995). Anxiolytic effects of chlordiazepoxide blocked by injection of $GABA_A$ and benzodiazepine receptor antagonists in the region of the anterior basolateral amygdala of rats. *Biol. Psychiatry* 37, 473–476. doi: 10.1016/0006-3223(94)00183-4

Schindelin, J., Arganda-Carreras, I., Frise, E., Kaynig, V., Longair, M., Pietzsch, T., et al. (2012). Fiji: an open-source platform for biological-image analysis. *Nat. Methods* 9, 676–682. doi: 10.1038/nmeth.2019

Scholten, A. C., Haagsma, J. A., Cnossen, M. C., Olff, M., van Beeck, E. F., and Polinder, S. (2016). Prevalence of and risk factors for anxiety and depressive disorders after traumatic brain injury: a systematic review. *J. Neurotrauma* 33, 1969–1994. doi: 10.1089/neu.2015.4252

Schultz, B. A., Cifu, D. X., McNamee, S., Nichols, M., and Carne, W. (2011). Assessment and treatment of common persistent sequelae following blast induced mild traumatic brain injury. *Neurorehabilitation* 28, 309–320. doi: 10.3233/NRE-2011-0659

Schwarzbold, M. L., Rial, D., De Bem, T., Machado, D. G., Cunha, M. P., dos Santos, A. A., et al. (2010). Effects of traumatic brain injury of different severities on emotional, cognitive, and oxidative stress-related parameters in mice. *J. Neurotrauma* 27, 1883–1893. doi: 10.1089/neu.2010.1318

Scott, S. K., Young, A. W., Calder, A. J., Hellawell, D. J., Aggleton, J. P., and Johnsons, M. (1997). Impaired auditory recognition of fear and anger following bilateral amygdala lesions. *Nature* 385, 254–257. doi: 10.1093/neucas/3.4.267-h

Shear, D. A., Lu, X.-C. M., Bombard, M. C., Pedersen, R., Chen, Z., Davis, A., et al. (2010). Longitudinal characterization of motor and cognitive deficits in a model of penetrating ballistic-like brain injury. *J. Neurotrauma* 27, 1911–1923. doi: 10.1089/neu.2010.1399

Sierra-Mercado, D., McAllister, L. M., Lee, C. C. H., Milad, M. R., Eskandar, E. N., and Whalen, M. J. (2015). Controlled cortical impact before or after fear conditioning does not affect fear extinction in mice. *Brain Res.* 1606, 133–141. doi: 10.1016/j.brainres.2015.02.031

Sönmez, A., Sayın, O., Gürgen, S. G., and Çaliş ir, M. (2015). Neuroprotective effects of MK-801 against traumatic brain injury in immature rats. *Neurosci. Lett.* 597, 137–142. doi: 10.1016/j.neulet.2015.05.001

Tai, C.-Y., Mysore, S. P., Chiu, C., and Schuman, E. M. (2007). Activity-regulated N-cadherin endocytosis. *Neuron* 54, 771–785. doi: 10.1016/j.neuron.2007.05.013

Thau-Zuchman, O., Gomes, R. N., Dyall, S. C., Davis, M., Priestley, J. V., Groenendijk, M., et al. (2019). Brain phospholipid precursors administered post-injury reduce tissue damage and improve neurological outcome in experimental traumatic brain injury. *J. Neurotrauma* 36, 25–42. doi: 10.1089/neu.2017.5579

Treit, D., Menard, J., and Royan, C. (1993). Anxiogenic stimuli in the elevated plus-maze. *Pharmacol. Biochem. Behav.* 44, 463–469. doi: 10.1016/0091-3057(93)90492-c

Tucker, L. B., Burke, J. F., Fu, A. H., and McCabe, J. T. (2017). Neuropsychiatric symptom modeling in male and female C57BL/6J mice after experimental traumatic brain injury. *J. Neurotrauma* 34, 890–905. doi: 10.1089/neu.2016.4508

Tye, K. M., Prakash, R., Kim, S.-Y., Fenno, L. E., Grosenick, L., Zarabi, H., et al. (2011). Amygdala circuitry mediating reversible and bidirectional control of anxiety. *Nature* 471, 358–362. doi: 10.1038/nature09820

Wagner, A. K., Postal, B. A., Darrah, S. D., Chen, X., and Khan, A. S. (2007). Deficits in novelty exploration after controlled cortical impact. *J. Neurotrauma* 24, 1308–1320. doi: 10.1089/neu.2007.0274

Wakade, C., Sukumari-Ramesh, S., Laird, M. D., Dhandapani, K. M., and Vender, J. R. (2010). Delayed reduction in hippocampal postsynaptic density protein-95 expression temporally correlates with cognitive dysfunction following controlled cortical impact in mice. *J. Neurosurg.* 113, 1195–1201. doi: 10.3171/2010.3.jns091212

Walf, A. A., and Frye, C. A. (2007). The use of the elevated plus maze as an assay of anxiety-related behavior in rodents. *Nat. Protoc.* 2, 322–328. doi: 10.1038/nprot.2007.44

Wang, Y., Liu, Y., Lopez, D., Lee, M., Dayal, S., Hurtado, A., et al. (2018). Protection against TBI-induced neuronal death with post-treatment with a selective calpain-2 inhibitor in mice. *J. Neurotrauma* 35, 105–117. doi: 10.1089/neu.2017.5024

Washington, P. M., Forcelli, P. A., Wilkins, T., Zapple, D. N., Parsadanian, M., and Burns, M. P. (2012). The effect of injury severity on behavior: a phenotypic study of cognitive and emotional deficits after mild, moderate, and severe controlled cortical impact injury in mice. *J. Neurotrauma* 29, 2283–2296. doi: 10.1089/neu.2012.2456

Werner, C., and Engelhard, K. (2007). Pathophysiology of traumatic brain injury. *Br. J. Anaesth.* 99, 4–9. doi: 10.1093/bja/aem131

Xiong, Y., Mahmood, A., and Chopp, M. (2013). Animal models of traumatic brain injury. *Nat. Rev. Neurosci.* 14, 128–142. doi: 10.1038/nrn3407

Conflict of Interest Statement: The authors declare that the research was conducted in the absence of any commercial or financial relationships that could be construed as a potential conflict of interest.

frontiers in Behavioral Neuroscience

ORIGINAL RESEARCH
published: 01 May 2019
doi: 10.3389/fnbeh.2019.00085

Neuroanatomical and Functional Correlates of Cognitive and Affective Empathy in Young Healthy Adults

Carme Uribe[1†], Arnau Puig-Davi[1†], Alexandra Abos[1], Hugo C. Baggio[1], Carme Junque[1,2,3] and Barbara Segura[1,2]*

[1] Medical Psychology Unit, Department of Medicine, Institute of Neuroscience, University of Barcelona, Barcelona, Spain, [2] Centro de Investigación Biomédica en Red sobre Enfermedades Neurodegenerativas, Hospital Clínic de Barcelona, Barcelona, Spain, [3] Institut d'Investigacions Biomèdiques August Pi i Sunyer, Barcelona, Spain

OPEN ACCESS

Edited by:
Gennady Knyazev,
State Scientific-Research Institute of Physiology and Basic Medicine, Russia

Reviewed by:
Christopher Chad Woodruff,
Northern Arizona University, United States
Sien Hu,
State University of New York at Oswego, United States
Kai Yuan,
Xidian University, China

***Correspondence:**
Carme Junque
cjunque@ub.edu

[†] These authors have contributed equally to this work

Received: 05 November 2018
Accepted: 11 April 2019
Published: 01 May 2019

Citation:
Uribe C, Puig-Davi A, Abos A, Baggio HC, Junque C and Segura B (2019) Neuroanatomical and Functional Correlates of Cognitive and Affective Empathy in Young Healthy Adults. Front. Behav. Neurosci. 13:85. doi: 10.3389/fnbeh.2019.00085

Neural substrates of empathy are mainly investigated through task-related functional MRI. However, the functional neural mechanisms at rest underlying the empathic response have been poorly studied. We aimed to investigate neuroanatomical and functional substrates of cognitive and affective empathy. The self-reported empathy questionnaire Cognitive and Affective Empathy Test (TECA), T1 and T2*-weighted 3-Tesla MRI were obtained from 22 healthy young females (mean age: 19.6 ± 2.4) and 20 males (mean age: 22.5 ± 4.4). Groups of low and high empathy were established for each scale. FreeSurfer v6.0 was used to estimate cortical thickness and to automatically segment the subcortical structures. FSL v5.0.10 was used to compare resting-state connectivity differences between empathy groups in six defined regions: the orbitofrontal, cingulate, and insular cortices, and the amygdala, hippocampus, and thalamus using a non-parametric permutation approach. The high empathy group in the Perspective Taking subscale (cognitive empathy) had greater thickness in the left orbitofrontal and ventrolateral frontal cortices, bilateral anterior cingulate, superior frontal, and occipital regions. Within the affective empathy scales, subjects with high Empathic Distress had higher thalamic volumes than the low-empathy group. Regarding resting-state connectivity analyses, low-empathy individuals in the Empathic Happiness scale had increased connectivity between the orbitofrontal cortex and the anterior cingulate when compared with the high-empathy group. In conclusion, from a structural point of view, there is a clear dissociation between the brain correlates of affective and cognitive factors of empathy. Neocortical correlates were found for the cognitive empathy dimension, whereas affective empathy is related to lower volumes in subcortical structures. Functionally, affective empathy is linked to connectivity between the orbital and cingulate cortices.

Keywords: cognitive empathy, affective empathy, healthy subjects, cortical thickness, fMRI, resting-state connectivity, young adults, orbitofrontal cortex

INTRODUCTION

Empathy is the ability to understand the thoughts and feelings of others, and to respond to these feelings in an appropriate way. The construct of empathy can be divided into cognitive and affective dimensions (Walter, 2012; Gonzalez-Liencres et al., 2013; Dvash and Shamay-Tsoory, 2014), although the literature on this subject is not always clear due to the multidimensionality of the concept. Cognitive empathy-related processes such as the Perspective Taking dimension "occur through interactions between limbic and cognitive structures" (Decety et al., 2012). Indeed, literature on perception of others in distress or pain have linked somatosensory information with limbic affective and motivational components (Lamm et al., 2011; Decety et al., 2012).

In the past decades, there has been increasing interest in studying the neural basis of empathy with the emergence of magnetic resonance imaging (MRI) techniques in social neuroscience. Recent functional MRI (fMRI) studies have reported limbic structures such as the amygdala, the anterior insula, and the anterior cingulate cortex to be part of the neural bases of affective empathy (Lamm et al., 2011; Bernhardt and Singer, 2012; Gonzalez-Liencres et al., 2013). The prefrontal cortex, including dorsolateral, ventromedial, and orbitofrontal regions, would in turn be related to cognitive empathy (Van Overwalle and Baetens, 2009; Bernhardt and Singer, 2012). A meta-analysis carried out by Fan et al. (2011) including 40 studies concluded that the left anterior insula is recruited for both affective and cognitive empathy. By contrast, the right anterior insula and the right inferior frontal gyrus seem to be more related to affective-perceptual empathy while the left anterior cingulate cortex is involved in the process of cognitive empathy (Fan et al., 2011). In many of the functional MRI studies, empathy has been assessed as a state in performing a task-based MRI design rather than a trait (Lamm et al., 2007; Harvey et al., 2013; Braadbaart et al., 2014; Moore et al., 2015). Lately, few studies have investigated the functional connectivity of the brain at rest linked to the ability to empathize as an intrinsic feature (Takeuchi et al., 2014, 2018; Bilevicius et al., 2018) measured by questionnaires.

Similarly, there are few published structural MRI studies addressing the neuroanatomical substrate of empathic ability measured by questionnaires. The majority of these studies used regions selected *a priori* and a voxel-based morphometry (VBM) approach. Using VBM, Banissy et al. (2012) found negative correlations between scores of affective empathy and gray matter (GM) volumes in the left precuneus, inferior frontal gyrus, anterior cingulate cortex, somatosensory cortex, and the insula. By contrast, employing GM density measures, Eres et al. (2015) reported positive correlations in the insula. Cognitive empathy has been related to cingulate, dorsolateral, and dorsomedial prefrontal cortices (Banissy et al., 2012; Eres et al., 2015). Considering both affective and cognitive empathy, Goerlich-Dobre et al. (2015) described a positive correlation between GM volumes in the left amygdala, bilateral thalamus, and the left parahippocampal gyrus. In line with the findings on fMRI by Fan et al. (2011), the left anterior insula would also be a neuroanatomical substrate for global empathy (Mutschler et al., 2013). To date, only one previous study investigated the correlation between empathy scores and whole-brain cortical thickness (Valk et al., 2016). The authors found a positive correlation between empathy scores and cortical thickness in left inferior frontal, opercular, and insular gyri.

To the best of our knowledge, no previous studies have investigated structural and functional dissociations of affective and cognitive empathy in the same sample of subjects. The aim of the present study was to investigate the structural and functional substrates of empathy in the same sample of healthy young persons. We were interested specially in differences within regions of the limbic system. We hypothesized that cognitive and affective empathy would present distinct regional cortical thickness patterns in neocortical regions and subcortical volumetric differences. Similarly, individuals would differentiate in their functional brain connectivity depending on empathy levels (low empathy and high empathy groups).

MATERIALS AND METHODS

Participants and Instruments

Fifty-six volunteers were recruited from advertising the study between students of the first course of the Nursing Bachelor of the University of Barcelona, Campus Clinic. These students were also invited to recruit friends or relatives of similar age and education. The inclusion criterion was that individuals would be between 18 and 35-years old. The exclusion criteria were: (1) presence of neurological or psychiatric disorders, (2) MRI incompatibilities such as metal implants that could not be extracted, (3) claustrophobia, (4) meeting DSM-IV criteria for substance abuse or dependence within the past year, and (5) current use of psychoactive medication.

Fourteen subjects were excluded due to the following reasons: 1 male met criteria of substance dependence, 1 male and 2 females were on psychoactive medication, 2 males and 3 females did not respond/did not show up on the day of the scan, 1 male and 3 females had a history of neurological or psychiatric disorders, and 1 female had MRI incompatibilities. Finally, 42 participants (22 females and 20 males) were included in the study. Additionally, for resting-state analysis 1 male was excluded due to excessive head motion.

Written informed consent was obtained from all participants after full explanation of procedures. The study was approved by the ethics committee of the Hospital Clinic of Barcelona. Subjects of this study were participants of an ongoing study funded by the Spanish Ministry of Science and Innovation (PSI2014-58004-P).

To exclude the presence of psychiatric disorders, the Mini International Neuropsychiatric Interview (Sheehan et al., 1998) was administered. Empathy was assessed with the Cognitive and Affective Empathy Test (TECA, López Pérez et al., 2008), which provides a global score of empathy and is divided into 4 subscales: 2 assessing cognitive empathy (Perspective Taking and Emotional Understanding) and 2 assessing affective empathy (Empathic Distress and Empathic Happiness).

Briefly, the Perspective Taking scale assesses the intellectual ability of putting oneself in someone else's place. The Emotional

Understanding scale measures the ability of acknowledging and understanding the emotional states, intentions, and impressions of others. Within the affective scales, Emotional Distress is the ability of sharing others' negative emotions, such as pain (Bernhardt and Singer, 2012). Finally, Empathic Happiness is the ability of sharing others' positive emotions; in other words, to be happy when something good happens to another person (López Pérez et al., 2008).

Scores were transformed into T scores as recommended in the TECA manual (López Pérez et al., 2008) and two groups were established: T scores ≤55 were considered as low empathy and T scores ≥56 were considered as high empathy.

MRI Acquisition and Preprocessing

Magnetic resonance images were acquired with a 3T scanner (MAGNETOM Trio, Siemens, Germany), using an 8-channel head coil. The scanning protocol included high-resolution three-dimensional T1-weighted images acquired in the sagittal plane (TR = 2,300 ms, TE = 2.98 ms, TI = 900 ms, 240 slices, FOV = 256 mm; matrix size = 256 × 256; 1 mm isotropic voxel) and a resting-state 10-min-long functional gradient-echo echo-planar imaging sequence (240 T2* weighted images, TR = 2.5 s, TE = 28 ms, flip angle = 80°, slice thickness = 3 mm, FOV = 240 mm). Subjects were instructed to keep their eyes closed, not to fall asleep, and not to think anything in particular.

Cortical Thickness

Cortical thickness was estimated using the automated FreeSurfer stream (version 6.0[1]). The procedures carried out by FreeSurfer include removal of non-brain data, intensity normalization (Fischl et al., 2001), tessellation of the GM / white matter (WM) boundary, automated topology correction (Dale et al., 1999; Ségonne et al., 2007), and accurate surface deformation to identify tissue borders (Dale and Sereno, 1993; Fischl and Dale, 2000; Fischl et al., 2002). Cortical thickness is then calculated as the distance between the WM and GM surfaces at each vertex of the reconstructed cortical mantle (Fischl et al., 2002). After FreeSurfer preprocessing, results for each subject were visually inspected to ensure accuracy of registration, skull stripping, segmentation, and cortical surface reconstruction. Maps were smoothed using a circularly symmetric Gaussian kernel across the surface with a full width at half maximum (FWHM) of 15 mm.

Subcortical Volumes

Six subcortical volumes (amygdala, hippocampus, nucleus accumbens, thalamus, caudate, and putamen) and estimated total intracranial volume (eTIV) were obtained via whole-brain segmentation (Fischl et al., 2002). Ratios were calculated for all subcortical structures to eTIV (left or right-hemisphere subcortical structure / eTIV)*100).

Resting-State Images

Basic functional image preprocessing, using AFNI[2] tools, included: discarding the first 5 volumes to allow magnetization stabilization, despiking, motion correction, grand-mean scaling, linear detrending, and temporal filtering (maintaining frequencies above 0.01 Hz).

For connectivity analysis, based on previous literature we defined 6 regions of interest: the bilateral orbitofrontal, cingulate, and insular cortices, amygdala, hippocampus, and thalamus. The corresponding masks were extracted from the Brainnetome Atlas, which is built on functional and anatomical images[3]. We merged all brainnetome subregions corresponding to each selected region (see **Supplementary Table 1**). Since this atlas is registered to MNI space, (unsmoothed) resting-state images normalized to standard MNI space (voxel size: 3 mm × 3 mm × 3 mm) were used to extract the signal variation time course of the regions of interest.

Noise Correction and Head Motion

Regarding head motion parameters, an exclusion cut-off was established for mean interframe head motion at ≥0.3 mm translation or 0.3° rotation; and for maximum interframe head motion at ≥1 mm translation or 1° rotation. As described in the participants section, we excluded 1 male participant due to excessive head movement (maximum rotation: 3.06°).

In order to remove the effects of head motion and other non-neural sources of signal variation from the functional data, we used an Independent Component Analysis (ICA)-based strategy for Automatic Removal of Motion Artifacts (ICA-AROMA, Pruim et al., 2015). ICA-AROMA decomposes the data via ICA and automatically identifies which of these components are related to head motion, by using four robust and standardized features.

As quality control measure to assess the efficacy of ICA-AROMA in reducing relationship between signal variation and motion, we performed correlations between framewise head displacement (Power et al., 2012) and overall signal variation (defined as the voxel-wise root mean square intensity difference between subsequent time points) after regressing the ICA-AROMA components. These two measures should not correlate significantly because signal change should not be explained by head motion. **Supplementary Table 2** summarizes groups' means of all motion parameters.

Statistical Analysis

Demographics and Empathy Scores

Demographic and volumetric statistical analyses were conducted using IBM SPSS Statistics 25.0 (2011; IBM Corp, Armonk, NY, United States). We tested for group differences in demographics between females and males and between groups of high and low empathy for each test scale using the Mann-Whitney *U*-test for non-normally distributed quantitative measures as indicated by the Shapiro-Wilk test; for normally distributed measures, Student's *T*-test was used. Fisher's exact test was used for categorical measures.

Cortical Thickness Analyses

Intergroup cortical thickness comparisons were performed using a vertex-by-vertex general linear model with FreeSurfer.

[1]https://surfer.nmr.mgh.harvard.edu/

[2]https://afni.nimh.nih.gov/afni

[3]https://atlas.brainnetome.org/bnatlas.html

The model included cortical thickness as a dependent factor and the low/high groups of empathy from each subscale as independent factors. Scores in the Vocabulary subtest from the Wechsler Adults Intelligence Scale-IV (Wechsler, 2008) were entered as a covariate of no interest. All results were corrected for multiple comparisons using pre-cached cluster-wise Monte Carlo simulation with 10,000 iterations. Reported cortical regions reached a two-tailed corrected significance level of $p < 0.05$. Mean thickness (mm) from significant clusters was extracted for plotting results.

Subcortical Volumes

Group differences between groups of high and low empathy in subcortical volumes were tested with the Hotelling's T-squared distribution test for multivariate ANOVA and *F*-test for univariate test stats.

Resting-State Analyses

The first eigenvariate of the time series of all voxels included in each of the six masks described above (see Resting-state images section) was extracted with the fslmeants tool[4]. The first eigenvariate represents the weighted mean of the data that results in the time series with maximum possible variance. We then fitted a general linear model with the preprocessed images and the time series extracted. At this step, we used smoothed images (smoothed at full width half maximum of 6) to include them into the general linear model. Nuisance factors from ICA-AROMA, the six head motion parameters extracted during motion correction, and the mean ventricular and WM time series were included as regressors. Finally, six binary masks were created from the five other regions left and we tested for group differences within each TECA scale group using FSL's randomize permutation-testing tool (5,000 permutations, Winkler et al., 2014). Therefore, for each TECA scale, six permutation testing analyses were performed. To correct for multiple comparisons across voxels we used the threshold-free cluster enhancement (TFCE, Smith and Nichols, 2009) method and significance *p*-value threshold was set at $P < 0.05 / (2*6) = 0.004$ after Bonferroni multiple comparison correction; being 2 the number of contrasts per region of interest and 6 the number of masks used. We also set a cluster-size threshold of 50 voxels in intergroup analyses.

RESULTS

Demographics

There were no significant differences in demographical variables between gender groups. Females scored significantly higher than males in all the empathic scales except for the Perspective Taking scale. However, no gender differences were found between groups of low and high empathy (**Table 1**). Additionally, there were no other demographical differences between groups of high and low empathy for each of the five test scales.

[4]https://fsl.fmrib.ox.ac.uk/fsl/fslwiki/Fslutils

Whole-Brain Cortical Thickness

Whole-brain cortical thickness comparisons showed that subjects grouped in the high Perspective Taking scores (cognitive empathy) showed thicker cortex in left lateral and medial orbitofrontal gyrus, lateral pars opercularis extending to pars triangularis, and inferior frontal gyrus, as well as in bilateral medial superior frontal, anterior and middle cingulate gyrus, and lateral and medial occipital regions (**Figures 1A,B**). There were no other significant differences between groups in other subscales or in the TECA global score.

Subcortical Regions

Subcortical volumetric analyses showed that participants grouped in the high Empathic Distress scale had significantly higher bilateral thalamus volumes than the low-empathy group, although the multivariate test was not statistically significant (**Supplementary Table 3**).

Seed-Based Resting-State

For the resting-state permutation testing analyses, no head motion parameters (e.g., framewise displacement, rotation, and translation) were considered as covariates since there were no significant differences between high and low empathy groups.

Significant differences were found in one of the affective empathy scales, the Empathic Happiness. Subjects classified as having low empathy had increased connectivity between the bilateral orbitofrontal and the anterior cingulate regions (x,y,z MNI coordinates: 12,45,3; 67 voxels in the cluster; max *t*-test = 4.440; *P*-value = 0.003) when compared with the high empathy group (**Figure 2**). There were no other group differences in resting-state connectivity in any other selected regions at *P*-corrected < 0.004.

DISCUSSION

The novelty of this study is the characterization of distinct neuroanatomical and functional correlates of cognitive and affective empathy in the same sample of healthy young adults. Overall, our findings showed that the orbitofrontal and cingulate cortices were related to both empathic dimensions. Higher cognitive empathy was associated with orbitofrontal thickening extending to the ventrolateral prefrontal cortex and bilateral superior frontal, cingulate, and occipital cortices. On the other hand, high negative affective empathy was linked to higher bilateral thalamus volumetry. The low positive affective empathy group had higher connectivity at rest between the bilateral orbitofrontal and cingulate cortices.

According to our structural and functional results, the orbitofrontal and anterior cingulate cortices seem to be key structures involved in empathy. However, cortical thickness was better able to discriminate between individuals with high and low empathy than resting state functional connectivity. The fact that the structural neuroanatomical information was more informative than functional connectivity is compatible with the notion that empathy was measured as a personality trait (e.g., "to

TABLE 1 | Demographical and empathy variables.

	Males (n = 20)	Females (n = 22)	Test stat	p-value	Total sample (n = 42)
Age, median (IQR)	22.5 (8.0)	19.0 (2.0)	150.500[1]	0.071	19.0 (5.0)
Education, years, median (IQR)	13.5 (6.0)	13.00 (2.0)	184.500[1]	0.353	13.0 (4.0)
Vocabulary test*, median (IQR)	38.0 (8.0)	38.0 (6.0)	224.000[1]	0.714	38.0 (6.0)
TECA total score, mean (SD)	114.2 (12.0)	132.4 (13.4)	4.641[2]	<0.001	123.7 (15.6)
TECA total, low/high (%)	10 (50.0) / 10 (50.0)	6 (27.3) / 16 (72.7)	0.204	0.116	16 (38.1) / 26 (61.9)
Perspective taking, mean (SD)	31.4 (4.5)	33.4 (4.3)	1.492[2]	0.144	32.4 (4.4)
Perspective taking, low/high (%)	8 (40.0) / 12 (60.0)	6 (27.3) / 16 (72.7)	0.515	0.293	14 (33.3) / 28 (66.7)
Emotional understanding, mean (SD)	31.9 (5.7)	35.6 (4.2)	2.440[2]	0.019	33.9 (5.2)
Emotional understanding, low/high (%)	9 (45.0) / 11 (55.0)	7 (31.8) / 15 (68.2)	0.527	0.288	16 (38.1) / 26 (61.9)
Empathic distress, mean (SD)	19.5 (6.5)	28.0 (5.7)	4.494[2]	<0.001	24.0 (7.4)
Empathic distress, low/high (%)	16 (80.0) / 4 (20.0)	13 (59.1) / 9 (40.9)	0.190	0.129	29 (69.0) / 13 (31.0)
Empathic happiness, median (IQR)	32.0 (7.0)	36.5 (7.0)	333.000[1]	0.004	34.0 (7.0)
Empathic happiness, low/high (%)	11 (55.0) / 9 (45.0)	9 (40.9) / 13 (59.1)	0.537	0.273	20 (47.6) / 22 (52.4)

[1]*Mann-Whitney U-test;* [2]*Student's t-test; *Vocabulary subtest of the Wechsler Adult Intelligence Scale-IV; SD, standard deviation; IQR, interquartile range; TECA, Test of Cognitive and Affective Empathy. Data are shown as mean (SD) for normally distributed quantitative measures; median (IQR) for non-normally distributed measures and as frequency (percentage) for categorical variables. Fisher's exact test was used for categorical variables. Test stats are group comparisons between males and females.*

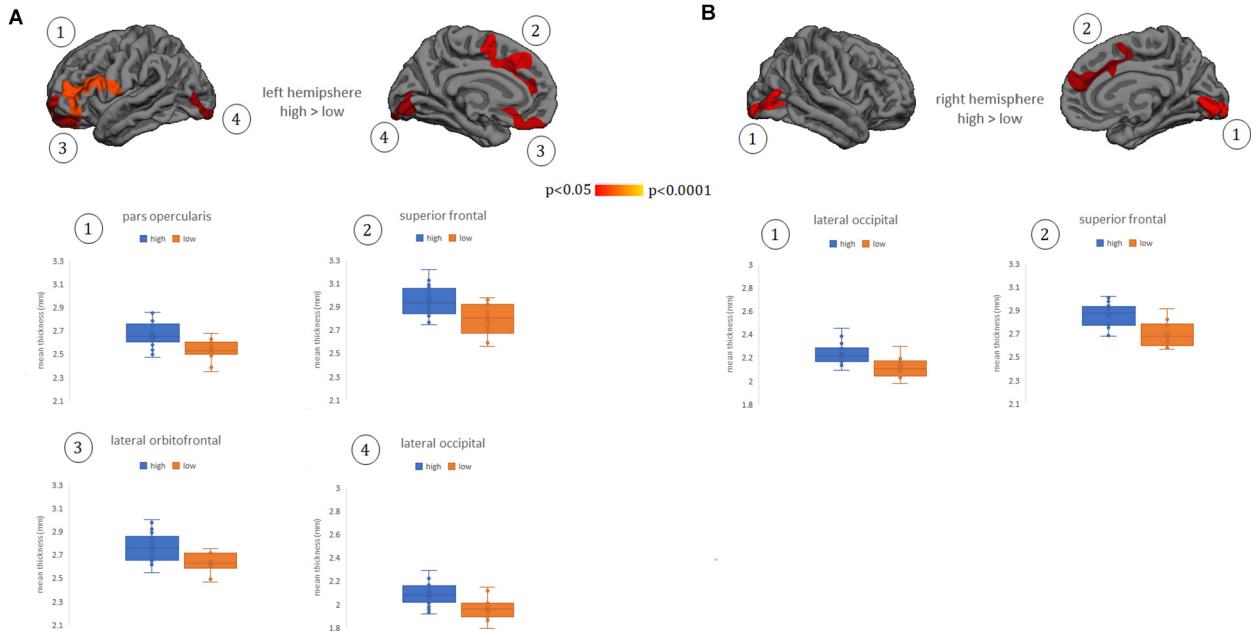

FIGURE 1 | Cortical thickness differences between groups of low and high empathy within the Perspective Taking subscale. **(A)** left hemisphere. **(B)** right hemisphere. Numbers indicate each cluster of significance that in turn are plotted below the cortical maps. Results were corrected using Monte Carlo simulation at two-tailed $p < 0.05$. Color maps indicate significant cortical thickening in the high group compared with the low group. Boxplots show the mean thickness values of each participant within the clusters that reached significant differences between groups. Vocabulary test scores were used as a covariate. The box of the graphs indicates the second and third quartile and middle lines are medians.

understand how another person feels is something really easy to me") rather than a state (Leiberg and Anders, 2006).

Group differences in cortical thickness between groups of high and low empathy within the Perspective Taking subtest were observed in both medial and lateral orbital cortices. Previous structural MRI studies also pointed to the dorsomedial prefrontal cortex as an anatomical substrate of empathy in healthy subjects using cortical thickness measures both studying cortical parcellations (Massey et al., 2017) and from a whole-brain approach (Valk et al., 2016). Earlier studies evidenced dorsomedial prefrontal correlations with empathy using a different methodological approach based on GM density (Eres et al., 2015).

In pathological conditions, cortical thickness correlates in lateral and medial prefrontal cortices have been described. For example, in pathological narcissism, which is characterized by arrogant behavior and lack of empathy, volumetric reductions, and cortical thinning in the right dorsolateral prefrontal cortex

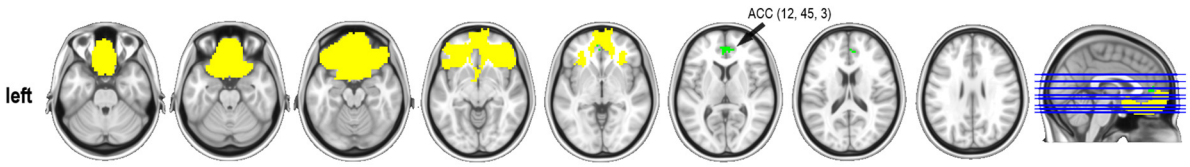

FIGURE 2 | Resting-state connectivity group differences in the Empathic Happiness subscale. ACC, anterior cingulate cortex (MNI coordinates). Represented in yellow, the orbital mask from the Brainnetome atlas and in green the cluster that reached statistical significance at *P*-corrected < 0.004 after Bonferroni multiple comparisons correction. Contrast group was low empathy > high empathy. Cluster-size threshold was set at 50 voxels. Thus, low empathic individuals had stronger functional connectivity between the orbitofrontal cortex and the anterior cingulate gyrus than the high empathic group in the Empathic happiness scale.

have been found (Mao et al., 2016). Also, reduced cortical thickness in inferior, middle, and superior frontal gyri was related to cognitive empathy in individuals at high risk of alcohol abuse (Schmidt et al., 2017). Dysfunctions in social cognition have also been described in neurological disorders (Henry et al., 2016). In a study with patients diagnosed with the behavioral variant of frontotemporal dementia, Perspective Taking scores correlated with atrophy in extensive parts of the right dorsolateral prefrontal cortex (Eslinger et al., 2011). From fMRI task-based studies, Fan et al. (2011) suggest that the left anterior insula is the core of the empathy network while there is regional specificity for both cognitive and affective dimensions, being the left orbitofrontal a cognitive-related region.

Structurally, we also found thicker bilateral cingulate cortex in the group with high perspective-taking empathy than in the low-empathy group. Positive correlations between cognitive empathy and the anterior cingulate (Banissy et al., 2012; Massey et al., 2017) as well as the middle cingulate cortex (Eres et al., 2015) have been reported in healthy individuals. In a study of patients with frontal lesions, it has been found that patients with lesions located in the medial prefrontal cortex extending to the anterior cingulate gyrus had poor cognitive empathic abilities (Shamay-Tsoory et al., 2009).

In the present study, group connectivity differences were found between the bilateral orbitofrontal with the anterior cingulate in the scale evaluating positive affective empathy. Within the limbic system, the cingulate cortex has been reported as a hub region, defined as a region that integrates different brain processes (Van Den Heuvel and Sporns, 2013). Indeed, the rostral anterior cingulate cortex projects to lateral and orbital regions of the prefrontal cortex (Bernhardt and Singer, 2012). Interestingly, we found regional thickening in these regions. Recent psychopathological studies using resting state images, showed orbitofrontal anomalies in conditions characterized by a lack of empathy including individuals with autism (Bi et al., 2018) and psychopathic subjects (Espinoza et al., 2018). In this last study, brain anomalies were also reported in the anterior and posterior cingulate. Our results suggest that subjects with low affective empathy with no previous psychiatric condition would over-engage cognitive-empathic pathways. However, it is important to highlight that in the literature of empathy in autism and psychopathy, there is an ongoing discussion in whether a lack of empathy is genuine or not (Decety et al., 2013; Richman and Bidshahri, 2018).

In our results, we also found regional thickness differences in bilateral occipital cortex involving the pericalcarine and lingual gyri using whole-brain cortical thickness analysis. Since most of the structural studies performed with healthy subjects have focused on regions selected *a priori*, literature relating cognitive empathy to non-limbic brain areas is scant. Similarly to our results, Valk et al. (2016), performing a whole-brain approach, reported the right occipital and fusiform gyri as anatomical substrates of mentalizing. This work is relevant since they combined structural vertex-wise whole brain analyses with an empathic fMRI task. In pathological conditions, Hadjikhani et al. (2006) found cortical thickness reductions in the left inferior occipital region in high-functioning autism spectrum disorders adults, and Schmidt et al. (2017) found reduced cortical thickness in the right precuneus in subjects at high risk of alcoholism and low empathy.

In the current study, analyses of volumetric subcortical structures showed that participants with high Empathic Distress scale scores had significantly higher bilateral thalamus volumes compared with those in the low-empathy group. Previous MRI structural studies have also found a link between the thalamus and both affective and cognitive empathy. One study investigated the neural correlates of both empathy and alexithymia in a sample of healthy participants and reported the thalamus, together with other structures including left amygdala, hippocampus and parahippocampal gyrus as significant correlates of both constructs (Goerlich-Dobre et al., 2015). Similarly, lower affective and cognitive empathy in individuals with temporal lobe epilepsy was associated with smaller fronto-limbic regions including the thalamus (Toller et al., 2015). The thalamus is a complex structure that makes multiple projections to other subcortical structures and the neocortex. The so-called limbic thalamus connects with other limbic structures and has been associated with stress and anxiety states (Vertes et al., 2015).

Global TECA scores did not reveal any significant differences between groups either in cortical or subcortical structures or in functional connectivity, thus emphasizing the importance of differentiating between the cognitive and the affective empathy, with different underlying neural bases. Sex differences were found in all TECA subscales and global scores as previously reported in the literature (Bratek et al., 2015; Esquerda et al., 2016), although these differences disappeared when considering the construct of empathy as binomial (high/low empathy). The actual influence of sex in empathy is still under debate.

Previous studies mainly focused on *a priori* regions already described in the literature from functional MRI studies. One of the strengths and novelty of the present study is the whole-brain vertex-wise methodology used to compare groups in the structural analyses. A second strength is that all participants were similar on demographical variables (i.e., age and education level). Regarding functional connectivity analyses, results reported in the text survived all multiple comparison corrections applied.

The main limitation is the small sample size. Unlike in the whole-brain approach used in the structural analysis, we decided to select *a priori* regions for resting-state connectivity analyses to increase the detection power. Additionally, the study sample was composed of healthy young subjects with no neurological or psychiatric conditions, which makes subtler the neuroanatomical correlates linked to personality traits.

CONCLUSION

In conclusion, we found that structural differences between individuals with high and low empathy are more marked than functional ones. Cognitive empathy had clear correlates with cortical structures, namely medial and lateral prefrontal cortices and associative occipital ones. For affective empathy, only a link with the thalamus was observed. However, in the absence of neuroanatomical differences in positive affective empathy, individuals with low empathy showed increased orbital functional connectivity with the anterior cingulate.

ETHICS STATEMENT

The study was approved by the ethics committee of the Hospital Clinic of Barcelona. Subjects of this study were participants of an ongoing study funded by the Spanish Ministry of Science and Innovation (PSI2014-58004-P). Written informed consent was obtained from all participants after full explanation of procedures.

AUTHOR CONTRIBUTIONS

CJ contributed in the design of the study. CU, AP-D, and AA contributed to the analysis of the data. CU, AP-D, AA, HB, BS, and CJ contributed to the interpretation of the data, revised the manuscript critically for important intellectual content, and approved the final version of the manuscript. AP-D wrote a first draft. CU and CJ modified the first draft of the article.

FUNDING

CU was supported by a fellowship from 2014, Spanish Ministry of Economy and Competitiveness (BES-2014-068173) and cofinanced by the European Social Fund (ESF). AA was supported by a 2016 fellowship from the Departament d'Empresa i Coneixement de la Generalitat de Catalunya, AGAUR (2016FI_B 00360). This study was partially funded by the Generalitat de Catalunya (2017SGR748).

ACKNOWLEDGMENTS

We thank Dr. Antonio Guillamon for facilitating the MRI data for the study. We appreciate the cooperation of the participants. We are also indebted to the Magnetic Resonance Imaging core facility of the IDIBAPS for the technical support, especially to C. Garrido and G. Lasso and we acknowledge the CERCA Programme/Generalitat de Catalunya.

SUPPLEMENTARY MATERIAL

The Supplementary Material for this article can be found online at: https://www.frontiersin.org/articles/10.3389/fnbeh.2019.00085/full#supplementary-material

REFERENCES

Banissy, M. J., Kanai, R., Walsh, V., and Rees, G. (2012). Inter-individual differences in empathy are reflected in human brain structure. *Neuroimage* 62, 2034–2039. doi: 10.1016/j.neuroimage.2012.05.081

Bernhardt, B. C., and Singer, T. (2012). The neural basis of empathy. *Annu. Rev. Neurosci.* 35, 1–23. doi: 10.1146/annurev-neuro-062111-150536

Bi, X.-A., Wang, Y., Shu, Q., Sun, Q., and Xu, Q. (2018). Classification of autism spectrum disorder using random support vector machine cluster. *Front. Genet.* 9:18. doi: 10.3389/fgene.2018.00018

Bilevicius, E., Kolesar, T. A., Smith, S. D., Trapnell, P. D., and Kornelsen, J. (2018). Trait emotional empathy and resting state functional connectivity in default mode, salience, and central executive networks. *Brain Sci.* 8, 1–11. doi: 10.3390/brainsci8070128

Braadbaart, L., de Grauw, H., Perrett, D. I., Waiter, G. D., and Williams, J. H. G. (2014). The shared neural basis of empathy and facial imitation accuracy. *Neuroimage* 84, 367–375. doi: 10.1016/j.neuroimage.2013.08.061

Bratek, A., Bulska, W., Bonk, M., Seweryn, M., and Krysta, K. (2015). Empathy among physicians, medical students and candidates. *Psychiatr. Danub.* 27, S48–S52.

Dale, A. M., Fischl, B., and Sereno, M. I. (1999). Cortical surface-based analysis: I. Segmentation and surface reconstruction. *Neuroimage* 9, 179–194. doi: 10.1006/nimg.1998.0395

Dale, A. M., and Sereno, M. I. (1993). Improved localizadon of cortical activity by combining EEG and MEG with MRI cortical surface reconstruction: a linear approach. *J. Cogn. Neurosci.* 5, 162–176. doi: 10.1162/jocn.1993.5.2.162

Decety, J., Chen, C., Harenski, C., and Kiehl, K. A. (2013). An fMRI study of affective perspective taking in individuals with psychopathy: imagining another in pain does not evoke empathy. *Front. Hum. Neurosci.* 7:489. doi: 10.3389/fnhum.2013.00489

Decety, J., Norman, G. J., Berntson, G. G., and Cacioppo, J. T. (2012). A neurobehavioral evolutionary perspective on the mechanisms underlying empathy. *Prog. Neurobiol.* 98, 38–48. doi: 10.1016/j.pneurobio.2012.05.001

Dvash, J., and Shamay-Tsoory, S. G. (2014). Theory of mind and empathy as multidimensional constructs: neurological foundations. *Top. Lang. Disord.* 34, 282–295. doi: 10.1097/TLD.0000000000000040

Eres, R., Decety, J., Louis, W. R., and Molenberghs, P. (2015). Individual differences in local gray matter density are associated with differences in affective and cognitive empathy. *Neuroimage* 117, 305–310. doi: 10.1016/j.neuroimage.2015.05.038

Eslinger, P. J., Moore, P., Anderson, C., and Grossman, M. (2011). Social cognition, executive functioning, and neuroimaging correlates of empathic deficits in frontotemporal dementia. *J. Neuropsychiatry Clin. Neurosci.* 23, 74–82. doi: 10.1176/jnp.23.1.jnp74

Espinoza, F. A., Vergara, V. M., Reyes, D., Anderson, N. E., Harenski, C. L., Decety, J., et al. (2018). Aberrant functional network connectivity in psychopathy from a large (N = 985) forensic sample. *Hum. Brain Mapp.* 39, 2624–2634. doi: 10.1002/hbm.24028

Esquerda, M., Yuguero, O., Viñas, J., and Pifarré, J. (2016). La empatía médica, ¿nace o se hace? Evolución de la empatía en estudiantes de medicina. *Atención Primaria* 48, 8–14. doi: 10.1016/j.aprim.2014.12.012

Fan, Y., Duncan, N. W., de Greck, M., and Northoff, G. (2011). Is there a core neural network in empathy? An fMRI based quantitative meta-analysis. *Neurosci. Biobehav. Rev.* 35, 903–911. doi: 10.1016/j.neubiorev.2010.10.009

Fischl, B., and Dale, A. M. (2000). Measuring the thickness of the human cerebral cortex from magnetic resonance images. *Proc. Natl. Acad. Sci. U.S.A.* 97, 11050–11055. doi: 10.1073/pnas.200033797

Fischl, B., Liu, A., and Dale, A. M. (2001). Automated manifold surgery: constructing geometrically accurate and topologically correct models of the human cerebral cortex. *IEEE Trans. Med. Imaging* 20, 70–80. doi: 10.1109/42.906426

Fischl, B., Salat, D. H., Busa, E., Albert, M., Dieterich, M., Haselgrove, C., et al. (2002). Whole brain segmentation: automated labeling of neuroanatomical structures in the human brain. *Neuron* 33, 341–355.

Goerlich-Dobre, K. S., Lamm, C., Pripfl, J., Habel, U., and Votinov, M. (2015). The left amygdala: a shared substrate of alexithymia and empathy. *Neuroimage* 122, 20–32. doi: 10.1016/j.neuroimage.2015.08.014

Gonzalez-Liencres, C., Shamay-Tsoory, S. G., and Brüne, M. (2013). Towards a neuroscience of empathy: ontogeny, phylogeny, brain mechanisms, context and psychopathology. *Neurosci. Biobehav. Rev.* 37, 1537–1548. doi: 10.1016/j.neubiorev.2013.05.001

Hadjikhani, N., Joseph, R. M., Snyder, J., and Tager-Flusberg, H. (2006). Anatomical differences in the mirror neuron system and social cognition network in autism. *Cereb. Cortex* 16, 1276–1282. doi: 10.1093/cercor/bhj069

Harvey, P.-O., Zaki, J., Lee, J., Ochsner, K., and Green, M. F. (2013). Neural substrates of empathic accuracy in people with schizophrenia. *Schizophr. Bull.* 39, 617–628. doi: 10.1093/schbul/sbs042

Henry, J. D., Von Hippel, W., Molenberghs, P., Lee, T., and Sachdev, P. S. (2016). Clinical assessment of social cognitive function in neurological disorders. *Nat. Rev. Neurol.* 12, 28–39. doi: 10.1038/nrneurol.2015.229

Lamm, C., Batson, C. D., and Decety, J. (2007). The neural substrate of human empathy: effects of perspective-taking and cognitive appraisal. *J. Cogn. Neurosci.* 19, 42–58. doi: 10.1162/jocn.2007.19.1.42

Lamm, C., Decety, J., and Singer, T. (2011). Meta-analytic evidence for common and distinct neural networks associated with directly experienced pain and empathy for pain. *Neuroimage* 54, 2492–2502. doi: 10.1016/j.neuroimage.2010.10.014

Leiberg, S., and Anders, S. (2006). The multiple facets of empathy: a survey of theory and evidence. *Prog. Brain Res.* 156, 419–440. doi: 10.1016/S0079-6123(06)56023-6

López Pérez, B., Fernández Pinto, I., and Abad García, F. J. (2008). *Test de Empatía Cognitiva y Afectiva*. Madrid: TEA.

Mao, Y., Sang, N., Wang, Y., Hou, X., Huang, H., Wei, D., et al. (2016). Reduced frontal cortex thickness and cortical volume associated with pathological narcissism. *Neuroscience* 328, 50–57. doi: 10.1016/j.neuroscience.2016.04.025

Massey, S. H., Stern, D., Alden, E. C., Petersen, J. E., Cobia, D. J., Wang, L., et al. (2017). Cortical thickness of neural substrates supporting cognitive empathy in individuals with schizophrenia. *Schizophr. Res.* 179, 119–124. doi: 10.1016/j.schres.2016.09.025

Moore, R. C., Dev, S. I., Jeste, D. V., Dziobek, I., and Eyler, L. T. (2015). Distinct neural correlates of emotional and cognitive empathy in older adults. *Psychiatry Res. Neuroimaging* 232, 42–50. doi: 10.1016/j.pscychresns.2014.10.016

Mutschler, I., Reinbold, C., Wankerl, J., Seifritz, E., and Ball, T. (2013). Structural basis of empathy and the domain general region in the anterior insular cortex. *Front. Hum. Neurosci.* 7:177. doi: 10.3389/fnhum.2013.00177

Power, J. D., Barnes, K. A., Snyder, A. Z., Schlaggar, B. L., and Petersen, S. E. (2012). Spurious but systematic correlations in functional connectivity MRI networks arise from subject motion. *Neuroimage* 59, 2142–2154. doi: 10.1016/j.neuroimage.2011.10.018

Pruim, R. H. R., Mennes, M., van Rooij, D., Llera, A., Buitelaar, J. K., and Beckmann, C. F. (2015). ICA-AROMA: a robust ICA-based strategy for removing motion artifacts from fMRI data. *Neuroimage* 112, 267–277. doi: 10.1016/j.neuroimage.2015.02.064

Richman, K. A., and Bidshahri, R. (2018). Autism, theory of mind, and the reactive attitudes. *Bioethics* 32, 43–49. doi: 10.1111/bioe.12370

Schmidt, T., Roser, P., Ze, O., Juckel, G., Suchan, B., and Thoma, P. (2017). Cortical thickness and trait empathy in patients and people at high risk for alcohol use disorders. *Psychopharmacology* 234, 3521–3533. doi: 10.1007/s00213-017-4741-3

Ségonne, F., Pacheco, J., and Fischl, B. (2007). Geometrically accurate topology-correction of cortical surfaces using nonseparating loops. *IEEE Trans. Med. Imaging* 26, 518–529. doi: 10.1109/TMI.2006.887364

Shamay-Tsoory, S. G., Aharon-Peretz, J., and Perry, D. (2009). Two systems for empathy: a double dissociation between emotional and cognitive empathy in inferior frontal gyrus versus ventromedial prefrontal lesions. *Brain* 132, 617–627. doi: 10.1093/brain/awn279

Sheehan, D. V., Lecrubier, Y., Sheehan, K. H., Amorim, P., Janavs, J., Weiller, E., et al. (1998). The mini-international neuropsychiatric interview (M.I.N.I.): the development and validation of a structured diagnostic psychiatric interview for DSM-IV and ICD-10. *J. Clin. Psychiatry* 59(Suppl. 20), 22–33. doi: 10.1016/S0924-9338(99)80239-9

Smith, S. M., and Nichols, T. E. (2009). Threshold-free cluster enhancement: addressing problems of smoothing, threshold dependence and localisation in cluster inference. *Neuroimage* 44, 83–98. doi: 10.1016/J.NEUROIMAGE.2008.03.061

Takeuchi, H., Taki, Y., Nouchi, R., Sekiguchi, A., Hashizume, H., Sassa, Y., et al. (2014). Association between resting-state functional connectivity and empathizing/systemizing. *Neuroimage* 99, 312–322. doi: 10.1016/j.neuroimage.2014.05.031

Takeuchi, H., Taki, Y., Nouchi, R., Sekiguchi, A., Hashizume, H., Sassa, Y., et al. (2018). The neural substrate of human empathy: effects of perspective-taking and cognitive appraisal. *Neuroimage* 8, 312–322. doi: 10.1162/jocn.2007.19.1.42

Toller, G., Adhimoolam, B., Rankin, K. P., Huppertz, H.-J., Kurthen, M., and Jokeit, H. (2015). Right fronto-limbic atrophy is associated with reduced empathy in refractory unilateral mesial temporal lobe epilepsy. *Neuropsychologia* 78, 80–87. doi: 10.1016/j.neuropsychologia.2015.09.010

Valk, S. L., Bernhardt, B. C., Böckler, A., Trautwein, F. M., Kanske, P., and Singer, T. (2016). Socio-cognitive phenotypes differentially modulate large-scale structural covariance networks. *Cereb. Cortex* 27, 1358–1368. doi: 10.1093/cercor/bhv319

Van Den Heuvel, M. P., and Sporns, O. (2013). Special issue: the connectome-feature review network hubs in the human brain. *Trends Cogn. Sci.* 17, 683–696. doi: 10.1016/j.tics.2013.09.012

Van Overwalle, F., and Baetens, K. (2009). Understanding others' actions and goals by mirror and mentalizing systems: a meta-analysis. *Neuroimage* 48, 564–584. doi: 10.1016/j.neuroimage.2009.06.009

Vertes, R. P., Linley, S. B., and Hoover, W. B. (2015). Limbic circuitry of the midline thalamus. *Neurosci. Biobehav. Rev.* 54, 89–107. doi: 10.1016/J.NEUBIOREV.2015.01.014

Walter, H. (2012). Social cognitive neuroscience of empathy: concepts, circuits, and genes. *Emot. Rev.* 4, 9–17. doi: 10.1177/1754073911421379

Wechsler, D. (2008). *Wechsler Adult Intelligence Test*, Fourth Edn. San Antonio, TX: Psychological Corporation.

Winkler, A. M., Ridgway, G. R., Webster, M. A., Smith, S. M., and Nichols, T. E. (2014). Permutation inference for the general linear model. *Neuroimage* 92, 381–397. doi: 10.1016/j.neuroimage.2014.01.060

Conflict of Interest Statement: The authors declare that the research was conducted in the absence of any commercial or financial relationships that could be construed as a potential conflict of interest.

frontiers in Behavioral Neuroscience

ORIGINAL RESEARCH
published: 08 May 2019
doi: 10.3389/fnbeh.2019.00098

Distinct Time-Course of Alterations of Groups I and II Metabotropic Glutamate Receptor and GABAergic Receptor Expression Along the Dorsoventral Hippocampal Axis in an Animal Model of Psychosis

*Valentyna Dubovyk[1,2] and Denise Manahan-Vaughan[1]**

[1] *Department of Neurophysiology, Medical Faculty, Ruhr-University Bochum, Bochum, Germany,* [2] *International Graduate School of Neuroscience, Ruhr-University Bochum, Bochum, Germany*

OPEN ACCESS

Edited by:
Gregg Stanwood, Florida State University, United States

Reviewed by:
Juan Olaya, Neuroscience Research Australia (NeuRA), Australia
Devon L. Graham, Florida State University College of Medicine, United States

***Correspondence:**
Denise Manahan-Vaughan
denise.manahan-vaughan@rub.de; dmv-igsn@rub.de

Received: *21 December 2018*
Accepted: *23 April 2019*
Published: *08 May 2019*

Citation:
Dubovyk V and Manahan-Vaughan D (2019) Distinct Time-Course of Alterations of Groups I and II Metabotropic Glutamate Receptor and GABAergic Receptor Expression Along the Dorsoventral Hippocampal Axis in an Animal Model of Psychosis. Front. Behav. Neurosci. 13:98. doi: 10.3389/fnbeh.2019.00098

Psychosis is a clinical state that encompasses a range of abnormal conditions, including distortions in sensory information processing and the resultant delusional thinking, emotional discordance and cognitive impairments. Upon developing this condition, the rate at which cognitive and behavioral deteriorations progress steadily increases suggesting an active contribution of the first psychotic event to the progression of structural and functional abnormalities and disease establishment in diagnosed patients. Changes in GABAergic and glutamatergic function, or expression, in the hippocampus have been proposed as a key factor in the pathophysiology of psychosis. However, little is known as to the time-point of onset of putative changes, to what extent they are progressive, and their relation to disease stabilization. Here, we characterized the expression and distribution patterns of groups I and II metabotropic glutamate (mGlu) receptors and GABA receptors 1 week and 3 months after systemic treatment with an *N*-methyl-D-aspartate receptor (NMDAR) antagonist (MK801) that is used to model a psychosis-like state in adult rats. We found an early alteration in the expression of mGlu1, mGlu2/3, and $GABA_B$ receptors across the hippocampal dorsoventral and transverse axes. This expanded to include an up-regulation of mGlu5 levels across the entire CA1 region and a reduction in $GABA_B$ expression, as well as GAD67-positive interneurons particularly in the dorsal hippocampus that appeared 3 months after treatment. Our findings indicate that a reduction of excitability may occur in the hippocampus soon after first-episode psychosis. This changes, over time, into increased excitability. These hippocampus-specific alterations are likely to contribute to the pathophysiology and stabilization of psychosis.

Keywords: psychosis, MK801, hippocampus, dorsoventral axis, mGlu receptors, GABA receptors, rodent

INTRODUCTION

Schizophrenia is a chronic mental disorder, distinguished by a rich spectrum of symptoms that are clustered into the cognitive, negative, and psychotic domains (McGhie and Chapman, 1961; Kapur, 2003; Bowie and Harvey, 2005; Bürgy, 2008; Velligan and Alphs, 2008; Davis et al., 2014). Whilst a decline in learning and memory ability (cognitive symptoms) and social withdrawal (negative symptoms) become apparent early on, in the course of the disease (Keshavan et al., 2011; Keefe and Harvey, 2012), it is the manifestation of hallucinatory and delusionary experiences (psychotic symptoms) that lead to clinical diagnosis. Following the first major psychotic event, also known as the first-episode of psychosis (Larson et al., 2010; Keshavan et al., 2011; Ruby et al., 2014), the rate at which cognitive and behavioral deteriorations occur progressively increases (Häfner et al., 1994; Cheung et al., 2010; Alvarez-Jimenez et al., 2011). This suggests an active involvement of the first-episode of psychosis in the progression of structural and functional abnormalities in diagnosed patients (Borgwardt et al., 2008; Haijima et al., 2012; Guo et al., 2013).

It has been proposed that a dysfunction of the glutamatergic and GABAergic systems are key elements to the etiology of schizophrenia and psychosis (Belforte et al., 2010; Nakazawa et al., 2012; Snyder and Gao, 2013). In particular, it is believed that hypofunction of *N*-methyl-D-aspartate receptors (NMDAR) on GABAergic interneurons, particularly on parvalbumin-containing (PV) interneurons, leads to disinhibition of glutamatergic terminals and a hyperglutamatergic state (Marek et al., 2010; Riebe et al., 2016). This disinhibition further results in functional deficits of neurons, circuits and behavior that are characteristic of psychosis and can be emulated by NMDAR antagonists (Krystal et al., 1994; Lahti et al., 1995), and in transgenic animal models of NMDAR hypofunction (Belforte et al., 2010).

Importantly, reduced inhibitory and increased excitatory neurotransmission may, in turn, modulate the function of other glutamatergic and GABAergic receptors, as well as be modulated by them. Here, the (group I) metabotropic glutamate receptor 5 (mGlu5) is of prime interest as it shares a unique interrelationship, both in terms of physical coupling and functional modulation, with NMDAR (Tu et al., 1999; Marino and Conn, 2002; Alagarsamy et al., 2005). Another group I mGlu receptor, mGlu1, potentiates NMDAR currents (Benquet et al., 2002; Heidinger et al., 2002). Furthermore, mGlu1 and mGlu5 receptors both facilitate long-term potentiation (LTP) in the hippocampus (Mukherjee and Manahan-Vaughan, 2013), a brain region that is among the most affected in patients suffering from schizophrenia and psychosis (Heckers and Konradi, 2002; Kolomeets et al., 2007; Adriano et al., 2012; Yin et al., 2012). Group II mGlu receptors, mGlu2 and mGlu3, serve as autoreceptors at glutamatergic terminals (Shigemoto et al., 1997; Schoepp, 2001) and are critically required for persistent forms of hippocampal long-term depression (LTD) (Kobayashi et al., 1996; Manahan-Vaughan, 1998; Pöschel and Manahan-Vaughan, 2007; Altinbilek and Manahan-Vaughan, 2009). Thus, both group I and group II receptors play an intrinsic role in the regulation and support of NMDAR-dependent information processing and storage, as well as in the regulation of activity-dependent neural excitability.

GABA is the primary inhibitory neurotransmitter in the mammalian brain. The ionotropic $GABA_A$ receptor is a ligand-gated chloride channel that is responsible for tonic inhibition in the brain. Because of their high affinity for GABA, along with their relatively slow desensitization rates, it has been proposed that $GABA_A$ receptors sense both the ambient concentration of GABA, as well as the activity- dependent spill-over of GABA from the synaptic cleft (Wlodarczyk et al., 2013). The $GABA_B$ receptor is a metabotropic receptor that serves as an autoreceptor (Waldmeier et al., 2008), but also can modulate GABAergic responses of neurons (Shen et al., 2017). The efficacy of both receptors is regulated by synaptic activity: activation of calcium calmodulin kinase II (CAMKII), a downstream target of NMDAR activation, results in phosphorylation of $GABA_B$ receptors (Zemoura et al., 2018). Furthermore, both protein kinase A (PKA) and protein kinase C (PKC) can mediate phosphorylation of $GABA_A$ receptors (Connelly et al., 2013). $GABA_A$ and $GABA_B$ receptors serve to keep local cellular and network excitation within a functional physiological range and enable the precise spatiotemporal conditions that are required for information encoding through synaptic plasticity (Kaila, 1994; Paulsen and Moser, 1998; Bettler et al., 2004; Kullmann et al., 2005). A disruption of GABAergic inhibitory control can, thus, be expected not only to have a potent effect at the level of tonic inhibition, but also at the level of excitation-inhibition balance. The effectivity of information processing related to cognition, learning and memory will consequently be compromised.

The hippocampus is a critical processing hub for a wide range of sensory and cognitive information (Kesner and Rolls, 2015) and is a primary site for activity-dependent synaptic plasticity that in turn enables both short- and long-term declarative memory (Kemp and Manahan-Vaughan, 2007). Patients with schizophrenia and psychosis exhibit a wide range of sensory and cognitive abnormalities (McGhie and Chapman, 1961; Kapur, 2003; Bowie and Harvey, 2005; Bürgy, 2008) that have been ascribed, at least in part, to dysfunctions in sensory information processing by the hippocampus (Arnold, 1999; Bast and Feldon, 2003; Behrendt, 2010; Bak et al., 2014; Kalweit et al., 2017). Not only is the trisynaptic circuit [dentate gyrus (DG) and CA regions (CA3 and CA1)] of the hippocampus responsible for the formation of multimodal memory representations (Hasselmo, 2005; Kesner, 2013a,b; Kesner and Rolls, 2015), but its longitudinal (dorso-ventral) axis is pivotal to the processing of visuo-spatial and socio-emotional elements of cognition (Bast et al., 2009; Fanselow and Dong, 2010; Strange et al., 2014). Strikingly, changes in GABAergic and groups I and II mGlu receptor function or expression in the hippocampus have been proposed to form a key factor in psychotic events in schizophrenia (Linden et al., 2006; Behrendt, 2010; Matosin et al., 2015; Zurawek et al., 2018). Nonetheless, little is known as to the time-point of onset of putative changes on these receptor systems, or to what extent changes are progressive during the course of chronification of the disease. Evidence

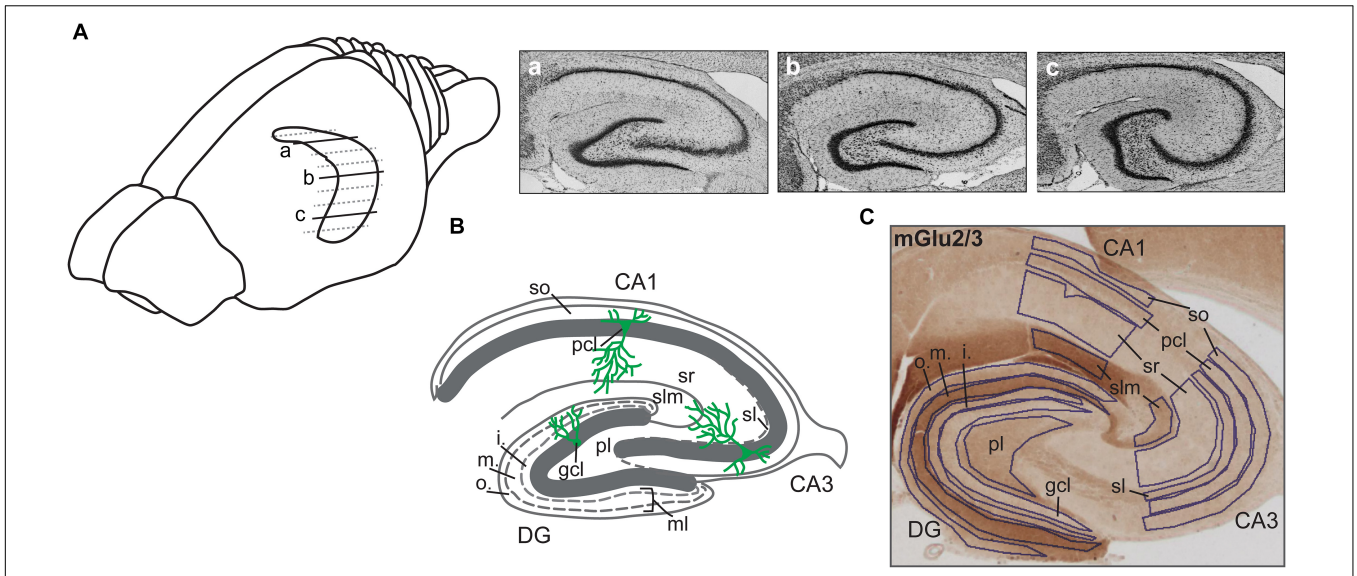

FIGURE 1 | Illustration of hippocampal sections. **(A)** Drawing of the rat brain showing the horizontally sectioned hippocampus along its longitudinal axis. Nissl-stained sections correspond to dorsal **(a)**, intermediate **(b)**, and ventral **(c)** subdivisions. **(B)** Schematic illustration of the hippocampal transverse axis depicting its trisynaptic circuit with the laminar view. o., outer band of the ml of the DG; m., middle band of the ml of the DG; i., inner band of the ml of the DG; gcl, granule cell layer of the DG; ml, molecular layer of the DG; pl, polymorphic layer of the DG; so, Stratum oriens of CA3/CA1; pcl, pyramidal cell layer of CA3/CA1; sl, Stratum lucidum of the CA3; sr, Stratum radiatum of CA3/CA1; and slm, Stratum lacunosum-moleculare of CA3/CA1. **(C)** A representative example of the dorsal hippocampus showing the expression of mGlu2/3 receptors across its transverse axis. Laminal delineation across the DG, CA3, and CA1 regions is shown.

for early changes in receptor function, soon after the first-episode of psychosis could offer novel possibilities for therapy and disease intervention.

In the present study our goal was to study putative changes in the abovementioned receptor systems by examining receptor expression in a rodent model of first-episode psychosis. Here, an acute systemic injection of MK801, an NMDAR antagonist, was used to mimic the first-episode of psychosis (Manahan-Vaughan et al., 2008a; Wiescholleck and Manahan-Vaughan, 2013a,b). Rodent features of a psychosis-like episode comprise significant deficits in prepulse inhibition of the acoustic startle response and startle inhibition, increased stereotypy and hyperactivity (Manahan-Vaughan et al., 2008a; Wiescholleck and Manahan-Vaughan, 2013a) that parallel symptoms exhibited by patients during the first episode of psychosis (Ludewig et al., 2003; Kim et al., 2011; Compton et al., 2015).

The first episode-like event in rodents is followed by a persistent loss of hippocampal LTP, deficits in hippocampus-dependent learning and memory (Manahan-Vaughan et al., 2008b; Wiescholleck and Manahan-Vaughan, 2013b; Wlodarczyk et al., 2013), changes in hippocampal neuronal oscillations (Kehrer et al., 2007; Kalweit et al., 2017), persistent elevations of neuronal excitability and somatic immediate early gene expression (Grüter et al., 2015). In patients, overt changes in brain function comprise decreases in hippocampal functional connectivity and deficits in relational memory (Samudra et al., 2015; Avery et al., 2018), increased cortical excitability (Díez et al., 2017), and abnormal neural oscillations (Uhlhaas and Singer, 2010). These changes form the fundament of the "disconnection hypothesis" (Friston, 1998; Díez et al., 2017) and are widely believed to be caused by a combination of focal brain changes and a disruption of synaptic plasticity that leads to impairments of functional integration at the cognitive level (Stephan et al., 2006, 2009). As mentioned above, changes in GABA and glutamate receptor function have been proposed to underlie these changes (Stephan et al., 2006, 2009; Corlett et al., 2011; Gonzalez-Burgos and Lewis, 2012). In line with this, changes in expression of NMDAR subunits along the dorsoventral axis of the hippocampus have been reported in a rodent model of psychosis (Dubovyk and Manahan-Vaughan, 2018a). Less is known about changes in GABA receptors, or subunits of mGlu receptors that may accompany disease progression.

We characterized the expression and distribution patterns of metabotropic glutamatergic and GABAergic receptors 1 week and 3 months after the emulation of the first psychotic event in adult rats. In particular, we looked for changes in the expression of mGlu1, mGlu2/3, mGlu5, $GABA_A$, and $GABA_B$ receptors across the laminar structure of the trisynaptic circuit and along the longitudinal axis of the hippocampus. We detected time-dependent and neural subcompartment-specific changes in the expression of these receptors across the longitudinal axis of the hippocampus. Our findings indicate that an early adaptive reorganization of the hippocampus occurs after first-episode psychosis that contributes to a reduction of network excitation, and is superseded by a state of permanently increased network excitability and reduced interneuron number. These changes are likely to support loss of synaptic gain control that have been proposed by others

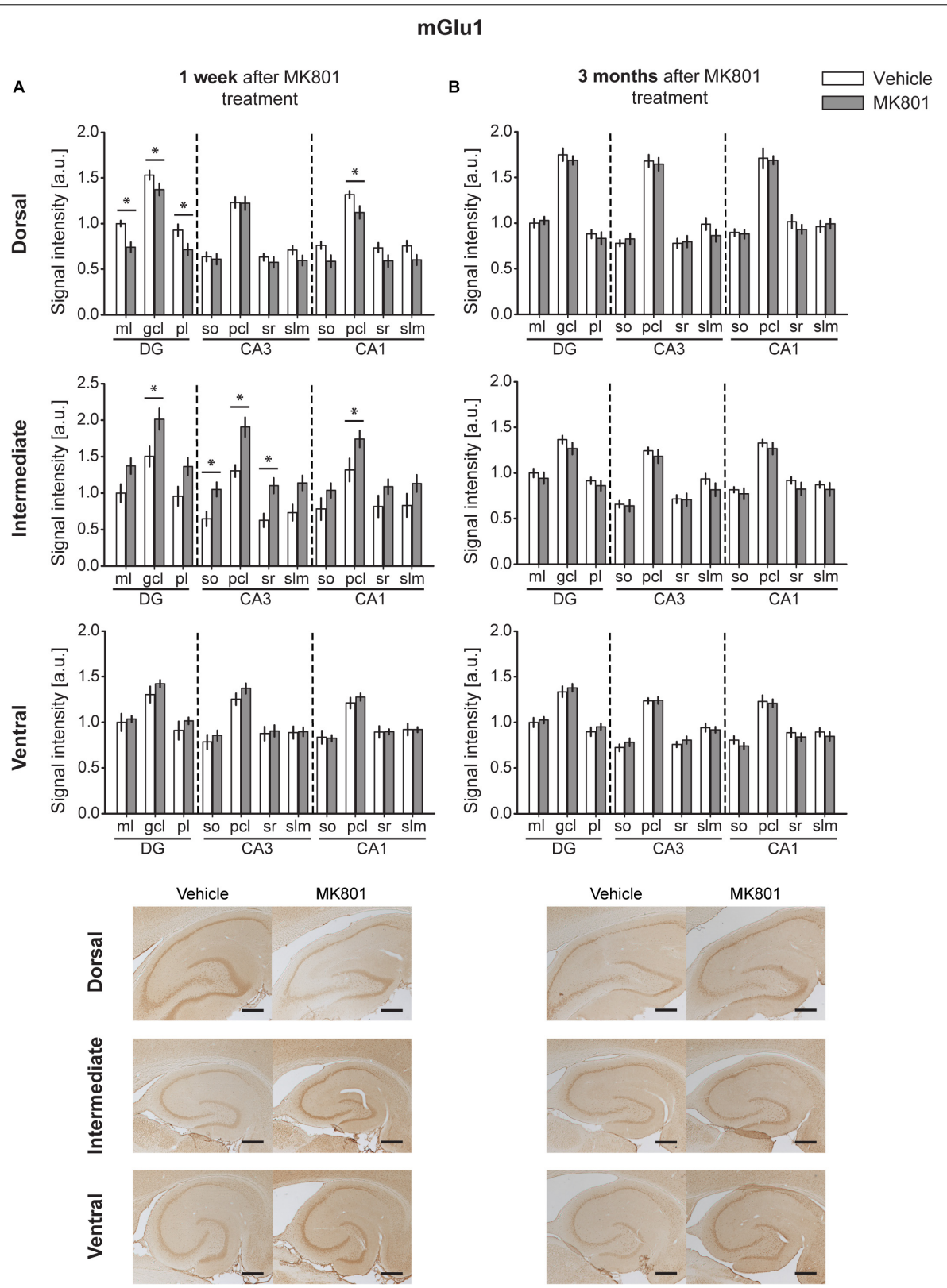

FIGURE 2 | MK801 treatment leads to a transient change of mGlu1 receptor protein expression. Bar charts represent relative changes in protein levels 1 week and 3 months after MK801 treatment across the somato-dendritic layers of the transverse and longitudinal hippocampal axes. **(A)** mGlu1 receptor levels were

(*Continued*)

FIGURE 2 | Continued
down-regulated in the dorsal hippocampus, but up-regulated in the intermediate hippocampus 1 week after MK801 treatment. **(B)** No changes in mGlu1 receptor expression were detected 3 months after MK801 administration. Scale bar: 500 μm. Values expressed in arbitrary units (a.u.). Error bars indicate SEM. $*p < 0.05$ or $**p < 0.01$. ml, molecular layer of the DG; gcl, granule cell layer of the DG; pl, polymorphic layer of the DG; so, Stratum oriens of CA3/CA1; pcl, pyramidal cell layer of CA3/CA1; sr, Stratum radiatum of CA3/CA1; and slm, Stratum lacunosum-moleculare of CA3/CA1. Photomicrographs provide examples of mGlu1 receptor-stained sections from the dorsal, intermediate and ventral hippocampal subdivisions that originated from the same vehicle- or MK801-treated animal and correspond to 1 week (left) or 3 months (right) after treatment.

(Adams et al., 2013; Díez et al., 2017) to contribute importantly to the pathophysiology and stabilization of psychosis.

MATERIALS AND METHODS

Animals

All experiments were done with healthy male Wistar rats (Charles River Laboratories, Germany). Animals were housed in custom-made climatised and ventilated holding cupboards in an animal-housing room with a controlled 12-h light/dark cycle. No female rats were housed in the room. Animals had free access to food and water. The study was carried out in accordance with the European Communities Council Directive of September 22nd, 2010 (2010/63/EU) for care of laboratory animals. Prior permission was obtained from the ethics commission of the local government authority (Landesamt für Arbeitsschutz, Umwelt- und Naturschutz, Nordrhein-Westfalen).

Drug Treatment

Seven-to-eight-week-old Wistar rats were divided into two groups where each animal received a single intraperitoneal (i.p.) injection of the NMDAR antagonist [+]-5-methyl-10,11-dihydro-5Hdibenzo-[a,d]-cyclohepten-5,10-imine hydrogen maleate (MK801, Tocris, Germany). The compound was dissolved in 0.9% physiological saline and administered in a concentration of 5 mg/kg, in accordance with previous studies conducted by our group (Manahan-Vaughan et al., 2008a,b). This treatment protocol results in a first-episode-like state in rodents (Wöhrl et al., 2007; Manahan-Vaughan et al., 2008a,b, 2013a,b; Wiescholleck and Manahan-Vaughan, 2012). Two control animal groups of identical age and strain received a single i.p. injection of 0.9% physiological saline (10 ml/kg). Animals were sacrificed 1 week or 3 months after the injection. Each group included 5 animals, with the exception of the 3-month-group where 3 additional animals were added to confirm a strong statistical tendency in the original dataset. From each animal, one section of the DH, IH, or VH was analyzed with regard to a specific receptor. Both, right and left hippocampi were used for the analysis and considered as replicates.

Slice Preparation

Wistar rats were deeply anesthetized with sodium pentobarbital and transcardially perfused with cold Ringer's solution + heparin (0.2%) followed by 4% paraformaldehyde (PFA) in phosphate buffered saline (PBS, 0.025 M). Brains were removed, fixed in 4% PFA for 24 h, and cryoprotected in 30% sucrose in 0.1 M PBS for at least 3 days. Serial 30-μm thick horizontal sections were collected with a freezing microtome. For each animal, three horizontal sections from the most dorsal (between 3.6 and 4.1 mm posterior to bregma), middle intermediate (around 5.6 mm posterior to bregma) and most ventral hippocampal parts (between 7.1 and 7.6 mm posterior to bregma) were simultaneously used for immunohistochemical staining (**Figure 1A**). Sections from the Vehicle- and MK801-treated animals were always analyzed in pairs.

Immunohistochemistry

Antibody specificity was verified in our previous studies (Grüter et al., 2015; Dubovyk and Manahan-Vaughan, 2018a,b). Endogenous peroxidase was blocked by pretreating the free-floating brain sections in 0.3% H_2O_2 for 20 min. They were then rinsed in PBS and incubated with blocking solution containing 10% normal serum and 20% avidin in PBS with 0.2% Triton X-100 (PBS-Tx) for 90 min at room temperature (RT). Sections were incubated overnight at room temperature with primary antibodies: mGlu2/3 (rabbit polyclonal, 1:200; ab1553, Chemicon), mGlu5 (rabbit polyclonal, 1:200; ab5675, Millipore), $GABA_A$ receptor (mouse monoclonal, 1:400; mab341, Millipore), $GABA_B$ receptor 1 (mouse monoclonal, 1:250; ab55051, Abcam) or GAD67 (mouse monoclonal, 1:100; mab-5406, Millipore) in medium containing 1% normal serum in 0.2% PBS-Tx + 20% biotin. Sections were then rinsed in PBS and incubated with biotinylated goat anti-rabbit (1:500; BA-1000, Vector), horse anti-mouse (1:500; BA-2001, Vector) or horse anti-goat (1:500; BA-9500, Vector) antibodies in 1% normal serum in 0.1% PBS-Tx for 90 min at RT. Afterwards, sections were washed in PBS and incubated for 90 min at RT with ABC kit (PK-6100, Vector) in 1% normal serum in 0.1% PBS-Tx.

Staining with mGlu1 receptor antibodies required an additional amplification step with biotinylated tyramide for 20 min. Here, the sections were incubated for 5 days at 4°C with primary mGlu1 receptor antibodies (rabbit polyclonal, 1:400; ab82211, Abcam) in 1% BSA in 0.2% TBS-Tx. PBS was replaced with TBS, normal serum + PBS-Tx with bovine serum albumin + TBS-Tx, and one ABC reaction with two for 30 min each with amplification step in between. Here, sections were incubated with 10 μl b-tyramide + 10 μl 0.01% H_2O_2 in 1,000 μl of TBS for 20 min. Finally, the sections were washed in PBS and treated with diaminobenzidine and 0.01% H_2O_2 for approximately 10 min.

Quantitative Analysis

Regions of interest were defined using the rat brain atlas of Paxinos and Watson (1982) and Nissl staining where every 12th section throughout the whole hippocampus was stained

TABLE 1 | An overview of statistically significant differences in the expression of metabotropic glutamatergic receptors.

Receptor	Time-point	Hippocampal axis part	Multifactorial ANOVA			
			TREATMENT factor (T)	**REGION factor (R)**	**T * R interaction**	**Duncan's *post hoc* test**
mGlu1	1 week	DH	$F_{(1,198)} = 32.364$, **$p < 0.001$**	$F_{(10,198)} = 55.487$, **$p < 0.001$**	$F_{(10,198)} = 0.968$, $p = 0.472$	**ml/DG: $p = 0.002$** **gcl/DG: $p = 0.047$** **pl/DG: $p = 0.017$** so/CA3: $p = 0.748$ pcl/CA3: $p = 0.909$ sr/CA3: $p = 0.557$ slm/CA3: $p = 0.218$ so/CA1: $p = 0.069$ **pcl/CA1: $p = 0.023$** sr/CA1: $p = 0.127$ slm/CA1: $p = 0.111$
		IH	$F_{(1,161)} = 58.727$, **$p < 0.001$**	$F_{(10,161)} = 14.245$, **$p < 0.001$**	$F_{(10,161)} = 0.354$, $p = 0.963$	ml/DG: $p = 0.077$ **gcl/DG: $p = 0.005$** pl/DG: $p = 0.052$ **so/CA3: $p = 0.048$** **pcl/CA3: $p = 0.001$** **sr/CA3: $p = 0.021$** slm/CA3: $p = 0.053$ so/CA1: $p = 0.208$ **pcl/CA1: $p = 0.027$** sr/CA1: $p = 0.187$ slm/CA1: $p = 0.146$
		VH	$F_{(1,165)} = 3.209$, $p = 0.075$	$F_{(10,165)} = 18.678$, **$p < 0.001$**	$F_{(10,165)} = 0.286$, $p = 0.983$	ml/DG: $p = 0.714$ gcl/DG: $p = 0.224$ pl/DG: $p = 0.309$ so/CA3: $p = 0.49$ pcl/CA3: $p = 0.246$ sr/CA3: $p = 0.784$ slm/CA3: $p = 0.931$ so/CA1: $p = 0.908$ pcl/CA1: $p = 0.502$ sr/CA1: $p = 0.989$ slm/CA1: $p = 0.996$
	3 months	DH	$F_{(1,198)} = 0.885$, $p = 0.347$	$F_{(10,198)} = 76.594$, **$p < 0.001$**	$F_{(10,198)} = 0.398$, $p = 0.946$	ml/DG: $p = 0.737$ gcl/DG: $p = 0.507$ pl/DG: $p = 0.617$ so/CA3: $p = 0.605$ pcl/CA3: $p = 0.684$ sr/CA3: $p = 0.844$ slm/CA3: $p = 0.21$ so/CA1: $p = 0.854$ pcl/CA1: $p = 0.807$ sr/CA1: $p = 0.407$ slm/CA1: $p = 0.742$
		IH	$F_{(1,187)} = 6.962$, **$p < 0.01$**	$F_{(10,187)} = 36.306$, **$p < 0.001$**	$F_{(10,187)} = 0.195$, $p = 0.996$	ml/DG: $p = 0.454$ gcl/DG: $p = 0.233$ pl/DG: $p = 0.492$ so/CA3: $p = 0.838$ pcl/CA3: $p = 0.41$ sr/CA3: $p = 0.924$ slm/CA3: $p = 0.198$

(Continued)

TABLE 1 | Continued

Receptor	Time-point	Hippocampal axis part	Multifactorial ANOVA			
			TREATMENT factor (T)	**REGION factor (R)**	**T * R interaction**	**Duncan's *post hoc* test**
		VH	$F_{(1,194)} = 0.03$, $p = 0.866$	$F_{(10,194)} = 45.12$, $p < 0.001$	$F_{(10,194)} = 0.54$, $p = 0.863$	so/CA1: $p = 0.584$ pcl/CA1: $p = 0.424$ sr/CA1: $p = 0.282$ slm/CA1: $p = 0.555$ ml/DG: $p = 0.687$ gcl/DG: $p = 0.482$ pl/DG: $p = 0.433$ so/CA3: $p = 0.391$ pcl/CA3: $p = 0.906$ sr/CA3: $p = 0.472$ slm/CA3: $p = 0.705$ so/CA1: $p = 0.366$ pcl/CA1: $p = 0.742$ sr/CA1: $p = 0.451$ slm/CA1: $p = 0.504$
mGlu2/3	1 week	DH	$F_{(1,238)} = 5.687$, **$p < 0.05$**	$F_{(13,238)} = 46.561$, **$p < 0.001$**	$F_{(13,238)} = 0.969$, $p = 0.482$	o./DG: $p = 0.839$ m./DG: $p = 0.563$ i./DG: $p = 0.936$ gcl/DG: $p = 0.317$ pl/DG: $p = 0.897$ so/CA3: $p = 0.11$ pcl/CA3: $p = 0.29$ sl/CA3: $p = 0.22$ sr/CA3: $p = 0.118$ slm/CA3: $p = 0.23$ so/CA1: $p = 0.483$ pcl/CA1: $p = 0.583$ sr/CA1: $p = 0.297$ slm/CA1: $p = 0.097$
		IH	$F_{(1,238)} = 18.317$, **$p < 0.001$**	$F_{(13,238)} = 68.422$, **$p < 0.001$**	$F_{(13,238)} = 1.28$, $p = 0.225$	o./DG: $p = 0.552$ m./DG: $p = 0.91$ i./DG: $p = 0.604$ gcl/DG: $p = 0.216$ pl/DG: $p = 0.524$ **so/CA3: $p = 0.047$** **pcl/CA3: $p = 0.044$** sl/CA3: $p = 0.118$ **sr/CA3: $p = 0.016$** slm/CA3: $p = 0.064$ so/CA1: $p = 0.374$ pcl/CA1: $p = 0.315$ sr/CA1: $p = 0.253$ slm/CA1: $p = 0.076$
		VH	$F_{(1,238)} = 36.241$, **$p < 0.001$**	$F_{(13,238)} = 35.252$, **$p < 0.001$**	$F_{(13,238)} = 0.4$, $p = 0.968$	o./DG: $p = 0.539$ m./DG: $p = 0.28$ i./DG: $p = 0.215$ gcl/DG: $p = 0.195$ pl/DG: $p = 0.181$ **so/CA3: $p = 0.03$** pcl/CA3: $p = 0.052$ **sl/CA3: $p = 0.037$**

(Continued)

TABLE 1 | Continued

Receptor	Time-point	Hippocampal axis part	Multifactorial ANOVA			
			TREATMENT factor (T)	**REGION factor (R)**	**T * R interaction**	**Duncan's *post hoc* test**
	3 months	DH	$F_{(1,252)} = 9.8$, $\mathbf{p < 0.01}$	$F_{(13,252)} = 145.45$, $\mathbf{p < 0.001}$	$F_{(13,252)} = 0.27$, $p = 0.995$	**sr/CA3: $p = 0.039$** slm/CA3: $p = 0.062$ so/CA1: $p = 0.275$ pcl/CA1: $p = 0.233$ sr/CA1: $p = 0.306$ slm/CA1: $p = 0.567$ o./DG: $p = 0.267$ m./DG: $p = 0.407$ i./DG: $p = 0.252$ gcl/DG: $p = 0.286$ pl/DG: $p = 0.465$ so/CA3: $p = 0.405$ pcl/CA3: $p = 0.472$ sl/CA3: $p = 0.483$ sr/CA3: $p = 0.256$ slm/CA3: $p = 0.668$ so/CA1: $p = 0.8$ pcl/CA1: $p = 0.862$ sr/CA1: $p = 0.589$
		IH	$F_{(1,252)} = 0.00$, $p = 0.961$	$F_{(13,252)} = 195.77$, $\mathbf{p < 0.001}$	$F_{(13,252)} = 0.19$, $p = 0.999$	**slm/CA1: $p = 0.041$** o./DG: $p = 0.551$ m./DG: $p = 0.539$ i./DG: $p = 0.901$ gcl/DG: $p = 0.551$ pl/DG: $p = 0.717$ so/CA3: $p = 0.75$ pcl/CA3: $p = 0.741$ sl/CA3: $p = 0.882$ sr/CA3: $p = 0.915$ slm/CA3: $p = 0.659$ so/CA1: $p = 0.586$ pcl/CA1: $p = 0.535$ sr/CA1: $p = 0.818$ slm/CA1: $p = 0.971$
		VH	$F_{(1,248)} = 1.53$, $p = 0.217$	$F_{(13,248)} = 103.07$, $\mathbf{p < 0.001}$	$F_{(13,248)} = 0.15$, $p = 0.999$	o./DG: $p = 0.918$ m./DG: $p = 0.714$ i./DG: $p = 0.467$ gcl/DG: $p = 0.382$ pl/DG: $p = 0.779$ so/CA3: $p = 0.703$ pcl/CA3: $p = 0.511$ sl/CA3: $p = 0.828$ sr/CA3: $p = 0.674$ slm/CA3: $p = 0.872$ so/CA1: $p = 0.653$ pcl/CA1: $p = 0.95$ sr/CA1: $p = 0.912$ slm/CA1: $p = 0.521$
mGlu5	1 week	DH	$F_{(1,198)} = 0.87$, $p = 0.351$	$F_{(10,198)} = 5.93$, $\mathbf{p < 0.001}$	$F_{(10,198)} = 0.44$, $p = 0.927$	ml/DG: $p = 0.841$ gcl/DG: $p = 0.877$ pl/DG: $p = 0.904$

(Continued)

TABLE 1 | Continued

Receptor	Time-point	Hippocampal axis part	Multifactorial ANOVA			
			TREATMENT factor (T)	**REGION factor (R)**	**T * R interaction**	**Duncan's *post hoc* test**
		IH	$F_{(1,198)} = 13.08$, ***p* < 0.001**	$F_{(10,198)} = 7.65$, ***p* < 0.001**	$F_{(10,198)} = 0.21$, $p = 0.995$	so/CA3: $p = 0.265$ pcl/CA3: $p = 0.238$ sr/CA3: $p = 0.507$ slm/CA3: $p = 0.461$ so/CA1: $p = 0.86$ pcl/CA1: $p = 0.943$ sr/CA1: $p = 0.723$ slm/CA1: $p = 0.505$ ml/DG: $p = 0.176$ gcl/DG: $p = 0.285$ pl/DG: $p = 0.168$ so/CA3: $p = 0.278$ pcl/CA3: $p = 0.133$ sr/CA3: $p = 0.332$ slm/CA3: $p = 0.375$ so/CA1: $p = 0.848$ pcl/CA1: $p = 0.484$ sr/CA1: $p = 0.506$ slm/CA1: $p = 0.532$
		VH	$F_{(1,198)} = 2.66$, $p = 0.104$	$F_{(10,198)} = 7.34$, ***p* < 0.001**	$F_{(10,198)} = 0.06$, $p = 0.999$	ml/DG: $p = 0.745$ gcl/DG: $p = 0.497$ pl/DG: $p = 0.567$ so/CA3: $p = 0.883$ pcl/CA3: $p = 0.789$ sr/CA3: $p = 0.505$ slm/CA3: $p = 0.468$ so/CA1: $p = 0.814$ pcl/CA1: $p = 0.759$ sr/CA1: $p = 0.696$ slm/CA1: $p = 0.63$
	3 months	DH	$F_{(1,330)} = 20.77$, ***p* < 0.001**	$F_{(10,330)} = 64.67$, ***p* < 0.001**	$F_{(10,330)} = 0.71$, $p = 0.718$	ml/DG: $p = 0.354$ gcl/DG: $p = 0.258$ pl/DG: $p = 0.619$ so/CA3: $p = 0.386$ pcl/CA3: $p = 0.438$ sr/CA3: $p = 0.426$ slm/CA3: $p = 0.586$ **so/CA1: *p* = 0.004** **pcl/CA1: *p* = 0.03** **sr/CA1: *p* = 0.031** slm/CA1: $p = 0.223$
		IH	$F_{(1,330)} = 58.18$, ***p* < 0.001**	$F_{(10,330)} = 21.4$, ***p* < 0.001**	$F_{(10,330)} = 0.75$, $p = 0.678$	**ml/DG: *p* = 0.043** **gcl/DG: *p* = 0.037** **pl/DG: *p* = 0.005** so/CA3: $p = 0.083$ pcl/CA3: $p = 0.331$ sr/CA3: $p = 0.195$ slm/CA3: $p = 0.408$ **so/CA1: *p* = 0.002** **pcl/CA1: *p* = 0.005** **sr/CA1: *p* = 0.005**

(Continued)

TABLE 1 | Continued

Receptor	Time-point	Hippocampal axis part	Multifactorial ANOVA			
			TREATMENT factor (T)	**REGION factor (R)**	**T * R interaction**	**Duncan's *post hoc* test**
		VH	$F_{(1,330)} = 34.16$, **$p < 0.001$**	$F_{(10,330)} = 48.02$, **$p < 0.001$**	$F_{(10,330)} = 1.47$, $p = 0.149$	**slm/CA1: $p = 0.024$** ml/DG: $p = 0.299$ gcl/DG: $p = 0.377$ pl/DG: $p = 0.296$ so/CA3: $p = 0.129$ pcl/CA3: $p = 0.44$ sr/CA3: $p = 0.212$ slm/CA3: $p = 0.675$ **so/CA1: $p < 0.001$** **pcl/CA1: $p = 0.004$** **sr/CA1: $p = 0.012$** slm/CA1: $p = 0.215$

The table describes the mean ± SEM values. Significant differences are highlighted in bold font. DH, dorsal hippocampus; IH, intermediate hippocampus; VH, ventral hippocampus; ml, molecular layer of the DG; o., outer band of the ml; m., middle band of the ml; i., inner band of the ml; gcl, granule cell layer of the DG; pl, polymorphic layer of the DG; so, Stratum oriens of CA3/CA1; pcl, pyramidal cell layer of CA3/CA1; sl, Stratum lucidum of the CA3; sr, Stratum radiatum of CA3/CA1; and slm, Stratum lacunosum-moleculare of CA3/CA1.

with 0.1% Cresyl violet (c5042, Sigma) as a reference. Eleven areas of interest included: molecular layer (ml) of the dentate gyrus (DG); granule cell layer (gcl) of the DG; polymorphic layer (pl) of the DG; Stratum oriens (so) of CA3/CA1; pyramidal cell layer (pcl) of CA3/CA1; Stratum radiatum (sr) of CA3/CA1; and Stratum lacunosum-moleculare (slm) of CA3/CA1 on sections taken from the dorsal, intermediate and ventral hippocampal subdivisions. Due to the expression profile of mGlu2/3 receptors, a specific delineation of the ml of the DG into outer, middle and inner bands was possible. The Stratum lucidum (sl) of the CA3 could also be clearly identified and was therefore quantified, resulting in 15 areas of interest for the mGlu2/3 receptor (**Figures 1B,C**). Importantly, for background subtraction we used receptor-devoid tissue, which in the dorsal sections was the fimbria; in the intermediate sections was either the fimbria or the superior thalamic radiation; and in the ventral sections was the internal capsule. Pictures of stained sections were acquired with a light microscope (Leica DMR, Germany), equipped with a digital camera (MBF Bioscience) and stored in TIFF format. The regions of interest were analyzed at 2.5× lens magnification. The digitized high-resolution pictures were obtained using Neurolucida software (MBF Bioscience) and quantified using open-source ImageJ software (National Institutes of Health). Given that images were acquired with a RGB camera the 'Color Deconvolution' plugin in ImageJ was used to deconvolve the color information as well as to convert images to 8-bit format, thus increasing the dynamic range of the signal. R software was used to scale data from several independent stainings/plates using generalized residual sum of squares algorithm to account for batch variability in staining intensities (Kreutz et al., 2007; von der Heyde et al., 2014).

The amount of GAD67 positive cells was manually calculated in sections stained with anti-GAD67 antibodies. Quantification was limited to the DG, CA3, and CA1 regions across their respective laminal structures of the DH, IH, and VH sections.

Statistical Analysis

Data obtained in the immunohistochemical experiments were statistically analyzed by means of factorial analysis of variance (ANOVA) followed by Duncan's *post hoc* test, which allowed detection of significant factors in a two-factor model. Here, the Vehicle and MK801 treatment data were considered as the TREATMENT factor (factor one), while the laminar organization of the trisynaptic circuit as the REGION factor (factor two). The cell count results were analyzed using the Students *t*-test. All significant differences were defined as $p < 0.05$ or $p < 0.01$. Values are expressed as mean values ± the standard error of the mean (SEM).

RESULTS

To allow for detailed scrutiny of the hippocampus we studied the following hippocampal subcompartments: the molecular layer (ml), the granule cell layer (gcl), and the polymorphic layer (pl) of the dentate gyrus (DG), as well as the Stratum oriens (so), pyramidal cell layer (pcl), Stratum radiatum (sr), and Stratum lacunosum-moleculare (slm) of CA3/CA1. Sections from the dorsal hippocampus (DH), intermediate hippocampus (IH), and ventral hippocampus (VH) were examined (**Figure 1**). Expression of mGlu1, mGlu5, mGlu2/3, $GABA_A$, and $GABA_B$ receptors was examined 1 week and 3 months after treatment with vehicle, or the NMDAR antagonist, MK801.

MGlu1 Expression Is Altered 1 Week, but Not 3 Months After MK801 Administration

One week after MK801 treatment, mGlu1 receptor protein levels were significantly changed in DH, and IH [multifactorial ANOVA, Treatment factor, DH: $F_{(1,198)} = 32.364$, $p < 0.001$;

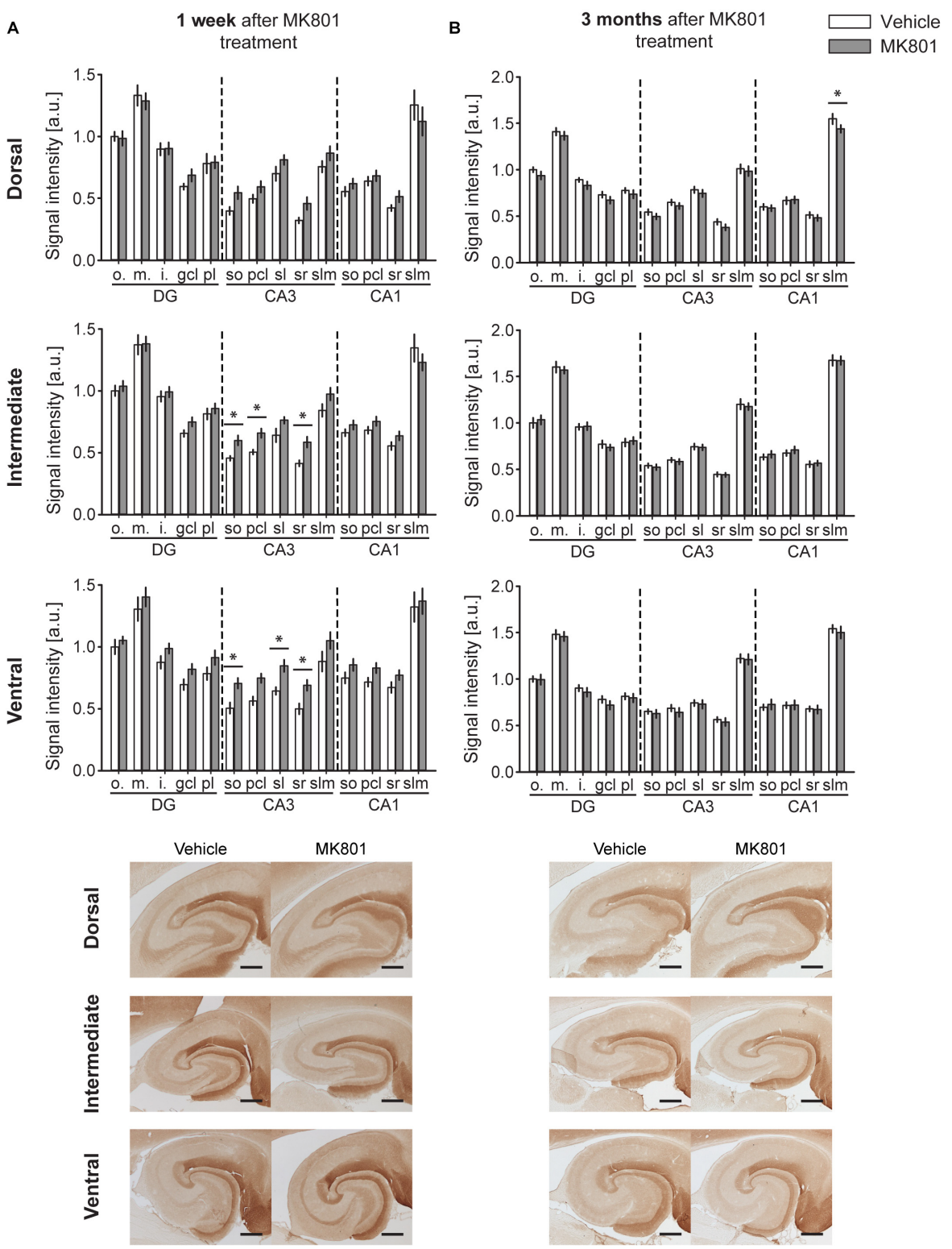

FIGURE 3 | mGlu2/3 receptor levels are transiently up-regulated early after MK801 treatment. Bar charts represent relative changes in protein levels 1 week and 3 months after MK801 treatment across the somato-dendritic layers of the transverse and longitudinal hippocampal axes. **(A)** mGlu2/3 protein expression is

(*Continued*)

FIGURE 3 | Continued
significantly increased across the ventro-intermediate hippocampal CA3 region 1 week after MK801 treatment. **(B)** No overall changes were detected 3 months after MK801 application. Scale bar: 500 μm. Values expressed in arbitrary units (a.u.). Error bars indicate SEM. *$p < 0.05$. ml, molecular layer of the DG; gcl, granule cell layer of the DG; pl, polymorphic layer of the DG; so, Stratum oriens of CA3/CA1; pcl, pyramidal cell layer of CA3/CA1; sr, Stratum radiatum of CA3/CA1; and slm, Stratum lacunosum-moleculare of CA3/CA1. Photomicrographs provide examples of mGlu2/3 receptor-stained sections from the dorsal, intermediate and ventral hippocampal subdivisions that originated from the same vehicle- or MK801-treated animal and correspond to 1 week (left) or 3 months (right) after treatment.

IH: $F(_{1,161}) = 58.727$, $p < 0.001$]. In the DH, protein expression was reduced in the ml, gcl, and pl of the DG and in the pcl of the CA1 (**Figure 2A** and **Table 1**). In contrast, the IH showed an up-regulation of mGlu1 receptor levels in the gcl of the DG, so, pcl and sr of the CA3; and pcl of the CA1. The VH remained unaltered [multifactorial ANOVA, Treatment factor, VH: $F(_{1,165}) = 3.209$, $p = 0.075$] (**Figure 2A** and **Table 1**).

Three months after MK801-treatment receptor expression was equivalent in hippocampi from MK801- and vehicle-treated animals [multifactorial ANOVA, Treatment factor, DH: $F(_{1,198}) = 0.885$, $p = 0.347$; IH: $F(_{1,187}) = 6.962$, $p < 0.01$; VH: $F(_{1,194}) = 0.03$, $p = 0.866$] (**Figure 2B** and **Table 1**).

MGlu2/3 Levels Are Upregulated 1 Week After MK801 Treatment, With No Overall Changes Evident 3 Months After Treatment

A significant up-regulation in the levels of mGlu2/3 receptors was found 1 week after MK801 administration in the CA3 region of both the IH and VH [multifactorial ANOVA, Treatment factor, IH: $F(_{1,238}) = 18.317$, $p < 0.001$; VH: $F(_{1,238}) = 36.241$, $p < 0.001$]. The layers affected included so, pcl, and sr of the IH CA3; and so, sl and sr of the VH CA3 (**Figure 3A** and **Table 1**). The DH was unaffected [multifactorial ANOVA, Treatment factor, DH: $F(_{1,238}) = 5.687$, $p < 0.05$].

Overall, no changes occurred in mGlu2/3 expression 3 months after treatment [multifactorial ANOVA, Treatment factor, DH: $F(_{1,252}) = 9.8$, $p < 0.01$; IH: $F(_{1,252}) = 0.00$, $p = 0.961$; VH: $F(_{1,248}) = 1.53$, $p = 0.217$]. There was one exception to this, however: we detected a significant decrease in mGlu2/3 expression in the slm of the DH CA1 (**Figure 3B** and **Table 1**).

MGlu5 Expression Is Increased 3 Months After MK801 Application

One week after MK801-treatment, mGlu5 receptor expression was unchanged in the hippocampus [multifactorial ANOVA, Treatment factor, DH: $F(_{1,198}) = 0.87$, $p = 0.351$; IH: $F(_{1,198}) = 13.08$, $p < 0.001$; VH: $F(_{1,198}) = 2.66$, $p = 0.104$] (**Figure 4A** and **Table 1**). By contrast, 3 months after treatment, a widespread up-regulation of mGlu5 receptor expression was evident across the entire CA1 region (dorsal, intermediate and ventral CA1) and in the intermediate DG compared to controls [multifactorial ANOVA, Treatment factor, DH: $F(_{1,330}) = 20.77$, $p < 0.001$; IH: $F(_{1,330}) = 58.18$, $p < 0.001$; VH: $F(_{1,330}) = 34.16$, $p < 0.001$]. The layers affected included the so, pcl, and sr of the DH CA1, the so, pcl, and sr of the VH CA1, and the so, pcl, sr, and slm of the intermediate CA1. In addition, increased mGlu5 receptor expression occurred in the ml, gcl, and pl of the intermediate DG (**Figure 4B** and **Table 1**).

$GABA_A$ Levels Remained Largely Unaltered Following MK801 Treatment

One week after MK801 treatment, a potent decrease in $GABA_A$ expression occurred in the pcl of the DH CA1 region (**Figure 5A**). No changes were found in any other subcompartment of the hippocampus [multifactorial ANOVA, Treatment factor, IH: $F(_{1,187}) = 8.805$, $p < 0.01$; VH: $F(_{1,183}) = 8$, $p < 0.01$] (**Figure 5A** and **Table 2**). Three months after treatment a significant increase in $GABA_A$ expression was evident in the slm of the DH CA3 region (**Figure 5B**). Expression levels in all other subcompartments were not different from controls at this time-point [multifactorial ANOVA, Treatment factor, IH: $F(_{1,190}) = 1.52$, $p = 0.219$; VH: $F(_{1,198}) = 1.308$, $p = 0.254$] (**Figure 5B** and **Table 2**).

$GABA_B$ Expression Is Downregulated After MK801 Application

One week following MK801 treatment, $GABA_B$ receptor changes occurred in the IH compared to controls (**Figure 6A**) [multifactorial ANOVA, Treatment factor, IH: $F(_{1,198}) = 37.22$, $p < 0.001$]. Here, a significant down-regulation was seen in the so and slm of the IH CA3 and in the slm of the IH CA1 (**Figure 6A** and **Table 2**). Receptor expression in the DH and VH was equivalent to controls [multifactorial ANOVA, Treatment factor, DH: $F(_{1,198}) = 1.547$, $p = 0.215$; VH: $F(_{1,187}) = 0.576$, $p = 0.449$] (**Table 2**).

Three months after MK801 treatment, no receptor changes were evident in the IH or VH [multifactorial ANOVA, Treatment factor, IH: $F(_{1,198}) = 1.82$, $p = 0.178$; VH: $F(_{1,187}) = 0.19$, $p = 0.662$] (**Table 2**), but a significant down-regulation in $GABA_B$ receptor levels was found across the entire DH cornus ammonis (**Figure 6B**): All layers (so, pcl, sr, and slm) of the CA1 and CA3 regions were significantly affected (**Table 2**).

MK801 Treatment Reduces the Amount of GAD67+ Cells in the Hippocampus

Our finding that $GABA_B$ receptor expression was potently downregulated 3 months after MK801-treatment might be explained by a loss of interneurons. To check this possibility, we assessed the number of GAD-expressing interneurons in the hippocampus 3 months after MK801 application (**Figure 7**). Here, we found a significant reduction in the amount of GAD67-positive cells in the DG (t-test, Vehicle: 69.21 ± 1.86 vs. MK801: 63.45 ± 1.86, $p = 0.03$, $t = 2.185$ with 90 degrees of freedom), CA3 (t-test, Vehicle: 54.06 ± 1.43 vs. MK801: 45.08 ± 1.4, $p < 0.001$,

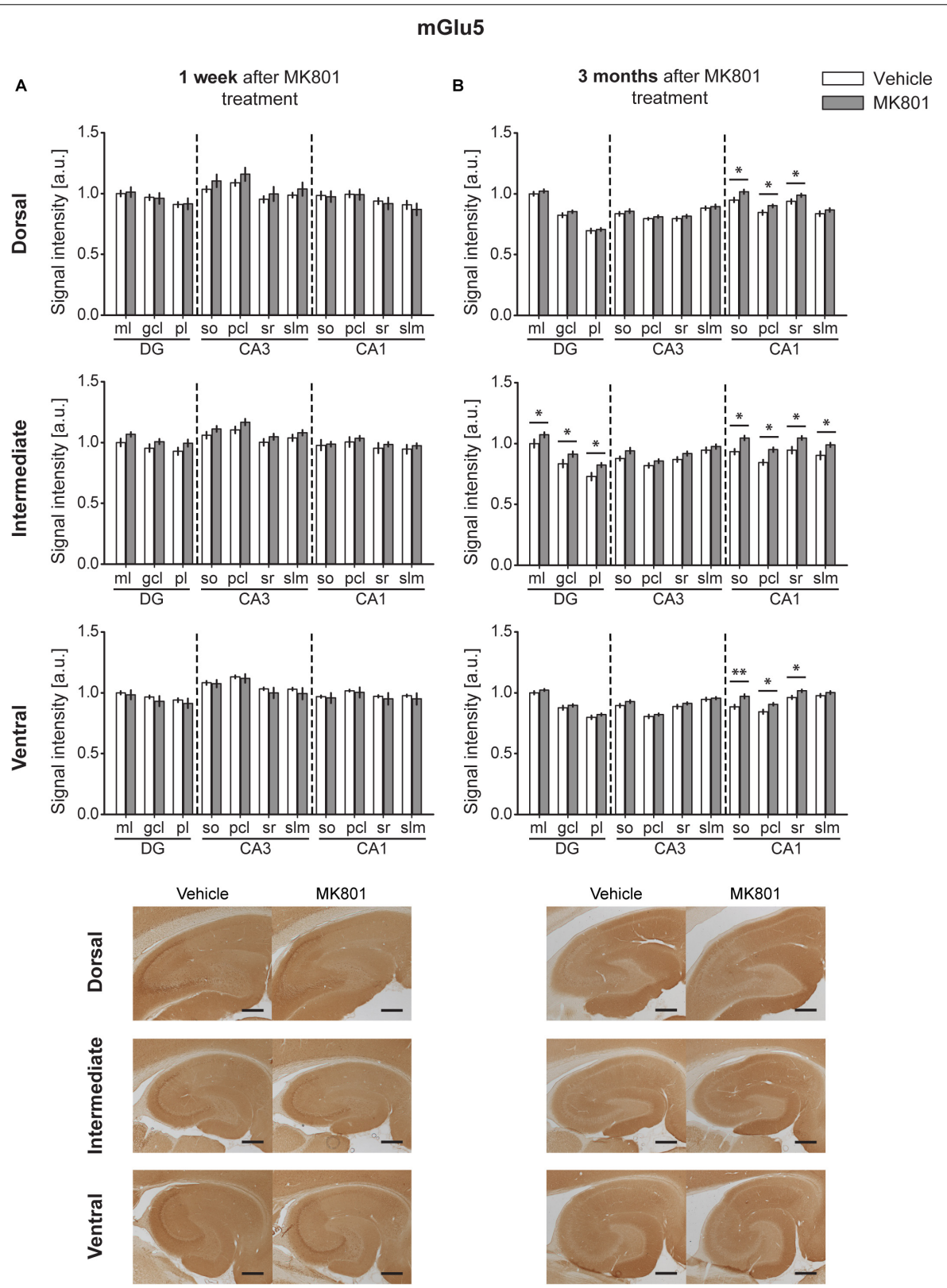

FIGURE 4 | Late up-regulation of mGlu5 receptor levels occurs after MK801 treatment. Bar charts represent relative changes in protein levels 1 week and 3 months after MK801 treatment across the somato-dendritic layers of the transverse and longitudinal hippocampal axes. **(A)** mGlu5 receptor expression remained unaltered

(*Continued*)

FIGURE 4 | Continued
1 week after MK801 treatment. **(B)** Three months after MK801 injection led to an extensive up-regulation of mGlu5 receptor levels across an entire hippocampus. Scale bar: 500 μm. Values expressed in arbitrary units (a.u.). Error bars indicate SEM. *$p < 0.05$. ml, molecular layer of the DG; gcl, granule cell layer of the DG; pl, polymorphic layer of the DG; so, Stratum oriens of CA3/CA1; pcl, pyramidal cell layer of CA3/CA1; sr, Stratum radiatum of CA3/CA1; and slm, Stratum lacunosum-moleculare of CA3/CA1. Photomicrographs provide examples of mGlu5 receptor-stained sections from the dorsal, intermediate and ventral hippocampal subdivisions that originated from the same vehicle- or MK801-treated animal and correspond to 1 week (left) or 3 months (right) after treatment.

$t = 4.471$ with 88 degrees of freedom), and CA1 (t-test, Vehicle median: 52 vs. MK801 median: 45, Mann–Whitney $U = 668$, $n_{Vehicle} = 44$, $n_{MK801} = 47$, $p = 0.004$) regions of the DH and in the CA3 (t-test, Vehicle: 51.27 ± 1.14 vs. MK801: 44.86 ± 1.27, $p < 0.001$, $t = 3.736$ with 88 degrees of freedom) and CA1 (t-test, Vehicle median: 41.5 vs. MK801 median: 36, Mann–Whitney $U = 719$, $n_{Vehicle} = 44$, $n_{MK801} = 46$, $p = 0.01$) regions of the IH. No changes could be observed in the VH (t-test, DG, Vehicle: 53.78 ± 1.96 vs. MK801: 54.53 ± 2.08, $p = 0.79$, $t = -0.263$ with 83 degrees of freedom; CA3, Vehicle: 55.53 ± 1.55 vs. MK801: 54.84 ± 1.97, $p = 0.78$, $t = 0.276$ with 85 degrees of freedom), although a trend toward a decrease was detected in the CA1 region (t-test Vehicle: 43.19 ± 1.8 vs. MK801: 39.09 ± 1.75, $p = 0.1$, $t = 1.628$ with 84 degrees of freedom).

DISCUSSION

In this study, we demonstrate that acute induction of hypoglutamatergic signaling in rats persistently alters the expression of several metabotropic glutamatergic and GABAergic receptors across the hippocampus. Importantly, the profile of rapid (1 week) changes differs from subsequent (3 month) changes. These alterations in receptor expression are also specific to the region (longitudinal axis), subregion (transverse axis) and layer of the hippocampus. In addition, 3 months after treatment, a significant reduction in GAD67-positive interneurons is evident in both the dorsal and the intermediate hippocampus.

In line with evidence for disturbed glutamatergic neurotransmission in schizophrenia and psychosis (Lesage and Steckler, 2010; Lin et al., 2012; Matosin and Newell, 2013), we observed an early impairment in the expression of mGlu1 receptors across the dorso-intermediate hippocampal axis, as well as an upregulation of expression in the intermediate hippocampus. An early up-regulation in mGlu2/3 levels across the ventro-intermediate CA3 region also occurred, whereas $GABA_B$ receptor expression was reduced in the intermediate hippocampus. Three months after MK801-treatment, an increase in mGlu5 expression was evident across the entire CA1 region and intermediate DG. At the same time-point a down-regulation in the levels of $GABA_B$ receptors occurred across the dorsal hippocampus. These changes can be expected to affect information transfer along the longitudinal axis of the hippocampus (Tóth and Freund, 1992; Andersen et al., 2000), and contribute to disturbed hippocampal-prefrontal cortex communication in psychosis (Heckers et al., 1998; Grüter et al., 2015; Hartung et al., 2016).

The changes in receptor expression that occurred 1 week after MK801-treatment may reflect a rapid adaptive response of the brain to the first episode of psychosis. This in turn, may contribute to the pathological steps that increase brain vulnerability toward disease progression and establishment. These changes are transient, however. Three months after treatment, expression of $GABA_A$, mGlu1, and mGlu2/3 receptors had largely normalized, with the exception of a focal decrease of mGlu2/3 receptor expression in the Stratum lacunosum-moleculare of the dorsal CA1 region and a focal elevation of $GABA_A$ expression in the Stratum lacunosum-moleculare of the dorsal CA3 region. At this time-point, an extensive elevation of mGlu5 receptor expression had developed across the CA1 region of the entire dorsoventral axis. Strikingly, this result matches a recent post-mortem finding of increased expression of mGlu5 receptors in the hippocampal CA1 region of subjects with schizophrenia (Matosin et al., 2015), possibly suggesting an established phenotype of receptor changes in our animal model 3 months after MK801 administration.

The rodent model of a psychosis-like event that we used here involves an acute treatment of adults rats with the NMDAR antagonist, MK801 (Wozniak et al., 1996; Manahan-Vaughan et al., 2008a,b; Wiescholleck and Manahan-Vaughan, 2013a,b). It triggers widespread changes in NMDAR expression across the hippocampus (Dubovyk and Manahan-Vaughan, 2018b). NMDAR hypofunction in GABAergic interneurons appears to be an important component of models defining impairments in both, humans with psychosis and in relevant animal models (Belforte et al., 2010; Nakazawa et al., 2012; Snyder and Gao, 2013; Cohen et al., 2015; Jézéquel et al., 2018). It offers an explanation for a wide-range of schizophrenia's positive, negative and cognitive symptoms. A primary alteration in glutamate-GABA levels and consequent destabilization of the levels of other neurotransmitters throughout the brain are believed to underlie these effects (Snyder and Gao, 2013; Perez and Lodge, 2014). Both glutamatergic and GABAergic neurotransmission are linked to a multitude of intrinsic sensory and cognitive processes such as perception, learning and memory (Kaila, 1994; Paulsen and Moser, 1998; Bettler et al., 2004; Malenka and Bear, 2004; Kullmann et al., 2005; Mukherjee and Manahan-Vaughan, 2013; Kesner and Rolls, 2015). Interestingly, both metabotropic glutamate and GABAergic receptors modulate NMDAR function, as well as glutamate and GABA release (Tu et al., 1999; Benquet et al., 2002; Heidinger et al., 2002; Marino and Conn, 2002; Bettler et al., 2004; Kullmann et al., 2005).

The changes in $GABA_B$ receptor expression that we detected, is in line with a reported decrease in $GABA_B$ receptor expression in the hippocampus of patients suffering from schizophrenia (Mizukami et al., 2000) and is especially interesting given the reported role of $GABA_B$ receptors in maintaining neuronal homeostasis in hippocampal networks (Vertkin et al., 2015).

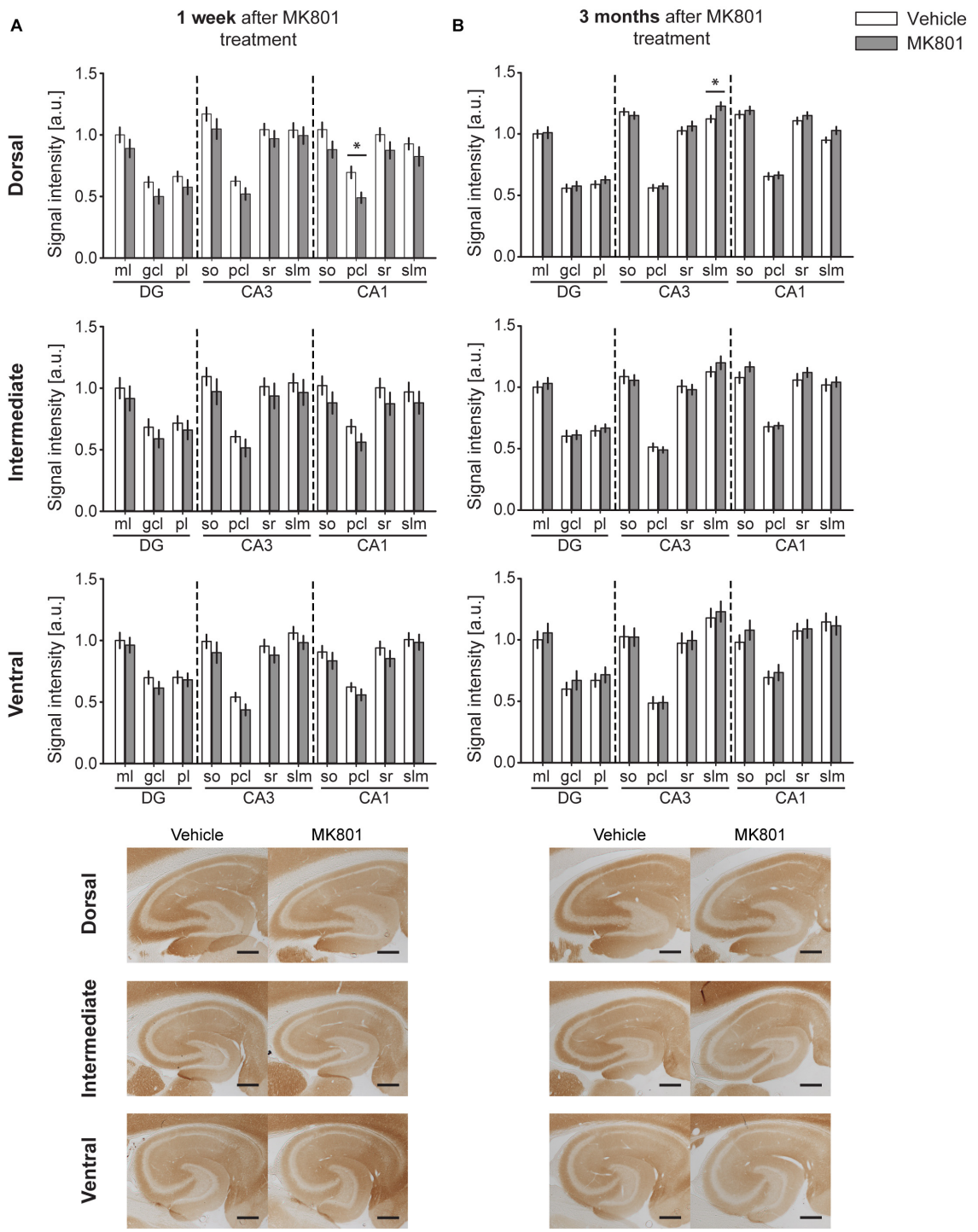

FIGURE 5 | GABA$_A$ protein levels display no substantial changes 1 week or 3 months after MK801 treatment. Bar charts illustrate relative changes in receptor protein levels across the somato-dendritic layers of the transverse and longitudinal hippocampal axes. **(A)** No overall changes were detected 1 week after MK801 treatment. **(B)** Similarly, no overall changes were detected 3 months after MK801 treatment. Scale bar: 500 μm. Values expressed in arbitrary units (a.u.). Error bars indicate SEM. *$p < 0.05$. ml, molecular layer of the DG; gcl, granule cell layer of the DG; pl, polymorphic layer of the DG; so, Stratum oriens of CA3/CA1; pcl, pyramidal cell layer of CA3/CA1; sr, Stratum radiatum of CA3/CA1; and slm, Stratum lacunosum-moleculare of CA3/CA1. Photomicrographs provide examples of GABA$_A$ receptor-stained sections from the dorsal, intermediate and ventral hippocampal subdivisions that originated from the same vehicle- or MK801-treated animal, and correspond to 1 week (left) or 3 months (right) after treatment.

TABLE 2 | An overview of statistically significant differences in the expression of GABAergic receptors.

Receptor	Time-point	Hippocampal axis part	Multifactorial ANOVA			
			TREATMENT factor (T)	**REGION factor (R)**	**T * R interaction**	**Duncan's *post hoc* test**
GABA A	1 week	DH	$F_{(1,176)} = 21.775$, **$p < 0.001$**	$F_{(10,176)} = 26.225$, **$p < 0.001$**	$F_{(10,176)} = 0.279$, $p = 0.985$	ml/DG: $p = 0.233$ gcl/DG: $p = 0.195$ pl/DG: $p = 0.338$ so/CA3: $p = 0.134$ pcl/CA3: $p = 0.247$ sr/CA3: $p = 0.437$ slm/CA3: $p = 0.626$ so/CA1: $p = 0.094$ **pcl/CA1: $p = 0.027$** sr/CA1: $p = 0.187$ slm/CA1: $p = 0.266$
		IH	$F_{(1,187)} = 8.805$, **$p < 0.01$**	$F_{(10,187)} = 10.303$, **$p < 0.001$**	$F_{(10,187)} = 0.06$, $p = 0.999$	ml/DG: $p = 0.521$ gcl/DG: $p = 0.447$ pl/DG: $p = 0.649$ so/CA3: $p = 0.349$ pcl/CA3: $p = 0.459$ sr/CA3: $p = 0.56$ slm/CA3: $p = 0.56$ so/CA1: $p = 0.301$ pcl/CA1: $p = 0.321$ sr/CA1: $p = 0.346$ slm/CA1: $p = 0.494$
		VH	$F_{(1,183)} = 8$, **$p < 0.01$**	$F_{(10,183)} = 22.144$, **$p < 0.001$**	$F_{(10,183)} = 0.128$, $p = 0.999$	ml/DG: $p = 0.672$ gcl/DG: $p = 0.332$ pl/DG: $p = 0.794$ so/CA3: $p = 0.33$ pcl/CA3: $p = 0.179$ sr/CA3: $p = 0.412$ slm/CA3: $p = 0.402$ so/CA1: $p = 0.423$ pcl/CA1: $p = 0.453$ sr/CA1: $p = 0.338$ slm/CA1: $p = 0.803$
	3 months	DH	$F_{(1,190)} = 6.12$, **$p < 0.05$**	$F_{(10,190)} = 147.24$, **$p < 0.001$**	$F_{(10,190)} = 0.7$, $p = 0.719$	ml/DG: $p = 0.799$ gcl/DG: $p = 0.735$ pl/DG: $p = 0.385$ so/CA3: $p = 0.503$ pcl/CA3: $p = 0.736$ sr/CA3: $p = 0.416$ **slm/CA3: $p = 0.033$** so/CA1: $p = 0.46$ pcl/CA1: $p = 0.835$ sr/CA1: $p = 0.362$ slm/CA1: $p = 0.109$
		IH	$F_{(1,190)} = 1.52$, $p = 0.219$	$F_{(10,190)} = 64.58$, **$p < 0.001$**	$F_{(10,190)} = 0.44$, $p = 0.927$	ml/DG: $p = 0.632$ gcl/DG: $p = 0.847$ pl/DG: $p = 0.708$ so/CA3: $p = 0.662$ pcl/CA3: $p = 0.714$ sr/CA3: $p = 0.678$ slm/CA3: $p = 0.26$

(Continued)

TABLE 2 | Continued

Receptor	Time-point	Hippocampal axis part	Multifactorial ANOVA			
			TREATMENT factor (T)	**REGION factor (R)**	**T * R interaction**	**Duncan's *post hoc* test**
		VH	$F_{(1,198)} = 1.308$, $p = 0.254$	$F_{(10,198)} = 23.24$, $\mathbf{p < 0.001}$	$F_{(10,198)} = 0.139$, $p = 0.999$	so/CA1: $p = 0.189$ pcl/CA1: $p = 0.859$ sr/CA1: $p = 0.357$ slm/CA1: $p = 0.714$ ml/DG: $p = 0.611$ gcl/DG: $p = 0.473$ pl/DG: $p = 0.673$ so/CA3: $p = 0.983$ pcl/CA3: $p = 0.975$ sr/CA3: $p = 0.836$ slm/CA3: $p = 0.606$
GABA B	1 week	DH	$F_{(1,198)} = 1.547$, $p = 0.215$	$F_{(10,198)} = 24.281$, $\mathbf{p < 0.001}$	$F_{(10,198)} = 0.081$, $p = 0.999$	so/CA1: $p = 0.403$ pcl/CA1: $p = 0.699$ sr/CA1: $p = 0.85$ slm/CA1: $p = 0.748$ ml/DG: $p = 0.873$ gcl/DG: $p = 0.554$ pl/DG: $p = 0.984$ so/CA3: $p = 0.772$ pcl/CA3: $p = 0.616$ sr/CA3: $p = 0.835$ slm/CA3: $p = 0.368$
		IH	$F_{(1,198)} = 37.22$, $\mathbf{p < 0.001}$	$F_{(10,198)} = 19.34$, $\mathbf{p < 0.001}$	$F_{(10,198)} = 0.22$, $p = 0.993$	so/CA1: $p = 0.505$ pcl/CA1: $p = 0.715$ sr/CA1: $p = 0.738$ slm/CA1: $p = 0.991$ ml/DG: $p = 0.065$ gcl/DG: $p = 0.119$ pl/DG: $p = 0.192$ so/CA3: $p = 0.0507$ pcl/CA3: $p = 0.283$ sr/CA3: $p = 0.136$ **slm/CA3: $p = 0.019$**
		VH	$F_{(1,187)} = 0.576$, $p = 0.449$	$F_{(10,187)} = 17.222$, $\mathbf{p < 0.001}$	$F_{(10,187)} = 0.512$, $p = 0.88$	so/CA1: $p = 0.098$ pcl/CA1: $p = 0.264$ sr/CA1: $p = 0.16$ **slm/CA1: $p = 0.028$** ml/DG: $p = 0.81$ gcl/DG: $p = 0.573$ pl/DG: $p = 0.753$ so/CA3: $p = 0.431$ pcl/CA3: $p = 0.438$ sr/CA3: $p = 0.28$ slm/CA3: $p = 0.259$
	3 months	DH	$F_{(1,190)} = 44.32$, $\mathbf{p < 0.001}$	$F_{(10,190)} = 48.54$, $\mathbf{p < 0.001}$	$F_{(10,190)} = 0.55$, $p = 0.852$	so/CA1: $p = 0.92$ pcl/CA1: $p = 0.986$ sr/CA1: $p = 0.913$ slm/CA1: $p = 0.667$ ml/DG: $p = 0.123$ pl/DG: $p = 0.061$ **so/CA3: $p = 0.03$**

(Continued)

TABLE 2 | Continued

Receptor	Time-point	Hippocampal axis part	Multifactorial ANOVA			
			TREATMENT factor (T)	**REGION factor (R)**	**T * R interaction**	**Duncan's *post hoc* test**
						pcl/CA3: $p = 0.163$ sr/CA3: $p = 0.378$ slm/CA3: $p = 0.483$ **so/CA1: $p = 0.012$** **pcl/CA1: $p = 0.009$** **sr/CA1: $p = 0.009$** **slm/CA1: $p = 0.036$**
		IH	$F_{(1,198)} = 1.82$, $p = 0.178$	$F_{(10,198)} = 34.01$, **$p < 0.001$**	$F_{(10,198)} = 0.18$, $p = 0.997$	ml/DG: $p = 0.914$ gcl/DG: $p = 0.824$ pl/DG: $p = 0.907$ so/CA3: $p = 0.214$ pcl/CA3: $p = 0.44$ sr/CA3: $p = 0.82$ slm/CA3: $p = 0.851$ so/CA1: $p = 0.579$ pcl/CA1: $p = 0.893$ sr/CA1: $p = 0.657$ slm/CA1: $p = 0.955$
		VH	$F_{(1,187)} = 0.19$, $p = 0.662$	$F_{(10,187)} = 24.44$, **$p < 0.001$**	$F_{(10,187)} = 0.2$, $p = 0.995$	ml/DG: $p = 0.811$ gcl/DG: $p = 0.737$ pl/DG: $p = 0.727$ so/CA3: $p = 0.629$ pcl/CA3: $p = 0.988$ sr/CA3: $p = 0.866$ slm/CA3: $p = 0.955$ so/CA1: $p = 0.947$ pcl/CA1: $p = 0.634$ sr/CA1: $p = 0.941$ slm/CA1: $p = 0.305$

The table describes the mean ± SEM values. Significant differences are highlighted in bold font. DH, dorsal hippocampus; IH, intermediate hippocampus; VH, ventral hippocampus; ml, molecular layer of the DG; gcl, granule cell layer of the DG; pl, polymorphic layer of the DG; so, Stratum oriens of CA3/CA1; pcl, pyramidal cell layer of CA3/CA1; sr, Stratum radiatum of CA3/CA1; and slm, Stratum lacunosum-moleculare of CA3/CA1.

$GABA_B$ receptors regulate neuronal population firing rate through sensing of ambient GABA levels. This is then transduced into homeostatic changes in synaptic strength (Gassmann and Bettler, 2012; Degro et al., 2015). In addition to the loss of $GABA_B$ receptors, 3 months after MK801 treatment, a significant loss of hippocampal interneurons was also detected in our study. A loss of interneurons combined with a decrease of $GABA_B$ receptors can be expected to result in a loss of experience-dependent GABA release, of GABA sensitivity and inhibitory tonus in the hippocampus. In line with this, a decrease in $GABA_B$ receptors is associated with aberrantly increased neuronal activity in rodents (Schuler et al., 2001; Gassmann et al., 2004). Furthermore, elevations in hippocampal excitability, coupled to aberrant somatic immediate early gene expression and deficits in hippocampus-dependent learning occur several weeks after MK801 treatment of rats (Grüter et al., 2015).

Both mGlu1 (Aiba et al., 1994; Naie and Manahan-Vaughan, 2005; Gil-Sanz et al., 2008; Neyman and Manahan-Vaughan, 2008) and mGlu5 receptors are required for the persistence of hippocampal synaptic plasticity and hippocampus-dependent spatial memory (Naie and Manahan-Vaughan, 2004; Manahan-Vaughan and Braunewell, 2005; Popkirov and Manahan-Vaughan, 2011). In the hippocampus, mGlu1 receptors are predominantly expressed on interneurons (Baude et al., 1993; Ferraguti et al., 1998, 2004). Their activation evokes slow oscillatory inward currents and elevates the frequency of spontaneous inhibitory postsynaptic currents and their amplitude in principal cells (van Hooft et al., 2000; Mannaioni et al., 2001; Lapointe et al., 2004). Hippocampal interneurons dampen neuronal excitability via mGlu1 receptor signaling that increases activation of interneurons and GABA release, (van Hooft et al., 2000; Lapointe et al., 2004). Furthermore, mGlu5 receptors support information transfer through neuronal oscillations in the hippocampus (Bikbaev et al., 2008; Bikbaev and Manahan-Vaughan, 2017). Thus, the changes in expression of these receptors may underlie changes in synaptic plasticity and neuronal oscillations that have been described in the rodent model studied here (Kalweit et al., 2017), as well neuronal

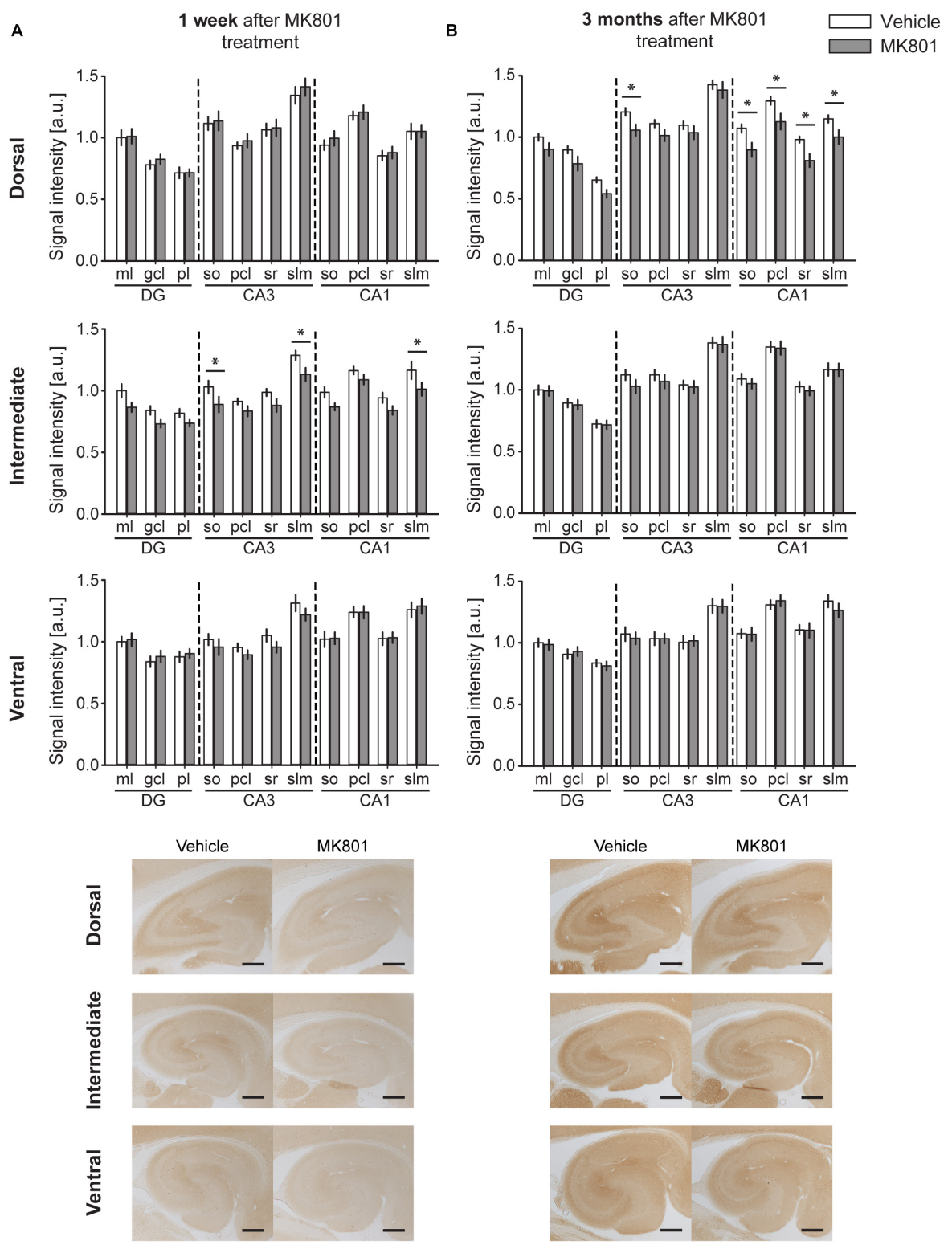

FIGURE 6 | MK801 treatment leads to a down-regulation of $GABA_B$ receptor protein expression. Bar charts illustrate relative changes in receptor protein levels across the somato-dendritic layers of the transverse and longitudinal hippocampal axes. **(A)** A reduction of $GABA_B$ receptor expression was evident across the CA

(*Continued*)

FIGURE 6 | Continued
regions of the intermediate hippocampus 1 week after MK801 treatment. **(B)** Similarly, a reduction of $GABA_B$ receptor levels was detected across the dorsal CA regions 3 months after MK801 treatment. Scale bar: 500 μm. Values expressed in arbitrary units (a.u.). Error bars indicate SEM. *$p < 0.05$. ml, molecular layer of the DG; gcl, granule cell layer of the DG; pl, polymorphic layer of the DG; so, Stratum oriens of CA3/CA1; pcl, pyramidal cell layer of CA3/CA1; sr, Stratum radiatum of CA3/CA1; and slm, Stratum lacunosum-moleculare of CA3/CA1. Photomicrographs provide examples of $GABA_B$ receptor-stained sections from the dorsal, intermediate and ventral hippocampal subdivisions that originated from the same vehicle- or MK801-treated animal, and correspond to 1 week (left) or 3 months (right) after treatment.

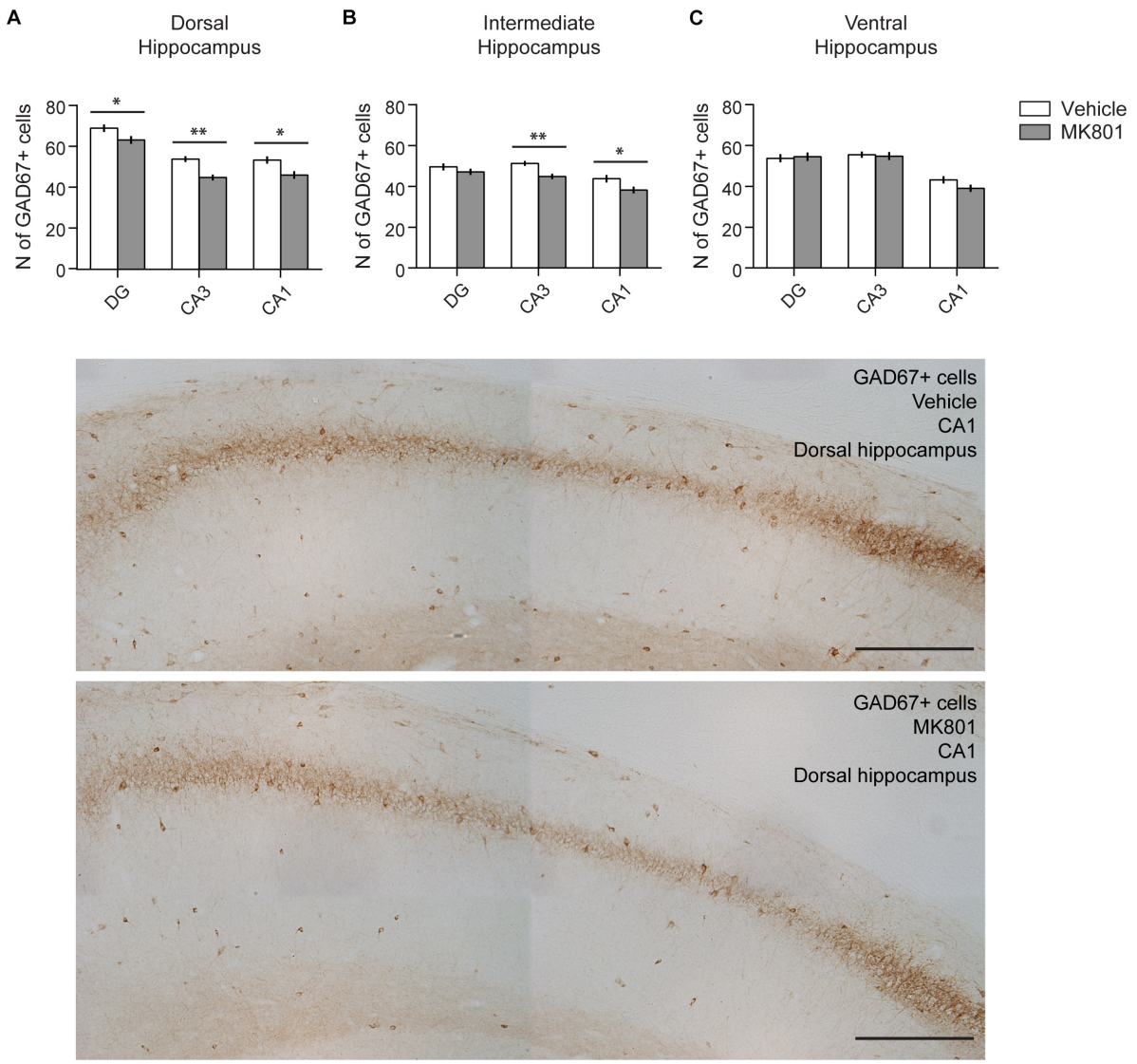

FIGURE 7 | The amount of GAD67+ cells is reduced in the hippocampus after MK801 treatment. Bar charts summarize the number of interneurons 3 months after MK801 treatment across the transverse and longitudinal hippocampal axes: **(A)** dorsal, **(B)** intermediate, **(C)** ventral hippocampus. Whereas significant decreases were detected in subregions of the dorsal and intermediate hippocampus, no changes were observed in the ventral subdivision. Error bars indicate SEM. *$p < 0.05$, **$p < 0.01$. Examples of GAD67-stained sections from the dorsal, intermediate and ventral hippocampal subdivisions are shown below. Specifically, the CA1 region from vehicle and MK801-treated animals is shown. Scale bar: 300 μm.

oscillations in patients who have experienced a first-episode (Uhlhaas and Singer, 2010).

'Synaptic gain control' determines how neurons respond to their inputs as well as the intrinsic excitation-inhibition balance in neural networks (Díez et al., 2017). We propose that changes in the relative balance and distribution of GABA and glutamate receptors underlie the loss of synaptic gain control that has been previously described in this animal model of

psychosis (Grüter et al., 2015; Kalweit et al., 2017) and may possibly comprise a fundamental mechanism underlying loss of synaptic gain control as proposed to occur in patients suffering from psychosis (Adams et al., 2013; Ranlund et al., 2016; Díez et al., 2017).

Of the hippocampal subdivisions affected by MK801 treatment, the dorsal hippocampus was the most vulnerable and the ventral hippocampus was the most resistant. Functionally, the convergence of long-term receptor changes in the dorsal hippocampal CA1 region suggests that impairments in memory retrieval and prediction error function will develop (Schultz and Dickinson, 2000). This means that mismatches will occur between external sensory information and internal representations (Hasselmo, 2005; Ji and Maren, 2008). In our animal model, this is reflected by impairments of object recognition memory, object-place memory, sensory gating and spatial reference memory (Grüter et al., 2015; Manahan-Vaughan et al., 2008a). In psychotic patients, this might be reflected by attention and motivation being applied to unimportant events, the formation of erroneous thoughts, disrupted cognition, and possibly delusions (Corlett et al., 2009; Schobel et al., 2013).

In summary, our findings suggest that in an animal model of psychosis that is accompanied by both short-term changes in NMDAR expression and long-term NMDAR hypofunction (Dubovyk and Manahan-Vaughan, 2018a), rapid changes in the expression of metabotropic glutamate receptors and GABA receptors are superseded by an extensive long-term upregulation of mGlu5 receptors in the CA1 regions of the entire dorsoventral hippocampal axis, along with a decrease of $GABA_B$ receptor expression across all layers of the dorsal CA1 region and a loss of interneurons. The CA1 region is arguably the output structure of the hippocampus that engages in mismatch detection and has been proposed to be especially vulnerable to NMDAR hypofunction (Lisman and Otmakhova, 2001). Our findings indicate that this structure is particularly susceptible to changes elicited by the instigation of a first episode psychosis-like state in rodents that in turn triggers receptor expression changes that are similar to those reported in schizophrenic patients. We propose that these chronic changes in glutamatergic and GABAergic receptor expression comprise a primary mechanism underlying loss of synaptic gain control that is believed to underlie many features of psychosis including functional disconnectivity, abnormal neuronal oscillations and loss of sensory attenuation (Adams et al., 2013; Díez et al., 2017).

ETHICS STATEMENT

This study was carried out in accordance with the European Communities Council Directive of September 22nd, 2010 (2010/63/EU) for care of laboratory animals. Prior permission was obtained from the local authorities (Landesamt für Arbeitsschutz, Umwelt- und Naturschutz, Nordrhein-Westfalen).

AUTHOR CONTRIBUTIONS

DM-V created the concept and strategy of the study. VD carried out the experiments. DM-V and VD conducted data analysis and interpretation, as well as the writing of the manuscript.

FUNDING

This project was supported by grants (SFB 874/B1, Project No: 122679504 and SFB1280/A4, Project No: 316803389) from the German Research Foundation (Deutsche Forschungsgemeinschaft, DFG) to DM-V.

ACKNOWLEDGMENTS

We gratefully thank Ute Neubacher and Beate Krenzek for technical assistance and both Nadine Kollosch and Petra Küsener for animal care.

REFERENCES

Adams, R. A., Stephan, K. E., Brown, H. R., Frith, C. D., and Friston, K. J. (2013). The computational anatomy of psychosis. *Front. Psychiatry* 4:47.

Adriano, F., Caltagirone, C., and Spalletta, G. (2012). Hippocampal volume reduction in first-episode and chronic schizophrenia: a review and meta-analysis. *Neuroscientist* 18, 180–200. doi: 10.1177/1073858410395147

Aiba, A., Chen, C., Herrup, K., Rosenmund, C., Stevens, C. F., and Tonegawa, S. (1994). Reduced hippocampal long-term potentiation and context-specific deficit in associative learning in mGluR1 mutant mice. *Cell* 79, 365–375. doi: 10.1016/0092-8674(94)90204-6

Alagarsamy, S., Saugstad, J., Warren, L., Mansuy, I. M., Gereau, I. V. R. W., and Conn, P. J. (2005). NMDA-induced potentiation of mGlu5 is mediated by activation of protein phosphatase 2B/calcineurin. *Neuropharmacology* 49, 135–145. doi: 10.1016/j.neuropharm.2005.05.005

Altinbilek, B., and Manahan-Vaughan, D. (2009). A specific role for group II metabotropic glutamate receptors in hippocampal long-term depression and spatial memory. *Neuroscience* 158, 149–158. doi: 10.1016/j.neuroscience.2008.07.045

Alvarez-Jimenez, M., Gleeson, J. F., Henry, L. P., Harrigan, S. M., Harris, M. G., Amminger, G. P., et al. (2011). Prediction of a single psychotic episode: a 7.5-year, prospective study in first-episode psychosis. *Schizophr. Res.* 125, 236–246. doi: 10.1016/j.schres.2010.10.020

Andersen, P., Soleng, A. F., and Raastad, M. (2000). The hippocampal lamella hypothesis revisited. *Brain Res.* 886, 165–171. doi: 10.1016/s0006-8993(00)02991-7

Arnold, O. H. (1999). Schizophrenia – a disturbance of signal interaction between the entorhinal cortex and the dentate dyrus? The contribution of experimental dibenamine psychosis to the pathogenesis of schizophrenia: a hypothesis. *Neuropsychobiology* 40, 21–32. doi: 10.1159/000026593

Avery, S. N., Rogers, B. P., and Heckers, S. (2018). Hippocampal network modularity is associated with relational memory dysfunction in schizophrenia. *Biol. Psychiatry Cogn. Neurosci. Neuroimaging* 3, 423–432. doi: 10.1016/j.bpsc.2018.02.001

Bak, N., Rostrup, E., Larsson, H. B., Glenthoj, B. Y., and Oranje, B. (2014). Concurrent functional magnetic resonance imaging and electroencephalography assessment of sensory gating in schizophrenia. *Hum. Brain Mapp.* 35, 3578–3587. doi: 10.1002/hbm.22422

Bast, T., and Feldon, J. (2003). Hippocampal modulation of sensorimotor processes. *Prog. Neurobiol.* 70, 319–345. doi: 10.1016/s0301-0082(03)00112-6

Bast, T., Wilson, I. A., Witter, M. P., and Morris, R. G. M. (2009). From rapid place learning to behavioral performance: a key role for the intermediate hippocampus. *PLoS Biol.* 7:e1000089. doi: 10.1371/journal.pbio.1000089

Baude, A., Nusser, Z., Roberts, J. D. B., Mulvihill, E., Mcllhinney, R. A. J., and Somogyi, P. (1993). The metabotropic glutamate receptor (mGluR1a) is concentrated at perisynaptic membrane of neuronal subpopulations as detected by immunogold reaction. *Neuron* 11, 771–787. doi: 10.1016/0896-6273(93)90086-7

Behrendt, R. P. (2010). Contribution of hippocampal region CA3 to consciousness and schizophrenic hallucinations. *Neurosci. Biobehav. Rev.* 34, 1121–1136. doi: 10.1016/j.neubiorev.2009.12.009

Belforte, J. E., Zsiros, V., Sklar, E. R., Jiang, Z., Yu, G., Li, Y., et al. (2010). Postnatal NMDA receptor ablation in corticolimbic interneurons confers schizophrenia-like phenotypes. *Nat. Neurosci.* 13, 76–83. doi: 10.1038/nn.2447

Benquet, P., Gee, C. E., and Gerber, U. (2002). Two distinct signaling pathways upregulate NMDA receptor responses via two distinct metabotropic glutamate receptor subtypes. *J. Neurosci.* 22, 9679–9686. doi: 10.1523/jneurosci.22-22-09679.2002

Bettler, B., Kaupmann, K., Mosbacher, J., and Gassmann, M. (2004). Molecular structure and physiological functions of GABAB receptors. *Physiol. Rev.* 84, 835–867.

Bikbaev, A., and Manahan-Vaughan, D. (2017). Metabotropic glutamate receptor, mGlu5, regulates hippocampal synaptic plasticity and is required for tetanisation-triggered changes in theta and gamma oscillations. *Neuropharmacology* 115, 20–29. doi: 10.1016/j.neuropharm.2016.06.004

Bikbaev, A., Neyman, S., Ngomba, R., Nicoletti, F., Conn, P. J., and Manahan-Vaughan, D. (2008). The metabotropic glutamate receptor, mGluR5, mediates the functional interaction between late-LTP, hippocampal network activity, and learning by a mechanism involving regulation of mGluR1 expression. *PLoS One* 3:e2155. doi: 10.1371/journal.pone.0002155

Borgwardt, S. J., McGuire, P. K., Aston, J., Gschwandtner, U., Pflüger, M. O., Stieglitz, R. D., et al. (2008). Reductions in frontal, temporal and parietal volume associated with the onset of psychosis. *Schizophr. Res.* 106, 108–114. doi: 10.1016/j.schres.2008.08.007

Bowie, C. R., and Harvey, P. D. (2005). Cognition in schizophrenia: impairments, determinants, and functional importance. *Psychiatr. Clin. N. Am.* 28, 613–633. doi: 10.1016/j.psc.2005.05.004

Bürgy, M. (2008). The concept of psychosis: historical and phenomenological aspects. *Schizophr. Bull.* 34, 1200–1210. doi: 10.1093/schbul/sbm136

Cheung, V., Chiu, C. P. Y., Law, C. W., Cheung, C., Hui, C. L. M., Chan, K. K. S., et al. (2010). Positive symptoms and white matter microstructure in never-medicated first episode schizophrenia. *Psychol. Med.* 41, 1709–1719. doi: 10.1017/S003329171000156X

Cohen, S. M., Tsien, R. W., Goff, D. C., and Halassa, M. M. (2015). The impact of NMDA receptor hypofunction on GABAergic neurons in the pathophysiology of schizophrenia. *Schizophr. Res.* 167, 98–107. doi: 10.1016/j.schres.2014.12.026

Compton, M. T., Fantes, F., Wan, C. R., Johnson, S., and Walker, E. F. (2015). Abnormal movements in first-episode, nonaffective psychosis: dyskinesias, stereotypies, and catatonic-like signs. *Psychiatry Res.* 226, 192–197. doi: 10.1016/j.psychres.2014.12.048

Connelly, W. M., Errington, A. C., Di Giovanni, G., and Crunelli, V. (2013). Metabotropic regulation of extrasynaptic GABAA receptors. *Front. Neural Circ.* 7:171. doi: 10.3389/fncir.2013.00171

Corlett, P. R., Honey, G. D., Krystal, J. H., and Fletcher, P. C. (2011). Glutamatergic model psychoses: prediction error, learning, and inference. *Neuropsychopharmacology* 36, 294–315. doi: 10.1038/npp.2010.163

Corlett, P. R., Krystal, J. H., Taylor, J. R., and Fletcher, P. C. (2009). Why do delusions persist? *Front. Hum. Neurosci.* 3:12. doi: 10.3389/neuro.09.012.2009

Davis, M. C., Horan, W. P., and Marder, S. R. (2014). Psychopharmacology of the negative symptoms: current status and prospects for progress. *Eur. Neuropsychopharmacol.* 24, 788–799. doi: 10.1016/j.euroneuro.2013.10.010

Degro, C. E., Kulik, A., Booker, S. A., and Vida, I. (2015). Compartmental distribution of GABAB receptor-mediated currents along the somatodendritic axis of hippocampal principal cells. *Front. Synaptic Neurosci.* 7:6. doi: 10.3389/fnsyn.2015.00006

Díez, Á, Ranlund, S., Pinotsis, D., Calafato, S., Shaikh, M., Hall, M. H., et al. (2017). Abnormal frontoparietal synaptic gain mediating the P300 in patients with psychotic disorder and their unaffected relatives. *Hum. Brain Mapp.* 38, 3262–3276. doi: 10.1002/hbm.23588

Dubovyk, V., and Manahan-Vaughan, D. (2018a). Less means more: the magnitude of synaptic plasticity along the hippocampal dorso-ventral axis is inversely related to the expression levels of plasticity-related neurotransmitter receptors. *Hippocampus* 28, 136–150. doi: 10.1002/hipo.22816

Dubovyk, V., and Manahan-Vaughan, D. (2018b). Time-dependent alterations in the expression of NMDA receptor subunits along the dorsoventral hippocampal axis in an animal model of nascent psychosis. *ACS Chem. Neurosci.* 9, 2241–2251. doi: 10.1021/acschemneuro.8b00017

Fanselow, M. S., and Dong, H. W. (2010). Are the dorsal and ventral hippocampus functionally distinct structures? *Neuron* 65, 1–20.

Ferraguti, F., Cobden, P., Pollard, M., Cope, D., Shigemoto, R., Watanabe, M., et al. (2004). Immunolocalization of metabotropic glutamate receptor 1a (mGluR1a) in distinct classes of interneuron in the CA1 region of the rat hippocampus. *Hippocampus* 14, 193–215. doi: 10.1002/hipo.10163

Ferraguti, F., Conquet, F., Corti, C., Grandes, P., Kuhn, R., and Knopfel, T. (1998). Immunohistochemical localization of the mGluR1β metabotropic glutamate receptor in the adult rodent forebrain: evidence for a differential distribution of mGluR1 splice variants. *J. Comp. Neurol.* 400, 391–407. doi: 10.1002/(sici)1096-9861(19981026)400:3<391::aid-cne8>3.0.co;2-3

Friston, K. J. (1998). The disconnection hypothesis. *Schizophr. Res.* 30, 115–125. doi: 10.1016/s0920-9964(97)00140-0

Gassmann, M., and Bettler, B. (2012). Regulation of neuronal GABAB receptor functions by subunit composition. *Nat. Rev.* 13, 380–394. doi: 10.1038/nrn3249

Gassmann, M., Shaban, H., Vigot, R., Sansig, G., Haller, C., Barbieri, S., et al. (2004). Redistribution of GABAB(1) protein and atypical GABAB responses in GABAB(2)-deficient mice. *J. Neurosci.* 24, 6086–6097. doi: 10.1523/jneurosci.5635-03.2004

Gil-Sanz, C., Delgado-Garcia, J. M., Fairen, A., and Gruart, A. (2008). Involvement of the mGluR1 receptor in hippocampal synaptic plasticity and associative learning in behaving mice. *Cereb Cortex* 18, 1653–1663. doi: 10.1093/cercor/bhm193

Gonzalez-Burgos, G., and Lewis, D. A. (2012). NMDA receptor hypofunction, parvalbumin-positive neurons, and cortical gamma oscillations in schizophrenia. *Schizophr. Bull.* 38, 950–957. doi: 10.1093/schbul/sbs010

Grüter, T., Wiescholleck, V., Dubovyk, V., Aliane, V., and Manahan-Vaughan, D. (2015). Altered neuronal excitability underlies impaired hippocampal function in an animal model of psychosis. *Front. Behav. Neurosci.* 9:117. doi: 10.3389/fnbeh.2015.00117

Guo, X., Li, J., Wei, Q., Fan, X., Kennedy, D. N., Shen, Y., et al. (2013). Duration of untreated psychosis is associated with temporal and occipitotemporal gray matted volume decrease in treatment naïve schizophrenia. *PLoS One* 8:e83679. doi: 10.1371/journal.pone.0083679

Häfner, H., Maurer, K., Löffler, W., Fätkenheuer, B., an der Heiden, W., Riecher-Rössler, A., et al. (1994). The epidemiology of early schizophrenia. Influence of age and gender on onset and early course. *Br. J. Psychiatry* 164, 29–38. doi: 10.1192/s0007125000292714

Haijima, S. V., Van Haren, N., Cahn, W., Koolschijn, P. C., Hulshoff, P. H., and Kahn, R. S. (2012). Brain volumes in schizophrenia: a meta-analysis in over 18 000 subjects. *Schizophr. Bull.* 39, 1129–1138. doi: 10.1093/schbul/sbs118

Hartung, H., Cichon, N., De Feo, V., Riemann, S., Schildt, S., Lindemann, C., et al. (2016). From shortage to surge: a developmental switch in hippocampal-prefrontal coupling in a gene-environment model of neuropsychiatric disorders. *Cereb Cortex* 26, 4265–4281. doi: 10.1093/cercor/bhw274

Hasselmo, M. E. (2005). The role of hippocampal regions CA3 and CA1 in matching entorhinal input with retrieval of associations between objects and context: theoretical comment on Lee et al. (2005). *Behav. Neurosci.* 119, 342–345. doi: 10.1037/0735-7044.119.1.342

Heckers, S., and Konradi, C. (2002). Hippocampal neurons in schizophrenia. *J. Neural Transm.* 109, 891–905. doi: 10.1007/s007020200073

Heckers, S., Rauch, S. L., Goff, D., Savage, C. R., Schacter, D. L., Fischman, A. J., et al. (1998). Impaired recruitment of the hippocampus during conscious recollection in schizophrenia. *Nat. Neurosci.* 1, 318–323. doi: 10.1038/1137

Heidinger, V., Manzerra, P., Wang, Z. Q., Strasser, U., Yu, S.-P., Choi, D. W., et al. (2002). Metabotropic glutamate receptor 1-induced upregulation of NMDA

receptor current: mediation through the Pyk2/Src-family kinase pathway in cortical neurons. *J. Neurosci.* 22, 5452–5461. doi: 10.1523/jneurosci.22-13-05452.2002

Jézéquel, J., Lepleux, M., Kahn, R. S., Honnorat, J., Leboyer, M., and Groc, L. (2018). Molecular pathogenicity of anti-NMDA receptor autoantibody from patients with first-episode psychosis. *Am. J. Psychiatry* 175, 382–383. doi: 10.1176/appi.ajp.2017.17091053

Ji, J., and Maren, S. (2008). Differential roles for hippocampal areas CA1 and CA3 in the contextual encoding and retrieval of extinguished fear. *Learn. Mem.* 15, 244–251. doi: 10.1101/lm.794808

Kaila, K. (1994). Ionic basis of GABA A receptor channel function in the nervous system. *Prog. Neurobiol.* 42, 489–537. doi: 10.1016/0301-0082(94)90049-3

Kalweit, A. N., Amanpour-Gharaei, B., Colitti-Klausnitzer, J., and Manahan-Vaughan, D. (2017). Changer in neuronal oscillations accompany the loss of hippocampal LTP that occurs in an animal model of psychosis. *Front. Behav. Neurosci.* 11:36. doi: 10.3389/fnbeh.2017.00036

Kapur, S. (2003). Psychosis as a state of aberrant salience: a framework linking biology, phenomenology, and pharmacology in schizophrenia. *Am. J. Psychiatry* 160, 13–23. doi: 10.1176/appi.ajp.160.1.13

Keefe, R. S. E., and Harvey, P. D. (2012). Cognitive impairment in schizophrenia. *Handb. Exp. Pharmacol.* 213, 11–37.

Kehrer, C., Dugladze, T., Maziashvili, N., Wójtowicz, A., Schmitz, D., Heinemann, U., et al. (2007). Increased inhibitory input to CA1 pyramidal cells alters hippocampal gamma frequency oscillations in the MK-801 model of acute psychosis. *Neurobiol. Dis.* 25, 545–552. doi: 10.1016/j.nbd.2006.10.015

Kemp, A., and Manahan-Vaughan, D. (2007). Hippocampal long-term depression: master or minion in declarative memory processes? *Trends Neurosci.* 30, 111–118. doi: 10.1016/j.tins.2007.01.002

Keshavan, M. S., DeLisi, L. E., and Seidman, L. J. (2011). Early and broadly defined psychotic risk mental states. *Schizophr. Res.* 126, 1–10. doi: 10.1016/j.schres.2010.10.006

Kesner, R. P. (2013a). An analysis of the dentate gyrus function. *Behav. Brain Res.* 254, 1–7. doi: 10.1016/j.bbr.2013.01.012

Kesner, R. P. (2013b). A process analysis of the CA3 subregion of the hippocampus. *Front. Cell Neurosci.* 7:78. doi: 10.3389/fncel.2013.00078

Kesner, R. P., and Rolls, E. T. (2015). A computational theory of hippocampal function, and tests of the theory: new developments. *Neurosci. Behav. Rev.* 48, 92–147. doi: 10.1016/j.neubiorev.2014.11.009

Kim, J. S., Baek, J. H., Choi, J. S., Lee, D., Kwon, J. S., and Hong, K. S. (2011). Diagnostic stability of first-episode psychosis and predictors of diagnostic shift from non-affective psychosis to bipolar disorder: a retrospective evaluation after recurrence. *Psychiatry Res.* 188, 29–33. doi: 10.1016/j.psychres.2010.09.017

Kobayashi, K., Manabe, T., and Takahashi, T. (1996). Presynaptic long-term depression at the hippocampal mossy fiber-CA3 synapse. *Science* 273, 648–650. doi: 10.1126/science.273.5275.648

Kolomeets, N. S., Orlovskaya, D. D., and Uranova, N. A. (2007). Decreased numerical density of CA3 hippocampal mossy fiber synapses in schizophrenia. *Synapse* 61, 615–621. doi: 10.1002/syn.20405

Kreutz, C., Bartolome Rodriguez, M. M., Maiwald, T., Seidl, M., Blum, H. E., Mohr, L., et al. (2007). An error model for protein quantification. *Bioinformatics* 20, 2747–2753. doi: 10.1093/bioinformatics/btm397

Krystal, J. H., Karper, L. P., Seibyl, J. P., Freeman, G. K., Delaney, R., Bremner, J. D., et al. (1994). Subanesthetic effects of the noncompetitive NMDA antagonist, ketamine, in humans. Psychotomimetic, perceptual, cognitive, and neuroendocrine responses. *Arch. Gen. Psychiatry* 51, 199–214.

Kullmann, D. M., Ruiz, A., Rusakov, D. M., Scott, R., Semyanov, A., and Walker, M. C. (2005). Presynaptic, extrasynaptic and axonal GABA A receptors in the CNS: where and why? *Prog. Biophys. Mol. Biol.* 87, 33–46. doi: 10.1016/j.pbiomolbio.2004.06.003

Lahti, A. C., Koffel, B., LaPorte, D., and Tamminga, C. A. (1995). Subanesthetic doses of ketamine stimulate psychosis in schizophrenia. *Neuropsychopharmacology* 13, 9–19. doi: 10.1016/0893-133x(94)00131-i

Lapointe, V., Morin, F., Ratte, S., Croce, A., Conquet, F., and Lacaille, J. C. (2004). Synapse-specific mGluR1-dependent long-term potentiation in interneurons regulates mouse hippocampal inhibition. *J. Physiol.* 555, 125–135. doi: 10.1113/jphysiol.2003.053603

Larson, M. K., Walker, E. F., and Compton, M. T. (2010). Early signs, diagnosis and therapeutics of the prodromal phase of schizophrenia and related psychotic disorders. *Expert Rev. Neurother.* 10, 1347–1359. doi: 10.1586/ern.10.93

Lesage, A., and Steckler, T. (2010). Metabotropic glutamate mGlu1 receptor stimulation and blockade: therapeutic opportunities in psychiatric illness. *Eur. J. Pharmacol.* 639, 2–16. doi: 10.1016/j.ejphar.2009.12.043

Lin, C.-H., Lane, H.-Y., and Tsai, G. E. (2012). Glutamate signaling in the pathophysiology and therapy of schizophrenia. *Pharmacol. Biochem. Behav.* 100, 665–677. doi: 10.1016/j.pbb.2011.03.023

Linden, A. M., Baez, M., Bergeron, M., and Schoepp, D. D. (2006). Effects of mGlu2 or mGlu3 receptor deletions on mGlu2/3 receptor agonist (LY354740)-induced brain c-Fos expression: specific roles for mGlu2 in the amygdala and subcortical nuclei, and mGlu3 in the hippocampus. *Neuropharmacology* 51, 213–228. doi: 10.1016/j.neuropharm.2006.03.014

Lisman, J. E., and Otmakhova, N. A. (2001). Storage, recall, and novelty detection of sequences by the hippocampus: elaborating on the SOCRATIC model to account for normal and aberrant effects of dopamine. *Hippocampus* 11, 551–568. doi: 10.1002/hipo.1071.abs

Ludewig, K., Geyer, M. A., and Vollenweider, F. X. (2003). Deficits in prepulse inhibition and habituation in never-medicated, first-episode schizophrenia. *Biol. Psychiatry* 54, 121–128. doi: 10.1016/s0006-3223(02)01925-x

Malenka, R. C., and Bear, M. F. (2004). LTP and LTD: an embarrassment of riches. *Neuron* 44, 5–21.

Manahan-Vaughan, D. (1998). Priming of group 2 metabotropic glutamate receptors facilitates induction of long-term depression in the dentate gyrus of freely moving rats. *Neuropharmacology* 37, 1459–1464. doi: 10.1016/s0028-3908(98)00150-6

Manahan-Vaughan, D., and Braunewell, K. H. (2005). The metabotropic glutamate receptor, mGluR5, is a key determinant of good and bad spatial learning performance and hippocampal synaptic plasticity. *Cereb Cortex* 15, 1703–1713. doi: 10.1093/cercor/bhi047

Manahan-Vaughan, D., von Haebler, D., Winter, C., Juckel, G., and Heinemann, U. (2008a). A single application of MK801 causes symptoms of acute psychosis, deficits in spatial memory, and impairment of synaptic plasticity in rats. *Hippocampus* 18, 125–134. doi: 10.1002/hipo.20367

Manahan-Vaughan, D., Wildförster, V., and Thomsen, C. (2008b). Rescue of hippocampal LTP and learning deficits in a rat model of psychosis by inhibition of glycine transporter-1 (GlyT1). *Eur. J. Neurosci.* 28, 1342–1350. doi: 10.1111/j.1460-9568.2008.06433.x

Mannaioni, G., Marino, M. J., Valenti, O., Traynelis, S. F., and Conn, P. J. (2001). Metabotropic glutamate receptors 1 and 5 differentially regulate CA1 pyramidal cell function. *J. Neurosci.* 21, 5925–5934. doi: 10.1523/jneurosci.21-16-05925.2001

Marek, G. J., Behl, B., Bespalov, A. Y., Gross, G., Lee, Y., and Schoemaker, H. (2010). Glutamatergic (N-methyl-D-aspartate receptor) hypofrontality in schizophrenia: too little juice or miswired brain? *Mol. Pharmacol.* 77, 317–326. doi: 10.1124/mol.109.059865

Marino, M. J., and Conn, P. J. (2002). Direct and indirect modulation of the N-methyl D-aspartate receptor. *Curr. Drug Targets CNS Neurol. Disord.* 1, 1–16. doi: 10.2174/1568007023339544

Matosin, N., Fernandez-Enright, F., Lum, J. S., Andrews, J. L., Engel, M., Huang, X.-F., et al. (2015). Metabotropic glutamate receptor 5, and its trafficking molecules Norbin and Tamalin, are increased in the CA1 hippocampal region of subjects with schizophrenia. *Schizophr. Res.* 166, 212–218. doi: 10.1016/j.schres.2015.05.001

Matosin, N., and Newell, K. A. (2013). Metabotropic glutamate receptor 5 in the pathology and treatment of schizophrenia. *Neurosci. Behav. Rev.* 37, 256–268. doi: 10.1016/j.neubiorev.2012.12.005

McGhie, A., and Chapman, J. (1961). Disorders of attention and perception in early schizophrenia. *Br. J. Med. Psychol.* 34, 103–116. doi: 10.1111/j.2044-8341.1961.tb00936.x

Mizukami, K., Sasaki, M., Ishikawa, M., Iwakiri, M., Hidaka, S., Shiraishi, H., et al. (2000). Immunohistochemical localization of γ-aminobutyric acidB receptor in the hippocampus of subjects with schizophrenia. *Neurosci. Lett.* 283, 101–104. doi: 10.1016/s0304-3940(00)00939-3

Mukherjee, S., and Manahan-Vaughan, D. (2013). Role of metabotropic glutamate receptors in persistent forms of hippocampal plasticity and learning. *Neuropharmacology* 66, 65–81. doi: 10.1016/j.neuropharm.2012.06.005

Naie, K., and Manahan-Vaughan, D. (2004). Regulation by metabotropic glutamate receptor 5 of LTP in the dentate gyrus of freely moving rats: relevance for learning and memory formation. *Cereb Cortex* 14, 189–198. doi: 10.1093/cercor/bhg118

Naie, K., and Manahan-Vaughan, D. (2005). Pharmacological antagonism of metabotropic glutamate receptor 1 regulates long-term potentiation and spatial reference memory in the dentate gyrus of freely moving rats via N-methyl-D-aspartate and metabotropic glutamate receptor-dependent mechanisms. *Eur. J. Neurosci.* 21, 411–421. doi: 10.1111/j.1460-9568.2005.03864.x

Nakazawa, K., Zsiros, V., Jiang, Z., Nakao, K., Kolata, S., Zhang, S., et al. (2012). GABAergic interneuron origin of schizophrenia pathophysiology. *Neuropharmacology* 62, 1574–1583. doi: 10.1016/j.neuropharm.2011.01.022

Neyman, S., and Manahan-Vaughan, D. (2008). Metabotropic glutamate receptor 1 (mGluR1) and 5 (mGluR5) regulate late phases of LTP and LTD in the hippocampal CA1 region in vitro. *Eur. J. Neurosci.* 27, 1345–1352. doi: 10.1111/j.1460-9568.2008.06109.x

Paulsen, O., and Moser, E. I. (1998). A model of hippocampal memory encoding and retrieval: GABAergic control of synaptic plasticity. *Trends Neurosci.* 21, 273–278. doi: 10.1016/s0166-2236(97)01205-8

Paxinos, G., and Watson, C. (1982). *The Rat Brain in Stereotaxic Coordinates*. San Diego, CA: Academic Press.

Perez, S. M., and Lodge, D. J. (2014). New approaches to the management of schizophrenia: focus on aberrant hippocampal drive of dopamine pathways. *Drug Design Dev. Ther.* 8, 887–896. doi: 10.2147/DDDT.S42708

Popkirov, S. G., and Manahan-Vaughan, D. (2011). Involvement of the metabotropic glutamate receptor mGluR5 in NMDA receptor-dependent, learning-facilitated long-term depression in CA1 synapses. *Cereb Cortex* 21, 501–509. doi: 10.1093/cercor/bhq093

Pöschel, B., and Manahan-Vaughan, D. (2007). Persistent (> 24h) long-term depression in the dentate gyrus of freely moving rats is not dependent on activation of NMDA receptors, L-type voltage-gated calcium channels or protein synthesis. *Neuropharmacology* 52, 46–54. doi: 10.1016/j.neuropharm.2006.07.019

Ranlund, S., Adams, R. A., Díez, Á, Constante, M., Dutt, A., Hall, M. H., et al. (2016). Impaired prefrontal synaptic gain in people with psychosis and their relatives during the mismatch negativity. *Hum. Brain Mapp.* 37, 351–365. doi: 10.1002/hbm.23035

Riebe, I., Seth, H., Culley, G., Dosa, Z., Radi, S., Strand, K., et al. (2016). Tonically active NMDA receptors – a signalling mechanism critical for interneuronal excitability in the CA1 stratum radiatum. *Eur. J. Neurosci.* 43, 169–178. doi: 10.1111/ejn.13128

Ruby, E., Polito, S., McMahon, K., Gorovitz, M., Corcoran, C., and Malaspina, D. (2014). Pathways associating childhood trauma to the neurobiology of schizophrenia. *Front. Psychol. Behav. Sci.* 3:1–17.

Samudra, N., Ivleva, E. I., Hubbard, N. A., Rypma, B., Sweeney, J. A., Clementz, B. A., et al. (2015). Alterations in hippocampal connectivity across the psychosis dimension. *Psychiatry Res.* 233, 148–157. doi: 10.1016/j.pscychresns.2015.06.004

Schobel, S. A., Chaudhury, N. H., Khan, U. A., Paniagua, B., Styner, M. A., Asllani, I., et al. (2013). Imaging patients with psychosis and a mouse model establishes a spreading pattern of hippocampal dysfunction and implicates glutamate as a driver. *Neuron* 78, 81–93. doi: 10.1016/j.neuron.2013.02.011

Schoepp, D. D. (2001). Unveiling the functions of presynaptic metabotropic glutamate receptors in the central nervous system. *J. Pharmacol. Exp. Ther.* 299, 12–20.

Schuler, V., Lüscher, C., Blanchet, C., Klix, N., Sansig, G., Klebs, K., et al. (2001). Epilepsy, hyperalgesia, impaired memory, and loss of pre- and postsynaptic GABA(B) responses in mice lacking GABA(B(1)). *Neuron* 31, 47–58. doi: 10.1016/s0896-6273(01)00345-2

Schultz, W., and Dickinson, A. (2000). Neural coding of prediction errors. *Annu. Rev. Neurosci.* 23, 473–500.

Shen, W., Nan, C., Nelson, P. T., Ripps, H., and Slaughter, M. M. (2017). GABAB receptor attenuation of GABAA currents in neurons of the mammalian central nervous system. *Physiol. Rep.* 5, 1–11.

Shigemoto, R., Kinoshita, A., Wada, E., Nomura, S., Ohishi, H., Takada, M., et al. (1997). Differential presynaptic localization of metabotropic glutamate receptor subtypes in the rat hippocampus. *J. Neurosci.* 17, 7503–7522. doi: 10.1523/jneurosci.17-19-07503.1997

Snyder, M. A., and Gao, W. J. (2013). NMDA hypofunction as a convergence point for progression and symptoms of schizophrenia. *Front. Cell. Neurosci.* 7:31. doi: 10.3389/fncel.2013.00031

Stephan, K. E., Baldeweg, T., and Friston, K. J. (2006). Synaptic plasticity and dysconnection in schizophrenia. *Biol. Psychiatry* 59, 929–939. doi: 10.1016/j.biopsych.2005.10.005

Stephan, K. E., Friston, K. J., and Frith, C. D. (2009). Dysconnection in schizophrenia: from abnormal synaptic plasticity to failures of self-monitoring. *Schizophr. Bull.* 35, 509–527. doi: 10.1093/schbul/sbn176

Strange, B. A., Witter, M. P., Lein, E. S., and Moser, E. I. (2014). Functional organization of the hippocampal longitudinal axis. *Nat. Rev. Neurosci.* 15, 655–669. doi: 10.1038/nrn3785

Tóth, K., and Freund, T. F. (1992). Calbindin D28k-containing nonpyramidal cells in the rat hippocampus: their immunoreactivity for GABA and projection to the medial septum. *Neuroscience* 49, 793–805. doi: 10.1016/0306-4522(92)90357-8

Tu, J. C., Xiao, B., Naisbitt, S., Yuan, J. P., Petralia, R. S., Brakeman, P., et al. (1999). Coupling of mGluR/Homer and PSD-95 complexes by the Shank family of postsynaptic density proteins. *Neuron* 23, 583–592. doi: 10.1016/s0896-6273(00)80810-7

Uhlhaas, P. J., and Singer, W. (2010). Abnormal neural oscillations and synchrony in schizophrenia. *Nat Rev Neurosci.* 11, 100–113. doi: 10.1038/nrn2774

van Hooft, J. A., Giuffrida, R., Blatow, M., and Monyer, H. (2000). Differential expression of group I metabotropic glutamate receptors in functionally distinct hippocampal interneurons. *J. Neurosci.* 20, 3544–3551. doi: 10.1523/jneurosci.20-10-03544.2000

Velligan, D. I., and Alphs, L. D. (2008). Negative symptoms in schizophrenia: the importance of identification and treatment. *Psychiatr. Times* 25, 1–6.

Vertkin, I., Styr, B., Slomowitz, E., Ofir, N., Shapira, I., Berner, D., et al. (2015). GABAB receptor deficiency causes failure of neuronal homeostasis in hippocampal networks. *Proc. Natl. Acad. Sci. U.S.A.* 112, E3291–E3299. doi: 10.1073/pnas.1424810112

von der Heyde, S., Sonntag, J., Kaschek, D., Bender, C., Bues, J., and Wachter, A. (2014). RPPanalyzer toolbox: an improved R package for analysis of reverse phase protein array data. *Biotechniques* 57, 125–135. doi: 10.2144/000114205

Waldmeier, P. C., Kaupmann, K., and Urwyler, S. (2008). Roles of GABAB receptor subtypes in presynaptic auto- and heteroreceptor function regulating GABA and glutamate release. *J. Neural Transm.* 115, 1401–1411. doi: 10.1007/s00702-008-0095-7

Wieschollek, V., and Manahan-Vaughan, D. (2012). PDE4 inhibition enchances hippocampal synaptic plasticity *in vivo* and rescues MK801-induced impairment of long-term potentiation and object recognition memory in an animal model of psychosis. *Transl. Psychiatry* 2:e89. doi: 10.1038/tp.2012.17

Wieschollek, V., and Manahan-Vaughan, D. (2013a). Long-lasting changes in hippocampal synaptic plasticity and cognition in an animal model of NMDA receptor dysfunction in psychosis. *Neuropharmacology* 74, 48–58. doi: 10.1016/j.neuropharm.2013.01.001

Wieschollek, V., and Manahan-Vaughan, D. (2013b). Persistent deficits in hippocampal synaptic plasticity accompany losses of hippocampus-dependent memory in a rat model of psychosis. *Front. Integr. Neurosci.* 7:12. doi: 10.3389/fnint.2013.00012

Wlodarczyk, A. I., Sylantyev, S., Herd, M. B., Kersante, F., Lambert, J. J., Rusakov, D. A., et al. (2013). GABA-independent GABAA receptor openings maintain tonic currents. *J. Neurosci.* 33, 3905–3914. doi: 10.1523/JNEUROSCI.4193-12.2013

Wöhrl, R., Eisenach, S., Manahan-Vaughan, D., Heinemann, U., and von Haebler, D. (2007). Acute and long-term effects of MK801 on direct cortical input evoked homosynaptic and heterosynaptic plasticity in the CA1 region of the female rat. *Eur. J. Neurosci.* 26, 2873–2883. doi: 10.1111/j.1460-9568.2007.05899.x

Wozniak, D. F., Brosnan-Watters, G., Nardi, A., McEwen, M., Corso, T. D., Olney, J. W., et al. (1996). MK-801 neurotoxicity in male mice: histologic effects and

chronic impairment in spatial learning. *Brain Res.* 707, 165–179. doi: 10.1016/0006-8993(95)01230-3

Yin, D. M., Chen, Y. J., Sathyamurthy, A., Xiong, W. C., and Mei, L. (2012). Synaptic dysfunction in schizophrenia. *Adv. Exp. Med. Biol.* 970, 493–516. doi: 10.1007/978-3-7091-0932-8_22

Zemoura, K., Balakrishnan, K., Grampp, T., and Benke, D. (2018). Ca2+/Calmodulin-dependent protein kinase II (CaMKII) β-dependent phosphorylation of GABAB1 triggers lysosomal degradation of GABAB receptors via Mind Bomb-2 (MIB2)-mediated Lys-63-linked ubiquitination. *Mol. Neurobiol.* 56, 1293–1309. doi: 10.1007/s12035-018-1142-5

Zurawek, D., Salerno-Kochan, A., Dziedzicka-Wasylewska, M., Nikiforuk, A., Kos, T., and Popik, P. (2018). Changes in the expression of metabotropic glutamate receptor 5 (mGluR5) in a ketamine-based animal model of schizophrenia. *Schizophr. Res.* 192, 423–430. doi: 10.1016/j.schres.2017.04.014

Conflict of Interest Statement: The authors declare that the research was conducted in the absence of any commercial or financial relationships that could be construed as a potential conflict of interest.

frontiers in Behavioral Neuroscience

ORIGINAL RESEARCH
published: 13 June 2019
doi: 10.3389/fnbeh.2019.00122

Localized Connectivity in Obsessive-Compulsive Disorder: An Investigation Combining Univariate and Multivariate Pattern Analyses

Xinyu Hu[1], Lianqing Zhang[1], Xuan Bu[1], Hailong Li[1], Bin Li[2], Wanjie Tang[2], Lu Lu[1], Xiaoxiao Hu[1], Shi Tang[1], Yingxue Gao[1], Yanchun Yang[2], Neil Roberts[3], Qiyong Gong[1] and Xiaoqi Huang[1]**

[1]Huaxi MR Research Center (HMRRC), West China Hospital of Sichuan University, Chengdu, China, [2]Mental Health Center, West China Hospital of Sichuan University, Chengdu, China, [3]Clinical Research Imaging Centre (CRIC), The Queen's Medical Research Institute (QMRI), University of Edinburgh, Edinburgh, United Kingdom

Recent developments in psychoradiological researches have highlighted the disrupted organization of large-scale functional brain networks in obsessive-compulsive disorder (OCD). However, whether abnormal activation of localized brain areas would affect network dysfunction remains to be fully characterized. We applied both univariate analysis and multivariate pattern analysis (MVPA) approaches to investigate the abnormalities of regional homogeneity (ReHo), an index to measure the localized connectivity, in 88 medication-free patients with OCD and 88 healthy control subjects (HCS). Resting-state functional magnetic resonance imaging (RS-fMRI) data of all the participants were acquired in a 3.0-T scanner. First, we adopted a traditional univariate analysis to explore ReHo alterations between the patient group and the control group. Subsequently, we utilized a support vector machine (SVM) to examine whether ReHo could be further used to differentiate patients with OCD from HCS at the individual level. Relative to HCS, OCD patients showed lower ReHo in the bilateral cerebellum and higher ReHo in the bilateral superior frontal gyri (SFG), right inferior parietal gyrus (IPG), and precuneus [$P < 0.05$, family-wise error (FWE) correction]. ReHo value in the left SFG positively correlated with Yale–Brown Obsessive Compulsive Scale (Y-BOCS) total score ($r = 0$ 0.241, $P = 0.024$) and obsessive subscale ($r = 0.224$, $P = 0.036$). The SVM classification regarding ReHo yielded an accuracy of 78.98% (sensitivity = 78.41%, specificity = 79.55%) with $P < 0.001$ after permutation testing. The most discriminative regions contributing to the SVM classification were mainly located in the frontal, temporal, and parietal regions as well as in the cerebellum while the right orbital frontal cortex was identified with the highest discriminative power. Our findings not only suggested that the localized activation disequilibrium between the prefrontal cortex (PFC) and the cerebellum appeared to be associated with the pathophysiology of OCD but also indicated the translational role of the localized connectivity as a potential discriminative pattern to detect OCD at the individual level.

Keywords: obsessive-compulsive disorder, resting-state functional magnetic resonance imaging, psychoradiology, localized connectivity, regional homogeneity, univariate analysis, multivariate pattern analysis, support vector machine

OPEN ACCESS

Edited by:
Walter Adriani,
Istituto Superiore di Sanità (ISS), Italy

Reviewed by:
Gianfranco Spalletta,
Fondazione Santa Lucia (IRCCS), Italy
Marcelo Hoexter,
University of São Paulo, Brazil

****Correspondence:***
Qiyong Gong
qiyonggong@hmrrc.org.cn
Xiaoqi Huang
julianahuang@163.com

Received: *28 August 2018*
Accepted: *20 May 2019*
Published: *13 June 2019*

Citation:
Hu X, Zhang L, Bu X, Li H, Li B, Tang W, Lu L, Hu X, Tang S, Gao Y, Yang Y, Roberts N, Gong Q and Huang X (2019) Localized Connectivity in Obsessive-Compulsive Disorder: An Investigation Combining Univariate and Multivariate Pattern Analyses. Front. Behav. Neurosci. 13:122. doi: 10.3389/fnbeh.2019.00122

INTRODUCTION

Obsessive-compulsive disorder (OCD) is among the most debilitating mental illnesses that influence nearly 2.3% of the general population (Abramowitz et al., 2009). In spite of the high morbidity as well as high levels of social burden (Ruscio et al., 2010), the pathological mechanisms of OCD remain elusive. The investigation of the neurobiological substrates of OCD is a fundamental point to shed light upon the underlying mechanisms, which may be of great value in gaining insights into improving the specificity of diagnosis and efficacy of treatment for OCD.

Over the past decade, advanced magnetic resonance imaging (MRI) techniques have dramatically facilitated the comprehension of the neural correlates in OCD (Nakao et al., 2014). Previous review of voxel-based morphometry studies reported gray matter alterations of both "affective" and "executive" circuits in OCD patients (Piras et al., 2015). Meta-analysis of diffusion MRI literature consistently showed microstructural alterations of the fronto-basal pathways and intra-hemispheric bundles in OCD (Piras et al., 2013). Meanwhile, aberrant structural connectivity of left superior longitudinal fasciculus and the body of corpus callosum has been identified in patients with OCD, which was associated with executive control function (Spalletta et al., 2014). For functional MRI (fMRI) researches in OCD, patients show abnormal activation in several brain regions, which are essential for some domains of neuropsychological function such as decision making [ventromedial orbitofrontal cortex (OFC)] (Norman et al., 2018), error monitoring [amygdala, presupplementary motor area (preSMA), and subgenual anterior cingulate cortex] (Grützmann et al., 2016), response inhibition [inferior parietal gyrus (IPG), inferior frontal gyrus, and preSMA] (de Wit et al., 2012), reward-based learning (hippocampus, putamen, and amygdala; Marsh et al., 2015), fear conditioning (caudate and hippocampus) and extinction recall (cerebellum, posterior cingulate cortex, and putamen; Milad et al., 2013), cognitive flexibility [caudate and ventrolateral prefrontal cortex (PFC)], as well as goal-directed planning (putamen and dorsolateral PFC; Vaghi et al., 2017). The results obtained from these functional neuroimaging researches appear to be highly inconsistent, which might be attributed to clinical heterogeneity (e.g., symptom severity, onset age, illness duration, medication exposure, and comorbidity profiles) of OCD participants. More importantly, findings from task-based neuroimaging studies varied remarkably as different paradigms or analytic methods were adopted.

Resting-state fMRI (RS-fMRI) is a popular psychoradiological approach to assess the brain function at rest without performing a task (Lui et al., 2016). Two derived RS-fMRI parameters including the amplitude low-frequency flow-frequency (ALFF) and functional connectivity (FC) are widely adopted to explore the cerebral dysfunction in mental disorders. ALFF reflects the intensity of spontaneous neural activity while the FC reflects the level of integration of local activity across brain regions (Biswal et al., 1995; Gusnard and Raichle, 2001). Besides applying these two methods to explore the regional and network-level neural function of the brain, we can alternatively characterize the local synchronization of spontaneous blood oxygen level-dependent (BOLD) signal fluctuation among neighboring voxels within a given cluster, using an index named as regional homogeneity (ReHo; Zang et al., 2004). Given the hypothesis that similar temporal patterns are shared by spatially neighboring voxels, Kendall's coefficient of concordance (KCC) between the time series of a single voxel and those of its neighbors was calculated in the ReHo analysis using a voxel-wise manner. Considering the computational basis of this parameter, ReHo could be best described as an index of "localized connectivity," which gives the researchers a chance to discover the disruptions of localized activation in disease states without *a priori* constraints and makes it possible to investigate the previously unconsidered regional alterations (Iwabuchi et al., 2015).

Previous RS-fMRI studies using conventional mass-univariate analytical techniques for investigating the alterations of ReHo in OCD have suggested that there may be anomalies of localized connectivity in cortico-striato-limbic regions (Yang et al., 2010, 2015; Ping et al., 2013; Chen et al., 2016; Niu et al., 2017). One important limitation of these studies is the small sample sizes, which reduce sensitivity and presumably result in the lack of reliability of findings. Additionally, all these published mass-univariate researches investigating ReHo alterations between OCD participants and healthy control subjects (HCS) aim to test whether there are any effects in one or more brain regions, rather than to test whether the effects are large enough to have the translational importance for clinical utility.

Recently, the researchers have developed a growing interest in applying multivariate pattern analysis (MVPA) to develop brain signatures for clinical diagnoses in relevant mental disorders (Woo et al., 2017). Relative to traditional univariate analysis, the MVPA bears two strengths. First, MVPA takes the inter-correlation between voxels into consideration and thus might be more sensitive in detecting subtle and spatially distributed alterations. Second, MVPA allows statistical inferences at the single-subject level and thus could be used to make diagnostic decisions of individual patients (Vieira et al., 2017). Meanwhile, MVPA methods have been successfully used to differentiate OCD participants from control subjects based on diffusion MRI (Li et al., 2014), structural MRI (Hu et al., 2016), as well as task-based fMRI (Weygandt et al., 2012). However, no MVPA studies have investigated the utility of ReHo maps for distinguishing OCD subjects from HCS.

Therefore, we aimed to apply both univariate analysis and support vector machine (SVM) method to evaluate the alterations of ReHo in a relatively large sample of medication-free patients with OCD. The SVM discrimination algorithm is a widely used MVPA approach. In the SVM analysis, the data points are first projected into the high-dimensional space and subsequently classified based on the principle of maximizing the margin between categories (Orrù et al., 2012). The SVM classification process constitutes two procedures: training and testing. In the training stage, a decision boundary is identified by the SVM classifier to

separate the examples into the input space according to their class labels (i.e., OCD vs. HCS). In the testing phase, as soon as the optimized hyperplane is established from the training dataset, it can be utilized to make predictions for the class label of a new testing example to determine its generalizability (Noble, 2006). We hypothesized that the SVM analysis of the ReHo maps: (1) would potentially be able to discriminate individual patients with OCD from healthy controls; and (2) provided information on neurobiological changes that will potentially help to elucidate the mechanisms that cause OCD.

MATERIALS AND METHODS

Participants

All the subjects were right-handed individuals with ages between 18 and 60 years. Patients with OCD were enrolled from the West China Hospital of Sichuan University. The diagnosis of OCD was determined by three experienced clinical psychiatrists (YY, BL, and WT with 32, 18, and 11 years of experience in clinical psychiatry, respectively) by using the Structured Clinical Interview for *Diagnostic and Statistical Manual of Mental Disorders, Fourth Edition* (*DSM-IV*; Patient Edition) to exclude anxiety disorder, Tourette syndrome, major depressive disorder, schizophrenia, bipolar disorder, or any other axis I psychiatric comorbid disorders. The symptom severity of OCD was rated according to the Yale–Brown Obsessive Compulsive Scale (Y-BOCS). The anxiety symptom severity was assessed by the 14-item Hamilton Anxiety Scale (HAMA). The depressive symptom severity was evaluated based on the 17-item Hamilton Depression Scale (HAMD). All the patients with OCD experienced a washout period of 4 weeks from any treatment before the image data acquisition. Healthy controls were recruited by a poster and were screened using the structured clinical interview for DSM-IV axis I disorders (SCID) (non-patient edition) in order to ensure the absence of neurological and mental diseases. All the HCS reported that their first-degree relatives did not have a history of mental illness or neurological diseases. The exclusion criteria applied to both OCD patients and HCS were listed as follows: (1) the existence of neurological diseases or other mental disorders; (2) any history of cardiovascular diseases, metabolic disorders, or major physical illness; (3) alcohol or drug dependance; and (4) pregnancy. The above assessments were evaluated by two experienced psychiatrists. Written informed agreement was obtained from each participant before the research procedure was initiated. The Ethics Committee of West China Hospital approved the present study.

Resting-State Functional Magnetic Resonance Imaging Data Acquisition

All participants were subjected to MRI scanning using a 3.0-T GE Signa EXCITE scanner with an 8-channel phase array head coil. The RS-fMRI sensitized to alterations in BOLD signal levels of the whole brain was obtained *via* an echo-planar imaging (EPI) sequence. The parameters of scanning were listed as follows: repetition time (TR) = 2,000 ms, echo time (TE) = 30 ms, flip angle = 90°, slice thickness = 5 mm with no slice gap, field of view (FOV) = 240 × 240 mm^2, 30 axial slices, and 200 time points in each run. In the MRI examination, participants were informed to be relaxed and keep their eyes closed without falling asleep. Foam padding was used to reduce head motion while earplugs were used for reducing the scanner noise.

Image Preprocessing

The image preprocessing procedures including slice timing, head motion correction, and normalization (voxel size = 3 × 3 × 3 mm^3) to Montreal Neurological Institute (MNI) space were performed using the data processing and analysis for (resting-state) brain imaging (DPABI) software (Yan et al., 2016). For the purposes of removing head motion artifacts, we applied the Friston 24-parameter model in the current study as a regressor, which has been shown to be advantageous to the six-parameter model (Yan et al., 2013). All the image data used in the present study met the criteria of spatial movement in any direction <1.5 mm or 1.5° and the mean framewise displacement (FD) value <0.2. Signal from the cerebrospinal fluid, white matter, and global mean signal intensity was used as covariates for decreasing the effects of non-neuronal BOLD fluctuations. Afterward, we removed the linear trend of the fMRI images, and band-pass filtering (0.01–0.08 Hz) was performed in order to reduce the effect of physiological noise with high frequency as well as the extreme low-frequency drift. After that, we adopted the REST software (Song et al., 2011) for the calculation of the ReHo maps.

Regional Homogeneity Calculation

The ReHo map of each subject was created by the calculation of KCC regarding the time series between a single voxel with adjacent 26 voxels of its neighbors in a voxel-wise manner (Zang et al., 2004). Subsequently, the REST software used a whole-brain mask to eliminate the non-brain tissues for the aims of standardization, Afterwards, individual ReHo maps were divided using the average global KCC, and this procedure was achieved in the whole-brain mask. Finally, a Gaussian kernel with a full width at half maximum of 8 mm was adopted to spatial smoothing for all the individual standardized ReHo maps.

Univariate Analysis

We performed a univariate analysis for exploring alterations of localized connectivity by comparing ReHo maps between patients with OCD and HCS using the two-sample *t*-test in SPM8. Meanwhile, we conducted subgroup analysis in medication-naive OCD patients compared with matched HCS to test the reliability of the main effects. The voxel-level statistical threshold was set at $P < 0.001$ with a minimum cluster extent of 100 voxels without correction. Meanwhile, the statistical threshold of cluster level was set at $P < 0.05$ with family-wise error (FWE) correction. Regions with significant ReHo alterations between groups were extracted as region of interest for Pearson correlation analyses with clinical variables including illness duration, HAMA scores, HAMD scores, and symptom severity evaluated

by Y-BOCS and subscale scores in the SPSS software (SPSS 16.0; Chicago, IL, USA).

Multivariate Pattern Analysis Approach

The SVM classifier was adopted to evaluate the classification accuracy of local connectivity in distinguishing individuals with OCD from HCS, and this step was conducted by the PROBID package running in the Matlab. The SVM approaches have been described in detail elsewhere (Li et al., 2014; Hu et al., 2016) and are briefly summarized here. Individual RS-fMRI images were regarded as points situated in a high-dimensional interspace defined by the ReHo maps in the preprocessed images. The SVM classifier identified a linear decision boundary to separate individual brain maps in a high-dimensional space based on the category label. The optimized hyperplane was computed on the basis of the whole multivariate pattern of the ReHo map across each RS-fMRI scan. For the purposes of lowering the risk of data overfitting and allowing direct extraction of the weight vector, the linear kernel SVM was applied. Additionally, we utilized a leave-one-out cross-validation (LOOCV) strategy to evaluate the performance of the SVM classifier. This LOOCV approach excluded an independent individual from each group and used the rest of the participants to train the SVM classifier. Then, the excluded subject pair was applied to test the differentiating ability of SVM to reliably discriminate between two sorts. We used a nonparametric test to determine the statistical significance of the general accuracy of discrimination, specifically, the nonparametric test repeated the classification step 1,000 times using permutation test of the labels in the training group and computed the specificity and sensitivity in respect to the true labels. Ultimately, the PROBID software generated the discriminative maps to display the relative contributions of each voxel to the SVM classification decision. We overlaid the voxels with top 30% of the maximum weighted value onto the brain template with high resolution (Mourão-Miranda et al., 2005).

RESULTS

A total of 88 participants with OCD and 88 gender- and age-matched control subjects were employed in the current study. Among them, 54 OCD patients and 54 control subjects were included in a previous analysis (Bu et al., 2019). **Table 1** displays the clinical characteristics and demographic information of all the subjects. No significant differences were identified with respect to gender (P = 1.000) and age (P = 0.381) between OCD patients and HCS. The mean (standard deviation) scores of Y-BOCS, HAMD, and HAMA were 21.47 (±5.38), 8.74 (±4.92), and 8.78 (±4.46), respectively. The illness duration of the OCD patient group was 7.32 ± 5.58 years.

Relative to HCS, OCD patients showed lower ReHo in the bilateral cerebellum and higher ReHo in the bilateral superior frontal gyri (SFG), right IPG, and precuneus ($P < 0.05$, with FWE correction at the cluster level; **Table 2**, **Figures 1**, **2**). The results regarding subgroup analysis of medication-naive OCD patients remained reproducible with the main effect (**Supplementary Figure S1**). The ReHo value in the left SFG positively correlated with Y-BOCS total score (r = 0.241, P = 0.024) and obsessive subscale (r = 0.224, P = 0.036; **Figure 3**). No significant correlations were identified between altered ReHo and any other clinical characteristics in OCD patients.

The plotting for SVM classification using ReHo maps are presented in **Figure 4** (left). The receiver operating characteristic (ROC) curve assessing the performance of the SVM classifier based on ReHo maps is displayed in **Figure 4** (right).

Based on the SVM classification approach, the diagnostic accuracy of ReHo maps for the contrast between OCD and

TABLE 1 | Clinical characteristics and demographic information for patients with obsessive-compulsive disorder (OCD) and healthy control subjects (HCS).

Characteristic	OCD (n = 88)		HCS (n = 88)		Significance	
	Mean	SD	Mean	SD	t/χ^2	P
Gender (male:female)	56:32	-	56:32	-	0.000	1.000
Age (years)	29.16	8.71	27.88	10.58	0.879	0.381
Duration of illness (years)	7.32	5.58	-	-	-	-
Age of onset	21.84	7.09	-	-	-	-
Y-BOCS total	21.47	5.38	-	-	-	-
Obsessions	13.15	5.07	-	-	-	-
Compulsions	8.32	5.35	-	-	-	-
HAMD 17	8.74	4.92	-	-	-	-
HAMA 14	8.78	4.46	-	-	-	-
Current treatment status	*n*	%				
Drug-free (>4 weeks)	88	100	-	-	-	-
Medication-naive	74	88.09	-	-	-	-
Previous treatment history	*n*	%	-	-	-	-
Clomipramine	4	4.55	-	-	-	-
Paroxetine	3	3.41	-	-	-	-
Fluoxetine	3	3.41	-	-	-	-
Sertraline	3	3.41	-	-	-	-
Quetiapine	1	1.14	-	-	-	-

Abbreviations: HAMA, Hamilton Anxiety Rating Scale; HAMD, Hamilton Depression Rating Scale; HCS, healthy control subjects; OCD, obsessive-compulsive disorder; SD, standard deviation; Y-BOCS, Yale–Brown Obsessive Compulsive Scale.

TABLE 2 | Significant differences of regional homogeneity (ReHo) alterations in OCD patients compared with HCS.

Region	Side	Voxel size	MNI coordinate			*T*	*P**
			x	*y*	*z*		
OCD patients > HCS							
Superior frontal gyrus	R	274	15	15	66	6.35	0.001
			15	27	60	5.55	
			9	9	69	5.37	
Inferior parietal gyrus	R	407	57	−60	39	6.25	<0.001
			63	−54	33	5.46	
			63	−54	24	5.39	
Precuneus	L/R	139	9	−69	57	5.13	0.018
			−9	−78	48	3.33	
			−6	−78	39	3.20	
Superior frontal gyrus	L	591	−12	0	72	5.10	<0.001
			−42	6	54	5.07	
			−48	36	12	5.06	
OCD patients < HCS							
Cerebellum	R	357	15	−51	−27	−5.20	<0.001
			6	−27	−15	−3.86	
Cerebellum	L	117	−18	−48	−27	−4.55	0.031
			−9	−60	−21	−4.04	

**P < 0.05 set at cluster level with whole-brain family-wise error correction. Abbreviations: HCS, healthy control subjects; MNI, Montreal Neurological Institute; OCD, obsessive-compulsive disorder; ReHo, regional homogeneity.*

HCS was 78.98% (sensitivity = 78.41% and specificity = 79.55%, $P < 0.001$). The most discriminative regions contributing to the SVM classification regarding ReHo were mainly located in frontal, temporal, and parietal regions as well as the cerebellum while the right OFC was identified with the highest discriminative power. The details concerning the brain areas that contributed to distinguishing OCD participants from controls are displayed in **Table 3** and **Figure 5**.

DISCUSSION

The current study applied both univariate analysis and MVPA approach to explore the alterations of ReHo in a relatively large cohort of medication-free patients with OCD. Our study revealed that OCD patients showed lower ReHo in the bilateral cerebellum and higher ReHo in the frontoparietal regions compared with HCS. ReHo value in the left SFG positively correlated with symptom severity. Additionally, OCD patients could be differentiated from HCS using SVM based on ReHo maps with high classification accuracy (78.98%, $P < 0.001$). Brain regions including the frontolimbic circuit, the temporo-parietal areas, and the cerebellum were identified to have high differentiating power. Meanwhile, both univariate analysis and MVPA approach detected abnormalities of frontoparietal regions and cerebellum in OCD based on ReHo maps.

The PFC has long been recognized to be a paramount part in the mediation of clinical manifestations including executive disturbance, low behavioral flexibility, and inability for decision making that are commonly observed in OCD patients (Chamberlain et al., 2008; Menzies et al., 2008; Samara et al., 2017). Furthermore, Ahmari et al. (2013) used optogenetics to prove that repeated stimulation of the OFC in mice would lead to persistent OCD-like behaviors. In agreement with findings from previous ReHo studies of OCD (Ping et al., 2013; Yang et al., 2015; Chen et al., 2016), the current study revealed higher ReHo in the bilateral SFG in OCD patients compared with HCS. Meanwhile, the right OFC was identified as the brain region that provided the greatest potential to discriminate OCD from HCS based on the MVPA approach. Thus, an abnormal hyperactivation in PFC might be related to the pathophysiological process of OCD. Additionally, the increased ReHo value in the left SFG was positively correlated with the Y-BOCS and obsession subscale scores. This finding indicated that ReHo might be an optimal measure for capturing the disease severity.

Neither univariate analysis nor MVPA revealed ReHo alterations of the striatum in OCD patients, which is inconsistent with evidence from meta- and mega-analyses of structural and functional neuroimaging studies (Menzies et al., 2008; Radua and Mataix-Cols, 2009; Rotge et al., 2010; Boedhoe et al., 2017). The striatum has long been regarded as a key hub for symptom mediation in OCD (Pauls et al., 2014) and recent evidence has suggested the striatum as a promising site for deep brain stimulation treatment of OCD (Pinhal et al., 2018). Two previous studies identified that OCD patients showed decreased ReHo in the caudate nucleus (Ping et al., 2013; Yang et al., 2015), which seemed to be inconsistent with the present finding. Several reasons might account for the discrepancies. First, there were more OCD participants enrolled in the present study than in the previous ReHo studies (Ping et al., 2013; Yang et al., 2015). The large sample size of the current study increased the power to detect potential localized functional disruptions in OCD and minimized the risk of false-positive findings. Second, clinical cohorts in previous ReHo studies included OCD patients who were being treated using serotonin reuptake inhibitors while all the subjects with OCD of our research were medication-free. This is especially relevant, given the report by Beucke et al. (2013) that antidepressant medication may reduce network-level neural function of cortico-striato-thalamo-cortical (CSTC) circuits in OCD. Third, two recent

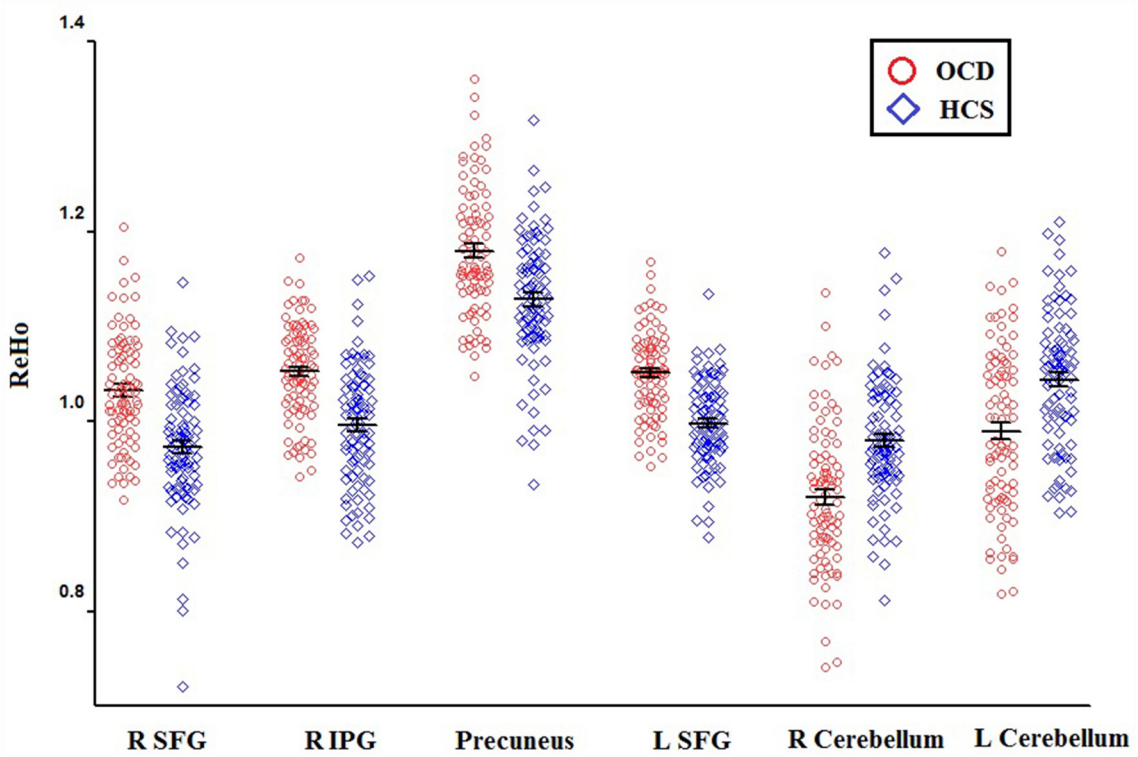

FIGURE 1 | The distributions of ReHo eigenvalue in six brain areas with altered ReHo in OCD patients relative to HCS. Abbreviations: HCS, healthy control subjects; IPG, inferior parietal gyrus; OCD, obsessive-compulsive disorder; ReHo, regional homogeneity; SFG, superior frontal gyrus.

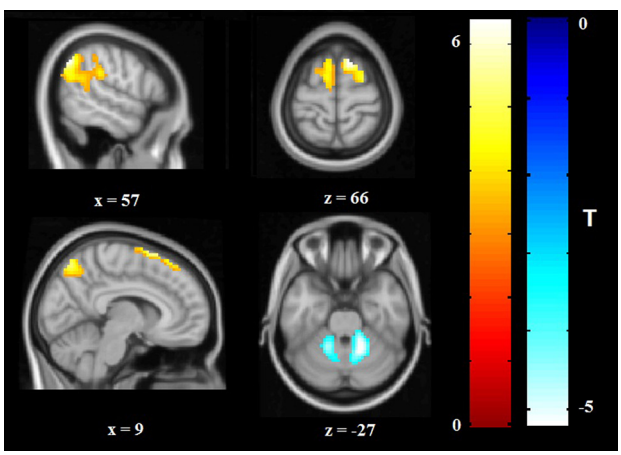

FIGURE 2 | Altered ReHo in OCD patients compared with HCS. ReHo increases are indicated in warm colors while ReHo reductions are indicated in cool colors. Abbreviations: HCS, healthy control subjects; OCD, obsessive-compulsive disorder; ReHo, regional homogeneity.

multicenter studies of 780 brain scans reported no structural alterations of striatum in OCD patients (de Wit et al., 2014; Fouche et al., 2017). Therefore, striatum may not directly relate to the pathophysiology of OCD, but be secondary to current medication use. Further longitudinal studies would be needed to clarify this hypothesis.

Both univariate analysis and MVPA demonstrated cerebellar dysfunction of OCD patients compared with healthy controls. The cerebellum has been identified to integrate the information flow of prefrontal-basal ganglia pathway as it is functionally and anatomically connected to the CSTC network (Middleton and Strick, 2000). Furthermore, an increasing number of evidence has reported that, besides the traditional role of motor control, the primate cerebellum is involved in cognitive control and emotional regulation (Ramnani, 2006). For example, the cerebellar hypoactivation in OCD patients was observed when fear conditioning tasks were performed (Milad et al., 2013), which was consistent with our current finding. Interestingly, a recent multicenter voxel based morphometry (VBM) mega-analysis reported smaller volumes of PFC and greater cerebellar gray matter volume bilaterally (de Wit et al., 2014), but our study found higher ReHo in the bilateral SFG and lower ReHo in the bilateral cerebellum. The opposite findings might suggest a functional compensatory response to regional anatomical alterations in OCD. Given all the OCD participants were treatment-free in the current study, we proposed that the activation disequilibrium between the PFC and the cerebellum might directly be associated with the psychopathology of OCD.

In addition to the significant cerebellar dysfunction, it is of special interest to find the involvement of parietal (including IPG and precuneus) and temporal regions with disrupted localized connectivity in patients with OCD

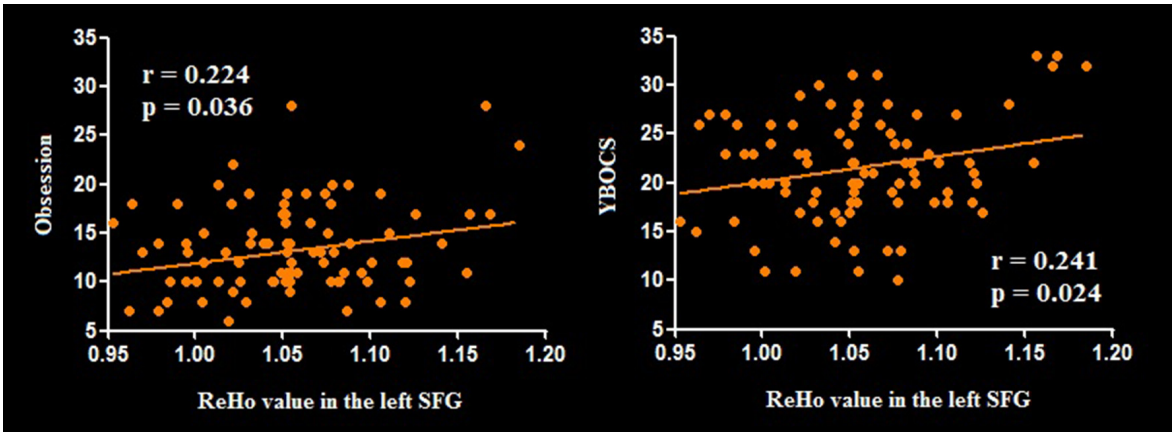

FIGURE 3 | Pearson correlation exhibiting positive association between ReHo in the left SFG and YBOCS as well as obsessive subscale scores in the OCD group. Abbreviations: OCD, obsessive-compulsive disorder; ReHo, regional homogeneity; SFG, superior frontal gyrus; YBOCS, Yale–Brown Obsessive Compulsive Scale.

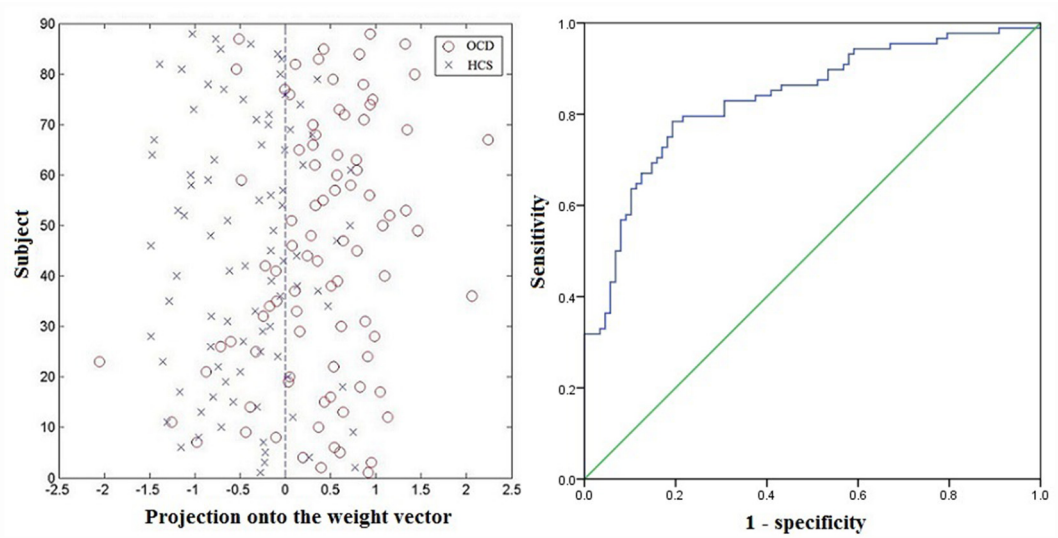

FIGURE 4 | Classification plot (left) and receiver operating characteristic (ROC) curve (right) for differentiating patients with OCD from HCS based on ReHo maps, yielding an accuracy of 78.98% (sensitivity = 78.41%, specificity = 79.55%, $P < 0.001$). Abbreviations: HCS, healthy control subjects; OCD, obsessive-compulsive disorder; ReHo, regional homogeneity.

compared to healthy volunteers, which is consistent with the reports of the engagement of the extended OCD anatomical model (Gürsel et al., 2018). Previous systematic review of structural neuroimaging studies had emphasized that the neural mechanism of OCD might involve more widespread regions such as parietal and temporal cortices, which may help explain the heterogeneity in clinical manifestations of OCD (Piras et al., 2013). By integrating evidence from functional neuroimaging and neuropsychological tests, Menzies et al. (2008) suggested the parietal cortex as a fundamental area outside the classical orbitofronto-striatal circuit in the psychopathology of OCD. Moreover, altered anatomical connectivity between lateral frontal and parietal regions is consistently identified in the meta-analysis of diffusion tensor imaging studies (Piras et al., 2015). The parietal activation may be related to emotion processing (Margulies et al., 2009) and decision making (Huk et al., 2017), which are also reported to be impaired in OCD patients. Meanwhile, de Vries et al. (2014) suggested that the compensatory activity of frontoparietal network (FPN) during working memory might constitute a neurocognitive endophenotype for OCD. The precuneus and temporal cortices are major components of the default mode network (DMN; Raichle, 2015). A recent task-based fMRI meta-analysis has demonstrated that OCD symptom severity was related to increased activation in the precuneus (Thorsen et al., 2018). Evidence from cognitive studies has demonstrated that temporal regions are involved in impairment of inhibitory control (Penadés et al., 2007) and

TABLE 3 | Brain areas that differentiated OCD patients from HCS based on ReHo maps.

Brain areas (SVM)	Coordinates (MNI)			w_i
	x	*y*	*z*	
OCD patients > HCS				
R orbit frontal	5	53	−19	17.18
OCD patients > HCS				
R cerebellum	50	−67	−46	−12.88
Vermis	5	−73	−37	−11.39
R inferior temporal	38	2	−40	−11.01
R middle temporal	23	2	−40	−10.88
R middle temporal	71	−34	−4	−12.69
R transverse temporal	62	−13	8	−12.28
L middle temporal	−45	−64	23	−13.26
Dorsal anterior cingulate	1	−13	38	−11.42
R inferior parietal	50	−46	54	−10.57

These areas were identified by setting the threshold to the top 30% of the weight vector scores. Abbreviations: HCS, healthy control subjects; MNI, Montreal Neurological Institute; OCD, obsessive-compulsive disorder; ReHo, regional homogeneity; SVM, support vector machine; w_i, weight of each cluster centroid i.

executive planning (van den Heuvel et al., 2005) in OCD. Research using graph theory analysis revealed decreased local efficiency and reduced intra-connectivity of DMN in OCD patients relative to HCS (Peng et al., 2014). Since the IPG is reported as an important node in both the FPN and the DMN (Boedhoe et al., 2018) while our present study identified higher ReHo in the IPG, we speculated that the parietal hyperactivation might contribute to the underlying mechanism of OCD.

The current research had some limitations. First, although our results were encouraging, multicenter research is still needed for testing the generalizability of the current findings. Second, we recruited drug-free OCD patients who went through a 4-week medication washout period before the MRI data acquisition. Therefore, we could not rule out the longer-term effects of treatment on the localized functional disruptions. Third, we only compared patients with OCD and HCS in the current investigation, Thus, it remained unknown whether the SVM classification of ReHo maps would distinguish OCD subjects from participants with different psychiatric disorders. Future investigations could address this issue by evaluating the discrimination accuracy of SVM classifier in differentiating OCD from other anxiety disorders (i.e., Tourette syndrome). Fourth, we did not recruit pediatric OCD patients in this study. Recent studies have identified distinct cortical and subcortical alterations in pediatric and adult OCD (Boedhoe et al., 2017, 2018; Hu et al., 2017). Future studies should involve pediatric OCD patients in order to provide an insight into the neurodevelopmental alterations in this disorder. Fifth, we did not evaluate the possible effect of comorbid apathy in the current study. Previous evidence indicated that apathy could modulate the microstructure of bundles related to OCD (Spalletta et al., 2013). Future investigations should adopt the Apathy Rating Scale to assess the apathetic conditions in OCD patients. Finally, we failed to perform separate analyses for childhood onset OCD and adulthood onset OCD since there were much fewer childhood onset OCD patients (n = 18) than adulthood onset OCD patients (n = 70). A recent world-wide mega-analysis reinforced the effects of onset age in the neural mechanism of OCD (Boedhoe et al., 2017). Thus, illustrating the differences of ReHo alterations between childhood onset OCD patients and adulthood onset OCD patients is still warranted.

In summary, our univariate analysis provided evidence that localized activation disequilibrium between the PFC and the cerebellum appeared to be associated with the pathophysiology of OCD. Additionally, positive correlations between ReHo

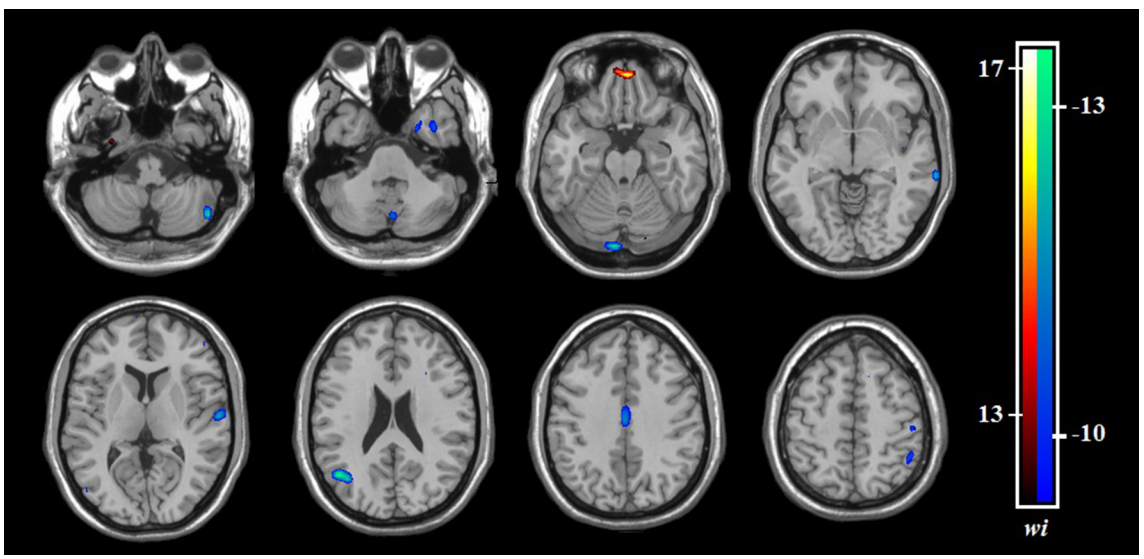

FIGURE 5 | The discrimination maps for ReHo. These areas were identified by setting the threshold to the top 30% of weight vector scores. Warm colors indicated higher discriminated values for OCD subjects than HCS. Cool colors indicate lower discriminated values for OCD participants than HCS. Abbreviations: HCS, healthy control subjects; OCD, obsessive-compulsive disorder; ReHo, regional homogeneity.

in left SFG and symptom severity were identified, which suggested that ReHo might be a paramount measure for studying the underlying cause of OCD. Furthermore, the SVM analysis of ReHo achieved modest accuracy (79.0%, $P < 0.001$) in classifying OCD patients and HCS at the individual level, which indicated the translational role of the localized connectivity as a potential psychoradiological biomarker for OCD diagnosis.

ETHICS STATEMENT

The study was approved by the Research Ethics Committee of the West China Hospital, Sichuan University, and written informed consent was obtained from each participant.

AUTHOR CONTRIBUTIONS

XQH, QG, and YY designed the study. XYH, BL, and WT acquired the data. XYH, LZ, XB, and HL analyzed the data. XQH, NR, XYH, and QG wrote the article, which BL, WT, LZ, XB, HL, LL, XXH, ST, YG, and YY reviewed. All authors approved the final version for publication.

FUNDING

This study was supported by the National Natural Science Foundation (Grant No. 81030027, 81171488, 81227002, 81671669, 81621003, 81761128023 and 81820108018), the Sichuan Provincial Youth Grant (Grant No. 2017JQ0001), the Programme for Changjiang Scholars and Innovative Research Team in University (PCSIRT, Grant No. IRT16R52) of China and the Post-Doctoral Interdisciplinary Research Project of Sichuan University.

ACKNOWLEDGMENTS

QG would like to acknowledge his Visiting Adjunct Professor appointment in the Department of Psychiatry at the Yale School of Medicine, Yale University, New Haven, CT, USA.

SUPPLEMENTARY MATERIAL

The Supplementary Material for this article can be found online at: https://www.frontiersin.org/articles/10.3389/fnbeh.2019.00122/full#supplementary-material

REFERENCES

Abramowitz, J. S., Taylor, S., and McKay, D. (2009). Obsessive-compulsive disorder. *Lancet* 374, 491–499. doi: 10.1016/S0140-6736(09)60240-3

Ahmari, S. E., Spellman, T., Douglass, N. L., Kheirbek, M. A., Simpson, H. B., Deisseroth, K., et al. (2013). Repeated cortico-striatal stimulation generates persistent OCD-like behavior. *Science* 340, 1234–1239. doi: 10.1126/science.1234733

Beucke, J. C., Sepulcre, J., Talukdar, T., Linnman, C., Zschenderlein, K., Endrass, T., et al. (2013). Abnormally high degree connectivity of the orbitofrontal cortex in obsessive-compulsive disorder. *JAMA Psychiatry* 70, 619–629. doi: 10.1001/jamapsychiatry.2013.173

Biswal, B., Yetkin, F. Z., Haughton, V. M., and Hyde, J. S. (1995). Functional connectivity in the motor cortex of resting human brain using echo-planar MRI. *Magn. Reson. Med.* 34, 537–541. doi: 10.1002/mrm.1910340409

Boedhoe, P. S. W., Schmaal, L., Abe, Y., Alonso, P., Ameis, S. H., Anticevic, A., et al. (2018). Cortical abnormalities associated with pediatric and adult obsessive-compulsive disorder: findings from the ENIGMA obsessive-compulsive disorder working group. *Am. J. Psychiatry* 175, 453–462. doi: 10.1176/appi.ajp.2017.17050485

Boedhoe, P. S., Schmaal, L., Abe, Y., Ameis, S. H., Arnold, P. D., Batistuzzo, M. C., et al. (2017). Distinct subcortical volume alterations in pediatric and adult OCD: a worldwide meta- and mega-analysis. *Am. J. Psychiatry* 174, 60–69. doi: 10.1176/appi.ajp.2016.16020201

Bu, X., Hu, X., Zhang, L., Li, B., Zhou, M., Lu, L., et al. (2019). Investigating the predictive value of different resting-state functional MRI parameters in obsessive-compulsive disorder. *Transl. Psychiatry* 9:17. doi: 10.1038/s41398-018-0362-9

Chamberlain, S. R., Menzies, L., Hampshire, A., Suckling, J., Fineberg, N. A., del Campo, N., et al. (2008). Orbitofrontal dysfunction in patients with obsessive-compulsive disorder and their unaffected relatives. *Science* 321, 421–422. doi: 10.1126/science.1154433

Chen, Y., Meng, X., Hu, Q., Cui, H., Ding, Y., Kang, L., et al. (2016). Altered resting-state functional organization within the central executive network in obsessive-compulsive disorder. *Psychiatry Clin. Neurosci.* 70, 448–456. doi: 10.1111/pcn.12419

de Vries, F. E., de Wit, S. J., Cath, D. C., van der Werf, Y. D., van der Borden, V., van Rossum, T. B., et al. (2014). Compensatory frontoparietal activity during working memory: an endophenotype of obsessive-compulsive disorder. *Biol. Psychiatry* 76, 878–887. doi: 10.1016/j.biopsych.2013.11.021

de Wit, S. J., Alonso, P., Schweren, L., Mataix-Cols, D., Lochner, C., Menchon, J. M., et al. (2014). Multicenter voxel-based morphometry mega-analysis of structural brain scans in obsessive-compulsive disorder. *Am. J. Psychiatry* 171, 340–349. doi: 10.1176/appi.ajp.2013.13040574

de Wit, S. J., de Vries, F. E., van der Werf, Y. D., Cath, D. C., Heslenfeld, D. J., Veltman, E. M., et al. (2012). Presupplementary motor area hyperactivity during response inhibition: a candidate endophenotype of obsessive-compulsive disorder. *Am. J. Psychiatry* 169, 1100–1108. doi: 10.1176/appi.ajp.2012.12010073

Fouche, J. P., du Plessis, S., Hattingh, C., Roos, A., Lochner, C., Soriano-Mas, C., et al. (2017). Cortical thickness in obsessive-compulsive disorder: multisite mega-analysis of 780 brain scans from six centres. *Br. J. Psychiatry* 210, 67–74. doi: 10.1192/bjp.bp.115.164020

Grützmann, R., Endrass, T., Kaufmann, C., Allen, E., Eichele, T., and Kathmann, N. (2016). Presupplementary motor area contributes to altered error monitoring in obsessive-compulsive disorder. *Biol. Psychiatry* 80, 562–571. doi: 10.1016/j.biopsych.2014.12.010

Gürsel, D. A., Avram, M., Sorg, C., Brandl, F., and Koch, K. (2018). Frontoparietal areas link impairments of large-scale intrinsic brain networks with aberrant fronto-striatal interactions in OCD: a meta-analysis of resting-state functional connectivity. *Neurosci. Biobehav. Rev.* 87, 151–160. doi: 10.1016/j.neubiorev.2018.01.016

Gusnard, D. A., and Raichle, M. E. (2001). Searching for a baseline: functional imaging and the resting human brain. *Nat. Rev. Neurosci.* 2, 685–694. doi: 10.1038/35094500

Hu, X., Du, M., Chen, L., Li, L., Zhou, M., Zhang, L., et al. (2017). Meta-analytic investigations of common and distinct grey matter alterations in youths and adults with obsessive-compulsive disorder. *Neurosci. Biobehav. Rev.* 78, 91–103. doi: 10.1016/j.neubiorev.2017.04.012

Hu, X., Liu, Q., Li, B., Tang, W., Sun, H., Li, F., et al. (2016). Multivariate pattern analysis of obsessive-compulsive disorder using structural neuroanatomy. *Eur. Neuropsychopharmacol.* 26, 246–254. doi: 10.1016/j.euroneuro.2015.12.014

Huk, A. C., Katz, L. N., and Yates, J. L. (2017). The role of the lateral intraparietal area in (the study of) decision making. *Annu. Rev. Neurosci.* 40, 349–372. doi: 10.1146/annurev-neuro-072116-031508

Iwabuchi, S. J., Krishnadas, R., Li, C., Auer, D. P., Radua, J., and Palaniyappan, L. (2015). Localized connectivity in depression: a meta-analysis of resting state functional imaging studies. *Neurosci. Biobehav. Rev.* 51, 77–86. doi: 10.1016/j.neubiorev.2015.01.006

Li, F., Huang, X., Tang, W., Yang, Y., Li, B., Kemp, G. J., et al. (2014). Multivariate pattern analysis of DTI reveals differential white matter in individuals with obsessive-compulsive disorder. *Hum. Brain Mapp.* 35, 2643–2651. doi: 10.1002/hbm.22357

Lui, S., Zhou, X. J., Sweeney, J. A., and Gong, Q. (2016). Psychoradiology: the frontier of neuroimaging in psychiatry. *Radiology* 281, 357–372. doi: 10.1148/radiol.2016152149

Margulies, D. S., Vincent, J. L., Kelly, C., Lohmann, G., Uddin, L. Q., Biswal, B. B., et al. (2009). Precuneus shares intrinsic functional architecture in humans and monkeys. *Proc. Natl. Acad. Sci. U S A* 106, 20069–20074. doi: 10.1073/pnas.0905314106

Marsh, R., Tau, G. Z., Wang, Z., Huo, Y., Liu, G., Hao, X., et al. (2015). Reward-based spatial learning in unmedicated adults with obsessive-compulsive disorder. *Am. J. Psychiatry* 172, 383–392. doi: 10.1176/appi.ajp.2014.13121700

Menzies, L., Chamberlain, S. R., Laird, A. R., Thelen, S. M., Sahakian, B. J., and Bullmore, E. T. (2008). Integrating evidence from neuroimaging and neuropsychological studies of obsessive-compulsive disorder: the orbitofronto-striatal model revisited. *Neurosci. Biobehav. Rev.* 32, 525–549. doi: 10.1016/j.neubiorev.2007.09.005

Middleton, F. A., and Strick, P. L. (2000). Basal ganglia output and cognition: evidence from anatomical, behavioral and clinical studies. *Brain Cogn.* 42, 183–200. doi: 10.1006/brcg.1999.1099

Milad, M. R., Furtak, S. C., Greenberg, J. L., Keshaviah, A., Im, J. J., Falkenstein, M. J., et al. (2013). Deficits in conditioned fear extinction in obsessive-compulsive disorder and neurobiological changes in the fear circuit. *JAMA Psychiatry* 70, 608–618. doi: 10.1001/jamapsychiatry.2013.914

Mourão-Miranda, J., Bokde, A. L., Born, C., Hampel, H., and Stetter, M. (2005). Classifying brain states and determining the discriminating activation patterns: support vector machine on functional MRI data. *Neuroimage* 28, 980–995. doi: 10.1016/j.neuroimage.2005.06.070

Nakao, T., Okada, K., and Kanba, S. (2014). Neurobiological model of obsessive-compulsive disorder: evidence from recent neuropsychological and neuroimaging findings. *Psychiatry Clin. Neurosci.* 68, 587–605. doi: 10.1111/pcn.12195

Niu, Q., Yang, L., Song, X., Chu, C., Liu, H., Zhang, L., et al. (2017). Abnormal resting-state brain activities in patients with first-episode obsessive-compulsive disorder. *Neuropsychiatr. Dis. Treat.* 13, 507–513. doi: 10.2147/NDT.s117510

Noble, W. S. (2006). What is a support vector machine? *Nat. Biotechnol.* 24, 1565–1567. doi: 10.1038/nbt1206-1565

Norman, L. J., Carlisi, C. O., Christakou, A., Murphy, C. M., Chantiluke, K., Giampietro, V., et al. (2018). Frontostriatal dysfunction during decision making in attention-deficit/hyperactivity disorder and obsessive-compulsive disorder. *Biol. Psychiatry Cogn. Neurosci. Neuroimaging* 3, 694–703. doi: 10.1016/j.bpsc.2018.03.009

Orrù, G., Pettersson-Yeo, W., Marquand, A. F., Sartori, G., and Mechelli, A. (2012). Using support vector machine to identify imaging biomarkers of neurological and psychiatric disease: a critical review. *Neurosci. Biobehav. Rev.* 36, 1140–1152. doi: 10.1016/j.neubiorev.2012.01.004

Pauls, D. L., Abramovitch, A., Rauch, S. L., and Geller, D. A. (2014). Obsessive-compulsive disorder: an integrative genetic and neurobiological perspective. *Nat. Rev. Neurosci.* 15, 410–424. doi: 10.1038/nrn3746

Penadés, R., Catalán, R., Rubia, K., Andrés, S., Salamero, M., and Gasto, C. (2007). Impaired response inhibition in obsessive compulsive disorder. *Eur. Psychiatry* 22, 404–410. doi: 10.1016/j.eurpsy.2006.05.001

Peng, Z., Shi, F., Shi, C., Yang, Q., Chan, R. C., and Shen, D. (2014). Disrupted cortical network as a vulnerability marker for obsessive-compulsive disorder. *Brain Struct. Funct.* 219, 1801–1812. doi: 10.1007/s00429-013-0602-y

Ping, L., Su-Fang, L., Hai-Ying, H., Zhang-Ye, D., Jia, L., Zhi-Hua, G., et al. (2013). Abnormal spontaneous neural activity in obsessive-compulsive disorder: a resting-state functional magnetic resonance imaging study. *PLoS One* 8:e67262. doi: 10.1371/journal.pone.0067262

Pinhal, C. M., van den Boom, B. J. G., Santana-Kragelund, F., Fellinger, L., Bech, P., Hamelink, R., et al. (2018). Differential effects of deep brain stimulation of the internal capsule and the striatum on excessive grooming in Sapap3 mutant mice. *Biol. Psychiatry* 84, 917–925. doi: 10.1016/j.biopsych.2018.05.011

Piras, F., Caltagirone, C., and Spalletta, G. (2013). Brain circuitries of obsessive compulsive disorder: a systematic review and meta-analysis of diffusion tensor imaging studies. *Neurosci. Biobehav. Rev.* 37, 2856–2877. doi: 10.1016/j.neubiorev.2013.10.008

Piras, F., Chiapponi, C., Girardi, P., Caltagirone, C., and Spalletta, G. (2015). Widespread structural brain changes in OCD: a systematic review of voxel-based morphometry studies. *Cortex* 62, 89–108. doi: 10.1016/j.cortex.2013.01.016

Radua, J., and Mataix-Cols, D. (2009). Voxel-wise meta-analysis of grey matter changes in obsessive-compulsive disorder. *Br. J. Psychiatry* 195, 393–402. doi: 10.1192/bjp.bp.108.055046

Raichle, M. E. (2015). The brain's default mode network. *Annu. Rev. Neurosci.* 38, 433–447. doi: 10.1146/annurev-neuro-071013-014030

Ramnani, N. (2006). The primate cortico-cerebellar system: anatomy and function. *Nat. Rev. Neurosci.* 7, 511–522. doi: 10.1038/nrn1953

Rotge, J. Y., Langbour, N., Guehl, D., Bioulac, B., Jaafari, N., Allard, M., et al. (2010). Gray matter alterations in obsessive-compulsive disorder: an anatomic likelihood estimation meta-analysis. *Neuropsychopharmacology* 35, 686–691. doi: 10.1038/npp.2009.175

Ruscio, A. M., Stein, D. J., Chiu, W. T., and Kessler, R. C. (2010). The epidemiology of obsessive-compulsive disorder in the National Comorbidity Survey Replication. *Mol. Psychiatry* 15, 53–63. doi: 10.1038/mp.2008.94

Samara, Z., Evers, E. A. T., Goulas, A., Uylings, H. B. M., Rajkowska, G., Ramaekers, J. G., et al. (2017). Human orbital and anterior medial prefrontal cortex: intrinsic connectivity parcellation and functional organization. *Brain Struct. Funct.* 222, 2941–2960. doi: 10.1007/s00429-017-1378-2

Song, X. W., Dong, Z. Y., Long, X. Y., Li, S. F., Zuo, X. N., Zhu, C. Z., et al. (2011). REST: a toolkit for resting-state functional magnetic resonance imaging data processing. *PLoS One* 6:e25031. doi: 10.1371/journal.pone.0025031

Spalletta, G., Fagioli, S., Caltagirone, C., and Piras, F. (2013). Brain microstructure of subclinical apathy phenomenology in healthy individuals. *Hum. Brain Mapp.* 34, 3193–3203. doi: 10.1002/hbm.22137

Spalletta, G., Piras, F., Fagioli, S., and Caltagirone, C. (2014). Brain microstructural changes and cognitive correlates in patients with pure obsessive compulsive disorder. *Brain Behav.* 4, 261–277. doi: 10.1002/brb3.212

Thorsen, A. L., Hagland, P., Radua, J., Mataix-Cols, D., Kvale, G., Hansen, B., et al. (2018). Emotional processing in obsessive-compulsive disorder: a systematic review and meta-analysis of 25 functional neuroimaging studies. *Biol. Psychiatry Cogn. Neurosci. Neuroimaging* 3, 563–571. doi: 10.1016/j.bpsc.2018.01.009

Vaghi, M. M., Vértes, P. E., Kitzbichler, M. G., Apergis-Schoute, A. M., van der Flier, F. E., Fineberg, N. A., et al. (2017). Specific frontostriatal circuits for impaired cognitive flexibility and goal-directed planning in obsessive-compulsive disorder: evidence from resting-state functional connectivity. *Biol. Psychiatry* 81, 708–717. doi: 10.1016/j.biopsych.2016.08.009

van den Heuvel, O. A., Veltman, D. J., Groenewegen, H. J., Cath, D. C., van Balkom, A. J., van Hartskamp, J., et al. (2005). Frontal-striatal dysfunction during planning in obsessive-compulsive disorder. *Arch. Gen. Psychiatry* 62, 301–309. doi: 10.1001/archpsyc.62.3.301

Vieira, S., Pinaya, W. H., and Mechelli, A. (2017). Using deep learning to investigate the neuroimaging correlates of psychiatric and neurological disorders: methods and applications. *Neurosci. Biobehav. Rev.* 74, 58–75. doi: 10.1016/j.neubiorev.2017.01.002

Weygandt, M., Blecker, C. R., Schäfer, A., Hackmack, K., Haynes, J. D., Vaitl, D., et al. (2012). fMRI pattern recognition in obsessive-compulsive disorder. *Neuroimage* 60, 1186–1193. doi: 10.1016/j.neuroimage.2012.01.064

Woo, C. W., Chang, L. J., Lindquist, M. A., and Wager, T. D. (2017). Building better biomarkers: brain models in translational neuroimaging. *Nat. Neurosci.* 20, 365–377. doi: 10.1038/nn.4478

Yan, C. G., Cheung, B., Kelly, C., Colcombe, S., Craddock, R. C., Di Martino, A., et al. (2013). A comprehensive assessment of regional variation in the impact of head micromovements on functional connectomics. *Neuroimage* 76, 183–201. doi: 10.1016/j.neuroimage.2013.03.004

Yan, C. G., Wang, X. D., Zuo, X. N., and Zang, Y. F. (2016). DPABI: data processing and analysis for (Resting-State) brain imaging. *Neuroinformatics* 14, 339–351. doi: 10.1007/s12021-016-9299-4

Yang, T., Cheng, Y., Li, H., Jiang, H., Luo, C., Shan, B., et al. (2010). Abnormal regional homogeneity of drug-naive obsessive-compulsive patients. *Neuroreport* 21, 786–790. doi: 10.1097/WNR.0b013e32833cadf0

Yang, X. Y., Sun, J., Luo, J., Zhong, Z. X., Li, P., Yao, S. M., et al. (2015). Regional homogeneity of spontaneous brain activity in adult patients with obsessive-compulsive disorder before and after cognitive behavioural therapy. *J. Affect. Disord.* 188, 243–251. doi: 10.1016/j.jad.2015.07.048

Zang, Y., Jiang, T., Lu, Y., He, Y., and Tian, L. (2004). Regional homogeneity approach to fMRI data analysis. *Neuroimage* 22, 394–400. doi: 10.1016/j.neuroimage.2003.12.030

Conflict of Interest Statement: The authors declare that the research was conducted in the absence of any commercial or financial relationships that could be construed as a potential conflict of interest.

frontiers in Behavioral Neuroscience

ORIGINAL RESEARCH
published: 06 August 2019
doi: 10.3389/fnbeh.2019.00169

Neurorestoration of Sustained Attention in a Model of HIV-1 Associated Neurocognitive Disorders

*Landhing M. Moran, Kristen A. McLaurin, Rosemarie M. Booze and Charles F. Mactutus**

Program in Behavioral Neuroscience, Department of Psychology, University of South Carolina, Columbia, SC, United States

Due to the sustained prevalence of human immunodeficiency virus (HIV)-1 associated neurocognitive disorders (HAND) in the post-combination antiretroviral therapy (cART) era, as well as the increased prevalence of older HIV-1 seropositive individuals, there is a critical need to develop adjunctive therapeutics targeted at preserving and/or restoring neurocognitive function. To address this knowledge gap, the present study examined the utility of S-Equol (SE), a phytoestrogen produced by gut microbiota, as an innovative therapeutic strategy. A signal detection operant task with varying signal durations (1,000, 500, 100 ms) was utilized to assess sustained attention in HIV-1 transgenic (Tg) and control animals. During the signal detection pretest assessment, HIV-1 Tg animals displayed profound deficits in stimulus-response learning and sustained attention relative to control animals. Subsequently, between 6 and 8 months of age, HIV-1 Tg and control animals were treated with a daily oral dose of either placebo or SE (0.05, 0.1, 0.2 mg) and a posttest assessment was conducted in the signal detection operant task with varying signal durations. In HIV-1 Tg animals, a linear decrease in the number of misses at 100 ms was observed as SE dose increased, suggesting a dose response with the most effective dose at 0.2 mg SE, approximating controls. Comparison of the number of misses across signal durations at the pretest and posttest revealed a preservation of neurocognitive function in HIV-1 Tg animals treated with 0.2 mg SE; an effect that was in sharp contrast to the neurocognitive decline observed in HIV-1 Tg animals treated with placebo. The results support the utility of 0.2 mg SE as a potential efficacious neuroprotective and/or neurorestorative therapeutic for sustained attention, in the absence of any adverse peripheral effects, in the HIV-1 Tg rat. Thus, the present study highlights the critical need for further *in vivo* studies to elucidate the full potential and generalizability of phytoestrogen treatment for HAND.

Keywords: S-Equol, gut-brain axis, phytoestrogen, dose response, HIV-1 transgenic rat

OPEN ACCESS

Edited by:
Carlos Tomaz,
Universidade Ceuma, Brazil

Reviewed by:
Eleni Konsolaki,
American College of Greece, Greece
Cândida Lopes Alves,
Universidade Ceuma, Brazil

****Correspondence:***
Charles F. Mactutus
mactutus@mailbox.sc.edu

Received: *25 February 2019*
Accepted: *12 July 2019*
Published: *06 August 2019*

Citation:
Moran LM, McLaurin KA, Booze RM and Mactutus CF (2019) Neurorestoration of Sustained Attention in a Model of HIV-1 Associated Neurocognitive Disorders. Front. Behav. Neurosci. 13:169. doi: 10.3389/fnbeh.2019.00169

INTRODUCTION

Worldwide, approximately 36.7 million individuals are living with human immunodeficiency virus type 1 (HIV-1; UNAIDS, 2017), including approximately 4.2 million older adults (>50 years of age; UNAIDS, 2014). Combination antiretroviral therapy (cART), introduced in 1996, serves as the primary treatment regimen for HIV-1 seropositive individuals and dramatically shifted

the epidemiological features of both HIV-1 (Justice, 2010) and HIV-1 associated neurocognitive disorders (HAND). Specifically, cART increased the life expectancy for HIV-1 seropositive individuals (e.g., Romley et al., 2014; Teeraananchai et al., 2017) and decreased the prevalence of the most severe forms of neurocognitive impairment (NCI; Ances and Ellis, 2007). Milder forms of NCI (i.e., HAND), however, persist (Cysique et al., 2004; Garvey et al., 2009; Heaton et al., 2011), afflicting between 40% and 70% of HIV-1 seropositive individuals (Letendre et al., 2010; McArthur et al., 2010; Heaton et al., 2011). Due to the sustained prevalence of HAND in the post-cART era, as well as the increased prevalence of older HIV-1 seropositive individuals, there is a critical need to develop adjunctive therapeutics targeted at slowing/preventing neurocognitive decline and/or restoring neurocognitive function.

The gut-brain axis (or the gut-brain-microbiota axis) is a complex network that includes the central nervous system (CNS), the enteric nervous system, and the gastrointestinal tract (Mayer et al., 2015). Trillions of gut microbiota, which comprise the gastrointestinal tract, play a prominent role in the gut-brain axis. Functionally, gut microbiota have been implicated in the modulation of neurocognitive functions (e.g., Gareau et al., 2011; Manderino et al., 2017), emotional behavior (e.g., anxiety: Diaz Heijtz et al., 2011; Neufeld et al., 2011; depression: Kelly et al., 2016), and social interactions (e.g., Tung et al., 2015). Furthermore, alterations in microbiome composition have been observed in multiple neurodegenerative diseases (e.g., HIV-1: Gori et al., 2008; Mutlu et al., 2014; Parkinson's disease: Keshavarzian et al., 2015; Perez-Pardo et al., 2018; Alzheimer's disease: Harach et al., 2017).

Alterations in the gut microbiome in HIV-1 seropositive individuals, independent of treatment with cART, include decreased diversity (e.g., Mutlu et al., 2014; Monaco et al., 2016; Hamad et al., 2018) and prominent alterations in gut microbiome composition (e.g., Gori et al., 2008; Dillon et al., 2014; Hamad et al., 2018). Gut dysbiosis in HIV-1 has been associated with both CD4+ T-cell count (e.g., Pérez-Santiago et al., 2013; Nowak et al., 2015) and inflammation (e.g., Ancuta et al., 2008; Dinh et al., 2015; Nowak et al., 2015); pathologic indicators correlated with NCI (e.g., Marcotte et al., 2003; Abassi et al., 2017; Eckard et al., 2017). However, antiretroviral therapy seems to at least partially restore gut integrity (Guadalupe et al., 2006). Furthermore, targeting the gut microbiota *via* probiotic supplementation enhanced neurocognitive function during a pilot study in HIV-1 seropositive individuals (Ceccarelli et al., 2017); results which validate the potential utility of targeting the gut-brain axis for the development of adjunctive therapeutic treatments for NCI commonly observed in HIV-1 seropositive individuals.

sDue to the reported gut dysbiosis in HIV-1 seropositive individuals Equol, the active metabolite produced by the gut microbiota following ingestion of the soy-derived phytoestrogen daidzein (Setchell et al., 1984), was assessed as an adjunctive therapeutic approach for HAND. Although Equol can exist in either the R- or S- conformation, given its chiral center at carbon 3, S-Equol (SE) is the only enantiomer produced by humans (Setchell et al., 2005). The neuroprotective effects of SE occur *via* its selective affinity for estrogen receptor β (ERβ), with SE showing an even greater affinity for ERβ than daidzein (Setchell et al., 2005). Functionally, the benefits of a soy food-based diet, such as a reduced risk for certain cancers and increased bone density, are typically found in adults who produce SE (Setchell et al., 2002; Lampe, 2009; Jackson et al., 2011), representing approximately 25%–30% of the Western population (Rowland et al., 2000; Setchell and Cole, 2006). The caveat that therapeutic efficacy and potential may be limited as only 25%–30% of the adults of western countries convert daidzein to SE is fully embraced with our emphasis on use of the metabolite SE, rather than the parent compound, rendering moot the concern of heterogeneity of responses in human gut microbiota as well as any potential differences in gut microflora induced by HIV and/or aging.

Thus, the present study addressed three key questions in the HIV-1 Tg rat. First, do HIV-1 Tg animals exhibit an impairment in sustained attention relative to control animals? Assessments of sustained attention have revealed prominent alterations in both HIV-1 seropositive children (Watkins et al., 2000) and adults (e.g., Fein et al., 1995); deficits which were characterized by a failure of response inhibition (Watkins et al., 2000) and alterations in the temporal dimension of attention (Fein et al., 1995). Furthermore, in the HIV-1 Tg rat, profound alterations in sustained attention (Moran et al., 2014; McLaurin et al., 2017b, 2019a), have been previously reported. Second, utilizing a dose-response experimental design (i.e., placebo, 0.05, 0.1, or 0.2 mg SE), is SE an efficacious therapeutic for the treatment of sustained attention deficits in the HIV-1 Tg rat? *In vitro* studies demonstrate the neuroprotective and/or neurorestorative properties of daidzein (Bertrand et al., 2014) and SE (Bertrand et al., 2015) in rat neuronal cultures treated with the HIV-1 protein, Tat. Doses selected for the present experiment yielded a daily amount of 0.25–1.0 mg/kg SE; an amount equivalent to a 2.5–10 mg dose in a 60 kg human (see most elderly Japanese have a daily isoflavone intake of 30–50 mg, Akaza, 2012). Third, how does the most effective dose of SE change sustained attention across time (i.e., Pre-SE vs. Post-SE) in HIV-1 Tg animals? It was hypothesized that SE may support an efficacious neurorestorative therapeutic for at least a subset of HIV-1 Tg animals.

MATERIALS AND METHODS

Animals

The efficacy of SE as a neuroprotective and/or neurorestorative treatment for NCI was assessed in ovariectomized (OVX) female Fisher (F344/N; Harlan Laboratories Inc., Indianapolis, IN, USA) rats (HIV-1 Tg, n = 41; control, n = 43). Due to health issues, two HIV-1 Tg animals were euthanized prior to beginning treatment with SE, yielding HIV-1 Tg, n = 39 and control, n = 43 for the post-SE assessments. The HIV-1 Tg rat, originally reported in 2001 by Reid et al. (2001) expresses seven of the nine HIV-1 genes constitutively

throughout development and displays intact functional health through advanced age (i.e., 18 months of age; Peng et al., 2010; McLaurin et al., 2018a, 2019a). Although the deletion of two viral proteins, including *-gag* and *–pol*, renders the HIV-1 Tg rat non-infectious, it resembles HIV-1 seropositive individuals on cART and serves as a valid and reliable animal system to translationally model NCI commonly observed in HAND (e.g., Vigorito et al., 2007; Moran et al., 2013, 2014; Repunte-Canonigo et al., 2014; McLaurin et al., 2017b, 2019a). Animals were received at the animal vivarium at approximately 2-months of age and were pair- or group-housed throughout the duration of sexperimentation.

All rats were OVX at Harlan Laboratories prior to arrival at the animal vivarium. Given that SE is a nonsteroidal estrogen, with preferential binding to ERβ (Setchell and Clerici, 2010), OVX animals were utilized to preclude the potential confounding effect of endogenous hormones. Additionally, HIV-1 Tg and control animals were fed a minimal phytoestrogen diet [≤20 ppm; Teklad 2020X Global Extruded Rodent Diet (Soy Protein-Free)] due to the structural similarities between phytoestrogen and estrogen. Beginning approximately 1 week before preliminary training, animals were placed on food restriction to maintain 85% of their *ad libitum* body weight. Pair- or group housing was maintained during food restriction. Water was available *ad libitum* throughout the duration of the study.

Animals were maintained according to National Institute of Health (NIH) guidelines in AAALAC-accredited facilities. The animal facility was maintained at 21° ± 2°C, 50% ± 10% relative humidity and had a 12-h light:12-h dark cycle with lights on at 07:00 h (EST). The project protocol was approved under federal assurance (#D16-00028) by the Institutional Animal Care and Use Committee (IACUC) at the University of South Carolina.

Apparatus

Operant training was conducted in 22 operant chambers located inside sound-attenuating chambers (Med Associates Inc., Fairfax, VT, USA). The front wall of each chamber had two retractable levers, a pellet dispenser (45 mg), located between the two levers, and three incandescent panel lights (20 ± 2 lux). The central panel light, located above the pellet dispenser, was used in the present experiment for the presentation of signals. A house light was located at the top of the rear wall of the operant chamber. Signal presentation, lever operation, reinforcement delivery, and data collection were controlled by a PC and Med-PC for Windows software (V 4.1.3; Med Associates, Inc., Fairfax, VT, USA).

Preliminary Training

Shaping

Beginning at approximately 3 months of age, animals were trained to lever-press using a standard shaping response protocol. The house light was illuminated throughout the duration of the 42-min test session. Animals were trained to press both levers on an FR-1 schedule of reinforcement for sucrose pellets (45 mg). To prevent side-bias, animals were limited to no more than five consecutive presses on a single lever. Successful acquisition of shaping required animals to achieve at least 40 reinforcers for three consecutive days, with less than 20% variance across days.

Signal Detection Task: Training

A signal detection operant task was utilized to train HIV-1 Tg and control animals on two light stimulus contingencies [i.e., central panel light illumination (signal) vs. no illumination (non-signal)]. A 160 trial test session was conducted in a darkened operant chamber, beginning with a 5 min habituation period. Signal presentation was randomized across trials throughout the session. During the signal trials, the central panel light was illuminated until the animal made a response, or until the levers retracted, whichever occurred first. Two seconds after each trial began, levers were extended until the animal made a response, or 6 s elapsed, whichever occurred first; during which time the light stimulus also remained illuminated during signal trials. Levers were retracted between trials [Intertrial Interval (ITI): 9 ± 3 s]. For half of the animals, responses on the left lever during signal trials (Hits) and on the right lever during non-signal trials (Correct Rejections) were reinforced with a sucrose pellet. In the same manner, responses on the right lever during signal trials (Misses) and on the left lever during non-signal trials (False Alarms) were not reinforced. The reverse set of rules was used for the other half of the subjects.

During training, if an animal responded incorrectly, they were given correction trials, which included up to three repetitions of the trial. If an animal failed to respond appropriately during the correction trials, a force-choice trial occurred. During the forced-choice trial, the same stimulus type was repeated (signal or non-signal) but only the correct lever was extended and remained extended until a correct response was made or 120 s elapsed, whichever occurred first.

HIV-1 Tg and control animals were trained for up to 1 month of daily testing. Animals were required to achieve at least 70% accuracy on three consecutive test sessions to be promoted (adapted from Arnold et al., 2003) to the signal detection task tapping sustained attention. Accuracy was calculated as the total number of hits and correct rejections divided by the total number of responses in a session. Animals had prior experience with basic signal detection, discrimination learning, reversal learning, and extradimensional shift tasks, as previously reported (Moran et al., 2014).

Experimental Design

A schematic of the experimental design illustrates the timeline for neurocognitive assessments and treatment with SE, the age of the animals during each phase of the experiment, and the length of each experiment (**Figure 1**).

Pre-S-Equol: Sustained Attention Assessments

Procedure

After reaching the criterion of 70% accuracy on three consecutive days during preliminary training, animals were assessed in a signal detection operant task with varying signal durations,

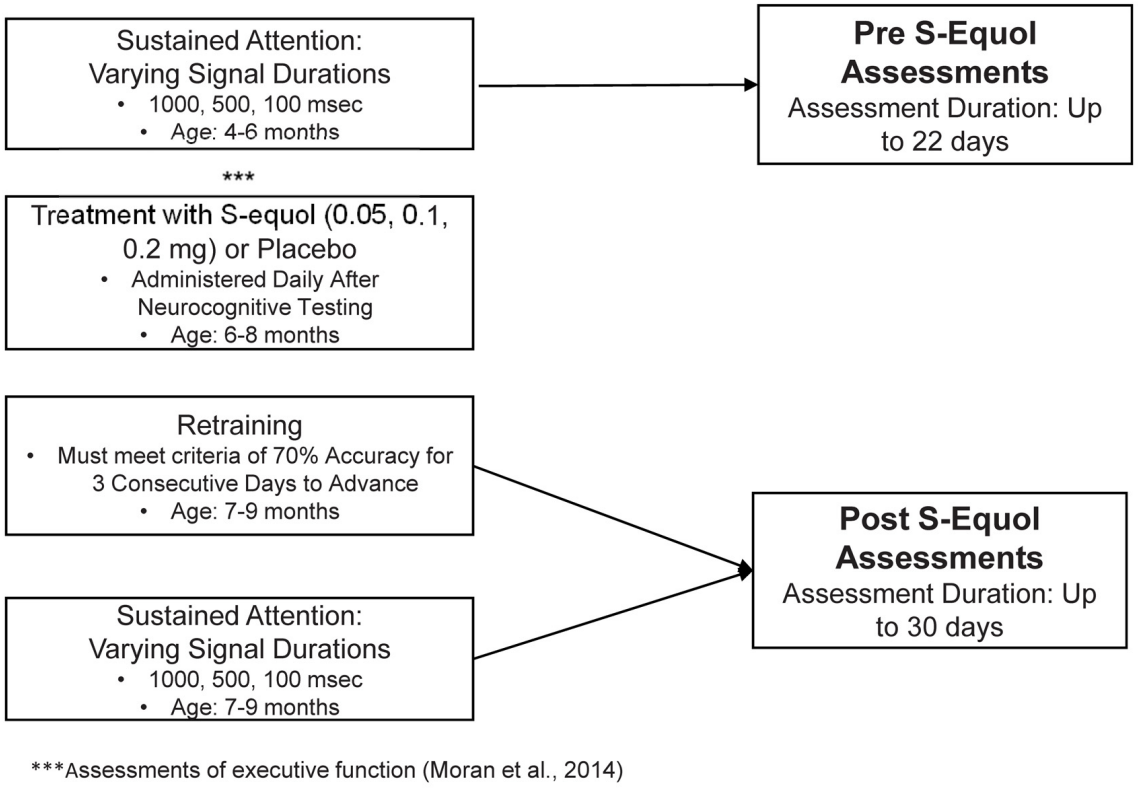

FIGURE 1 | Schematic of the experimental design.

tapping sustained attention. Each test session was conducted in a darkened operant chamber, beginning with a 5 min habituation period. The length of the light stimulus was manipulated (i.e., 1,000, 500, 100 ms) using a block randomized experimental design across the 162 trial test session. Following signal offset, both levers were presented for 6 s or until the animal made a response, whichever occurred first. Trials had ITIs of 9 ± 3 s, during which time the levers remained retracted. Each animal was trained on the task for up to 22 days.

Post S-Equol: Sustained Attention Assessments

Drugs

SE was obtained from Cayman Chemical Company (Ann Arbor, MI, USA) and incorporated into 90 mg sucrose pellets by Bio-Serv (Flemington, NJ, USA) to produce pellets containing 0.05 mg SE. Plain 90 mg sucrose pellets were also obtained from Bio-Serv for the placebo group.

Treatment

Beginning between approximately 6 and 8 months of age, HIV-1 Tg and control animals were treated daily with placebo or SE (0.05, 0.1, or 0.2 mg). A randomized-block experimental design, with percent accuracy on the signal detection operant task with varying signal duration as the blocking factor, was utilized to assign animals to dose groups (i.e., Placebo: Control, n = 10, HIV-1 Tg, n = 9; 0.05 mg SE: Control, n = 11, HIV-1 Tg, n = 10; 0.1 mg SE: Control, n = 11, HIV-1 Tg, n = 10; 0.2 mg SE: Control, n = 11, HIV-1 Tg, n = 10). Given that each SE pellet contained 0.05 mg, the 0.05 mg dose group received one pellet per day, the 0.1 mg dose group received two pellets per day, and the 0.2 mg dose group received four pellets per day. The placebo group received four sucrose pellets per day. Doses selected for the present experiment yielded a daily amount of 0.25–1.0 mg/kg SE; an amount equivalent to a 2.5–10 mg dose in a 60 kg human (see most elderly Japanese have a daily isoflavone intake of 30–50 mg, Akaza, 2012). Treatments were administered to animals at least 1 h after the completion of neurocognitive testing, and were typically consumed immediately.

Procedure

After 5 days of SE or placebo treatment, animals were retrained and retested in the signal detection operant task. Training and signal detection were conducted as described above. As in the assessment prior to SE treatment, animals were required to meet criteria of 70% accuracy for three consecutive days in retraining before advancing to the assessment of sustained attention. Animals were given up to 1 month to reacquire both training and the signal detection operant task.

Peripheral Effects of S-Equol

Potential peripheral effects of SE were assessed by dissecting the uterine horn from the peritoneal cavity of all rats. The uterine horns were separated from the underlying tissue and the uterine body was excised. Wet weights of the uterine horns were taken immediately following removal. A relative uterine weight was calculated for each animal by dividing the uterine weight (mg) by the body weight (g).

Statistics

T-test, analysis of variance (ANOVA) and regression statistical techniques were utilized for the analysis of all data. SPSS Statistics 25 (IBM Corp., Somers, NY, USA) was used for *t*-test and ANOVA statistical analyses. Figures and regression analyses were completed using GraphPad Prism 5 (GraphPad Software, Inc., La Jolla, CA, USA). R^2 values for all linear regression analyses reflect fits to the mean values and weighting with $1/SD^2$. Statistical tests were evaluated against a $p \leq 0.05$ alpha criterion. Sample sizes were chosen with the goal of sufficient statistical power (>0.80) to maximize the likelihood of detecting neurocognitive alterations resulting from HIV-1 transgene expression. Partial eta squared (η_p^2) is presented as a measurement of effect size.

A series of three analyses were conducted at the pre-SE assessment to evaluate NCI in the HIV-1 Tg rat. First, the temporal process of acquisition, an assessment of stimulus-response learning, was examined using regression analyses. Second, percent accuracy was analyzed using independent samples *t*-tests. Third, the number of responses for each response type (i.e., Hits, False Alarms, Correct Rejections, and Misses) was examined by calculating the average number of responses (and 95% confidence intervals) exhibited, independent of response type; a value reflecting the inability to distinguish response choices. The number of responses exhibited for each response type independently were then compared to the 95% confidence interval.

Sustained attention was assessed by conducting a mixed-factor ANOVA on the signal detection task with varying signal durations, with genotype (i.e., HIV-1 Tg vs. control) and SE dose (i.e., placebo, 0.05, 0.1, 0.2 mg) as between-subjects factors, as appropriate. Response type (i.e., hits and misses), and signal duration (i.e., 1,000, 500, or 100 ms) were included as within-subjects factors, as appropriate. At the pre-SE assessment, analyses were conducted on the number of hits and misses averaged across test sessions seven through nine; a point reflecting when approximately 50% of the control animals achieved criteria in the signal detection task with varying signal durations. At the post-SE assessment, analyses were conducted on an animal's final 3 days of testing; a point reflecting the maximal effect of SE. Due to *a priori* hypotheses, analyses at the post-SE assessment compared all of the control animals (reflecting the population sampled), independent of SE dose, to the top 40% performing HIV-1 Tg animals at each dose of SE. The HIV-1 Tg animals were chosen by selecting the animals with the highest average percent accuracy on the final three sessions in the signal detection operant task. The Greenhouse-Geisser *df* correction factor (Greenhouse and Geisser, 1959) and orthogonal decompositions were utilized to preclude potential violations of compound symmetry of the repeated-measures factors. Linear regression analyses were conducted to examine the number of misses as a function of signal duration, as well as to examine the effect of genotype and SE dose on the number of misses at 100 ms.

Based on results from our dose response analysis, time response analyses were conducted. Specifically, regression analyses were utilized to compare pre-SE performance to post-SE performance within groups. The performance at these two time points (i.e., pre-SE vs. post-SE) was compared in four groups, including control animals treated with placebo, control animals treated with 0.2 mg SE, HIV-1 Tg animals treated with placebo, and HIV-1 Tg animals treated with 0.2 mg SE.

The peripheral effects of SE were assessed with relative uterine weight, which was calculated by dividing uterine weight (g) by body weight (g). Statistical analyses were conducted on relative uterine weight using a two-way ANOVA with genotype and SE dose as between-subjects factors.

RESULTS

Pre S-Equol: Sustained Attention Assessments

Presence of the HIV-1 Transgene Significantly Influenced the Temporal Process of Acquisition During the Pre S-Equol Assessment of the Signal Detection Operant Task With Varying Signal Durations

HIV-1 Tg and control animals had up to 22 days to acquire the signal detection operant task with varying signal durations. Across the period of training in the signal detection operant task with varying signal durations, HIV-1 Tg animals exhibited a significantly slower rate of task acquisition, defined as achieving 70% accuracy on three consecutive days, relative to the control group. As illustrated in **Figure 2**, approximately 55% of the HIV-1 Tg animals acquired the task within the testing period (i.e., 22 days allotted for task acquisition), compared to 81% of the control animals. A one-phase association provided a well-described fit for both HIV-1 Tg (R^2 = 0.98) and control (R^2 = 0.98) animals. However, significant differences in the parameters of the function were observed ($F_{(3,22)}$ = 116.1, $p \leq 0.001$), supporting a profound alteration in stimulus-response learning in HIV-1 Tg animals relative to controls.

HIV-1 Tg Animals Exhibited a Marked Impairment in the Detection of Shorter Signal Durations, Supporting a Deficit in Sustained Attention

The effect of the HIV-1 transgene on sustained attention was examined by averaging each animal's performance from days 7 to 9 on the signal detection operant task with varying signal durations, a point reflecting when half of the control animals met criteria (i.e., 70% accuracy for three consecutive sessions; **Figure 3**).

Overall, HIV-1 Tg animals (n = 33) achieved a significantly lower percent accuracy (**Figure 3A**) relative to control animals

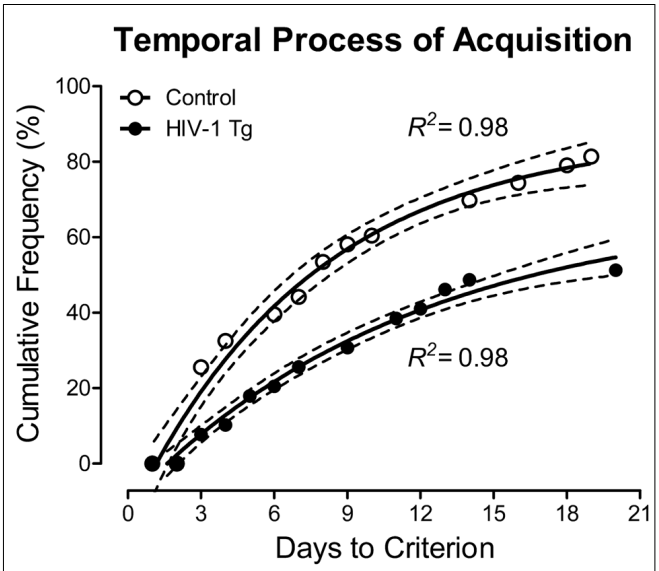

FIGURE 2 | The number of sessions required to meet criterion (70% accuracy on three consecutive sessions) is presented as a function of genotype human immunodeficiency virus (HIV-1 Tg vs. control; ±95% CI). HIV-1 Tg animals exhibited a slower rate of task acquisition relative to control animals, supporting a deficit in stimulus-response learning.

(n = 41; $t_{(72)}$ = 2.8, $p \leq 0.007$). Examination of the number of responses for each response type (i.e., Hits, False Alarms, Correct Rejections, and Misses) suggests that HIV-1 Tg and control animals are using different mechanisms to acquire the task (**Figure 3B**). The number of responses was compared to the average number of responses, independent of response type, and 95% confidence intervals. Control animals exhibited a significantly greater number of hits and correct rejections, in combination with a significantly fewer number of false alarms and misses, supporting learning all of the task contingencies. HIV-1 Tg animals, however, only exhibited an increased number of correct rejections and a decreased number of false alarms.

Presence of the HIV-1 transgene significantly influenced sustained attention during initial training on the signal detection operant task with varying signal durations (**Figure 3C**). A significant Response Type × Duration interaction ($F_{(2,144)}$ = 61.4, $p_{GG} \leq 0.001$, η_p^2 = 0.460) with a prominent linear component ($F_{(1,72)}$ = 78.8, $p \leq 0.001$, η_p^2 = 0.522), independent of genotype, supports the assessment of sustained attention. As the length of the signal duration decreased, the number of hits decreased and the number of misses increased. Most critically, however, HIV-1 Tg animals exhibited a prominent rightward shift in the loss of signal detection (i.e., where the number of hits and misses intersect) relative to control animals [approximately 479 ms vs. 247 ms, respectively; Genotype × Duration × Response Type Interaction with a prominent quadratic-linear component ($F_{(1,72)}$ = 4.3, $p \leq 0.05$, η_p^2 = 0.056)], supporting a deficit in sustained attention.

During the initial acquisition of the signal detection operant task with varying signal durations, HIV-1 Tg animals exhibited

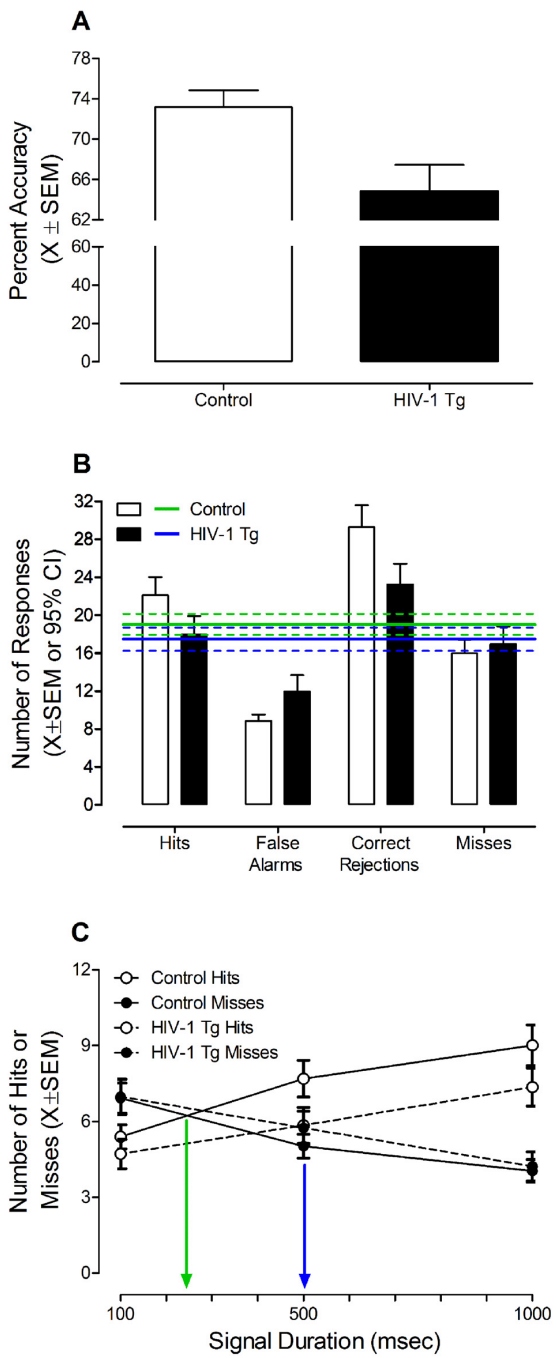

FIGURE 3 | HIV-1 Tg and control animals were tested in a signal detection operant task with varying signal durations prior to treatment with S-Equol. **(A)** HIV-1 animals exhibited a significantly lower percent accuracy relative to control animals ($p \leq 0.05$). **(B)** Control animals exhibited a significantly greater number of hits and correct rejections, in combination with a significantly fewer number of false alarms and misses, supporting learning all of the task contingencies. HIV-1 Tg animals, however, only exhibited an increased number of correct rejections and a decreased number of false alarms. **(C)** The assessment of sustained attention revealed that HIV-1 Tg animals exhibited a prominent rightward shift in the loss of signal detection (i.e., the intersection of hits and misses; $p \leq 0.05$) relative to control animals. Data are presented as mean ± SEM.

pronounced deficits, characterized by a slower rate of task acquisition, decreased percent accuracy, inability to distinguish hits and misses, and a prominent rightward shift in the loss of signal detection relative to control animals; deficits which suggest profound impairments in stimulus-response learning and sustained attention.

Post S-Equol: Dose Response

In HIV-1 Tg Animals, a Linear Dose Response Was Observed, With the Most Efficacious Dose as 0.2 mg S-Equol

Using a randomized-block design, with percent accuracy on the signal detection operant task with varying signal durations as the blocking factor, HIV-1 Tg and control animals were assigned to one of four SE dose groups (i.e., placebo, 0.05, 0.1, or 0.2 mg SE). After 5 days of treatment, animals were retrained and retested in the signal detection operant task with varying signal durations. Daily SE treatment continued throughout the duration of neurocognitive testing with administration occurring at least 1 h after the completion of assessments.

Given our *a priori* hypothesis that treatment with SE would only mitigate sustained attention deficits in a subset of HIV-1 Tg animals, statistical analyses were conducted on the top 40% of HIV-1 Tg animals at each SE dose. Performance was determined by examining percent accuracy on the final three sessions of SE treatment. All control animals were included in the statistical analysis.

Treatment with SE significantly influenced sustained attention, assessed in a signal detection operant task with varying signal durations, in a subset of HIV-1 Tg animals (**Figure 4**). Specifically, the overall mixed-design ANOVA revealed a significant Genotype × SE Dose × Response Type × Duration interaction with a prominent linear-quadratic component ($F_{(3,48)} = 4.1$, $p \leq 0.011$, $\eta_p^2 = 0.205$).

Complementary analyses were conducted at each SE dose to more fully elucidate the locus of the interaction. A significant Genotype × Duration × Response Type interaction was observed in animals treated with placebo (**Figure 4A**; $F_{(2,20)} = 7.7$, $p_{GG} \leq 0.009$, $\eta_p^2 = 0.436$) with a prominent linear-linear component ($F_{(1,10)} = 9.4$, $p \leq 0.012$, $\eta_p^2 = 0.486$), 0.05 mg SE (**Figure 4B**; $F_{(2,26)} = 4.8$, $p_{GG} \leq 0.02$, $\eta_p^2 = 0.272$) with a prominent linear-linear component ($F_{(1,13)} = 5.8$, $p \leq 0.032$, $\eta_p^2 = 0.309$), and 0.1 mg SE (**Figure 4C**; $F_{(2,26)} = 9.0$, $p_{GG} \leq 0.003$, $\eta_p^2 = 0.408$) with a prominent linear-linear component ($F_{(1,13)} = 9.5$, $p \leq 0.009$, $\eta_p^2 = 0.421$), suggesting that, despite treatment, HIV-1 Tg animals continued to exhibit deficits in sustained attention relative to control animals. The absence of a significant Genotype × Duration × Response Type interaction in animals treated with 0.2 mg SE (**Figure 4D**; $p > 0.05$) suggested that 0.2 mg SE is the most efficacious dose, ameliorating sustained attention deficits in a subset of HIV-1 Tg animals to the level of controls.

More specific investigations were targeted at examining if, and how, treatment with SE altered the number of misses (**Figure 5**), given that misses reflect a lapse of attention to the stimulus. A significant Genotype × SE Dose × Duration interaction was observed for misses with a prominent quadratic component ($F_{(3,48)} = 3.3$, $p \leq 0.027$, $\eta_p^2 = 0.172$). In control animals (**Figure 5A**), a global first-order polynomial provided a well-described fit ($R^2 = 0.75$), supporting no statistically significant differences in the number of misses as a function of SE dose ($p > 0.05$). However, in HIV-1 Tg animals (**Figure 5B**), a downward shift in the number of misses was observed as SE dose increased. Although a first-order polynomial provided a well-described fit for all SE doses (i.e., Placebo: $R^2 = 0.95$, 0.05 mg SE: $R^2 = 0.99$, 0.1 mg SE: $R^2 = 0.86$, 0.2 mg SE: $R^2 = 0.99$), significant differences were observed in the parameters of the function ($F_{(6,40)} = 2.5$, $p \leq 0.04$).

The most prominent difference in the number of misses was observed at the 100 ms duration; an effect that was subsequently investigated (**Figure 5C**). A horizontal line provided a well-described fit for the control animals, exhibiting a slope (i.e., β_1) that was not significantly different from 0 ($p > 0.05$). Results in control animals, therefore, support no significant difference in the number of misses at 100 ms as a function of SE dose. In sharp contrast, for HIV-1 Tg animals, as SE dose increased, a linear ($R^2 = 0.90$) decrease in the number of misses at 100 ms was observed, suggesting a dose response with the most effective dose as 0.2 mg SE to approximate levels of controls.

Treatment with 0.2 mg SE between 6 and 8 months of age, therefore, enhanced sustained attention, to the level of controls, in the top-performing 40% of the HIV-1 Tg animals sampled. Observations of enhanced sustained attention in HIV-1 Tg animals treated with 0.2 mg SE were due, at least in part, to a decreased number of misses, supporting fewer lapses of attention.

Pre S-Equol vs. Post S-Equol: Time Response

HIV-1 Tg Animals Treated With 0.2 mg S-Equol Exhibited a "Savings" of Sustained Attention

Given the beneficial effects of 0.2 mg SE observed in a subset of HIV-1 Tg animals, subsequent analyses compared the number of misses at the pre-SE assessment to the number of misses at the post-SE assessment across signal duration (**Figure 6**).

In control animals, a global first-order polynomial provided a well-described fit for animals treated with placebo ($R^2 = 0.80$, **Figure 6A**) and animals treated with 0.2 mg SE ($R^2 = 0.73$, **Figure 6B**). A global fit suggests no significant change in the number of misses as a function of time.

In sharp contrast, HIV-1 Tg animals treated with placebo displayed age-related disease progression, evidenced by an increased number of misses at the post-SE assessment relative to the pre-SE assessment. A first-order polynomial provided a well-described fit for HIV-1 Tg animals treated with placebo at both the pre-SE ($R^2 = 0.94$) and post-SE ($R^2 = 0.93$) assessment, however, significant differences in the parameters of the function were observed ($F_{(2,20)} = 4.4$, $p \leq 0.026$). Treatment with 0.2 mg of SE between 6 and 8 months of age, however, prevented neurocognitive decline, evidenced by

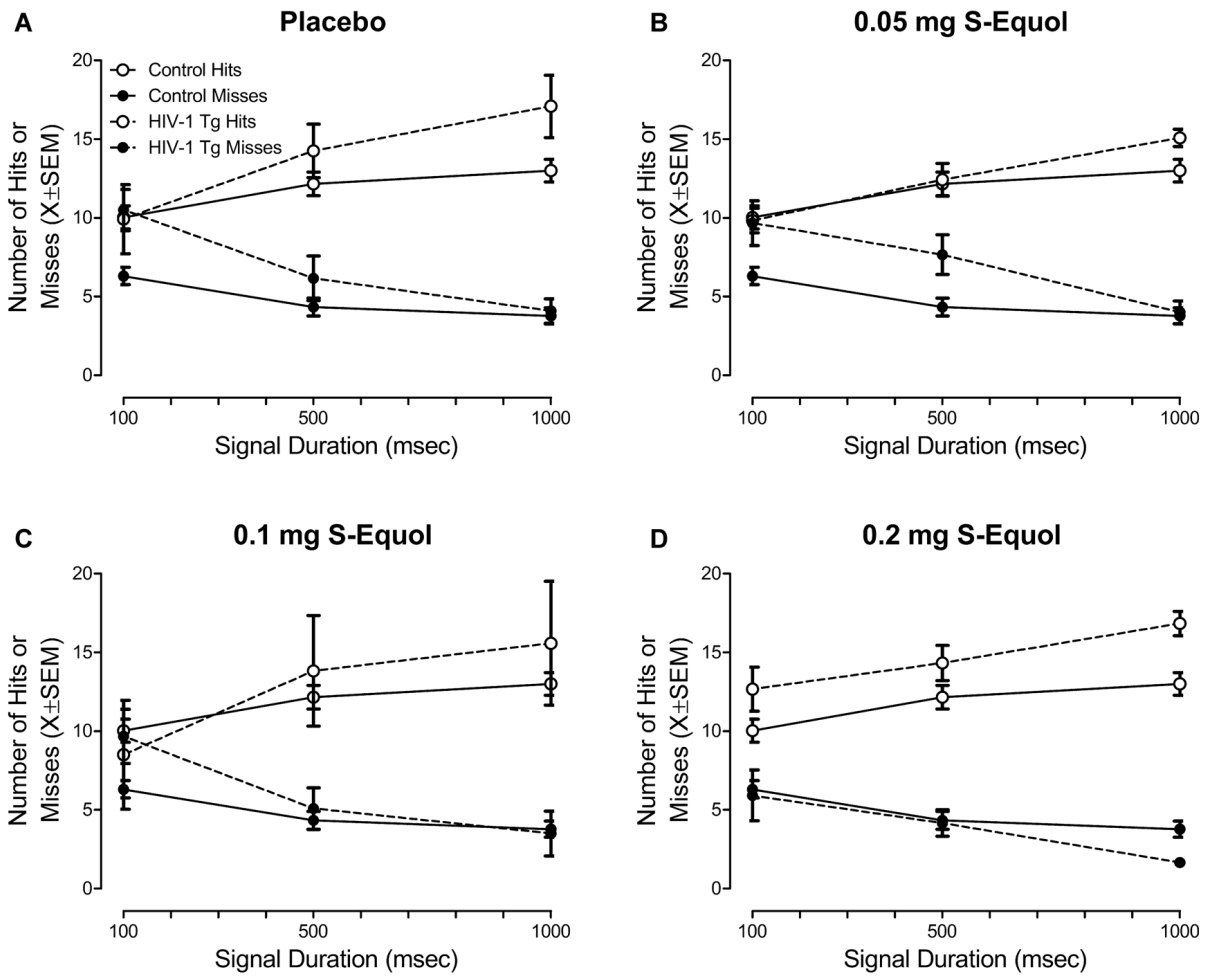

FIGURE 4 | The effect of S-Equol (SE) dose [Placebo **(A)**, 0.05 mg **(B)**, 0.1 mg **(C)**, 0.2 mg **(D)**] on sustained attention was assessed in a signal detection operant task with varying signal durations. There was no significant effect of SE dose on sustained attention in control animals, thus data for control animals were collapsed across all doses. The top 40% of HIV-1 Tg animals, determined using percent accuracy, are presented for each dose. HIV-1 Tg animals continued to exhibit deficits in sustained attention relative to control animals when treated with placebo, 0.05 mg SE, or 0.1 mg SE. However, sustained attention deficits were ameliorated, to the level of controls, in a subset (i.e., 40%) of HIV-1 Tg animals treated with 0.2 mg SE.

a global first-order polynomial fit (R^2 = 0.97). Thus, HIV-1 Tg animals treated with 0.2 mg of SE exhibited a "savings" of sustained attention.

Peripheral Effects of S-Equol: Uterine Weight

S-Equol Had no Peripheral Effects, Assessed Using Uterine Weight, in Either HIV-1 Tg or Control Animals, Independent of Dose

Uterine weight was assessed to examine the potential peripheral effects of SE treatment. A relative uterine weight was calculated by dividing uterine weight (g) by body weight (g). A horizontal line provided a well-described fit for relative uterine weight, exhibiting a slope (i.e., β_1) that was not significantly different from 0 (**Figure 7**; $p > 0.05$). Furthermore, a between-subject's ANOVA failed to reveal a significant Genotype × SE Dose interaction ($p > 0.05$) or main effects of either Genotype or SE dose ($p > 0.05$). Thus, independent of dose, SE had no adverse peripheral effects, assessed using relative uterine weight, in either HIV-1 Tg or control animals, suggesting that the treatment is more likely to act centrally.

DISCUSSION

At the pre-SE assessment, HIV-1 Tg animals exhibited profound deficits in task acquisition, tapping stimulus-response learning, and signal detection with varying signal durations, tapping sustained attention, relative to control animals, replicating and extending our previous reports (Moran et al., 2014; McLaurin et al., 2017b, 2019a). Between 6 and 8 months of age, HIV-1 Tg and control animals were treated with a daily oral dose of SE

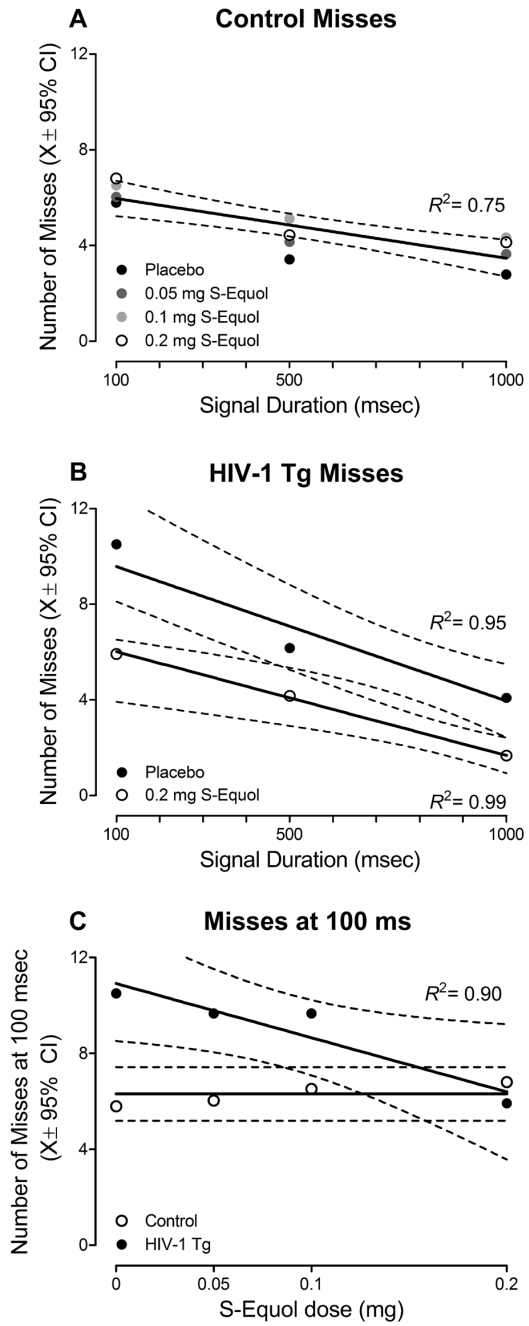

FIGURE 5 | The effect of S-Equol (SE) dose (Placebo, 0.05 mg, 0.1 mg, 0.2 mg) on the number of misses, which reflect a lapse of attention to the stimulus, was examined. **(A)** Treatment with SE did not significantly alter the number of misses across signal duration (i.e., 1,000, 500, 100 ms) in control animals. **(B)** For clarity, only the placebo and 0.2 mg SE dose groups are presented. A downward shift in the number of misses was observed as SE dose increased, with the most prominent shift observed in HIV-1 Tg animals treated with 0.2 mg SE. **(C)** HIV-1 Tg animals displayed a linear decrease in the number of misses at the 100 ms signal duration as the dose of SE increased. A horizontal line, however, provided a well-described fit for the control animals, supporting no change in the number of misses at 100 ms as a function of SE treatment. The number of misses in HIV-1 Tg animals treated with 0.2 mg SE approached the level of controls.

(placebo, 0.05, 0.1, 0.2 mg SE) and retested in the signal detection operant task with varying signal durations. In HIV-1 Tg animals, a linear decrease in the number of misses at 100 ms was observed as SE dose increased, suggesting a dose response with the most effective dose as 0.2 mg SE to approximate controls. Specifically, treatment with 0.2 mg SE enhanced sustained attention, to the level of controls, in a subset (i.e., 40%) of HIV-1 Tg animals; an improvement that was due, at least in part, to a downward shift in the number of misses. Comparison of the number of misses during the pre-SE and post-SE assessments revealed a preservation of neurocognitive function in HIV-1 Tg animals treated with 0.2 mg SE; an effect that was in sharp contrast to the neurocognitive decline observed in HIV-1 Tg animals treated with placebo. Treatment with 0.2 mg of SE in adulthood, therefore, may serve as an efficacious therapeutic strategy, slowing/preventing deficits in sustained attention and restoring sustained attention to the level of controls in a subset of HIV-1 Tg animals.

Sustained attention, or vigilance, an integral component of cognitive capacity, is the process by which one detects rare, unpredictable, and weak stimuli over long periods of time (Sarter et al., 2001). Changes in performance during a sustained attention task are often related to varying task parameters, including stimulus duration, intensity and frequency; changes which are analogous in both humans and rats (Parasuraman and Davies, 1977; McGaughy and Sarter, 1995; Bushnell, 1998). The experimental paradigm utilized in the present study, which has been validated for the assessment of sustained attention in animals (McGaughy and Sarter, 1995), required animals to attend to a randomly presented stimulus (i.e., central panel illumination), the presence or absence of which indicated the response required (i.e., which lever to press) to receive a reinforcer (i.e., sucrose pellet). Manipulation of the duration of the randomly presented stimulus (i.e., 1,000, 500, 100 ms), a key component in the assessment of sustained attention, afforded a critical opportunity to examine the temporal aspects of attention.

During the pretest assessment, the population of HIV-1 Tg animals sampled exhibited prominent alterations in stimulus-response learning and sustained attention relative to control animals; impairments which model those commonly observed in HIV-1 seropositive individuals (e.g., Fein et al., 1995; Watkins et al., 2000; Heaton et al., 2011). Deficits in stimulus-response learning, observed in HIV-1 Tg animals relative to controls, were characterized by a slower rate of task acquisition, with only 55% of the HIV-1 Tg animals acquiring the task within 22 days. Furthermore, the HIV-1 Tg rat displayed a profound deficit in sustained attention, characterized by a significantly lower percent accuracy, as well as a rightward shift in the loss of signal detection; alterations which extend those previously reported in the HIV-1 Tg rat (Moran et al., 2014; McLaurin et al., 2017b, 2019a).

Temporal processing deficits, assessed using prepulse inhibition (PPI) and gap prepulse inhibition (gap-PPI), have been implicated as a fundamental impairment in HAND (e.g., Chao et al., 2004; Matas et al., 2010; Moran et al., 2013). In PPI and gap-PPI, the manipulation of interstimulus interval (i.e., the time interval between the prepulse and startle stimulus)

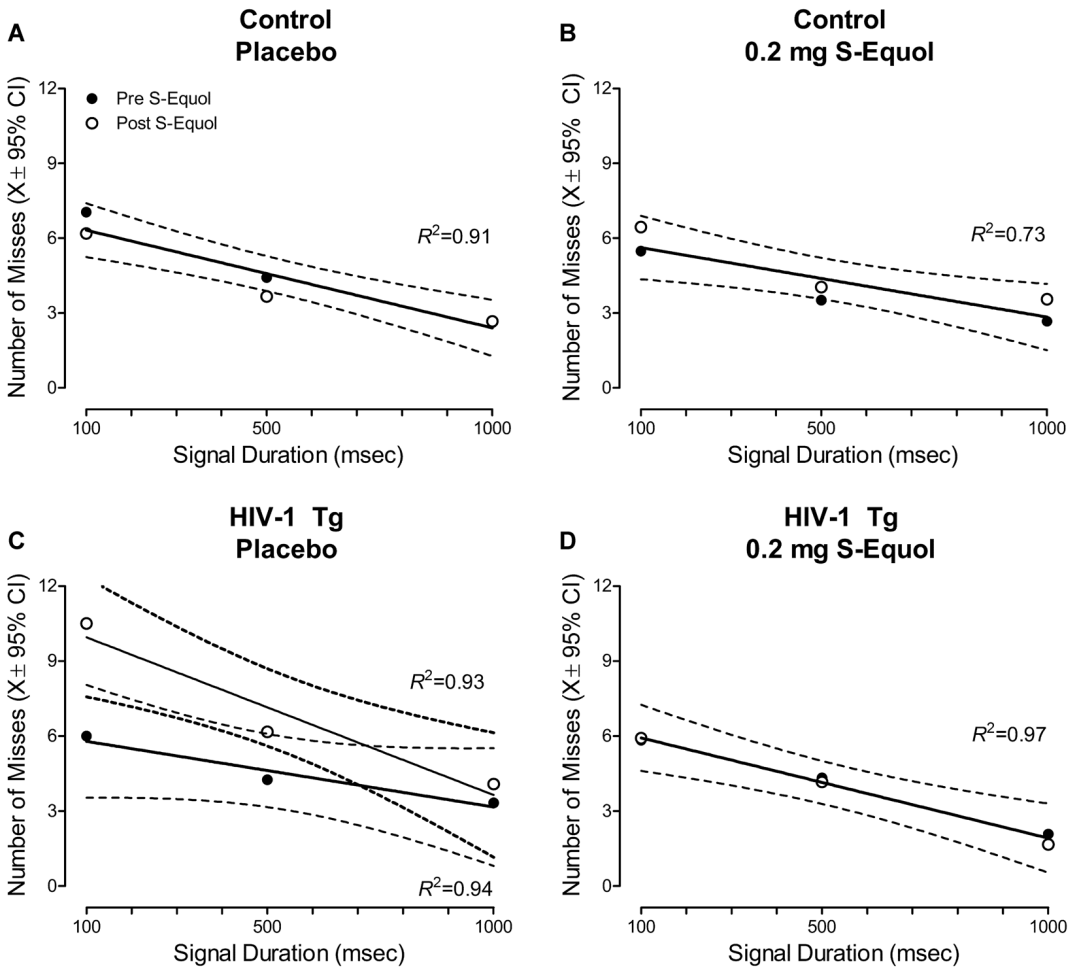

FIGURE 6 | A pretest-posttest experimental design was utilized to examine the effect of S-Equol [SE; Placebo **(A,C)** or 0.2 mg **(B,D)**] on the number of misses across time in control **(A,B)** and HIV-1 Tg **(C,D)** animals. Neither placebo nor 0.2 mg SE treatment altered the number of misses in control animals across time **(A,B)**, evidenced by a global first-order polynomial fit. HIV-1 Tg animals treated with placebo displayed an increase in the number of misses at the post-SE assessment relative to the pre-SE assessment **(C)**, supporting neurocognitive decline across time; an effect that was prevented by treatment with 0.2 mg SE **(D)**.

is utilized to evaluate the construct of temporal processing (McLaurin et al., 2019b). The generality (McLaurin et al., 2017a), progression (Moran et al., 2013; McLaurin et al., 2016, 2018a), and relative permanence (McLaurin et al., 2017a,c) of temporal processing deficits, assessed using PPI and gap-PPI, have been previously reported in the HIV-1 Tg rat across the functional lifespan. Observed alterations in the temporal aspects of attention in the HIV-1 Tg rat, as in the present study, build upon those previously reported in PPI and gap-PPI, establishing a critical need to characterize temporal processing alterations in other executive functions.

Between 6 and 8 months of age, HIV-1 Tg and control animals were treated with a daily oral dose of SE, an active metabolite produced by gut microbiota, using a dose-response experimental design to determine the lowest efficacious dose of SE. Sustained attention deficits were best ameliorated in a subset of HIV-1 Tg animals (i.e., 40%) following treatment with 0.2 mg SE. Specifically, in HIV-1 Tg animals, a downward shift in the number of misses at all signal durations (i.e., 1,000, 500, 100 ms) was observed as SE dose increased; an effect that was most prominent at the 100 ms signal duration. Subsequent time response analyses were conducted by comparing the number of misses at the pre-SE and post-SE assessment. HIV-1 Tg animals treated with 0.2 mg SE exhibited a preservation of neurocognitive function across time; an effect that was in sharp contrast to the neurocognitive decline observed in HIV-1 Tg animals treated with placebo. Critically, SE had neither a beneficial nor an adverse effect on sustained attention in control animals at any dose. Thus, in HIV-1 Tg animals, 0.2 mg SE served as an efficacious therapeutic for the restoration of neurocognitive function and prevention of neurocognitive decline.

The clinical importance of assessing selective estrogen receptor β agonists (SERBAs), including SE, as a therapeutic for HAND cannot be understated. First, selectively targeting ERβ for therapeutics minimizes the risk for undesirable side effects mediated by ERα in reproductive tissues (Schwen et al., 2012).

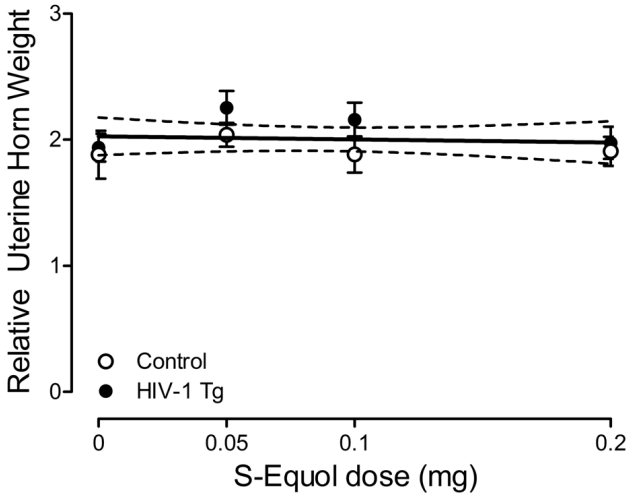

FIGURE 7 | Peripheral effects of S-Equol (SE) were examined by assessing the relative uterine horn weight [i.e., uterine weight (g)/by body weight (g)]. There was no significant effect of genotype ($p > 0.05$) or SE dose ($p > 0.05$) on relative uterine weight, suggesting that SE most likely exerts its effects centrally.

Furthermore, within the brain, SE crosses the blood-brain-barrier and distributes most significantly to the prefrontal cortex in rats (Lund et al., 2001). Second, the therapeutic potential of SERBAs for a wide range of neurocognitive disorders, including Alzheimer's disease (e.g., George et al., 2013; Zhao et al., 2013), and Parkinson's disease (e.g., McFarland et al., 2013) has been examined using preclinical animal model systems. Most critically, the translational relevance of SERBAs in the CNS is demonstrated *via* their progression into clinical trials for other neurocognitive disorders, ranging from Alzheimer's disease (Ausio Pharmaceuticls; NCT03101085) and memory loss (National Institutes on Aging; NCT01723917) to schizophrenia (Eli Lilly; NCT01874756). Given the translational value of preclinical studies on SERBAs, it seems appropriate to evaluate the therapeutic potential of SE for HAND, another neurodegenerative disease (McLaurin et al., 2019a).

The pathogenesis of HAND in the post-cART era is multidimensional, and may include neurotransmitter alterations (e.g., clinical: Kumar et al., 2011; HIV-1 Tg rat: Javadi-Paydar et al., 2017; Sinharay et al., 2017), synaptic dysfunction (e.g., clinical: Gelman et al., 2012; Desplats et al., 2013; HIV-1 Tg rat: Roscoe et al., 2014; McLaurin et al., 2018b, 2019a), and neuroinflammation (e.g., clinical: Meier et al., 2009; Royal et al., 2016; HIV-1 Tg rat: Royal et al., 2012). Functional alterations in neurons, however, more likely underlie the pathophysiology of HAND (Saylor et al., 2016). Pyramidal neurons, which are abundant throughout the prefrontal cortex (Spruston, 2008), a brain region critically involved in attention (Kim et al., 2016), have been examined in the HIV-1 Tg rat. Specifically, synaptic dysfunction in pyramidal neurons in the HIV-1 Tg rat is characterized by decreased branching complexity and profound alterations in synaptic connectivity; alterations which explain significant genotypic variance (McLaurin et al., 2019a).

Mechanistically, SE may exert therapeutic effects by slowing/preventing and/or restoring synaptic dysfunction. Specifically, *in vitro* studies revealed that pretreatment with SE prevented synaptodendritic damage induced by the HIV-1 viral protein, Tat (Bertrand et al., 2015). Other phytoestrogens, including daidzein and liquiritigenin, precursors to SE, also reduced HIV-1 viral protein (i.e., Tat) induced synaptodendritic damage and restored neuronal complexity (Bertrand et al., 2014). More broadly, strong evidence supports the effect of estrogen, including 17β-estradiol, on neuronal network complexity. In the prefrontal cortex, multiple studies reveal that treatment with 17β-estradiol increases dendritic spine density (Hao et al., 2006; Khan et al., 2013; Tuscher et al., 2016), enhances the formation of excitatory glutamatergic synapses (Khan et al., 2013), and induces morphological changes in dendritic spines (Hao et al., 2006). Furthermore, ERβ, the putative mechanism by which SE exerts effects (Setchell et al., 2005; Bertrand et al., 2015), plays a critical role in the modulation of 17β-estradiol on neuronal network complexity (Wang et al., 2018). There remains, however, a critical need for investigating the precise neural mechanism by which SE exerts neurorestorative effects in the HIV-1 Tg rat.

Despite the aforementioned strengths of the present study, a few caveats must be acknowledged. Specifically, the therapeutic efficacy of SE was assessed exclusively in one neurocognitive domain (i.e., sustained attention). HAND, however, is characterized by prominent alterations in multiple neurocognitive domains (e.g., Cysique et al., 2004; Heaton et al., 2011). Although the therapeutic efficacy of SE cannot be generalized across neurocognitive domains within the present study, results highlight the critical need to conduct further studies investigating the utility of SE. Furthermore, assessments were conducted in OVX female HIV-1 Tg and control animals in adulthood. Given prominent sex differences in HAND (e.g., Hestad et al., 2012; Rowson et al., 2016; Royal et al., 2016; McLaurin et al., 2017b; Maki et al., 2018), the ideal therapeutic would effectively ameliorate NCIs in both males and females. However, OVX female HIV-1 Tg and control animals were used to preclude the potential confounding effect of endogenous hormones. Thus, although the present study provides proof-of-concept that SE effectively ameliorates sustained attention deficits in HIV-1 Tg animals, further *in vivo* studies are required to elucidate the full potential of SE for HAND.

DATA AVAILABILITY

All datasets generated for this study are included in the manuscript.

ETHICS STATEMENT

Animals were maintained according to National Institute of Health (NIH) guidelines in AAALAC-accredited facilities. The animal facility was maintained at 21° ± 2°C, 50% ± 10% relative

humidity and had a 12-h light:12-h dark cycle with lights on at 07:00 h (EST). The project protocol was approved under federal assurance (#D16-00028) by the Institutional Animal Care and Use Committee (IACUC) at the University of South Carolina.

AUTHOR CONTRIBUTIONS

RB and CM conceived and designed the experiments. LM, CM and RB performed the experiments. LM, KM and CM analyzed the data. LM, KM, RB and CM wrote the article and critical appraisal and approval of final manuscript.

FUNDING

This work was supported in part by grants from NIH (National Institute on Drug Abuse, DA013137; Eunice Kennedy Shriver National Institute of Child Health and Human Development, HD043680; National Institute of Mental Health, MH106392; National Institute of Neurological Disorders and Stroke, NS100624) and the interdisciplinary research training program supported by the University of South Carolina Behavioral-Biomedical Interface Program. LM is currently a Scientific Officer at the NIDA Center for Clinical Trials Network.

REFERENCES

Abassi, M., Morawski, B. M., Nakigozi, G., Nakasujja, N., Kong, X., Meya, D. B., et al. (2017). Cerebrospinal fluid biomarkers and HIV-associated neurocognitive disorders in HIV-infected individuals in Rakai, Uganda. *J. Neurovirol.* 23, 369–375. doi: 10.1007/s13365-016-0505-9

Akaza, H. (2012). Prostate cancer chemoprevention by soy isoflavones: role of intestinal bacteria as the "second human genome". *Cancer Sci.* 103, 969–975. doi: 10.1111/j.1349-7006.2012.02257.x

Ances, B. M., and Ellis, R. J. (2007). Dementia and neurocognitive disorders due to HIV-1 infection. *Semin. Neurol.* 27, 86–92. doi: 10.1055/s-2006-956759

Ancuta, P., Kamat, A., Kunstman, K. J., Kim, E. Y., Autissier, P., Wurcel, A., et al. (2008). Microbial translocation is associated with increased monocyte activation and dementia in AIDS patients. *PLoS One* 3:e2516. doi: 10.1371/journal.pone.0002516

Arnold, H. M., Bruno, J. P., and Sarter, M. (2003). Assessment of sustained and divided attention in rats. *Curr. Protoc. Neurosci.* Chapter 8:Unit 8.5E. doi: 10.1002/0471142301.ns0805es22

Bertrand, S. J., Hu, C., Aksenova, M. V., Mactutus, C. F., and Booze, R. M. (2015). HIV-1 Tat and cocaine mediated synaptopathy in cortical and midbrain neurons is prevented by the isoflavone Equol. *Front. Microbiol.* 6:894. doi: 10.3389/fmicb.2015.00894

Bertrand, S. J., Mactutus, C. F., Aksenova, M. V., Espensen-Sturges, T. D., and Booze, R. M. (2014). Synaptodendritic recovery following HIV Tat exposure: neurorestoration by phytoestrogens. *J. Neurochem.* 128, 140–151. doi: 10.1111/jnc.12375

Bushnell, P. J. (1998). Behavioral approaches to the assessment of attention in animals. *Psychopharmacology* 138, 231–259. doi: 10.1007/s002130050668

Ceccarelli, G., Fratino, M., Selvaggi, C., Giustini, N., Serafino, S., Schietroma, I., et al. (2017). A pilot study on the effects of probiotic supplementation on neuropsychological performance and microRNA-29a-c levels in antiretroviral-treated HIV-1-infected patients. *Brain Behav.* 7:e00756. doi: 10.1002/brb3.756

Chao, L. L., Lindgren, J. A., Flenniken, D. L., and Weiner, M. V. (2004). ERP evidence of impaired central nervous system function in virally suppressed HIV patients on antiretroviral therapy. *Clin. Neurophysiol.* 115, 1583–1591. doi: 10.1016/j.clinph.2004.02.015

Cysique, L. A., Maruff, P., and Brew, B. J. (2004). Prevalence and pattern of neuropsychological impairment in human immunodeficiency virus infected/acquired immunodeficiency syndrome (HIV/AIDS) patients across pre and post-highly active antiretroviral therapy eras: a combined study of two cohorts. *J. Neurovirol.* 10, 350–357. doi: 10.1080/13550280490521078

Desplats, P., Dumaop, W., Smith, D., Adame, A., Everall, I., Letendre, S., et al. (2013). Molecular and pathologic insights from latent HIV-1 infection in the human brain. *Neurology* 80, 1415–1423. doi: 10.1212/WNL.0b013e31828c2e9e

Diaz Heijtz, R., Wang, S., Anuar, F., Qian, Y., Björkholm, B., Samuelsson, A., et al. (2011). Normal gut microbiota modulates brain development and behavior. *Proc. Natl. Acad. Sci. U S A* 108, 3047–3052. doi: 10.1073/pnas.1010529108

Dillon, S. M., Lee, E. J., Kotter, C. V., Austin, G. L., Dong, Z., Hecht, D. K., et al. (2014). An altered intestinal mucosal microbiome in HIV-1 infection is associated with mucosal and systemic immune activation and endotoxemia. *Mucosal Immunol.* 7, 983–994. doi: 10.1038/mi.2013.116

Dinh, D. M., Volpe, G. E., Duffalo, C., Bhalchandra, S., Tai, A. K., Kane, A. V., et al. (2015). Intestinal microbiota, microbial translocation, and systemic inflammation in chronic HIV infection. *J. Infect. Dis.* 211, 19–27. doi: 10.1093/infdis/jiu409

Eckard, A. R., Rosebush, J. C., O'Riodan, M. A., Graves, C. C., Alexander, A., Grover, A. K., et al. (2017). Neurocognitive dysfunction in HIV-infected youth: investigating the relationship with immune activation. *Antivir. Ther.* 22, 669–680. doi: 10.3851/imp3157

Fein, G., Biggins, C. A., and MacKay, S. (1995). Delayed latency of the event-related brain potential P3A component in HIV disease. Progressive effects with increasing cognitive impairment. *Arch. Neurol.* 52, 1109–1118. doi: 10.1001/archneur.1995.00540350103022

Gareau, M. G., Wine, E., Rodrigues, D. M., Cho, J. H., Whary, M. T., Philpott, D. J., et al. (2011). Bacterial infection causes stress-induced memory dysfunction in mice. *Gut* 60, 307–317. doi: 10.1136/gut.2009.202515

Garvey, L. J., Yerrakalva, D., and Winston, A. (2009). Correlations between computerized battery testing and a memory questionnaire for identification of neurocognitive impairment in HIV type 1-infected subjects on stable antiretroviral therapy. *AIDS Res. Hum. Retroviruses* 25, 765–769. doi: 10.1089/aid.2008.0292

Gelman, B. B., Lisinicchia, J. G., Chen, T. L., Johnson, K. M., Jennings, K., Freeman, D. H., et al. (2012). Prefrontal dopaminergic and enkephalinergic synaptic accomodiation in HIV-associated neurocognitive disorders and encephalitis. *J. Neuroimmune Pharmacol.* 7, 686–700. doi: 10.1007/s11481-012-9345-4

George, S., Petit, G. H., Gouras, G. K., Brundin, P., and Olsson, R. (2013). Nonsteroidal selective androgen receptor modulators and selective estrogen receptor β agonists moderate cognitive deficits and amyloid-β levels in a mouse model of Alzheimer's disease. *ACS Chem. Neurosci.* 4, 1537–1548. doi: 10.1021/cn400133s

Gori, A., Tincati, C., Rizzardini, G., Torti, C., Quirino, T., Haarman, M., et al. (2008). Early impairment of gut function and gut flora supporting a role for alteration of gastrointestinal mucosa in human immunodeficiency virus pathogenesis. *J. Clin. Microbiol.* 46, 757–758. doi: 10.1128/JCM.01729-07

Greenhouse, S. W., and Geisser, S. (1959). On methods in the analysis of profile data. *Psychometrika* 24, 95–112. doi: 10.1007/bf02289823

Guadalupe, M., Sankaran, S., George, M. D., Reay, E., Verhoeven, D., Shacklett, B. L., et al. (2006). Viral suppression and immune restoration in the gastrointestinal mucosa of human immunodeficiency virust type 1-infected patients initiating therapy during primary or chronic infection. *J. Virol.* 80, 8236–8247. doi: 10.1128/jvi.00120-06

Hamad, I., Abou Abdallah, R., Ravaux, I., Mokhtari, S., Tissot-Dupont, H., Michelle, C., et al. (2018). Metabarcoding analysis of eukaryotic microbiota in the gut of HIV-infected patients. *PLoS One* 13:e0191913. doi: 10.1371/journal.pone.0191913

Hao, J., Rapp, P. R., Leffler, A. E., Leffler, S. R., Janssen, W. G., Lou, W., et al. (2006). Estrogen alters spine number and morphology in prefrontal cortex of aged female rhesus monkeys. *J. Neurosci.* 26, 2571–2578. doi: 10.1523/JNEUROSCI.3440-05.2006

Harach, T., Marungruang, N., Duthilleul, N., Cheatham, V., McCoy, K. D., Frisoni, G., et al. (2017). Reduction of Aβ amyloid pathology in

APPPS1 transgenic mice in the absence of gut microbiota. *Sci. Rep.* 7:41802. doi: 10.1038/srep41802

Heaton, R. K., Franklin, D. R., Ellis, R. J., McCutchan, J. A., Letendre, S. L., LeBlanc, S., et al. (2011). HIV-associated neurocognitive disorders before and during the era of combination antiretroviral therapy: differences in rates, nature, and predictors. *J. Neurovirol.* 17, 3–16. doi: 10.1007/s13365-010-0006-1

Hestad, K. A., Menon, J. A., Silalukey-Ngoma, M., Franklin, D. R., Imasiku, M. L., Kalima, K., et al. (2012). Sex differences in neuropsychological performance as an effect of human immunodeficiency virus infection: a pilot study in Zambia, Africa. *J. Nerv. Ment. Dis.* 200, 336–342. doi: 10.1097/nmd.0b013e31824cc225

Jackson, R. L., Greiwe, J. S., and Schwen, R. J. (2011). Emerging evidence of the health benefits of S-equol, an estrogen receptor β agonist. *Nutr. Rev.* 69, 432–448. doi: 10.1111/j.1753-4887.2011.00400.x

Javadi-Paydar, M., Roscoe, R. F. Jr., Denton, A. R., Mactutus, C. F., and Booze, R. M. (2017). HIV-1 and cocaine disrupt dopamine reuptake and medium spiny neurons in female rat striatum. *PLoS One* 12:e0188404. doi: 10.1371/journal.pone.0188404

Justice, A. C. (2010). HIV and aging: time for a new paradigm. *Curr. HIV/AIDS Rep.* 7, 69–76. doi: 10.1007/s11904-010-0041-9

Kelly, J. R., Borre, Y., O'Brien, C., Patterson, E., El Aidy, S., Deane, J., et al. (2016). Transferring the blues: depression-associated gut microbiota induces neurobehavioural changes in the rat. *J. Psychiatr. Res.* 82, 109–118. doi: 10.1016/j.jpsychires.2016.07.019

Keshavarzian, A., Green, S. J., Engen, P. A., Voigt, R. M., Naqib, A., Forsyth, C. B., et al. (2015). Colonic bacterial composition in Parkinson's disease. *Mov. Disord.* 30, 1351–1360. doi: 10.1002/mds.26307

Khan, M. M., Dhandapani, K. M., Zhang, Q. G., and Brann, D. W. (2013). Estrogen regulation of spine density and excitatory synapses in rat prefrontal and somatosensory cerebral cortex. *Steroids* 78, 614–623. doi: 10.1016/j.steroids.2012.12.005

Kim, H., Ährlund-Richter, S., Wang, X., Deisseroth, K., and Carlén, M. (2016). Prefrontal parvalbumin neurons in control of attention. *Cell* 164, 208–218. doi: 10.1016/j.cell.2015.11.038

Kumar, A. M., Ownby, R. L., Waldrop-Valverde, D., Fernandez, B., and Kumar, M. (2011). Human immunodeficiency virus infection in the CNS and decreased dopamine availability: relationship with neuropsychological performance. *J. Neurovirol.* 17, 26–40. doi: 10.1007/s13365-010-0003-4

Lampe, J. W. (2009). Is equol the key to the efficacy of soy foods? *Am. J. Clin. Nutr.* 89, S1664–S1667. doi: 10.3945/ajcn.2009.26736t

Letendre, S. L., Ellis, R. J., Ances, B. M., and McCutchan, J. A. (2010). Neurologic complications of HIV disease and their treatment. *Top. HIV Med.* 18, 45–55.

Lund, T. D., Rhees, R. W., Setchell, K. D., and Lephart, E. D. (2001). Alterd sexually dimorphic nucleus of the preoptic area (SDN-POA) volume in adult Long-Evans rats by dietary soy phytoestrogens. *Brain Res.* 914, 92–99. doi: 10.1016/s0006-8993(01)02779-2

Maki, P. M., Rubin, L. H., Springer, G., Seaberg, E. C., Sacktor, N., Miller, E. N., et al. (2018). Differences in cognitive function between women and men with HIV. *J. Acquir. Immune Defic. Syndr.* 79, 101–107. doi: 10.1097/QAI.0000000000001764

Manderino, L., Carroll, I., Azcarate-Peril, M. A., Rochette, A., Heinberg, L., Peat, C., et al. (2017). Preliminary evidence for an association between the composition of the gut microbiome and cognitive function in neurologically healthy older adults. *J. Int. Neuropsychol. Soc.* 23, 700–705. doi: 10.1017/s1355617717000492

Marcotte, T. D., Deutsch, R., McCutchan, J. A., Moore, D. J., Letendre, S., Ellis, R. J., et al. (2003). Plasma Prediction of incident neurocognitive impairment by plasma HIV RNA and CD4 levels early after HIV seroconversion. *Arch. Neurol.* 60, 1406–1412. doi: 10.1001/archneur.60.10.1406

Matas, C. G., Silva, S. M., Marcon Bde, A., and Gonçalves, I. C. (2010). Electrophysiological manifestations in adults with HIV/AIDS submitted and not submitted to antiretroviral therapy. *Pro Fono* 22, 107–113. doi: 10.1590/S0104-56872010000200007

Mayer, E. A., Tillisch, K., and Gupta, A. (2015). Gut/brain axis and the microbiota. *J. Clin. Invest.* 125, 926–938. doi: 10.1172/JCI76304

McArthur, J. C., Steiner, J., Sacktor, N., and Nath, A. (2010). Human immunodeficiency virus-associated neurocognitive disorders mind the gap. *Ann. Neurol.* 67, 699–714. doi: 10.1002/ana.22053

McFarland, K., Price, D. L., Davis, C. N., Ma, J. N., Bonhaus, D. W., Burstein, E. S., et al. (2013). AC-186, a selective nonsteroidal estrogen receptor β agonist, shows gender specific neuroprotection in a Parkinson's disease rat model. *ACS Chem. Neurosci.* 4, 1249–1255. doi: 10.1021/cn400132u

McGaughy, J., and Sarter, M. (1995). Behavioral vigilance in rats: task validation and effects of age, amphetamine, and benzodiazepine receptor ligands. *Psychopharmacology* 117, 340–357. doi: 10.1007/bf02246109

McLaurin, K. A., Booze, R. M., and Mactutus, C. F. (2016). Progression of temporal processing deficits in the HIV-1 transgenic rat. *Sci. Rep.* 6:32831. doi: 10.1038/srep32831

McLaurin, K. A., Booze, R. M., and Mactutus, C. F. (2017a). Temporal processing demands in the HIV-1 transgenic rat: amodal gating and implications for diagnostics. *Int. J. Dev. Neurosci.* 57, 12–20. doi: 10.1016/j.ijdevneu.2016.11.004

McLaurin, K. A., Booze, R. M., Mactutus, C. F., and Fairchild, A. J. (2017b). Sex matters: robust sex differences in signal detection in the HIV-1 transgenic rat. *Front. Behav. Neurosci.* 11:212. doi: 10.3389/fnbeh.2017.00212

McLaurin, K. A., Moran, L. M., Li, H., Booze, R. M., and Mactutus, C. F. (2017c). A gap in time: extending our knowledge of temporal processing deficits in the HIV-1 transgenic rat. *J. Neuroimmune Pharmacol.* 12, 171–179. doi: 10.1007/s11481-016-9711-8

McLaurin, K. A., Booze, R. M., and Mactutus, C. F. (2018a). Evolution of the HIV-1 transgenic rat: utility in assessing the progression of HIV-1-associated neurocognitive disorders. *J. Neurovirol.* 24, 229–245. doi: 10.1007/s13365-017-0544-x

McLaurin, K. A., Cook, A. K., Li, H., League, A. F., Mactutus, C. F., and Booze, R. M. (2018b). Synaptic connectivity in medium spiny neurons of the nucleus accumbens: a sex-dependent mechanism underlying apathy in the HIV-1 transgenic rat. *Front. Behav. Neurosci.* 12:285. doi: 10.3389/fnbeh.2018.00285

McLaurin, K. A., Li, H., Booze, R. M., and Mactutus, C. F. (2019a). Disruption of timing: NeuroHIV progression in the post-cART era. *Sci. Rep.* 9:827. doi: 10.1038/s41598-018-36822-1

McLaurin, K. A., Moran, L. M., Li, H., Booze, R. M., and Mactutus, C. F. (2019b). The power of interstimulus interval for the assessment of temporal processing in rodents. *J. Vis. Exp.* 146:e58659. doi: 10.3791/58659

Meier, A., Chang, J. J., Chan, E. S., Pollard, R. B., Sidhu, H. K., Kulkarni, S., et al. (2009). Sex differences in the Toll-like receptor-mediated response of plasmacytoid dendritic cells to HIV-1. *Nat. Med.* 15, 955–959. doi: 10.1038/nm.2004

Monaco, C. L., Gootenberg, D. B., Zhao, G., Handley, S. A., Ghebremichael, M. S., Lim, E. S., et al. (2016). Altered virome and bacterial microbiome in human immunodeficiency virus -associated acquired immunodeficiency syndrome. *Cell Host Microbe* 19, 311–322. doi: 10.1016/j.chom.2016.02.011

Moran, L. M., Booze, R. M., and Mactutus, C. F. (2013). Time and time again: temporal processing demands implicate perceptual and gating deficits in the HIV-1 transgenic rat. *J. Neuroimmune Pharmacol.* 8, 988–997. doi: 10.1007/s11481-013-9472-6

Moran, L. M., Booze, R. M., and Mactutus, C. F. (2014). Modeling deficits in attention, inhibition, and flexibility in HAND. *J. Neuroimmune Pharmacol.* 9, 508–521. doi: 10.1007/s11481-014-9539-z

Mutlu, E. A., Keshavarzian, A., Losurdo, J., Swanson, G., Siewe, B., Forsyth, C., et al. (2014). A compositional look at the human gastrointestinal microbiome and immune activation parameters in HIV infected subjects. *PLoS Pathog.* 10:e1003829. doi: 10.1371/journal.ppat.1003829

Neufeld, K. M., Kang, N., Bienenstock, J., and Foster, J. A. (2011). Reduced anxiety-like behavior and central neurochemical changes in germ-free mice. *Neurogastroenterol. Motil.* 23, 255–264. doi: 10.1111/j.1365-2982.2010.01620.x

Nowak, P., Troseid, M., Avershina, E., Barqasho, B., Neogi, U., Holm, K., et al. (2015). Gut microbiota diversity predicts immune status in HIV-1 infection. *AIDS* 29, 2409–2418. doi: 10.1097/qad.0000000000000869

Parasuraman, R., and Davies, D. R. (1977). "A taxonomic analysis of vigilance performance," in *Vigilance: Theory, Operational Performance, and Physiological Correlates*, ed. R. R. Mackie (New York, NY: Plenum), 559–574.

Peng, J., Vigorito, M., Liu, X., Zhou, D., Wu, X., and Chang, S. L. (2010). The HIV-1 transgenic rat as a model for HIV-1 infected individuals on HAART. *J. Neuroimmunol.* 218, 94–101. doi: 10.1016/j.jneuroim.2009.09.014

Perez-Pardo, P., Dodiya, H. B., Engen, P. A., Naqib, A., Forsyth, C. B., Green, S. J., et al. (2018). Gut bacterial composition in a mouse

model of Parkinson's disease. *Benef. Microbes* 9, 799–814. doi: 10.3920/BM2017.0202

Pérez-Santiago, J., Gianella, S., Massanella, M., Spina, C. A., Karris, M. Y., Var, S. R., et al. (2013). Gut *Lactobacillales* are associated with higher CD4 and less microbial translocation during HIV infection. *AIDS* 27, 1921–1931. doi: 10.1097/QAD.0b013e3283611816

Reid, W., Sadowska, M., Denaro, F., Rao, S., Foulke, J., Hayes, N., et al. (2001). An HIV-1 transgenic rat that develops HIV-related pathology and immunologic dysfunction. *Proc. Natl. Acad. Sci. U S A* 98, 9271–9276. doi: 10.1073/pnas.161290298

Repunte-Canonigo, V., Lefebvre, C., George, O., Kawamura, T., Morales, M., Koob, G. F., et al. (2014). Gene expression changes consistent with neuroAIDS and impaired working memory in HIV-1 transgenic rats. *Mol. Neurodegener.* 9:26. doi: 10.1186/1750-1326-9-26

Romley, J. A., Juday, T., Solomon, M. D., Seekins, D., Brookmeyer, R., and Goldman, D. P. (2014). Early HIV treatment led to life expectancy gains valued at $80 billion for people infected in 1996–2009. *Health Aff.* 33, 370–377. doi: 10.1377/hlthaff.2013.0623

Roscoe, R. F., Mactutus, C. F., and Booze, R. M. (2014). HIV-1 transgenic female rat: synaptodendritic alterations of medium spiny neurons in the nucleus accumbens. *J. Neuroimmune Pharmacol.* 9, 642–653. doi: 10.1007/s11481-014-9555-z

Rowland, I. R., Wiseman, H., Sanders, T. A., Adlercreutz, H., and Bowey, E. A. (2000). Interindividual variation in metabolism of soy isoflavones and lignans: influence of habitual diet on equol production by the gut microflora. *Nutr. Cancer* 36, 27–32. doi: 10.1207/s15327914nc3601_5

Rowson, S. A., Harrell, C. S., Bekhbat, M., Gangavelli, A., Wu, M. J., Kelly, S. D., et al. (2016). Neuroinflammation and behavior in HIV-1 transgenic rats exposed to chronic adolescent stress. *Front. Psychiatry* 7:102. doi: 10.3389/fpsyt.2016.00102

Royal, W., Cherner, M., Burdo, T. H., Umlauf, A., Letendre, S. L., Jumare, J., et al. (2016). Associations between cognition, gender and monocyte activation among HIV infected individuals in Nigeria. *PLoS One* 11:e0147182. doi: 10.1371/journal.pone.0147182

Royal, W., Zhang, L., Guo, M., Jones, O., Davis, H., and Bryant, J. L. (2012). Immune activation, viral gene product expression and neurotoxicity in the HIV-1 transgenic rat. *J. Neuroimmunol.* 247, 16–24. doi: 10.1016/j.jneuroim.2012.03.015

Sarter, M., Givens, B., and Bruno, J. P. (2001). The cognitive neuroscience of sustained attention: where top-down meets bottom up. *Brain Res. Rev.* 35, 146–160. doi: 10.1016/s0165-0173(01)00044-3

Saylor, D., Dickens, A. M., Sacktor, N., Haughey, N., Slusher, B., Pletnikov, M., et al. (2016). HIV-associated neurocognitive disorder-pathogenesis and prospects for treatment. *Nat. Rev. Neurol.* 12:309. doi: 10.1038/nrneurol.2016.53

Schwen, R. J., Nguyen, L., Plomley, J. B., and Jackson, R. L. (2012). Toxicokinetics and lack of uterotropic effect of orally administered S-equol. *Food Chem. Toxicol.* 50, 1741–1748. doi: 10.1016/j.fct.2012.02.039

Setchell, K. D., Borriello, S. P., Hulme, P., Kirk, D. N., and Axelson, M. (1984). Nonsteroidal estrogens of dietary origin: possible roles in hormone-dependent disease. *Am. J. Clin. Nutr.* 40, 569–578. doi: 10.1093/ajcn/40.3.569

Setchell, K. D., Brown, N. M., and Lydeking-Olsen, E. (2002). The clinical importance of the metabolite equol-a clue to the effectiveness of soy and its isoflavones. *J Nutr* 132, 3577–3584. doi: 10.1093/jn/132.12.3577

Setchell, K. D., and Clerici, C. (2010). Equol: pharmacokinetics and biological actions. *J. Nutr.* 140, 1363S–1368S. doi: 10.3945/jn.109.119784

Setchell, K. D., and Cole, S. J. (2006). Method of defining equol-producer status and its frequency among vegetarians. *J. Nutr.* 136, 2188–2193. doi: 10.1093/jn/136.8.2188

Setchell, K. D., Clerici, C., Lephart, E. D., Cole, S. J., Heenan, C., Castellani, D., et al. (2005). S-equol, a potent ligand for estrogen receptor β, is the exclusive enantiomeric form of the soy isoflavone metabolite produced by human intestinal bacterial flora. *Am. J. Clin. Nutr.* 81, 1072–1079. doi: 10.1093/ajcn/81.5.1072

Sinharay, S., Lee, D., Shah, S., Muthusamy, S., Papadakis, G. Z., Zhang, X., et al. (2017). Cross-sectional and longitudinal small animal PET shows pre and post-synaptic striatal dopaminergic deficits in an animal model of HIV. *Nucl. Med. Biol.* 55, 27–33. doi: 10.1016/j.nucmedbio.2017.08.004

Spruston, N. (2008). Pyramidal neurons: dendritic structure and synaptic investigation. *Nat. Rev. Neurosci.* 9, 206–221. doi: 10.1038/nrn2286

Teeraananchai, S., Kerr, S. J., Amin, J., Ruxrungtham, K., and Law, M. G. (2017). Life expectancy of HIV-positive people after starting combination antiretroviral therapy: a meta-analysis. *HIV Med.* 18, 256–266. doi: 10.1111/hiv.12421

Tung, J., Barreiro, L. B., Burns, M. B., Grenier, J. C., Lynch, J., Grieneisen, L. E., et al. (2015). Social networks predict gut microbiome composition in wild baboons. *Elife* 4:e05224. doi: 10.7554/eLife.05224

Tuscher, J. J., Luine, V., Frankfurt, M., and Frick, K. M. (2016). Estradiol-mediated spine changes in the dorsal hippocampus and medial prefrontal cortex of ovariectomized female mice depend on ERK and mTOR activation in the dorsal hippocampus. *J. Neurosci.* 36, 1483–1489. doi: 10.1523/jneurosci.3135-15.2016

UNAIDS. (2017). *Fact Sheet-World AIDS Day 2018.* Available online at: http://www.unaids.org/sites/default/files/media_asset/UNAIDS_FactSheet_en.pdf. Accessed January 19, 2019.

UNAIDS. (2014). *People Aged 50 Years and Older.* Available online at: http://www.unaids.org/sites/default/files/media_asset/12_Peopleaged50yearsandolder.pdf. Accessed January 19, 2019.

Vigorito, M., LaShomb, A. L., and Chang, S. L. (2007). Spatial learning and memory in HIV-1 transgenic rats. *J. Neuroimmune Pharmacol.* 2, 319–328. doi: 10.1007/s11481-007-9078-y

Wang, S., Zhu, J., and Xu, T. (2018). 17β-estradiol (E2) promotes growth and stability of new dendritic spines *via* estrogen receptor β pathway in intact mouse cortex. *Brain Res. Bull.* 137, 241–248. doi: 10.1016/j.brainresbull.2017.12.011

Watkins, J. M., Cool, V. A., Usner, D., Stehbens, J. A., Nichols, S., Loveland, K. A., et al. (2000). Attention in HIV-infected children: results from the hemophilia growth and development study. *J. Int. Neuropsychol. Soc.* 6, 443–454. doi: 10.1017/s1355617700644028

Zhao, L., Mao, Z., Chen, S., Schneider, L. S., and Brinton, R. D. (2013). Early intervention with an estrogen receptor β-selective phytoestrogenic formulation prolongs survival, improves spatial recognition memory and slows progression of amyloid pathology in a female mouse model of Alzheimer's disease. *J. Alzheimers Dis.* 37, 403–419. doi: 10.3233/JAD-122341

Conflict of Interest Statement: The authors declare that the research was conducted in the absence of any commercial or financial relationships that could be construed as a potential conflict of interest.

frontiers in Behavioral Neuroscience

REVIEW
published: 22 August 2019
doi: 10.3389/fnbeh.2019.00190

Why Brain Oscillations Are Improving Our Understanding of Language

Antonio Benítez-Burraco[1] *and Elliot Murphy*[2]*

[1]Faculty of Philology, University of Seville, Seville, Spain, [2]Division of Psychology and Language Sciences, University College London, London, United Kingdom

We explore the potential that brain oscillations have for improving our understanding of how language develops, is processed in the brain, and initially evolved in our species. The different synchronization patterns of brain rhythms can account for different perceptual and cognitive functions, and we argue that this includes language. We aim to address six distinct questions—the What, How, Where, Who, Why, and When questions—pertaining to oscillatory investigations of language. Language deficits found in clinical conditions like autism, schizophrenia and dyslexia can be satisfactorily construed in terms of an abnormal, disorder-specific pattern of brain rhythmicity. Lastly, an eco-evo-devo approach to language is defended with explicit reference to brain oscillations, embracing a framework that considers language evolution to be the result of a changing environment surrounding developmental paths of the primate brain.

Keywords: oscillations, gamma, delta, theta, cross-frequency coupling, schizophrenia, autism, Neanderthals

OPEN ACCESS

Edited by:
Bahar Güntekin,
Istanbul Medipol University School of Medicine, Turkey

Reviewed by:
Birgit Mathes,
University of Bremen, Germany
Claudio Lucchiari,
University of Milan, Italy

***Correspondence:**
Elliot Murphy
elliotmurphy91@gmail.com

Speciality section:
This article was submitted to Pathological Conditions, a section of the journal Frontiers in Behavioral Neuroscience

Received: *08 May 2019*
Accepted: *06 August 2019*
Published: *22 August 2019*

Citation:
Benítez-Burraco A and Murphy E (2019) Why Brain Oscillations Are Improving Our Understanding of Language. Front. Behav. Neurosci. 13:190. doi: 10.3389/fnbeh.2019.00190

WHAT: THE OSCILLATORY NATURE OF LANGUAGE

During the last 150 years, neurolinguistic research has mostly focused on mapping language to the brain. The advent of various neuroimaging facilities (MRI, EEG/MEG, PET) has allowed neurolinguists to draw precise maps of the "language-ready" brain (that is, our species-specific brain configuration that allows us to learn and use language), both in pathological and neurotypical populations. It is now evident that language results from the coordinated activity of several widespread brain networks, encompassing different areas of both hemispheres (e.g., Poeppel et al., 2012; Chai et al., 2016, among many others). Nonetheless, as Poeppel (2012) has often stated, "mapping is not explaining."

Research into neural oscillations can allow us to circumvent this crucial limitation of neurolinguistics and provide robust, motivated explanations of how the brain processes language. Oscillations enable the construction of coherently organized neuronal assemblies through establishing transitory temporal correlations. They reflect synchronized fluctuations in neuronal excitability and are grouped by frequency, with the most common rhythms being delta (δ: ∼0.5–4 Hz), theta (θ: ∼4–8 Hz), alpha (α: ∼8–12 Hz), beta (β: ∼12–30 Hz) and gamma (γ: ∼30–150 Hz). These are generated by various cortical and subcortical structures and form a hierarchical structure. For example, slow rhythms can phase-modulate the power of faster rhythms (see Buzsáki and Draguhn, 2004; Buzsáki and Watson, 2012).

There are many reasons why oscillations are a promising candidate with respect to addressing Poeppel's (2012) mapping problem. For instance, they are primitive components of brain function and appear to be both domain-general (i.e., individual oscillations intervene in different cognitive and perceptual functions) and domain-specific (i.e., there exists a specific pattern of coupling between oscillations related to, and explaining, each cognitive function); an observation clearly

grounded by Başar and Stampfer (1985), Başar (2006) and Güntekin and Başar (2016; see also Hancock et al., 2017; Murphy, 2018). Importantly, the different "grammars" or "neural syntax" (Buzsáki and Watson, 2012) of brain rhythms accounting for different perceptual and cognitive functions are believed to be species-specific, but the atoms encompassing these grammars (i.e., individual rhythms) are shared across many species (Buzsáki et al., 2013; Brincat and Miller, 2015; Esghaei et al., 2015; Başar and Düzgün, 2016; Kikuchi et al., 2017; Murphy and Benítez-Burraco, 2018b). This circumstance grants a noteworthy evolutionary continuity to cognitive functions, which is particularly important in the case of language; meaning, certain elementary computational processes seem to be realized by brain oscillations (e.g., representational merging, working memory processes like search and maintain, and the coordination of distinct memory buffers; Murphy, 2018), and as such small tweaks to their phasal and coupling properties can yield modifications to their scope and format. This helps us cover the "What" question of our target of inquiry; namely, what the object of neurobiological inquiry is with respect to the implementational basis of language as conceived as a computational system. The remaining sections will cover some other questions surrounding the neural implementation of language, argue for a particular oscillatory model of language, and uniquely cover a large number of domains which bear some form of relation to the central theme of brain oscillations. Due to the rapidly expanding size of neurolinguistic research into oscillations, our discussion will include a selective overview of current themes in the literature.

HOW: OSCILLATIONS AND THE LINGUISTIC BRAIN

As also discussed extensively by Poeppel (e.g., Poeppel and Embick, 2005), current neurolinguistic research suffers from two crucial shortcomings. On the one hand, it relies on broad distinctions between components of language (e.g., the syntactic rules of grammar vs. the meanings of lexical representations), which actually involve multiple neural components, computations and representations. On the other hand, the core elements of linguistic theory (e.g., syntactic operations) do not map onto core neurobiological elements (neurons, nodes of Ranvier, etc.). It is consequently urgent for any neurolinguistic research to formulate a model of language in computational terms that can be processed by specific parts of the brain in real-time. For instance, we can decompose syntax into its constituent operations (MERGE, Labeling, Search; Adger, 2019) and representations [lexical and categorial features, such as N(oun) and A(djective); Adger and Svenonius, 2011]. Which seem generic enough to potentially make contact with certain neurobiological information processing frameworks. To take only the most commonly discussed cases, MERGE in its current formulation (Chomsky et al., Forthcoming) involves adding objects to a workspace, while Labeling involves attributing to a constructed set within a workspace a particular categorial identity.

Decomposing language into a specific pattern of "coupling" between different oscillations (whereby one feature of an oscillation, such as its phase, has its firing pattern synchronized with a feature of a distinct oscillation, such as its amplitude) appears feasible. Importantly, this approach satisfactorily accounts for core facets of language according to major linguistic theories, in particular, generative theories. For instance, the combinatorial power of MERGE (the basic operation in the modern generative approach to language, which adds an object to a given workspace) and the cyclic power of Labeling (the operation which chooses the lexical features to be assigned to the merged syntactic set) are able to be implemented/indexed *via* various oscillatory interactions such as forms of "cross-frequency" (i.e., between distinct frequencies) coupling (Murphy, 2015, 2018; Meyer, 2018). In the most recent and comprehensive oscillatory model of language comprehension defended in Murphy (2016, 2018) and which is briefly summarized in **Figure 1**, empirical and conceptual motivations are presented to defend the idea that δ-θ inter-regional phase-amplitude coupling constructs multiple sets of linguistic syntactic and semantic features. This occurs when the phase of δ is synchronized with the amplitude of θ. Causal directionality remains an open issue, though certain cases of θ-γ coupling appear to exhibit unidirectional prefrontal-hippocampal cortex coupling from γ activity to θ activity (Nandi et al., 2019). The full computational power of our model is achieved *via* distinct β and γ sources also being coupled with θ (e.g., θ-γ phase-amplitude coupling) for, respectively, syntactic prediction and conceptual binding. This framework goes considerably beyond the discussion of combinatorics, representational accommodation, and prediction presented in other recent accounts (e.g., Meyer, 2018). It also provides a specific neural code for *recursive hierarchical phrase structure*, the core distinctive feature of human language (reapplying the set-forming operation MERGE to its own output), with α also being involved in the early stages of binding (Pina et al., 2018) to synchronize distant cross-cortical γ sites required for the "θ-γ code" (θ-γ phase-amplitude coupling) of working memory and to modulate attentional resources (**Figure 1**).

Figure 2 contrasts the classical "language areas" with the model we are defending, revealing a considerably greater degree of complexity. To illustrate this point further, Murphy (2018) discusses the high likelihood that traveling oscillations are involved in language comprehension. These are oscillations which "move" across the brain; meaning, the spiking of neural clusters is coordinated not just across two fixed points (e.g., hippocampus and left inferior frontal cortex inter-regional phase-amplitude coupling) but across a particular extended path. These traveling oscillations have recently been shown to coordinate neural activity across widespread brain networks and across different temporal windows, and to support brain connectivity and function (Zhang et al., 2018). Accordingly, under the model in **Figure 2**, δ waves cycle across left inferior frontal parts of the cortex, building up the syntactic workspace phrase-by-phrase and potentially being endogenously reset by a newly constructed phrase, and being coupled to traveling θ waves which perform the same function (**Figure 2**; blue

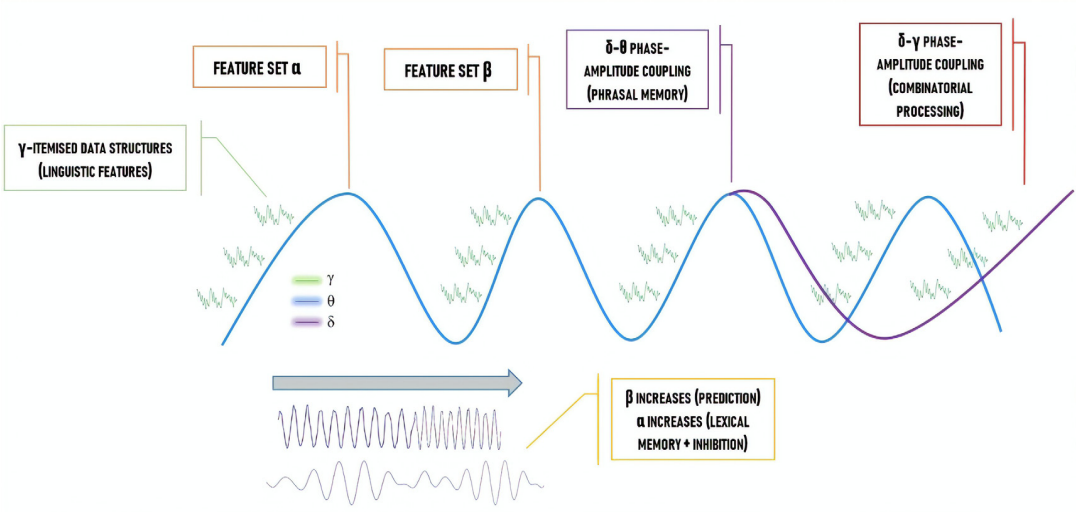

FIGURE 1 | The "How" Question: a neural code for language, representing the various cross-frequency coupling interactions proposed to implement hierarchical phrase structure building.

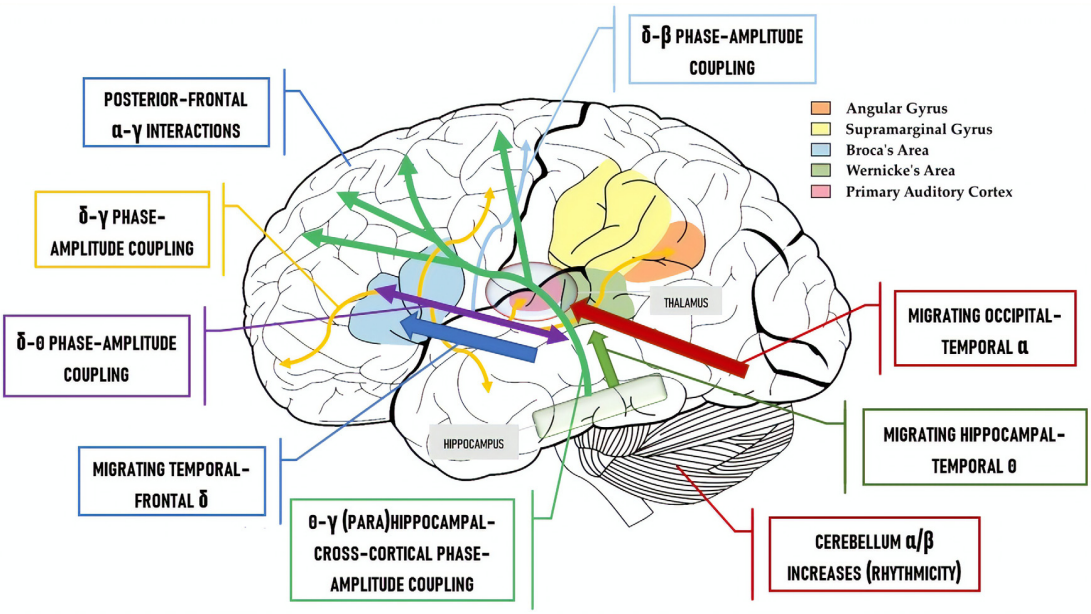

FIGURE 2 | The "Where" Question: a cartographic map of where the neural code for language is hypothesized to be implemented.

arrow and purple box). Traveling δ waves are assumed to be responsible for patterning spiking from single- to multi-unit lexical structures in each δ cycle. As such, δ would coordinate phrasal construction while θ-γ interactions (green arrows) would support the representational construction of linguistic feature-sets (Covington and Duff, 2016; Ding et al., 2016). Lastly, as Gągol et al. (2018) reveal, δ-γ coupling is involved in fluid intelligence (solving problems using a range of cognitive faculties on the fly, spontaneously), whereby δ embeds cross-cortical γ rhythms depending on the cortical areas needed for the particular task, i.e., geometric reasoning, visual processing, etc. Murphy (2018) proposes that δ-γ coupling may be a generic combinatorial process, combining representations from within and across domains (**Figure 2**; yellow box and yellow arrows), and the cerebellum has also been shown to play a role in processing linguistic rhythmicity and hence aids phrasal processing in frontotemporal regions (Murphy, 2019). Meanwhile, linguistic prediction seems to be implemented *via* coupling between frontal γ amplitude and posterior α phase (Wang et al., 2018) and prefrontal predictions facilitate

δ-entrained speech tracking in anterior superior temporal gyrus (Keitel et al., 2017).

Although we refer the reader to Murphy (2018) for further empirical details, we should briefly mention that there is increasing support for this model. For instance, Brennan and Martin (2019) analyzed a naturalistic story-listening EEG dataset and showed that δ-γ coupling increases with the number of predicates bound on a given word (the authors only analyzed the central Cz electrode, so further analysis is required to flesh out the picture). They also discovered an increasing scale of δ-θ coupling beginning at the point of a word completing a single phrase, through to words completing two and three phrases. As such, δ-γ and δ-θ coupling increases with predication. Overall, these observations illustrate how the presently defended analysis of interacting, traveling waves can help explain how such a complex thing as a fragment of discourse, which entails both linguistic and extralinguistic (i.e., encyclopaedic) knowledge, is processed.

WHERE: A SYSTEMS BIOLOGY APPROACH TO LANGUAGE

Mastering a language and being able to use it depends on having received the proper triggering environmental stimuli during development. But this is only possible because of complex biological processes, which are assembled mostly under genetic guidance. Thousands of biological factors interact to regulate language development and processing. Nevertheless, for many years it was not clear where the specificity of language resides—and if there is much biologically specific at all. Accordingly, although language seems to be a very specialized, human-specific faculty, it undoubtedly relies on biological components, such as its genetic basis, which may not be specific to language since "language genes" contribute to a range of biological functions.

Brain oscillations are highly heritable traits (van Beijsterveldt et al., 1996; Linkenkaer-Hansen et al., 2007; Müller et al., 2017), including oscillations related to language (Araki et al., 2016). As **Figure 3** proposes, a comprehensive model linking oscillations to neural wiring should be our goal. Murphy and Benítez-Burraco (2018a) show that the basic aspects of the language oscillome (that is, the particular phasal and cross-frequency coupling properties of neural oscillations involved in, and accounting for, language) result from genetic guidance, and a confident list of candidate genes for this guidance can be posited (although see Soloduchin and Shamir, 2018 for an alternative account through which oscillatory activity can emerge *via* an unsupervised learning process of spike timing-dependent plasticity). Moreover, a number of linking hypotheses connecting particular genes and oscillatory behavior implicated in language processing can be posited, suggesting that much of the oscillome is likely genetically-directed; the set of genes implicated here is termed the *oscillogenome* (see also **Figure 4** below). Importantly, these candidate genes map on to specific aspects of brain function, particularly on to neurotransmitter function, and through dopaminergic, GABAergic and glutamatergic synapses (see also Koch et al., 2016 for a neuropharmacological review of oscillations).

WHO: BRAIN OSCILLATIONS AND LANGUAGE DISORDERS

Most cognitive disorders entail problems with language. But there are many differences here depending on who we are focusing our attention on. Whereas each disorder can be said to exhibit a disorder-specific abnormal language profile (with deficits in the domains of phonology, syntax, semantics, or language use), each particular deficit is commonly found in several disorders, to the extent that most of them are shared by different disorders with a different symptomatology and etiology. This accounts for the frequent comorbidity of disorders. Moreover, these deficits are only indirectly related to (broad) cognitive deficits (for instance, certain syntactic deficits involve much broader working memory and attentional problems; Tilot et al., 2015). Finally, although most of these conditions have a genetic basis, the same gene can contribute to more than one cognitive disorder. This circumstance seemingly explains why the divide between the genetics and pathophysiology of prevalent cognitive/language disorders like autism spectrum disorder, schizophrenia or developmental dyslexia remains open. In recent years, a number of promising directions have emerged for investigating the neural and genetic basis of these disorders. Due to an emerging body of work concerning the oscillatory dynamics of language processing, it has become possible to associate certain features of the language deficit profile of autism, schizophrenia and developmental dyslexia with abnormal patterns of brain oscillations. Likewise, contemporary developments have allowed researchers to explore the genetic basis of particular cellular activity giving rise to oscillatory rhythms in distinct brain regions (e.g., Hancock et al., 2017) which appear to differ from neurotypical behavior in certain populations exhibiting language deficits, and which thereby allow us to make inferences about the likely genetic basis of these disorders.

In a series of related articles (Benítez-Burraco et al., 2016; Benítez-Burraco and Murphy, 2016; Murphy and Benítez-Burraco, 2016; Wilkinson and Murphy, 2016; Jiménez-Bravo et al., 2017; Murphy and Benítez-Burraco, 2018a) it has been shown that the distinctive language deficits found in clinical conditions like autism, schizophrenia and developmental dyslexia can be satisfactorily construed in terms of an abnormal, disorder-specific pattern of brain rhythmicity. Moreover, selected candidate genes for these conditions seemingly account for this abnormal rhythmicity and are differentially expressed in selected brain areas (see **Figure 4**), conferring a degree of specificity to this set of genes compared to other candidates for language dysfunction in these conditions. Ultimately, the genes encompassing the language oscillogenome are expected to exhibit a distinctive, disorder-specific pattern of up- and down-regulation in the brains of patients. In other words, the molecular signature of each disorder from this oscillogenomic perspective is expected to mostly rely not on the set of genes involved, which are thought to be essentially the same, but on their expression patterns in each brain region, which is hypothesized to be different in each condition. This is expected to contribute to the bridging of genes (with their disorder-specific expression profile) and oscillations (with their

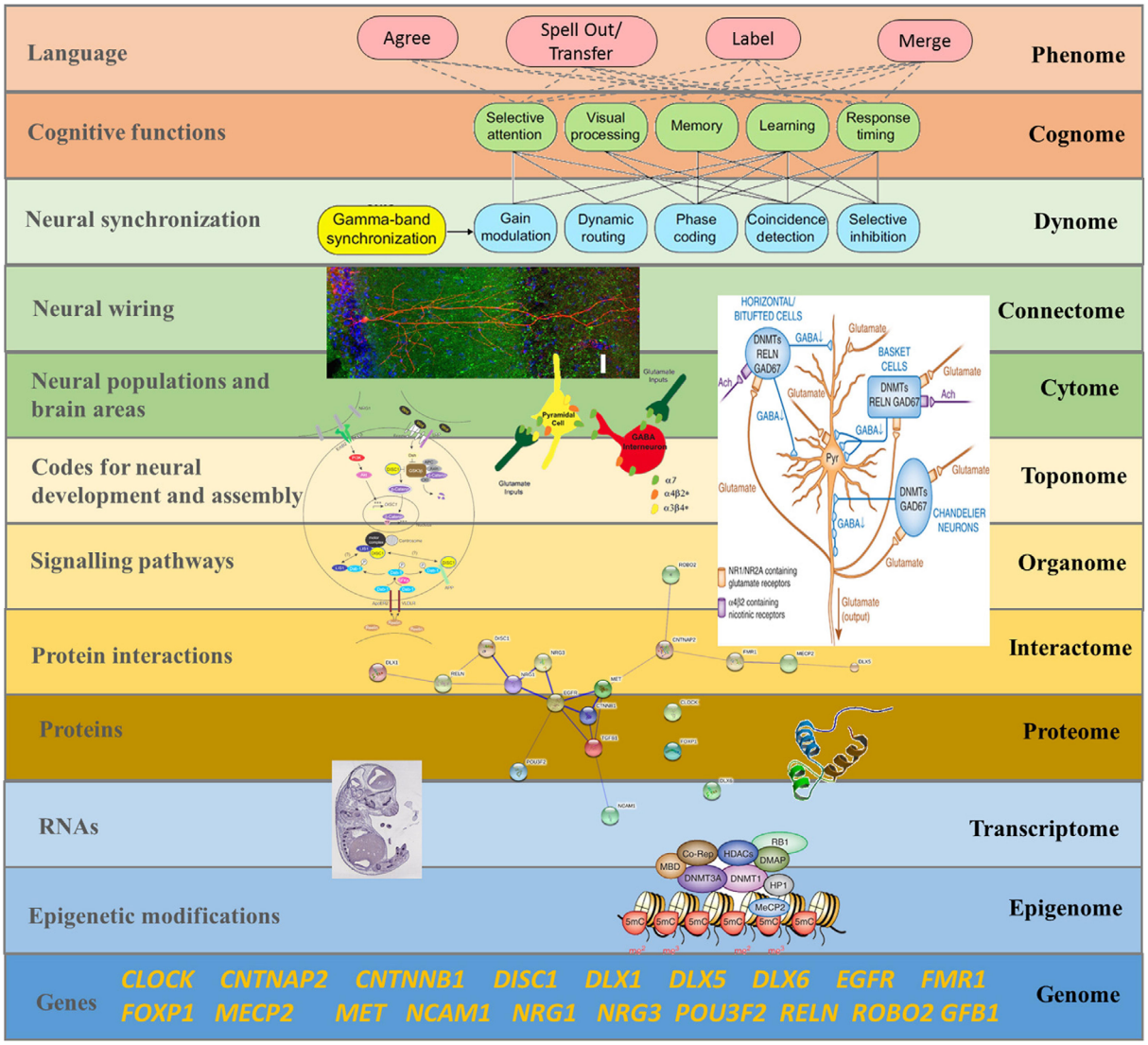

FIGURE 3 | The "Who" Question: a systems biology approach to language, focused on the dynamics of cellular and organismal function and on the (emergent) properties of the whole system, is suggested if one wants to understand how language emerges from these complex interactions (reproduced from Murphy and Benítez-Burraco, 2017; Figure 8).

disorder-specific rhythmic profile) and language (which is also impaired in a disorder-specific way).

As an example of this systems biology approach to language disorders that relies on brain oscillations, consider autism. Both structural and functional aspects of language are impaired in autism. Approximately one-third of children with autism exhibit difficulties with morphosyntax (Tager-Flusberg and Joseph, 2003) and both adults and children with autism typically use a low number of functional words (Tager-Flusberg et al., 1990). This population also integrates and consolidates semantic information differently from neurotypicals when processing sentences (Eigsti et al., 2011). More specific impairments include problems with relative clauses, *wh*-questions, raising and passives (Perovic and Janke, 2013). These difficulties all speak to a more general deficit in procedural memory. Concerning the oscillatory basis of these deficits, increased γ power has been documented for individuals with autism (e.g., Kikuchi et al., 2013), and since this rhythm is involved in the binding of semantic features this finding can likely contribute to a causal-explanatory oscillatory model of language deficits. Kikuchi et al. (2013) additionally found reduced cross-cortical θ, α and β in the brain of individuals with autism, while Bangel et al. (2014) documented lower β power during a number estimation task. Given the role of these slower rhythms in cross-cortical information integration, and the major role β likely plays in syntactic processing (Murphy, 2018), problems with executing complex syntactic operations like passivization and interpreting *wh*-dependencies seems not too surprising. At the same time, many of the differences in

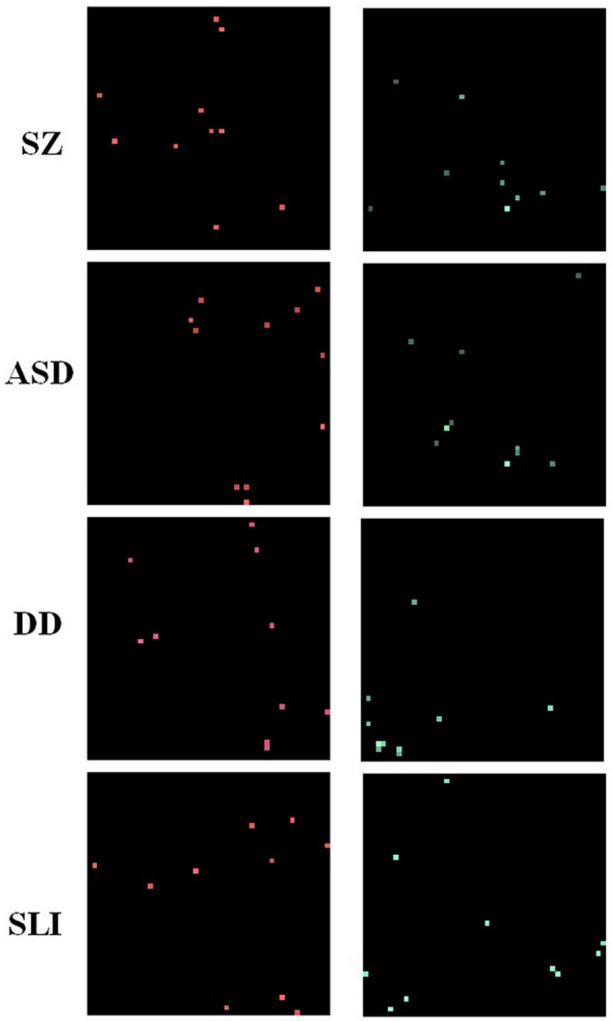

	SZ	ASD	DD	SLI	Oscillomic/oscillopathic features
AKT1	+				θ, α, β, γ
APOE	+				θ, α, δ
AUTS2	+			+	Epilepsy
CACNA1C	+	+			β, γ
CACNA1I	+	+			Sleep spindles
CNR1	+	+			θ, γ
CNTNAP2	+	+			α
COL4A2			+		Epilepsy
COMT	+	+			α
CX3CR1	+	+			θ
CYP19A1			+		Seizures
DCDC2			+		MMN 300-700 ms
DISC1	+	+			θ
DLX5	+	+			γ
DLX6	+	+			γ
DPP10	+	+			K^+ flux regulation
DYRK1A		+			Inhibition of neural activity
EGR1	+				Epilepsy
ELP4		+			High amplitude centrotemporal sharp waves
ERBB4	+	+			γ
FMR1	+	+			θ, γ
FOXP1	+	+		+	Epileptiform discharges
GABARAP			+		β, γ, paroxysmal sharp waves
GABRB3	+	+			β, γ, paroxysmal sharp waves
GAD1	+	+			Long-interval cortical inhibition
GRIN2A	+	+		+	γ
GRIN2B	+	+		+	EEG anomalies, epilepsy
GRM8	+	+			θ
HTR1A	+				γ
KANSL1			+		Epilepsy
KIAA0319			+		MMN 300-700 ms
MAPK14	+				Kainate-induced seizures
MBD5	+	+		+	Epilepsy
MECP2	+	+			γ , β
NRG1	+	+			γ
NSF			+		Epilepsy
PDGFRB	+	+			γ
PLAUR		+		+	Seizures
PTEN		+			Epilepsy, paroxysmal EEG
ROBO1	+	+	+		Epilepsy
S100B	+		+		γ
SCN1A		+			θ
SETBP1		+		+	Epilepsy
SHANK3	+	+			Seizures, abnormal EEG
SIRT1	+				Seizures
SNAP25	+	+	+		Epilepsy
SRPX2				+	Centrotemporal sharp waves
ZNF804A	+	+			γ

FIGURE 4 | The "Why" Question. Genes involved in brain rhythmicity are expected to exhibit a disorder-specific expression profile in the brain of affected people. The figure shows the expression grids of genes involved in brain rhythmicity that are also candidates for four prevalent conditions involving problems with language: schizophrenia (SZ), autism spectrum disorder (ASD), developmental dyslexia (DD) and specific language impairment (SLI). The grids were generated with Enrichr (amp.pharm.mssm.edu). Each grid square represents a brain region in the Allen Brain Atlas (portal.brain-map.org). Brain regions where genes of interest are upregulated are displayed in red (the brighter the square, the more upregulated the gene is in the selected region). Regions in which genes are downregulated are shown in green (the brighter the color, the more downregulated the gene is). The genes considered in the analysis, which can be regarded as robust candidates for the language oscillogenome, are displayed in the table, with an indication of their role in brain rhythmicity (adapted from Murphy and Benítez-Burraco, 2018a; Figure 2 and Table 1).

cognition and behavior found in autism are seemingly explained by differences in oscillatory activity resulting from pathogenic genetic diversity, mostly in genes indirectly or directly related to GABAergic activity, like *MECP2* (Liao et al., 2012), and genes encoding some of the GABAA-receptor subunits (particularly of β2 and β3; Porjesz et al., 2002; Heistek et al., 2010), or *PDGFRB* (Nguyen et al., 2011; Nakamura et al., 2015).

These oscillatory anomalies found in cognitive disorders in tandem with an increasingly sophisticated oscillatory model of language (see "How: Oscillations and the Linguistic Brain" section above) can yield predictions about the cortical profile of particular individuals exhibiting certain language deficits. Specifically, considering language disorders as "oscillopathic" traits (that is, involving abnormal patterns of brain rhythmicity) is a productive way to generate endophenotypes of the disorders and achieve earlier and more accurate diagnoses.

WHY: OSCILLATIONS AND LANGUAGE EVOLUTION

As discussed above, language is a complex system. Accordingly, and addressing the looming question of why our brains alone possess the capacity for language, we should expect that specific evolutionary changes in components of this complex system prompted the transition to language-readiness. At present, we have precise characterizations of the recent evolutionary changes

in our brain and in our genetic endowment that seemingly account for our language-readiness (see Boeckx and Benítez-Burraco, 2014; Neubauer et al., 2018; Gunz et al., 2019). Nonetheless, as noted above, brain anatomy and functional maps can only provide indirect and rough accounts of how the brain processes language. Moreover, because the specificity of language can seemingly be hosted at the oscillomic level, and because each species-specific pattern of brain coupling builds on a shared set of basic rhythms, we should expect that the human-specific pattern of coupling accounting for our language-readiness resulted from selected changes in the oscillatory signature of the hominin brain. These modifications can be traced *via* comparative studies, with humans exhibiting a species-specific richness in possible cross-frequency couplings (for references and discussion, see Murphy, 2018). Nevertheless, we should stress that these traces are not thoroughly well-established, and we must rely purely on current understanding.

Regarding extinct hominins, such as Neanderthals or Denisovans, it is evident that we cannot track the oscillatory activity of their brains. However, it is possible to rely on available (although still scarce) information from genes encompassing the language oscillogenome—as characterized above—to infer the particular changes in phasal and cross-frequency coupling properties of neural oscillations that resulted in the emergence of core features of language. Accordingly, as **Figure 5** depicts, several candidates for the language oscillogenome show differences in their methylation patterns (and hence, in their expression levels) between Neanderthals and anatomically-modern humans (we refer the reader to Murphy and Benítez-Burraco, 2018a). Some of these differences can confidently be related to neural function (i.e., directly impacting firing patterns), whereas others have (so far) simply been associated with particular conditions. These differences can be informative of differences in cognitive functions important for language; for instance, we can infer that the working memory capacity of Neanderthals likely differed from that of modern humans due to the differences in θ and γ expression (Murphy and Benítez-Burraco, 2018a). Nevertheless, while they gesture towards a concrete research programme, these suggestions remain highly speculative.

WHEN: AN ECO-EVO-DEVO APPROACH TO LANGUAGE

A growing body of evidence suggests that regions of the human genome showing signals of positive selection in our species are enriched in candidates for cognitive conditions entailing problems with language, like autism (Polimanti and Gelernter, 2017) or schizophrenia (Srinivasan et al., 2016). These findings suggest that these conditions may have mainly developed recently in our evolutionary history. This is seemingly due to the fact that the most recently evolved components of human cognition are more sensitive to the deleterious effect of developmental perturbations resulting from factors either internal to the organism or external to it. This is because of the lack of robust compensatory mechanisms to any damage; these mechanisms are typically found in more ancient biological functions which have been shaped by stronger selective pressures

GENE	FIXED AA CHANGE IN AMHS	POSITIVELY SELECTED IN AMHS	DIFFERENTIALLY METHYLATED IN AMH SKELETAL SAMPLES	ENRICHED IN AMH DMRS	OSCILLOMIC/OSCILLOPATHIC FEATURES
AUTS2		✓	↑(body gene)		Epilepsy
CACNA1C			↑ (body gene)		β, γ
CNTNAP2	✓				α
COL4A2			↑(body gene)		Epilepsy
COMT			↑(downstream the gene)		α
DYRK1A		✓			Inhibition of neural activity
EGR1				✓	Epilepsy
ELP4		✓			High amplitude centrotemporal sharp waves
FMR1	✓				θ, γ
FOXP1		✓	↑(body gene)		Epileptiform discharges
ROBO1		✓			Epilepsy

FIGURE 5 | The "Why" Question. Selected genes encompassing the language oscillogenome exhibit fixed derived changes in modern humans compared to extinct Neanderthals, either in their regulatory or coding regions, or in their methylation patterns (suggestive of differences in their expression levels; reproduced from Murphy and Benítez-Burraco, 2018b; Table 1).

(see Toro et al., 2010 for discussion). In a similar vein, when searching for the basis of genomic trade-offs potentially involved in the evolution of the human brain, Sikela and Searles Quick (2018; p. 2) have concluded that changes in the genome producing beneficial results might persist despite their ability to also produce diseases and that "the same genes that were responsible for the evolution of the human brain are also a significant cause of autism and schizophrenia". This is in line with current views of complex diseases as the consequence of the uncovering of cryptic variation resulting from the assorted changes (genomic, demographic, behavioral) promoting the transition from an ape-like biology to a human-specific biology.

As noted above, a systems biology approach to language is preferable since it allows us to understand how language emerges from the complex interactions among thousands of biological factors, most notably oscillations. It is now clear that because language evolved mostly as a result of specific changes in the developmental path of the hominin brain in response to changes in the environment in which our ancestors lived (the latter encompassing both physical and cultural factors), we need to consider developmental, evolutionary, and ecological aspects on a par. This can be viewed as an *eco-evo-devo* approach to language, that pays attention to language evolution (*evo*) and human ecology (*eco*) to better understand language development (*devo*; see Benítez-Burraco and Kimura, 2019). This approach should enable us to improve our understanding of how language is implemented in the brain, how it evolved, and how it is disrupted in language disorders. In addition, the evidence presented suggests that this can be ideally achieved by focusing on oscillations, in particular since oscillations can explicitly be linked, in some way, to *all* major topics in the study of the computational nature of language (i.e., online processing; timing of evolution; brain mapping; explanation for language deficits; development). Specifically, oscillations might be a better (or perhaps, the optimum) candidate for properly defining the morphospace or adaptive landscape of language growth in the species, either pathological or neurotypical; that is, defining the limited set of language faculties available during development.

CONCLUSIONS

Overall, the evidence presented in this article suggests that brain oscillations can be a very fruitful approach for understanding how language is implemented in our brain as a result of our evolutionary history. This is not just because oscillations are both domain-general and domain-specific, but because they help explain why and how *processing*, *evolution* and *development* are closely interwoven. Yet, we should stress that while oscillations are improving our understanding of the neural basis of language, they are not (currently) improving our understanding of the language system itself: programmatic and experimental direction from the theoretical linguistics literature will still be required, and care should be taken when attributing certain properties of "language" (however formulated, e.g., computational system, externalization system) to particular oscillatory behavior. Although new avenues for research are rapidly opening up, there remain a large number of unanswered questions: Which sub-domains of linguistics have the potential to make greater contact with the life sciences (e.g., pragmatics)? What are the anatomical similarities and differences regarding human and nonhuman temporal processing networks? How does the notion of a traveling oscillator tie in with existing findings concerning the supposedly fixed, regionalized oscillatory activity found in existing EEG and MEG experiments of language processing? How might one test the hypothesis that nonhuman primates exhibit a distinctly organized array of cortical cross-frequency couplings? Solving these and other complex questions will help refine our oscillatory view of human language.

AUTHOR CONTRIBUTIONS

Both authors contributed to all sections.

REFERENCES

Araki, T., Hirata, M., Yanagisawa, T., Sugata, H., Onishi, M., Watanabe, Y., et al. (2016). Language-related cerebral oscillatory changes are influenced equally by genetic and environmental factors. *Neuroimage* 142, 241–247. doi: 10.1016/j.neuroimage.2016.05.066

Adger, D. (2019). *Syntax Unlimited: The Science Behind Our Most Creative Power*. Oxford: Oxford University Press.

Adger, D., and Svenonius, P. (2011). "Features in minimalist syntax," in *The Handbook of Linguistic Minimalism*, ed. C. Boeckx (Oxford: Blackwell), 27–51.

Bangel, K. A., Batty, M., Ye, A. X., Meaux, E., Taylor, M. J., and Doesburg, S. M. (2014). Reduced beta band connectivity during number estimation in autism. *Neuroimage Clin.* 6, 202–213. doi: 10.1016/j.nicl.2014.08.020

Başar, E. (2006). The theory of the whole-brain-network. *Int. J. Psychophysiol.* 60, 133–138. doi: 10.1016/j.ijpsycho.2005.12.007

Başar, E., and Düzgün, A. (2016). How is the brain working?: research on brain oscillations and connectives in a new "Take-Off" state. *Int. J. Psychophysiol.* 103, 3–11. doi: 10.1016/j.ijpsycho.2015.02.007

Başar, E., and Stampfer, H. G. (1985). Important associations among EEG-dynamics, event related potentials, short-term memory and learning. *Int. J. Neurosci.* 26, 161–180. doi: 10.3109/00207458508985615

Benítez-Burraco, A., and Kimura, R. (2019). Robust candidates for language development and evolution are significantly dysregulated in the blood of people with Williams syndrome. *Front. Neurosci.* 13:258. doi: 10.3389/fnins.2019.00258

Benítez-Burraco, A., Lattanzi, W., and Murphy, E. (2016). Language impairments in ASD resulting from a failed domestication of the human brain. *Front. Neurosci.* 10:373. doi: 10.3389/fnins.2016.00373

Benítez-Burraco, A., and Murphy, E. (2016). The oscillopathic nature of language deficits in autism: from genes to language evolution. *Front. Hum. Neurosci.* 10:120. doi: 10.3389/fnhum.2016.00120

Boeckx, C., and Benítez-Burraco, A. (2014). The shape of the human language-ready brain. *Front. Psychol.* 5:282. doi: 10.3389/fpsyg.2014.00282

Brennan, J. R., and Martin, A. E. (2019). "Delta-gamma phase-locking indexes composition of predicates," in *Poster Presented at 23rd Annual Meeting of the Cognitive Neuroscience Society*, San Fransisco, 23–26.

Brincat, S. L., and Miller, E. K. (2015). Frequency-specific hippocampal-prefrontal interactions during associative learning. *Nat. Neurosci.* 18, 576–581. doi: 10.1038/nn.3954

Buzsáki, G., and Draguhn, A. (2004). Neuronal oscillations in cortical networks. *Science* 304, 1926–1929. doi: 10.1126/science.1099745

Buzsáki, G., Logothetis, N., and Singer, W. (2013). Scaling brain size, keeping timing: evolutionary preservation of brain rhythms. *Neuron* 80, 751–764. doi: 10.1016/j.neuron.2013.10.002

Buzsáki, G., and Watson, B. O. (2012). Brain rhythms and neural syntax: implications for efficient coding of cognitive content and neuropsychiatric disease. *Dialogues Clin. Neurosci.* 14, 345–367.

Chai, L. R., Mattar, M. G., Blank, I. A., Fedorenko, E., and Bassett, D. S. (2016). Functional network dynamics of the language system. *Cereb. Cortex* 26, 4148–4159. doi: 10.1093/cercor/bhw238

Chomsky, N., Gallego, Á. J., and Ott, D. (Forthcoming). "Generative grammar and the faculty of language: insights, questions and challenges," in *Generative Syntax: Questions, Crossroads and Challenges. Special Issue of Catalan Journal of Linguistics*, eds Á. J. Gallego and D. Ott.

Covington, N. V., and Duff, M. C. (2016). Expanding the language network: direct contributions from the hippocampus. *Trends Cogn. Sci.* 20, 869–870. doi: 10.1016/j.tics.2016.10.006

Ding, N., Melloni, L., Zhang, H., Tian, X., and Poeppel, D. (2016). Cortical tracking of hierarchical linguistic structures in connected speech. *Nat. Neurosci.* 19, 158–164. doi: 10.1038/nn.4186

Eigsti, I. M., de Marchena, A. B., Schuh, J. M., and Kelley, E. (2011). Language acquisition in autism spectrum disorders: a developmental review. *Res. Autism. Spectr. Disord.* 5, 681–691. doi: 10.1016/j.rasd.2010.09.001

Esghaei, M., Mohammad Reza, D., and Stefan, T. (2015). Attention decreases phase-amplitude coupling, enhancing stimulus discriminability in cortical area MT. *Front. Neural Circuits* 9:82. doi: 10.3389/fncir.2015.00082

Gągol, A., Magnuski, M., Kroczek, B., Kaamaa, P., Ociepka, M., Santarnecchi, E., et al. (2018). Delta-gamma coupling as a potential neurophysiological mechanism of fluid intelligence. *Intelligence* 66, 54–63. doi: 10.1016/j.intell.2017.11.003

Güntekin, B., and Başar, E. (2016). Review of evoked and event-related delta responses in the human brain. *Int. J. Psychophysiol.* 103, 43–52. doi: 10.1016/j.ijpsycho.2015.02.001

Gunz, P., Tilot, A. K., Wittfeld, K., Teumer, A., Shapland, C. Y., van Erp, T. G. M., et al. (2019). Neandertal introgression sheds light on modern human endocranial globularity. *Curr. Biol.* 29:895. doi: 10.1016/j.cub.2019.02.008

Hancock, R., Pugh, K. R., and Hoeft, F. (2017). Neural noise hypothesis of developmental dyslexia. *Trends Cogn. Sci.* 21:909. doi: 10.1016/j.tics.2017.08.003

Heistek, T. S., Jaap Timmerman, A., Spijker, S., Brussaard, A. B., and Mansvelder, H. D. (2010). GABAergic synapse properties may explain genetic variation in hippocampal network oscillations in mice. *Front. Cell. Neurosci.* 4:18. doi: 10.3389/fncel.2010.00018

Jiménez-Bravo, M., Marrero, V., and Benítez-Burraco, A. (2017). An oscillopathic approach to developmental dyslexia: from genes to speech processing. *Behav. Brain Res.* 329, 84–95. doi: 10.1016/j.bbr.2017.03.048

Keitel, A., Ince, R. A. A., Gross, J., and Kayser, C. (2017). Auditory cortical delta-entrainment interacts with oscillatory power in multiple fronto-parietal networks. *Neuroimage* 147, 32–42. doi: 10.1016/j.neuroimage.2016.11.062

Kikuchi, Y., Attaheri, A., Wilson, B., Rhone, A. E., Nourski, K. V., Gander, P. E., et al. (2017). Sequence learning modulates neural responses and oscillatory coupling in human and monkey auditory cortex. *PLoS Biol.* 15:e2000219. doi: 10.1371/journal.pbio.2000219

Kikuchi, M., Shitamichi, K., Yoshimura, Y., Ueno, S., Hiraishi, H., Hirosawa, T., et al. (2013). Altered brain connectivity in 3-to 7-year-old children with autism spectrum disorder. *Neuroimage Clin.* 2, 394–401. doi: 10.1016/j.nicl.2013.03.003

Koch, M., Schmiedt-Fedr, C., and Mathes, B. (2016). Neuropharmacology of altered brain oscillations in schizophrenia. *Int. J. Psychophysiol.* 103, 62–68. doi: 10.1016/j.ijpsycho.2015.02.014

Liao, W., Gandal, M. J., Ehrlichman, R. S., Siegel, S. J., and Carlson, G. C. (2012). MeCP2+/− mouse model of RTT reproduces auditory phenotypes associated with Rett syndrome and replicate select EEG endophenotypes of autism spectrum disorder. *Neurobiol. Dis.* 46, 88–92. doi: 10.1016/j.nbd.2011.12.048

Linkenkaer-Hansen, K., Smit, D. J., Barkil, A., van Beijsterveldt, T. E., Brussaard, A. B., Boomsma, D. I., et al. (2007). Genetic contributions to long-range temporal correlations in ongoing oscillations. *J. Neurosci.* 27, 13882–13889. doi: 10.1523/JNEUROSCI.3083-07.2007

Meyer, L. (2018). The neural oscillations of speech processing and language comprehension: state of the art and emerging mechanisms. *Eur. J. Neurosci.* 48, 2609–2621. doi: 10.1111/ejn.13748

Müller, V., Anokhin, A. P., and Lindenberger, U. (2017). Genetic influences on phase synchrony of brain oscillations supporting response inhibition. *Int. J. Psychophysiol.* 115, 125–132. doi: 10.1016/j.ijpsycho.2016.06.001

Murphy, E. (2015). The brain dynamics of linguistic computation. *Front. Psychol.* 6:1515. doi: 10.3389/fpsyg.2015.01515

Murphy, E. (2016). The human oscillome and its explanatory potential. *Biolinguistics* 10, 6–20.

Murphy, E. (2018). "Interfaces (travelling oscillations) + recursion (delta-theta code) = language," in *The Talking Species: Perspectives on the Evolutionary, Neuronal and Cultural Foundations of Language*, eds E. Luef and M. Manuela (Graz: Unipress Graz Verlag), 251–269.

Murphy, E. (2019). No country for Oldowan men: emerging factors in language evolution. *Front. Psychol.* 10:1448. doi: 10.3389/fpsyg.2019.01448

Murphy, E., and Benítez-Burraco, A. (2016). Bridging the gap between genes and language deficits in schizophrenia: an oscillopathic approach. *Front. Hum. Neurosci.* 10:422. doi: 10.3389/fnhum.2016.00422

Murphy, E., and Benítez-Burraco, A. (2017). Language deficits in schizophrenia and autism as related oscillatory connectomopathies: an evolutionary account. *Neurosci. Biobehav. Rev.* 83, 742–764. doi: 10.1016/j.neubiorev.2016.07.029

Murphy, E., and Benítez-Burraco, A. (2018a). Toward the language oscillogenome. *Front. Psychol.* 9:1999. doi: 10.3389/fpsyg.2018.01999

Murphy, E., and Benítez-Burraco, A. (2018b). Paleo-oscillomics: inferring aspects of Neanderthal language abilities from gene regulation of neural oscillations. *J. Anthropol. Sci.* 96, 111–124. doi: 10.4436/JASS.96010

Nakamura, T., Matsumoto, J., Takamura, Y., Ishii, Y., Sasahara, M., Ono, T., et al. (2015). Relationships among parvalbumin-immunoreactive neuron density, phase-locked gamma oscillations and autistic/schizophrenic symptoms in PDGFR-β knock-out and control mice. *PLoS One* 10:e0119258. doi: 10.1371/journal.pone.0119258

Nandi, B., Swiatek, B., Kocsis, B., and Ding, M. (2019). Inferring the direction of rhythmic neural transmission via inter-regional phase-amplitude coupling (ir-PAC). *Sci. Rep.* 9:6933. doi: 10.1038/s41598-019-43272-w

Neubauer, S., Hublin, J. J., and Gunz, P. (2018). The evolution of modern human brain shape. *Sci. Adv.* 4:eaao5961. doi: 10.1126/sciadv.aao5961

Nguyen, P. T., Nakamura, T., Hori, E., Urakawa, S., Uwano, T., Zhao, J., et al. (2011). Cognitive and socio-emotional deficits in platelet-derived growth factor receptor-β gene knockout mice. *PLoS One* 6:e18004. doi: 10.1371/journal.pone.0018004

Perovic, A., and Janke, V. (2013). Issues in the acquisition of binding, control and raising in high-functioning children with autism. *UCL Work. Pap. Linguist.* 25, 131–143.

Pina, J. E., Bodner, M., and Ermentrout, B. (2018). Oscillations in working memory and neural binding: a mechanism for multiple memories and their interactions. *PLoS Comput. Biol.* 14:e1006517. doi: 10.1371/journal.pcbi.1006517

Poeppel, D. (2012). The maps problem and the mapping problem: two challenges for a cognitive neuroscience of speech and language. *Cogn. Neuropsychol.* 29, 34–55. doi: 10.1080/02643294.2012.710600

Poeppel, D., and Embick, D. (2005). "Defining the relation between linguis-tics and neuroscience," in *Twenty-First Century Psycho-linguistics: Four Cornerstones*, ed. A. Cutler (Hillsdale: Lawrence Erlbaum), 103–120.

Poeppel, D., Emmorey, K., Hickok, G., and Pylkkänen, L. (2012). Towards a new neurobiology of language. *J. Neurosci.* 32, 14125–14131. doi: 10.1523/JNEUROSCI.3244-12.2012

Polimanti, R., and Gelernter, J. (2017). Widespread signatures of positive selection in common risk alleles associated to autism spectrum disorder. *PLoS Genet.* 13:e1006618. doi: 10.1371/journal.pgen.1006618

Porjesz, B., Almasy, L., Edenberg, H. J., Wang, K., Chorlian, D. B., Foroud, T., et al. (2002). Linkage disequilibrium between the beta frequency of the human EEG and a GABAA receptor gene locus. *Proc. Natl. Acad. Sci. U S A* 99, 3729–3733. doi: 10.1073/pnas.052716399

Sikela, J. M., and Searles Quick, V. B. (2018). Genomic trade-offs: are autism and schizophrenia the steep price of the human brain? *Hum. Genet.* 137, 1–13. doi: 10.1007/s00439-017-1865-9

Soloduchin, S., and Shamir, M. (2018). Rhythmogenesis evolves as a consequence of long-term plasticity of inhibitory synapses. *Sci. Rep.* 8:13050. doi: 10.1038/s41598-018-31412-7

Srinivasan, S., Bettella, F., Mattingsdal, M., Wang, Y., Witoelar, A., Schork, A. J., et al. (2016). Genetic markers of human evolution are enriched in schizophrenia. *Biol. Psychiatry* 80, 284–292. doi: 10.1016/j.biopsych.2015.10.009

Tager-Flusberg, H., Calkins, S., Nolin, T., Baumberger, T., Anderson, M., Chadwick-Dias, A., et al. (1990). A longitudinal study of language acquisition in autistic and downs syndrome children. *J. Autism Dev. Disord.* 20, 1–21. doi: 10.1007/BF02206853

Tager-Flusberg, H., and Joseph, R. M. (2003). Identifying neurocognitive phenotypes in autism. *Philos. Trans. R. Soc. Lond. B Biol. Sci.* 358, 303–314. doi: 10.1098/rstb.2002.1198

Tilot, A. K., Frazier, T. W. I. I., and Eng, C. (2015). Balancing proliferation and connectivity in PTEN-associated autism spectrum disorder. *Neurotherapeutics* 12, 609–619. doi: 10.1007/s13311-015-0356-8

Toro, R., Konyukh, M., Delorme, R., Leblond, C., Chaste, P., Fauchereau, F., et al. (2010). Key role for gene dosage and synaptic homeostasis in autism spectrum disorders. *Trends Genet.* 26, 363–372. doi: 10.1016/j.tig.2010.05.007

van Beijsterveldt, C. E., Molenaar, P. C., De Geus, E. J., and Boomsma, D. I. (1996). Heritability of human brain functioning as assessed by electroencephalography. *Am. J. Hum. Genet.* 58, 562–573.

Wang, L., Hagoort, P., and Jensen, O. (2018). Language prediction is reflected by coupling between frontal gamma and posterior alpha oscillations. *J. Cogn. Neurosci.* 30, 432–447. doi: 10.1162/jocn_a_01190

Wilkinson, C., and Murphy, E. (2016). Joint interventions in autism spectrum disorder: relating oscillopathies and syntactic deficits. *UCL Work. Pap. Linguist.* 28, 1–7.

Zhang, H., Watrous, A. J., Patel, A., and Jacobs, J. (2018). Theta and alpha oscillations are travelling waves in the human neocortex. *Neuron* 98, 1269–1281. doi: 10.1016/j.neuron.2018.05.019

Conflict of Interest Statement: The authors declare that the research was conducted in the absence of any commercial or financial relationships that could be construed as a potential conflict of interest.

frontiers in Behavioral Neuroscience

ORIGINAL RESEARCH
published: 19 September 2019
doi: 10.3389/fnbeh.2019.00214

Reelin Signaling Controls the Preference for Social Novelty in Zebrafish

*Elisa Dalla Vecchia[1], Vincenzo Di Donato[2,3], Andrew M. J. Young[1], Filippo Del Bene[2] and William H. J. Norton[1]**

[1] Department of Neuroscience, Psychology and Behaviour, University of Leicester, Leicester, United Kingdom, [2] Institut Curie, Paris, France, [3] ZeClinics SL, Institute for Health Science Research Germans Trias i Pujol (IGTP), Barcelona, Spain

Reelin (Reln) is an extracellular glycoprotein that is important for brain patterning. During development Reln coordinates the radial migration of postmitotic cortical neurons, cerebellar and hippocampal neurons, whereas it promotes dendrite maturation, synaptogenesis, synaptic transmission, plasticity and neurotransmitter release in the postnatal and adult brain. Genetic studies of human patients have demonstrated association between the RELN locus and autism spectrum disorder, schizophrenia, bipolar disorder, and Alzheimer's disease. In this study we have characterized the behavioral phenotype of *reelin* (*reln*) mutant zebrafish, as well as two canonical signaling pathway targets *DAB adaptor protein 1a* (*dab1a*) and the *very low density lipoprotein receptor* (*vldlr*). Zebrafish *reln*$^{-/-}$ mutants display a selective reduction in preference for social novelty that is not observed in *dab1a*$^{-/-}$ or *vldlr*$^{-/-}$ mutant lines. They also exhibit an increase in 5-HT signaling in the hindbrain that parallels but does not underpin the alteration in social preference. These results suggest that zebrafish *reln*$^{-/-}$ mutants can be used to model some aspects of human diseases in which changes to Reln signaling alter social behavior.

Keywords: zebrafish, Reelin, behavior, autism, neurochemistry, social behavior, neuroscience, 5-HT

OPEN ACCESS

Edited by:
Allan V. Kalueff, Saint Petersburg State University, Russia

Reviewed by:
Eckart Förster, Ruhr University Bochum, Germany
Angelo Piato, Federal University of Rio Grande do Sul, Brazil

***Correspondence:**
William H. J. Norton
whjn1@le.ac.uk

Specialty section:
This article was submitted to Pathological Conditions, a section of the journal Frontiers in Behavioral Neuroscience

Received: *04 April 2019*
Accepted: *30 August 2019*
Published: *19 September 2019*

Citation:
Dalla Vecchia E, Di Donato V, Young AMJ, Del Bene F and Norton WHJ (2019) Reelin Signaling Controls the Preference for Social Novelty in Zebrafish. Front. Behav. Neurosci. 13:214. doi: 10.3389/fnbeh.2019.00214

INTRODUCTION

Reelin (Reln) is an extracellular glycoprotein that is important for brain patterning and synaptogenesis. During mammalian development Reln is secreted by Cajal-Retzius (C-R) neurons in cerebral cortex and granule cells in the external granule cell layer of the cerebellum (Pesold et al., 1998; Lee and D'Arcangelo, 2016). In the adult brain Reln is expressed by γ-aminobutyric acid (GABA)-positive interneurons in the cortex and hippocampus, and glutamatergic granule cells in the cerebellum (Pesold et al., 1998). The mammalian neocortex develops in an inside-out manner in which late-born neurons migrate past existing neurons to form a laminar structure (Rakic, 2009). Reln coordinates the radial migration of postmitotic cortical neurons, cerebellar and hippocampal neurons (D'Arcangelo, 2014). Reeler mice that lack Reln function display a disorganization of cortical lamination and cerebellar hypoplasia caused by the failure of Purkinje neurons to migrate (Goffinet, 1983; Miyata et al., 1997). Similar abnormalities have been identified in human patients with homozygous null mutations in *RELN*, who display lissencephaly and cerebellar hypoplasia (Hong et al., 2000). In the mature brain, RELN promotes dendrite maturation, synaptogenesis,

synaptic transmission, plasticity and the release of neurotransmitters (D'Arcangelo, 2005; Herz and Chen, 2006; Levenson et al., 2008; Förster et al., 2010; Levy et al., 2014).

Reln signaling is transduced by several downstream pathways including two low-density lipoprotein receptor family members: apolipoprotein E receptor 2 (ApoER2, also called low-density lipoprotein receptor-related protein 8, LRP8) and the very low density lipoprotein receptor (Vldlr) (Trommsdorff et al., 1999). ApoER2 and Vldlr are expressed on the membrane of target neurons. Their activation leads to internalization of Reln in endocytic vesicles, phosphorylation of the DAB adapter protein 1 (Dab1; Howell et al., 1997; Sheldon et al., 1997) and activation of Src/Fyn kinases as part of canonical Reln signaling (D'Arcangelo, 2006; Bock and May, 2016). ApoER2 and VLDLR have partially redundant functions and double *Apoer2/Vldlr* knock-out mice exhibit a *reeler*-like neuroanatomical phenotype (Trommsdorff et al., 1999). However, they also play specific roles in neuronal migration. ApoER2 is mostly expressed in hippocampal and cortical neurons and single *Apoer2* knock-out mice show defects in forebrain structures. *Vldlr* is mostly expressed in the Purkinje cells of the cerebellum, and these neurons fail to assemble in a tight layer in *Vldlr* knock-out mice (Trommsdorff et al., 1999). Other signaling pathways regulated by Reln include CrK/Rap1 (neuronal migration and lamination) and the P13K/Akt/mTOR pathway (dendrite and spine development). Activity at NMDA receptors and the MEK/Erk1/2 pathway enhances the expression of synaptic plasticity and learning genes (Chen et al., 2010).

Animal studies further support a link between decreased Reln signaling and behavioral abnormalities. Both homozygous and heterozygous *reeler* mice exhibit behavioral and cognitive defects (Tueting et al., 1999; Costa, 2002; Qiu et al., 2006). $Reln^{+/-}$ mice show impaired prepulse inhibition, a sensory motor gaiting phenotype associated with schizophrenia (Tueting et al., 1999; Barr et al., 2008; Kutiyanawalla et al., 2011; Teixeira et al., 2011) although not all studies agree (Qiu et al., 2006; Teixeira et al., 2011). $Reln^{+/-}$ mice also exhibit neophobia in the elevated plus maze, a decrease in cortical dendritic spine density and defects in hippocampus-based learning (Qiu et al., 2006), long-term potentiation and long-term depression (Iafrati et al., 2013). Cross-modal prepulse inhibition is increased in $Apoer2^{-/-}$ knock-out mice and decreased in $Vldlr^{-/-}$ (Weeber et al., 2002); and *Dab1*-conditional knockout mice exhibit hyperactivity and deficits in anxiety and working memory (Imai et al., 2016).

Abnormal Reln signaling has also been linked to several human psychiatric disorders. Genetic studies have demonstrated an association between the RELN locus and autism spectrum disorder (ASD; Wang et al., 2014), schizophrenia (Ovadia and Shifman, 2011; Li et al., 2015), bipolar disorder (Ovadia and Shifman, 2011), and Alzheimer's disease (Bufill et al., 2013). In humans, RELN is located at chromosome 7q22, the peak region of linkage and first autism susceptibility locus (AUTS1). Linkage and epidemiologic studies have yielded both positive and negative findings as to whether RELN plays a major role in ASD susceptibility (Persico et al., 2001; Krebs et al., 2002; Zhang et al., 2002; Bonora et al., 2003; Li et al., 2004; Dutta et al., 2006, 2008; Serajee et al., 2006; Li et al., 2008; He et al., 2011). Meta-analysis of several studies has identified a single nucleotide polymorphism that segregates with ASD (Wang et al., 2014) and unique inherited and *de novo* Reelin variants have been uncovered by exome sequencing of ASD patients (Bonora et al., 2003; Neale et al., 2012; Koshimizu et al., 2013; De Rubeis et al., 2014; Yuen et al., 2015; Zhang et al., 2015). Further evidence for a role of RELN in the etiology of ASD are the reduction of Reelin levels in the cerebellum, frontal cortices and blood of ASD patients (Fatemi, 2001; Fatemi et al., 2005); a reduction of *RELN* and *DAB1* mRNA levels; and an increase in *VLDLR* mRNA levels (Fatemi et al., 2005).

In this study we have characterized the behavior of three zebrafish lines with mutations in Reln signaling pathway components: *reelin*, *dab1a* and *vldlr* (Di Donato et al., 2018). We hypothesized that reduced Reln signaling would decrease social interaction in zebrafish (including shoaling, social preference and aggression) with parallel alterations to monoamine neurotransmitter signaling. Our results demonstrate that $reln^{-/-}$ mutants display a selective decrease in preference for social novelty that is not observed in $dab1a^{-/-}$ or $vldlr^{-/-}$ mutant lines.

MATERIALS AND METHODS

Zebrafish Strains, Care and Maintenance

Zebrafish (*Danio rerio*) were kept at the University of Leicester in accordance with institute animal welfare guidelines. The lighting conditions were 14:10 h (light:dark). Fish were fed twice per day with ZEBRAFEED 400–600 dry food (Sparos). Groups of 15 fish were kept in 3.5 l tanks (Tecniplast). All experiments were approved by a local Animal Welfare and Ethical Review board and were covered by a UK Home Office license to Will Norton. The following strains were used: heterozygous and homozygous $reelin^{\Delta 28-/-}$ mutants; *DAB adaptor protein* $1a^{\Delta 22-/-}$ mutants; *very low density lipoprotein receptor*$^{+13-/-}$ mutants (Di Donato et al., 2018); and AB wild-type (WT) zebrafish.

Behavioral Methods

Behavior was recorded using FlyCapture2 2.5.2.3 software and a digital camera (Point Grey Research). All behavioral experiments were carried out between 11:00 and 17:00. Experiments were performed in a dedicated room with light and temperature kept constant. Zebrafish were moved to the behavior room in holding tanks on the same day as the analysis. Fish were allowed to habituate to the testing room for 1 h. Previous research in our laboratory has demonstrated no sex differences in behavior in our recording setups (e.g., Norton et al., 2011). We therefore used mixed groups of male and female adult zebrafish (3–6 months old) in our analyses. The age and size of fish were carefully matched between genotypes. The sample size (n) for each animal group was calculated based upon power analysis of previous behavioral experiments carried out in our laboratory (e.g., Norton et al., 2011, 2019; Carreno Gutierrez et al., 2017). We only used one experimental setup for each behavioral test, but we cleaned the setup between recordings and changed the water in the tank for each fish tested. Ethovision XT (Noldus) software was used for video tracking. Each film was analyzed by

two researchers blind to the genotype or treatment. This removes observer bias in manual quantification.

Novel Tank Diving Test

Anxiety-like behavior and exploratory activity was recorded in the novel tank test (NTT) which was performed in a 1.5 L trapezoid tank (Egan et al., 2009). Fish were recorded in this setup for 5 min. We analyzed the time spent in the bottom (geotaxis) and the total distance swum. For *reln*: $n = 13$ WT, $n = 13$ *reln*$^{+/-}$, $n = 12$ *reln*$^{-/-}$. For *dab1a*: $n = 10$ WT, $n = 7$ *dab1a*$^{-/-}$. For *vldlr*: $n = 7$ WT, $n = 7$ *vldlr*$^{-/-}$.

Open Field Test

The open field test was carried out in a open tank (40 × 25 cm) filled with water to a depth of 8 cm. Single adult zebrafish were filmed from above for 5 min. The total distance swum, duration of thigmotaxis (time spent at a distance of 2 cm or less from the walls) and time in the center of the tank (representing half of the total tank area) were quantified. For *reln*: $n = 12$ WT, $n = 12$ *reln*$^{+/-}$, $n = 12$ *reln*$^{-/-}$. For *dab1a*: $n = 10$ WT, $n = 7$ *dab1a*$^{-/-}$. For *vldlr*: $n = 8$ WT, $n = 7$ *vldlr*$^{-/-}$.

Shoaling Test

Shoaling was recorded in tanks measuring 43 × 22 cm filled with water to a depth of 8 cm. Groups of five familiar adult fish were introduced to the tank, allowed to acclimatize and recorded from above for 10 min (Parker et al., 2013). A mix of males and females were examined. We tracked the fish and measured the average inter-individual distance, polarization and speed of locomotion using VpCore2 software (ViewPoint Life Sciences). $n = 2$ groups of 5 WT, $n = 2$ groups of 5 *reln*$^{+/-}$ and $n = 2$ groups of 5 *reln*$^{-/-}$.

Social Preference Test

The social preference test was carried out as described in Carreno Gutierrez et al. (2019). We used a transparent plastic tank containing five compartments: a central area (13 × 19 cm) with two small 6.5 × 9 cm areas either side. The walls separating the central and the side compartments contained holes (1 mm) to allow movement of water and odorants. A single fish was introduced into the central area and permitted to interact with a group of three fish placed in one of the side compartments. To analyze the interactions the central arena was divided in four equal sections and the time spent by the focal fish in each area was recorded. Social preference. In the first session (interaction 1) a group of three unfamiliar WT fish (1st strangers) were placed into one of the side compartments. The behavior of the focal fish was recorded for 5 min, and the time spent closest to the 1st group of strangers was compared to the time spent near the empty area diagonally opposite. Preference for social novelty. A second group of three unfamiliar WT fish (2nd strangers) were placed in the compartment diagonally opposite the first group. The focal fish was recorded for a further 5 min. The time in the area nearest the 1st strangers and the time spent in the quadrant nearest the 2nd strangers was compared. We used a mixture of size-matched males and females as stimuli since can attract both male and female zebrafish (Ruhl et al., 2009). The stimulus fish were changed after recording three focal fish, to standardize the stimulus used and reduce the amount of stress that each animal was exposed to. For *reln*: $n = 12$ WT, $n = 12$ *reln*$^{+/-}$, $n = 10$ *reln*$^{-/-}$. For *dab1a*: $n = 10$ WT, $n = 7$ *dab1a*$^{-/-}$. For *vldlr*: $n = 8$ WT, $n = 7$ *vldlr*$^{-/-}$.

Aggression

Aggression was measured using a mirror as a stimulus (Norton et al., 2011). Fish were recorded for 5 min from above. The time spent being aggressive (biting the mirror image and thrashing the tail fin) was quantified manually using LabWatcher (ViewPoint Life Sciences). Films were renamed so that the observer was blind to the genotype being analyzed. For *reln*: $n = 12$ WT, $n = 12$ *reln*$^{+/-}$, $n = 8$ *reln*$^{-/-}$. For *dab1a*: $n = 10$ WT, $n = 7$ *dab1a*$^{-/-}$. For *vldlr*: $n = 8$ WT, $n = 7$ *vldlr*$^{-/-}$.

Drug Administration

Buspirone hydrochloride was bought from Tocris (Cat. no. 0962), oxytocin was purchased from Sigma Aldrich (Cat. no. O3251) and risperidone was purchased from Tocris (Cat. no. 2865). Administration and concentration of the treatments were chosen according to previously published studies. Buspirone was applied by immersion in water containing 10 mg/L drug for 1 h (Bencan et al., 2009). Oxytocin was applied at a concentration of 10 ng/kg by intraperitoneal injection 30 min before recording (Zimmermann et al., 2016). Risperidone was applied by immersion in water containing 170 μg/L drug for 15 min (Idalencio et al., 2015). For buspirone: $n = 8$ WT, $n = 8$ *reln*$^{-/-}$. For oxytocin: $n = 9$ WT, $n = 9$ *reln*$^{-/-}$. For risperidone: $n = 9$ WT, $n = 9$ *reln*$^{-/-}$.

Reelin Immunohistochemistry

The anti-Reelin antibody was purchased from Millipore (Cat. no. MAB5366). Immunohistochemistry labeling was carried out using the following protocol. Dissected brains were fixed in 4% PFA for 24 h at 4°C. Brains were washed in phosphate buffered saline (PBS) and stored in methanol at −20°C until processing. Coronal and sagittal sections (100 μM) were cut using a Leica VT1000 S vibratome (Leica Biosystems). After blocking in PBS with 5% normal goat serum (Sigma Cat. no. G9023), 1% dimethyl sulphoxide (Sigma, Cat. no. 276855) and 0.2% Triton X-100 (Fisher, Cat. no. 10254640), sections were incubated in primary antibody for 24 h at 4°C. The secondary antibody (Biotinylated Universal Antibody anti-mouse and rabbit IgG (H + L); Vector Laboratories Cat. no. BA-1400) was incubated for 2 h at room temperature and staining was developed using diaminobenzidine (DAB). Stained sections were mounted and then photographed using an optical microscope (GXM L3200B, GT Vision) and images were assembled in Adobe Photoshop version CS2 (Adobe systems).

High Pressure Liquid Chromatography (HPLC) Analysis of Monoamines and Their Metabolites

HPLC was performed as described in Carreno Gutierrez et al. (2017). Fish were sacrificed using a schedule 1 procedure. Dissected brains were divided into telencephalon, diencephalon, optic tectum and hindbrain. Samples were prepared in 100 μl

ice-cold 0.1 N perchloric acid and centrifuged. HPLC with electrochemical detection was used to measure dopamine (DA), serotonin (5-HT), 3,4-dihydroxyphenylacetic acid (DOPAC), homovanillic acid (HVA) and 5-hydroxyindoleacetic acid (5-HIAA). Samples were compared to standard neurotransmitter solutions and the results were expressed as pmol/mg of brain. 8 $reln^{-/-}$ and 8 AB brains were processed for HPLC.

Data Analysis

All data were stored in Excel (Microsoft). Statistical analysis was performed in GraphPad Prism7. Bars represent average values and error bars denote standard error of the mean (SEM). The distribution of the data was verified before choosing an appropriate statistical test, using either the D'Agostino-Pearson or Shapiro–Wilk normality test. A Student's *t*-test (with Holm–Sidak correction) or Mann–Whitney *U*-test (with Welch correction if appropriate) was used to compare two data sets. When comparing three groups, a one-way ANOVA followed by a Dunnett's *post hoc* test was used. For non-parametric data a Kruskal–Wallis test followed by Dunn *post hoc* was used. Three-way ANOVA followed by Sidak's *post hoc* test for multiple comparisons was used to analyze the drug treatment experiments, and two-way ANOVA for the social interaction tests as described in the figure legends. The Statistical significance was shown as follows: $^{*}p < 0.05$, $^{**}p < 0.01$, $^{***}p < 0.001$, $^{****}p < 0.0001$. The number of animals used is denoted by n in the figure legends.

RESULTS

Localization of Reln in the Adult Zebrafish Brain

We first examined the location of Reelin (Reln) protein in the adult zebrafish brain. In agreement with other published studies, Reln was expressed in a restricted pattern in the adult zebrafish brain, including areas that are important for synaptic organization and plasticity (Costagli et al., 2002). In WT, Reln protein is detected in the medial part of the dorsal telencephalon (Dm) and the ventral nucleus of the ventral telencephalon (Vv, **Figure 1a**). In the diencephalon, Reelin is found in the ventral thalamic nuclei (Th, **Figure 1b**) and in the ventral hypothalamic nuclei (Hy, **Figure 1c**). In the midbrain Reelin is detected in the torus longitudinalis (TL, **Figure 1d**) as well as the stratum fibrosum marginale (sfm) and stratum opticum (so, **Figure 1e**) layers of the tectal neuropil. A few labeled cells were observed in the interpeduncular nucleus (nin, **Figure 1f**). In the hindbrain Reelin is localized to three areas of the cerebellum: the granular cell layer of the corpus cerebelli (CCe), the caudal lobe (LCa) and the crista cerebellaris (CC, **Figure 1g**). No Reelin expression is observed in the Purkinje and molecular cell layer. Scattered nuclei expressing Reelin are also seen in the intermediate and inferior part of the reticula formation (RF) of the medulla oblongata (**Figure 1h**). As expected, there is a strong reduction in the level of Reln protein detected in $reln^{-/-}$ mutant zebrafish (**Figures 1i,j**), confirming the specificity of our immunohistochemical analysis.

Reduction of *reln* Alters Social Behavior

The well-established links between Reelin and social behavior prompted us to measure shoaling and social preference in *reln* mutants. We examined social interaction and discrimination in the social preference. We introduced a focal WT or mutant fish in the central compartment of the social preference tank and measured its interaction with a group of unfamiliar WT stimulus fish (1st strangers) (**Figure 2C**). WT, $reln^{+/-}$ and $reln^{-/-}$ spent more time next to the strangers than in the empty control area [**Figure 2A**; $p < 0.0001$ for all genotypes; two-way ANOVA followed by Sidak's *post hoc*, genotype factor: $F(2,62) = 1.818$, $p = 0.17$, stranger factor: $F(1,62) = 2392$, $p < 0.0001$, interaction genotype × stranger: $F(2,62) = 4.418$, $p = 0.02$]. We assessed social novelty preference by placing a group of unfamiliar fish (2nd strangers) into the setup (**Figure 2D**). Although both WT and $reln^{+/-}$ changed their preference and spent an equal amount of time interacting with both groups of fish (**Figure 2B**; $p = 0.99$ for WT and $p = 0.38$ for $reln^{+/-}$), $reln^{-/-}$ mutants failed to switch preference and remained with the first group of strangers [**Figure 2B**; $p < 0.0001$; two-way ANOVA followed by Sidak's *post hoc*, genotype factor: $F(2,62) = 0.5184$, $p = 0.60$, stranger factor: $F(1,62) = 21.49$, $p < 0.0001$, interaction genotype × stranger: $F(2,62) = 6.886$, $p = 0.002$]. We next recorded shoaling in groups of WT or mutants. We placed 5 WT or *reln* mutants into a large tank and measured the inter-individual distance. In contrast to the social preference test, $reln^{-/-}$ displayed a similar inter-individual distance (Kruskal–Wallis test with Dunn's multiple comparisons test: chi-square = 3.71, $p = 0.36$), polarization (Kruskal–Wallis test with Dunn's multiple comparisons test: chi-square = 0, $p > 0.99$) and velocity [one-way ANOVA Dunnett's multiple comparisons test: $F(2,3) = 5.498$, $p = 0.07$) as WT when interacting with a group of conspecifics (**Figures 3A–C**)]. Taken together, these results suggest that $reln^{-/-}$ mutants display a selective reduction in their preference for social novelty in the absence of global changes to social interactions.

Exploration, Anxiety-Like Behavior and Aggression Are Not Altered in $reln^{-/-}$

We examined the selectivity of this behavioral phenotype by measuring changes to exploration, anxiety-like behavior and aggression in $reln^{-/-}$ mutant zebrafish. In the open field test, both WT and $reln^{-/-}$ spent a similar amount of time at the side [**Figure 3D**; thigmotaxis, $p = 0.13$ for WT vs. $reln^{+/-}$ and $p = 0.50$ for WT vs. $reln^{-/-}$; one-way ANOVA with Dunnett's multiple comparisons test: $F(2,33) = 1.687$, $p = 0.20$] and in the center of the tank [**Figure 3E**; $p = 0.25$ for $reln^{+/-}$ and $p = 0.99$ for $reln^{-/-}$; one-way ANOVA with Dunnett's multiple comparisons test: $F(2,33) = 1.431$, $p = 0.25$]. They also swam a similar distance suggesting that exploration is not altered in mutant fish [**Figure 3F**; $p = 0.14$ for $reln^{+/-}$ and $p = 0.61$ for $reln^{-/-}$; one-way ANOVA with Dunnett's multiple comparisons test: $F(2,33) = 1.625$, $p = 0.21$]. $reln^{-/-}$ also exhibited normal anxiety-like behavior in the NTT. They spent a similar amount of time at the bottom of the tank (**Figure 3G**; Kruskal–Wallis test with Dunn's multiple comparisons test: chi-square = 0.5705,

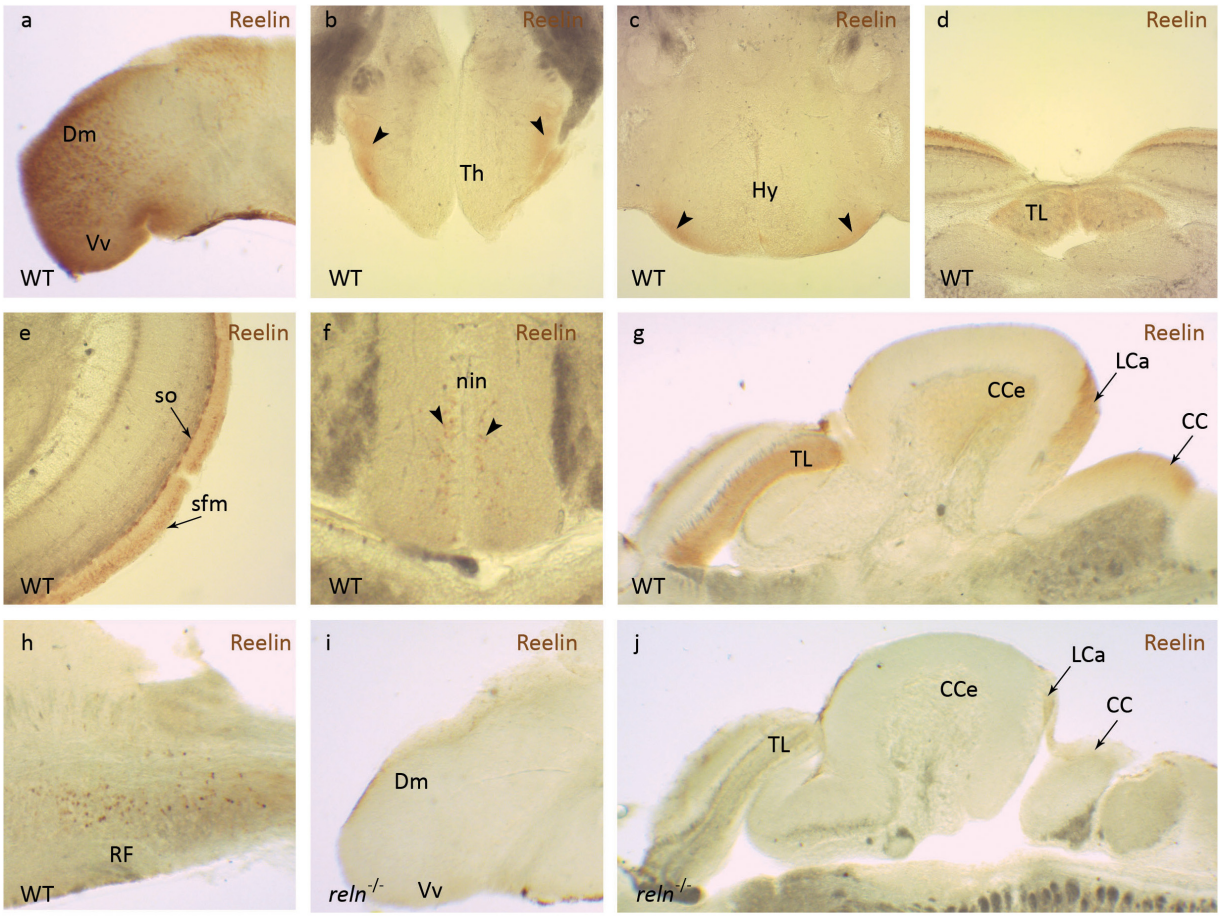

FIGURE 1 | Reelin immunohistochemistry. Anti-Reelin antibody labeling of coronal and sagittal sections of the adult zebrafish brain. In wild-type anti-Reelin antibody labeling is seen in the **(a)** medial part of the dorsal telencephalon (Dm) and in the ventral nucleus of the ventral telencephalon (Vm), in the **(b)** ventral thalamic nuclei (Th) and **(c)** the ventral hypothalamic nuclei (Hy). Labeling is also detected in the **(d)** torus longitudinalis (TL), **(e)** stratum fibrosum marginale (sfm) and the stratum opticum (so) of the optic tectum. **(f)** A few labeled cells are observed in the interpeduncular nucleus (nin). In the hindbrain, Reelin protein localizes to the **(g)** corpus cerebelli (CCe), the lobus caudalis cerebelli (LCa), crista cerebellaris (CC) and **(h)** the intermediate and inferior part of the reticular formation (RF). **(i,j)** Anti-Reelin antibody labeling is not detected in the brain of reln$^{-/-}$ mutants. Black arrowheads show position of Reelin-positive areas in **(b,c,f)**.

p = 0.93 for *reln*$^{+/-}$ and $p > 0.99$ for *reln*$^{-/-}$) and swam a similar distance [**Figure 3H**; $p = 0.75$ for *reln*$^{+/-}$ and $p = 0.43$ for *reln*$^{-/-}$; one-way ANOVA with Dunnett's multiple comparisons test: $F(2,35) = 1.54$, $p = 0.23$ as WT]. Both genotypes also spent a similar amount of time being aggressive in a mirror test, quantified as the amount of time spent biting the mirror image and thrashing the caudal fin (**Figure 3I**; Kruskal–Wallis test with Dunn's multiple comparisons test: chi-square = 3,372, $p = 0.97$ for *reln*$^{+/-}$ and $p = 0.13$ for *reln*$^{-/-}$). Taken together, these results suggest that *reln*$^{-/-}$ mutants exhibit a selective reduction in the reaction to social novelty.

Reaction to Social Novelty Is Not Mediated by the Canonical Reelin Signaling Pathway

Reelin activity is transduced by several downstream pathways including canonical signaling via DAB adaptor protein 1 and the Very low density lipoprotein receptor (Vldlr) (Trommsdorff et al., 1999; Bock and May, 2016). We characterized *dab1a*$^{-/-}$ (one of the zebrafish homologs of mammalian *Dab1*) and *vldlr*$^{-/-}$ mutant lines to examine the contribution of canonical signaling to the phenotype of *reln*$^{-/-}$ zebrafish. Interestingly, both *dab1a*$^{-/-}$ and *vldlr*$^{-/-}$ displayed different behavioral profiles. In the social preference test, *dab1a*$^{-/-}$ showed a similar social preference [**Figure 4A**; WT, $p = 0.0005$ and *dab1a*$^{-/-}$, $p < 0.0001$; two-way ANOVA followed by Sidak's *post hoc*, genotype factor: $F(1,30) = 0.9841$, $p = 0.3291$, stranger factor: $F(1,30) = 72.81$ $p < 0.0001$, interaction genotype × stranger: $F(1,30) = 7.716$ $p = 0.0093$] and reaction to social novelty as WT [**Figure 4B**; $p = 0.61$ for WT and $p = 0.44$ for *dab1a*$^{-/-}$; two-way ANOVA followed by Sidak's *post hoc*, genotype factor: $F(1,30) = 0.004$, $p = 0.95$, stranger factor: $F(1,30) = 0.1016$, $p = 0.75$, interaction genotype × stranger: $F(1,30) = 2.175$, $p = 0.15$]. Exploration in the open field test was similar in *dab1a*$^{-/-}$ and WT [**Figures 4C–E**; thigmotaxis, *t*-test

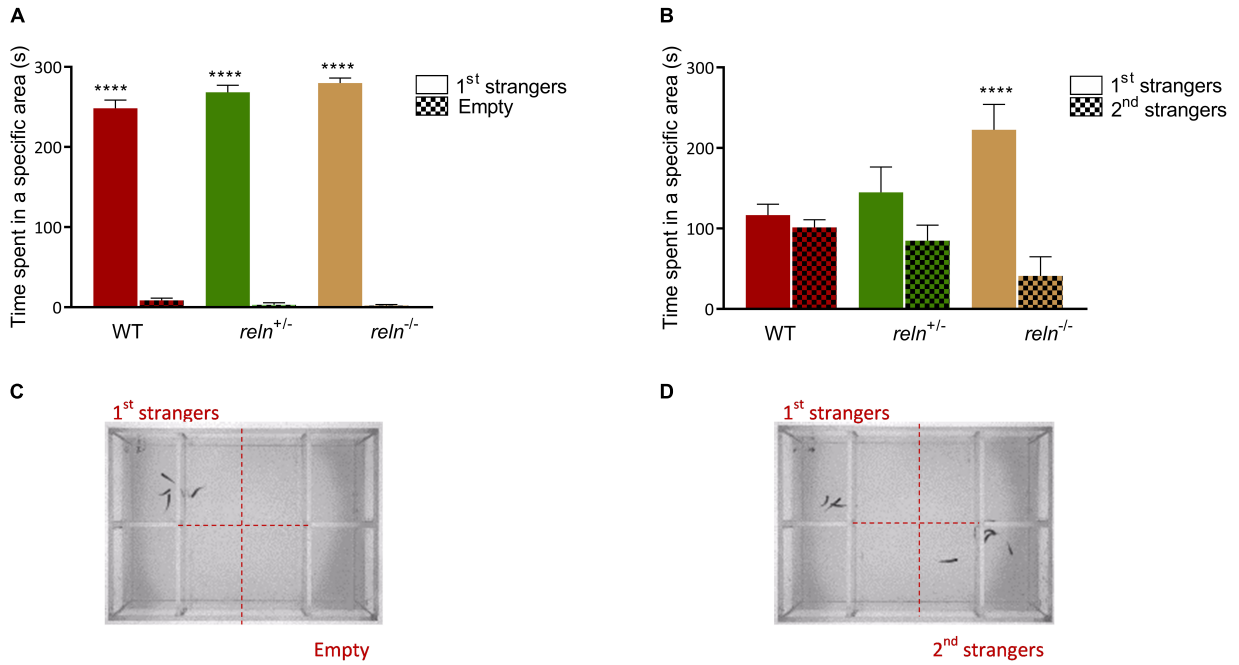

FIGURE 2 | Social preference test. **(A)** Social preference. WT, reln$^{+/-}$ and reln$^{-/-}$ show a significant preference to spend time near a group of unfamiliar fish [1st strangers; $p < 0.0001$ for all genotypes; two-way ANOVA followed by Sidak's *post hoc*, genotype factor: $F(2,62) = 1.818$, $p = 0.17$, stranger factor: $F(1,62) = 2392$, $p < 0.0001$, interaction genotype × stranger: $F(2,62) = 4.418$, $p = 0.02$]. **(B)** Preference for social novelty. Both WT and *reln*$^{+/-}$ spend an equal amount of time near both groups of unfamiliar fish (1st and 2nd strangers; $p = 0.99$ for WT and p = 0.38 for *reln*$^{+/-}$). *reln*$^{-/-}$ do not switch preference to the second group of unfamiliar fish [2nd strangers; $p < 0.0001$; two-way ANOVA followed by Sidak's *post hoc*, genotype factor: $F(2,62) = 0.5184$, $p = 0.60$, stranger factor: $F(1,62) = 21.49$, $p < 0.0001$, interaction genotype × stranger: $F(2,62) = 6.886$, $p = 0.002$]. $n = 12$ wild-type, $n = 12$ *reln*$^{+/-}$ and $n = 10$ *reln*$^{-/-}$. ****$p < 0.0001$. Mean ± SEM. **(C,D)** Photographs showing the experimental setup for social preference **(C)** and preference for social novelty **(D)**.

(Welch): $t_{(0.3262)} = 9.971$, $p = 0.75$; time in center of the tank, *t*-test (Welch): $t_{(0.1684)} = 14.64$, $p = 0.87$ and locomotion, *t*-test (Welch): $t_{(0.5277)} = 13.05$, $p = 0.61$]. Both genotypes also spent a similar amount of time at the bottom of a novel tank (**Figure 4F**; Mann–Whitney test: $U = 17$, $p = 0.06$), a readout of anxiety-like behavior, whereas mutants were hyperactive compared to WT [**Figure 4G**; *t*-test (Welch): $t_{(3.234)} = 7.409$, $p = 0.01$]. Finally, *dab1a*$^{-/-}$ mutants were more aggressive than WT in the mirror aggression test (**Figure 4H**; Mann–Whitney test: $U = 11.5$, $p = 0.0445$).

vldlr$^{-/-}$ mutants also showed both a similar interaction with the first group of strangers [**Figure 5A**; $p < 0.0001$ for both genotypes; two-way ANOVA followed by Sidak's *post hoc*, genotype factor: $F(1,24) = 0.0039$, $p = 0.95$, stranger factor: $F(1,24) = 120.1$, $p < 0.0001$, interaction genotype × stranger: $F(1,24) = 0.4912$, $p = 0.49$] and a normal reaction to social novelty [**Figure 5B**; $p = 0.58$ for WT and $p = 0.73$ for *vldlr*$^{-/-}$; two-way ANOVA followed by Sidak's *post hoc*, genotype factor: $F(1,24) = 1.353$, $p = 0.26$, stranger factor: $F(1,24) = 0.005$, $p = 0.94$, interaction genotype × stranger: $F(1,24) = 0.02779$, $p = 0.87$] as WT in the social preference test. In the open field test, *vldlr*$^{-/-}$ spent the same time at side of the tank [**Figure 5C**; *t*-test (Welch): $t(1.581) = 9.068$, $p = 0.15$] compared to WT but *vldlr*$^{-/-}$ mutants spent more significantly more time in the center of an open field tank than WT [**Figure 5D**; *t*-test (Welch): $t_{(2.595)} = 9.47$, $p = 0.03$]. However, the distance swum in the open field was the same as WT [**Figure 5E**; *t*-test (Welch): $t_{(0.3779)} = 12.84$, $p = 0.71$] suggesting that *vldlr*$^{-/-}$ are more explorative or less anxious than WT without being hyperactive. Anxiety-like behavior in the NTT was not altered in mutants [**Figures 5F,G**; time at bottom of tank, Mann–Whitney test: $U = 16$, $p = 0.32$ and locomotion, *t*-test (Welch): $t_{(0.1803)} = 10.92$, $p = 0.86$]. Finally, mutants also exhibited a trend decrease in aggression levels that did not reach significance [**Figure 5H**; *t*-test (Welch): $t_{(1.87)} = 11.41$, $p = 0.09$]. In summary, although mutation of *reln* leads to a specific alteration in social interactions, this phenotype does not appear to be mediated by the canonical Reln signaling components *dab1a* and *vldlr*, which display different behavioral alterations.

Increased Levels of 5-HT in the Hindbrain of *reln*$^{-/-}$

The control of social behavior, aggression and anxiety has been linked to monoamine signaling in the brain (Popova, 2008; Herculano and Maximino, 2014; Carreno Gutierrez et al., 2019). We used high pressure liquid chromatography (HPLC) to quantify the levels of 5-HT, DA and metabolites in WT and *reln* mutant zebrafish. Since heterozygous *reln*$^{+/-}$ mutants did not show behavioral alterations compared to WT we focused on *reln*$^{-/-}$ animals in these experiments. Using HPLC we uncovered a selective increase of 5-HT in

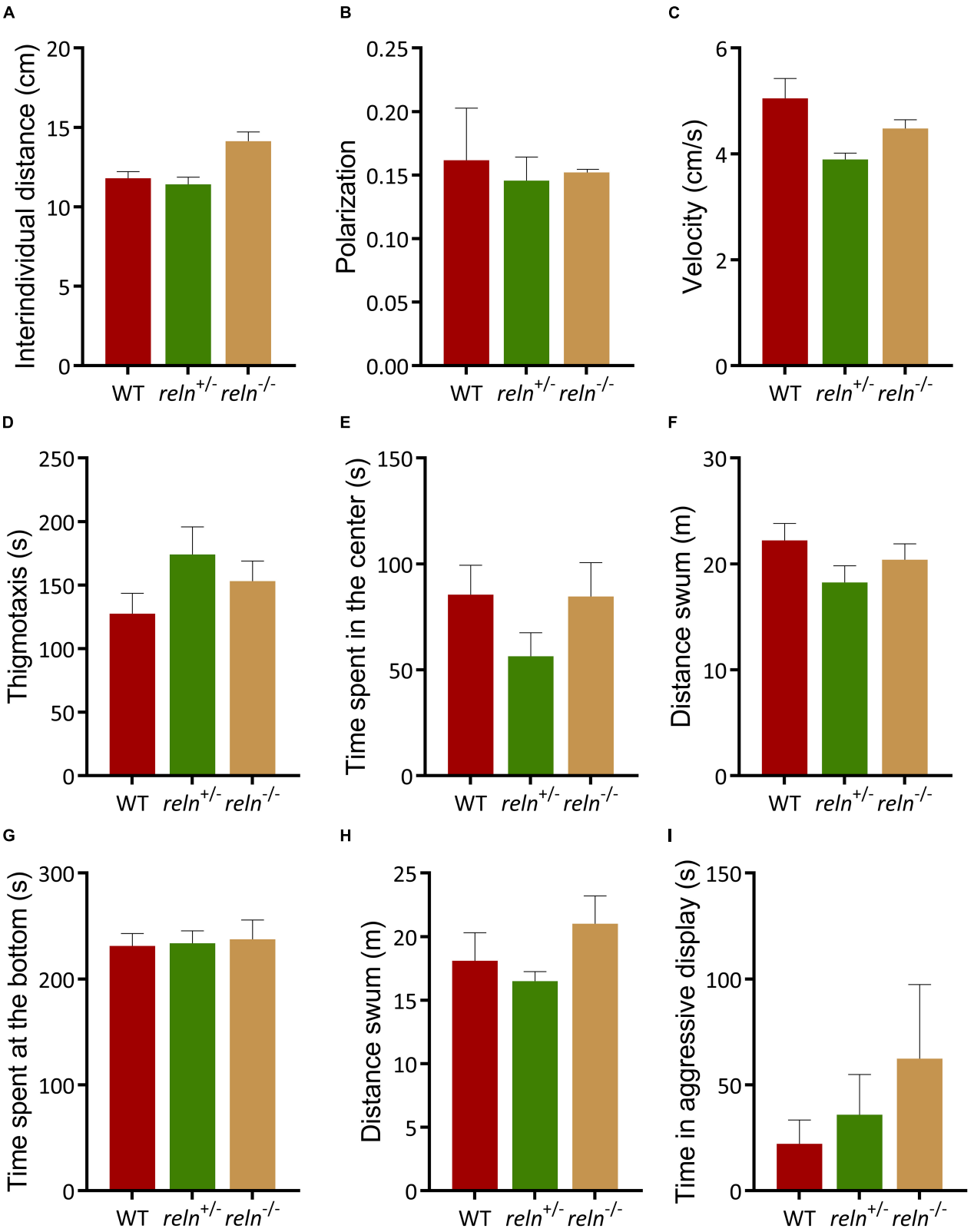

FIGURE 3 | Behavior of *reln*$^{+/-}$ and *reln*$^{-/-}$ zebrafish. **(A–C)** Both genotypes shoal normally. **(A)** Inter-individual distance (Kruskal–Wallis test with Dunn's multiple comparisons test: chi-square = 3.71, $p > 0.99$ for *reln*$^{+/-}$ and $p = 0.36$ for *reln*$^{-/-}$); **(B)** Polarization (Kruskal–Wallis test with Dunn's multiple comparisons

(Continued)

FIGURE 3 | Continued
test: chi-square = 0, $p > 0.99$ for both genotypes) and **(C)** velocity [one-way ANOVA Dunnett's multiple comparisons test: $F(2,3) = 5.498$, $p = 0.09$ for WT, $p = 0.31$ for *reln*$^{+/-}$ and $p = 0.07$ for *reln*$^{-/-}$]. $n = 2$ groups of 5 WT, $n = 2$ groups of 5 *reln*$^{+/-}$ and $n = 2$ groups of 5 *reln*$^{-/-}$. **(D–F)** Both *reln*$^{+/-}$ and *reln*$^{-/-}$ behave similarly to WT in the open field test. **(D)** Time at the side of the tank [thigmotaxis, one-way ANOVA Dunnett's multiple comparisons test: $F(2,33) = 1,687$, $p = 0.20$, $p = 0.13$ for WT vs. *reln*$^{+/-}$ and $p = 0.50$ for WT vs. *reln*$^{-/-}$]; **(E)** time spent in the center of the tank [one-way ANOVA Dunnett's multiple comparisons test: $F(2,33) = 1,431$, $p = 0.25$ for WT, $p = 0.25$ for *reln*$^{+/-}$ and $p = 0.99$ for *reln*$^{-/-}$]. **(F)** Locomotion is not affected in the open field test [one-way ANOVA Dunnett's multiple comparisons test: $F(2,33) = 1,625$, $p = 0.21$, $p = 0.14$ for *reln*$^{+/-}$ and $p = 0.61$ for *reln*$^{-/-}$]. $n = 12$ WT, $n = 12$ *reln*$^{+/-}$, $n = 12$ *reln*$^{-/-}$. **(G,H)** Both genotypes exhibit normal anxiety-like behavior. **(G)** Time at the bottom of a novel tank (Kruskal–Wallis test with Dunn's multiple comparisons test: chi-square = 0,5705, $p = 0.93$ for *reln*$^{+/-}$ and $p > 0.99$ for *reln*$^{-/-}$); **(H)** locomotion in a novel tank [one-way ANOVA Dunnett's multiple comparisons test: $F(2,35) = 1,54$, $p = 0.23$ for WT, $p = 0.75$ for *reln*$^{+/-}$ and $p = 0.43$ for *reln*$^{-/-}$) $n = 13$ wild-type, $n = 13$ reln$^{+/-}$, $n = 12$ *reln*$^{-/-}$. **(I)** No difference in aggression levels between WT, *reln*$^{+/-}$ and *reln*$^{-/-}$ (Kruskal–Wallis test with Dunn's multiple comparisons test: chi-square = 3,372, $p = 0.97$ for *reln*$^{+/-}$ and $p = 0.13$ for *reln*$^{-/-}$) $n = 12$ wild-type, $n = 12$ *reln*$^{+/-}$, $n = 8$ *reln*$^{-/-}$. Mean ± SEM.

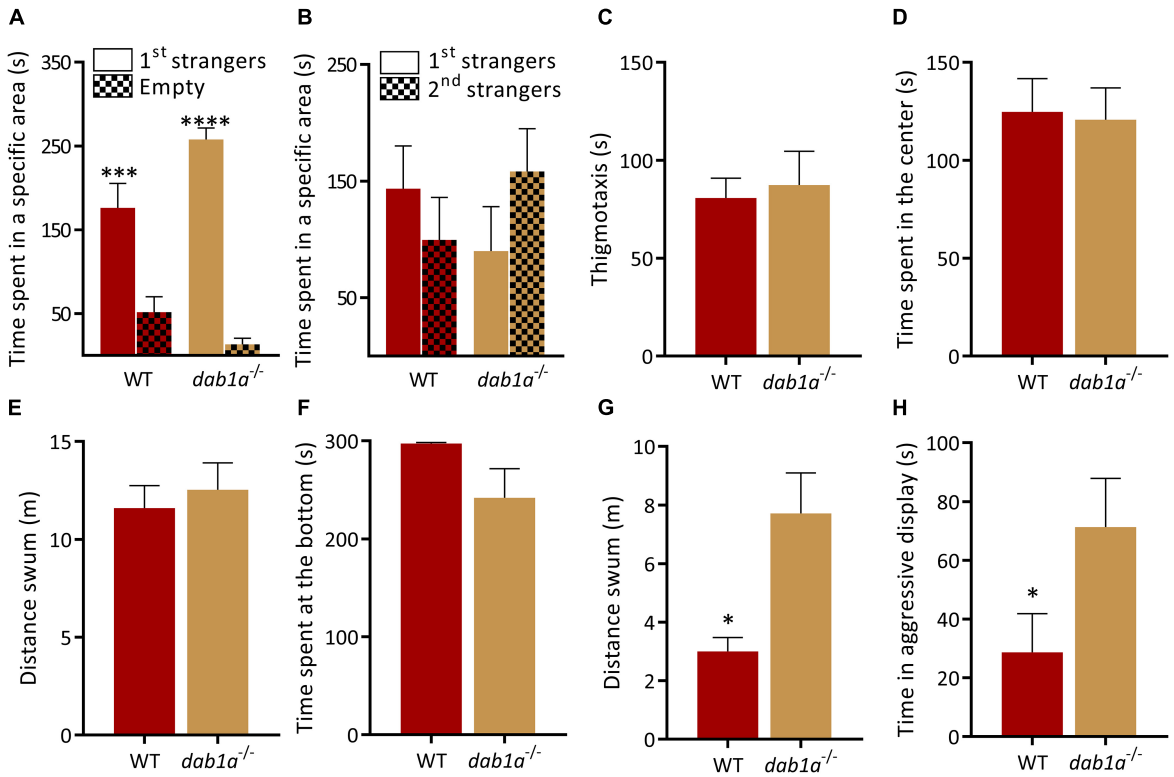

FIGURE 4 | Behavior of *dab1a*$^{-/-}$ zebrafish. **(A,B)** Social preference test. **(A)** Both genotypes prefer to spend time near a group of unfamiliar fish [1st strangers; $p = 0.0005$ and $p < 0.0001$ respectively; two-way ANOVA followed by Sidak's *post hoc*, genotype factor: $F(1,30) = 0.9841$, $p = 0.3291$, stranger factor: $F(1,30) = 72.81$, $p < 0.0001$, interaction genotype × stranger: $F(1,30) = 7.716$, $p = 0.0093$]. **(B)** WT and *dab1a*$^{-/-}$ spend equal time near both groups when a second unfamiliar group is added [$p = 0.61$ for WT and $p = 0.44$ for *dab1a*$^{-/-}$; two-way ANOVA followed by Sidak's *post hoc*, genotype factor: $F(1,30) = 0.004$, $p = 0.95$, stranger factor: $F(1,30) = 0.1016$, $p = 0.75$, interaction genotype × stranger: $F(1,30) = 2.175$, $p = 0.15$. $n = 10$ wild-type and $n = 7$ *dab1a*$^{-/-}$]. **(C–E)** *dab1a*$^{-/-}$ exhibit normal behavior in the open field test. **(C)** Time at side of the tank [thigmotaxis, *t*-test (Welch): $t_{(0.3262)} = 9.971$, $p = 0.75$] and **(D)** time in center of the tank [*t*-test (Welch): $t_{(0.1684)} = 14.64$, $p = 0.87$] **(E)** locomotion [*t*-test (Welch): $t_{(0.5277)} = 13.05$, $p = 0.61$. $n = 10$ wild-type and $n = 7$ *dab1a*$^{-/-}$]. **(F)** *dab1a*$^{-/-}$ exhibit normal anxiety-like behavior. Time at the bottom of novel tank (Mann–Whitney test: $U = 17$, $p = 0.06$). **(G)** *dab1a*$^{-/-}$ fish are more active than WT in the NTT [*t*-test (Welch): $t_{(3.234)} = 7.409$, $p = 0.0133$. $n = 10$ wild-type and $n = 7$ *dab1a*$^{-/-}$]. **(H)** *dab1a*$^{-/-}$ display heightened aggression levels compared to WT (Mann–Whitney test: $U = 11.5$, $p = 0.0445$. $n = 10$ wild-type and $n = 7$ *dab1a*$^{-/-}$). *$p < 0.05$, ***$p < 0.001$, ****$p < 0.0001$. Mean ± SEM.

the hindbrain of *reln*$^{-/-}$ compared to WT [**Figure 6D**; *t*-test: $t_{(3.694)} = 70$, $p = 0.0021$, multiple *t*-tests with Holm–Sidak multiple comparisons correction]. In contrast, we detected similar levels of dopamine (DA), homovanillic acid (HVA), dihydroxyphenylacetic acid (DOPAC) and 5-hydroxyindoleacetic acid (5HIAA) in the brain of both genotypes (**Figures 6A–D**). We also calculated the utilization ratio of each neurotransmitter. HPLC measures the sum basal level of analytes in the brain regardless of whether or not have been released at the synapse. Since neurotransmitters are broken down to their metabolites upon release the utilization ratio gives an approximation of neurotransmitter activity (Kilpatrick et al., 1986). The utilization ratio of 5-HT and DA was unaffected in *reln*$^{-/-}$ suggesting that release and reuptake of neurotransmitters is unaffected in these mutants (**Figures 6E–G**).

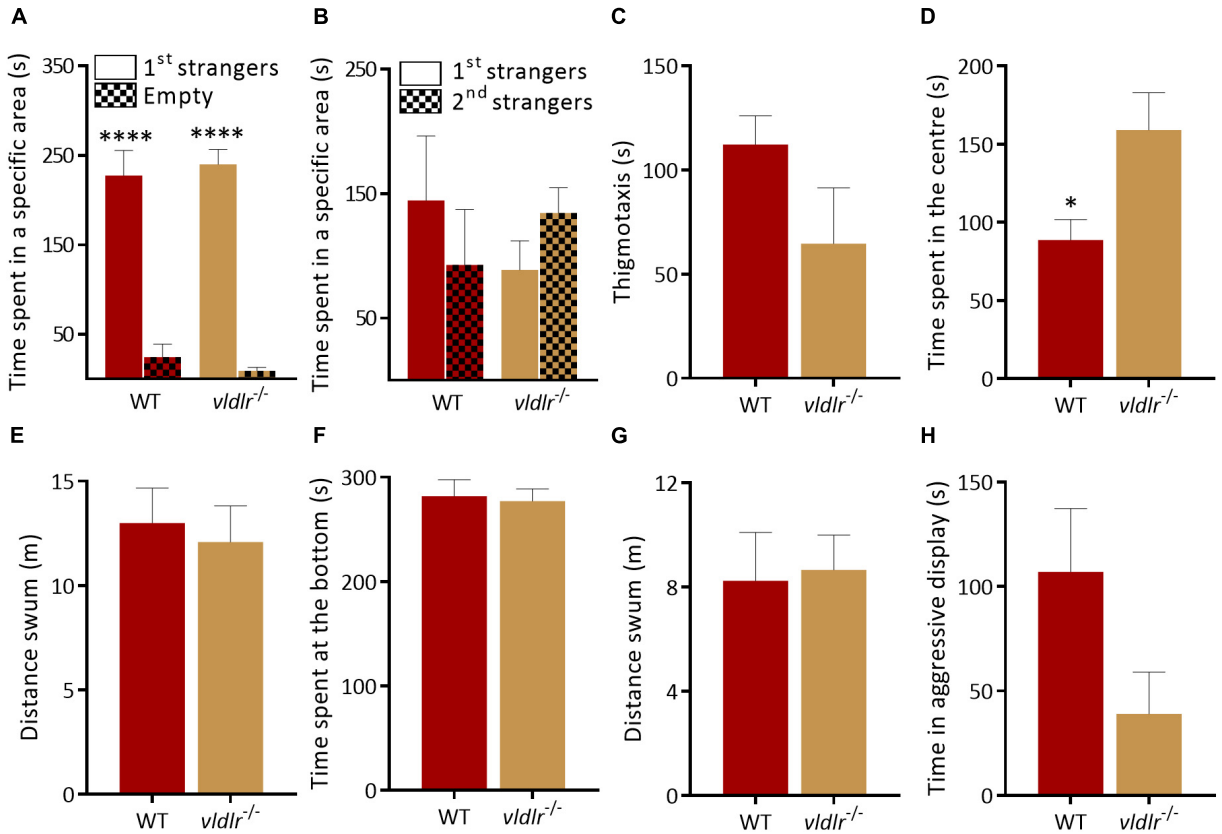

FIGURE 5 | Behavior of *vldlr*$^{-/-}$ zebrafish. **(A,B)** Social preference test. **(A)** Both genotypes prefer to spend time near a group of unfamiliar fish [1st strangers; $p < 0.0001$ for both genotypes; two-way ANOVA followed by Sidak's *post hoc*, genotype factor: $F(1,24) = 0.0039$, $p = 0.95$, stranger factor: $F(1,24) = 120.1$, $p < 0.0001$, interaction genotype × stranger: $F(1,24) = 0.4912$, $p = 0.49$]. **(B)** WT and *vldlr*$^{-/-}$ spend equal time near both groups when a second unfamiliar group is added [$p = 0.58$ for WT and $p = 0.73$ for *vldlr*$^{-/-}$; two-way ANOVA followed by Sidak's *post hoc*, genotype factor: $F(1,24) = 1.353$, $p = 0.26$, stranger factor: $F(1,24) = 0.005$, $p = 0.94$, interaction genotype × stranger: $F(1,24) = 0.02779$, $p = 0.87$. $n = 8$ wild-type and $n = 7$ *vldlr*$^{-/-}$]. **(C–E)** *vldlr*$^{-/-}$ behavior in the open field test. **(C)** *vldlr*$^{-/-}$ spent the same time at side of the tank [*t*-test (Welch): $t_{(1.581)} = 9.068$, $p = 0.15$] compared to WT but more **(D)** time in center of the tank [*t*-test (Welch): $t_{(2.595)} = 9.47$, $p = 0.03$]. **(E)** Locomotion [*t*-test (Welch): $t_{(0.3779)} = 12.84$, $p = 0.71$. $n = 8$ wild-type and $n = 7$ *vldlr*$^{-/-}$]. **(F)** *vldlr*$^{-/-}$ exhibit normal anxiety-like behavior. Time at the bottom of novel tank (Mann Whitney test: $U = 16$, $p = 0.32$), **(G)** locomotion in a novel tank [*t*-test (Welch): $t_{(0.1803)} = 10.92$, $p = 0.86$. $n = 7$ wild-type and $n = 7$ *vldlr*$^{-/-}$]. **(H)** No difference in aggression levels between WT and *vldlr*$^{-/-}$ [*t*-test (Welch): $t_{(1.87)} = 11.41$, $p = 0.09$. $n = 8$ WT and $n = 7$ *vldlr*$^{-/-}$]. $^{*}p < 0.05$, $^{****}p < 0.0001$.

5-HT Modulates the Preference for Social Interaction in Zebrafish

HPLC analysis identified a significant increase of 5-HT in the hindbrain of *reln*$^{-/-}$. We applied the 5HT-1A receptor agonist buspirone that decreases the concentration of 5-HT at the synapse (Loane and Politis, 2012) and measured behavior. Immersion in buspirone increased the interaction of WT with the second group of unfamiliar fish in the visually mediated social preference test (**Figure 7A**; first strangers $p = 0.51$ and second strangers $p = 0.004$). However, buspirone did not rescue the mutant phenotype, and *reln*$^{-/-}$ still failed to switch social preference following drug application [**Figure 7B**; second strangers $p = 0.01$; three-way ANOVA followed by Sidak's *post hoc*, genotype factor: $F(1,56) = 0.2488$, $p = 0.62$, stranger factor: $F(1,56) = 2.11$, $p = 0.16$, treatment factor: $F(1,56) = 0.0124$, $p = 0.91$, interaction genotype × stranger: $F(1,56) = 40.28$, $p < 0.0001$, interaction genotype × treatment: $F(1,56) = 0.01879$, $p = 0.89$, interaction stranger × treatment: $F(1,56) = 3.362$, $p = 0.07$, interaction stranger × genotype × treatment: $F(1,56) = 0.0566$, $p = 0.81$]. In humans, mutations in *RELN* are linked to autism spectrum disorder. We applied the autism treatment drugs oxytocin (Hollander et al., 2003; Andari et al., 2010; Guastella et al., 2010) and risperidone (Canitano and Scandurra, 2008) to *reln*$^{-/-}$ mutants and quantified individual social interactions in the social preference test. However, neither oxytocin nor risperidone altered the preference for social novelty in zebrafish of either genotype [**Figure 8A**; WT saline $p = 0.57$, WT oxytocin $p = 0.53$ and WT risperidone $p = 0.14$, **Figure 8B**; *reln*$^{-/-}$ saline $p = 0.014$, *reln*$^{-/-}$ oxytocin $p = 0.048$, *reln*$^{-/-}$ risperidone $p = 0.014$; Three-way ANOVA followed by Sidak's *post hoc* for oxytocin, genotype factor: $F(1,64) = 0.3928$, $p = 0.53$, stranger factor: $F(1,64) = 2.133$, $p = 0.15$, treatment factor: $F(1,64) = 0.0143$, $p = 0.90$, interaction genotype × stranger: $F(1,64) = 17.44$, $p < 0.0001$, interaction genotype × treatment: $F(1,64) = 0.0282$, $p = 0.87$, interaction stranger × treatment: $F(1,64) = 0.0707$, $p = 0.79$, interaction

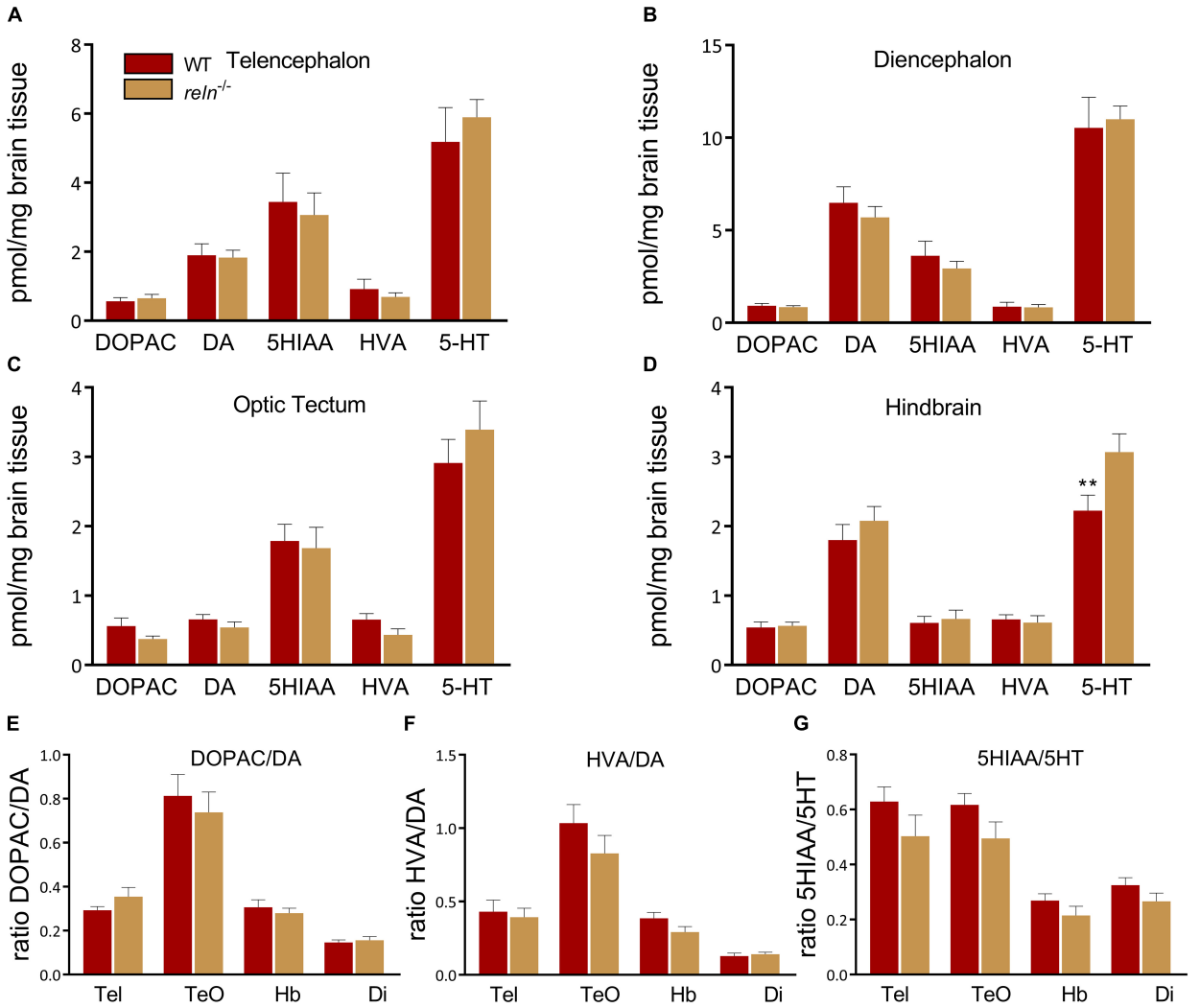

FIGURE 6 | High pressure liquid chromatography. 5-HT levels are increased in the hindbrain of *reln*$^{-/-}$ compared to WT [*t*-test: $t_{(3.694)} = 70$, $p = 0.0021$, multiple *t*-tests with Holm–Sidak multiple comparisons correction. $n = 8$ WT, $n = 8$ *reln*$^{-/-}$]. **(A)** Telencephalon, **(B)** diencephalon, **(C)** optic tectum and **(D)** hindbrain. No differences in the breakdown of **(E)** DOPAC/DA, **(F)** HVA/DA, **(G)** 5-HIAA/-5HT. DA, dopamine; Di, diencephalon; DOPAC, 3,4-Dihydroxyphenylacetic acid; Hb, Hindbrain; HVA, homovanillic acid; Tel, telencephalon; TeO, optic tectum; 5-HIAA, 5-hydroxyindoleacetic acid; 5-HT, 5-hydroxytryptamine. $^{**}p < 0.01$. Mean ± SEM.

stranger × genotype × treatment: $F(1,64) = 0.04759$, $p = 0.83$. Three-way ANOVA followed by Sidak's *post hoc* for risperidone, genotype factor: $F(1,64) = 1.073$, $p = 0.30$, stranger factor: $F(1,64) = 2.573$, $p = 0.11$, treatment factor: $F(1,64) = 0.8058$, $p = 0.37$, interaction genotype × stranger: $F(1,64) = 25.65$, $p < 0.0001$, interaction genotype × treatment: $F(1,64) = 0.3363$, $p = 0.56$, interaction stranger × treatment: $F(1,64) = 0.01244$, $p = 0.91$, interaction stranger × genotype × treatment: $F(1,64) = 0.4869$, $p = 0.49$].

DISCUSSION

In this study we have quantified the contribution of Reelin pathway signaling to adult zebrafish behavior. Zebrafish *reln*$^{-/-}$ mutants display a decrease in preference for social novelty, without altering shoaling, anxiety-like behavior, aggression or exploration. Conversely mutants for the canonical Reln targets *dab1a* and *vldlr* display normal social preference, but heightened aggression (*dab1a*$^{-/-}$) and exploration (*vldlr*$^{-/-}$). This suggests that Reln signaling has a pleiotropic role in controlling zebrafish behavior.

Reelin Localization in the Adult Zebrafish Brain

The zebrafish telencephalon has a non-laminar structure that develops through eversion, a process whereby the dorsal pallial region of the forebrain folds over the more ventral subpallium (Folgueira et al., 2012). Conversely, the mammalian cortex has a six-layered laminar structure that develops through evagination (Nieuwenhuys, 1994; Mueller, 2011). In zebrafish, Reln protein

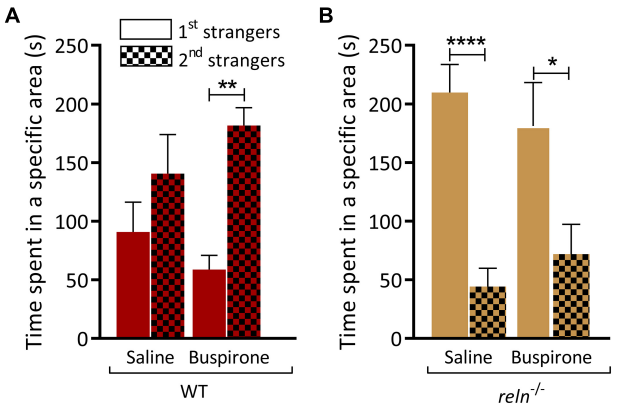

FIGURE 7 | Buspirone increase the social preference for novelty in WT but not *reln*$^{-/-}$. **(A)** WT treated with saline spend equal time near the two groups of unfamiliar fish, whereas WT treated with buspirone switch preference and spend more time near the new group of unfamiliar fish. **(B)** Buspirone treatment does not completely rescue the impaired preference for social novelty of *reln*$^{-/-}$ zebrafish (WT with saline $p = 0.51$; WT with buspirone $p = 0.0039$; *reln*$^{-/-}$ with saline $p < 0.0001$; *reln*$^{-/-}$ with buspirone $p = 0.012$). Three-way ANOVA followed by Sidak's *post hoc*, genotype factor: $F(1,56) = 0.2488$, $p = 0.62$, stranger factor: $F(1,56) = 2.11$, $p = 0.16$, treatment factor: $F(1,56) = 0.0124$, $p = 0.91$, interaction genotype × stranger: $F(1,56) = 40.28$, $p < 0.0001$, interaction genotype × treatment: $F(1,56) = 0.01879$, $p = 0.89$, interaction stranger × treatment: $F(1,56) = 3.362$, $p = 0.07$, interaction stranger × genotype × treatment: $F(1,56) = 0.0566$, $p = 0.81$). $n = 8$ WT and $n = 8$ *reln*$^{-/-}$. $^{*}p < 0.05$, $^{**}p < 0.01$, $^{****}p < 0.0001$. Mean ± SEM.

is secreted from superficial inhibitory interneurons (SINs) in a similar manner to the localization of Reln in interneurons in other adult vertebrates (Di Donato et al., 2018). However, Reln could have a different function in the non-laminar zebrafish brain compared to other vertebrates. Antibody labeling of the adult zebrafish brain agrees with the distribution of *reln* mRNA described by Costagli et al. (2002). The optic tectum is the principal retinorecipient brain region in zebrafish and is homologous to the superior colliculus in mammals (Gebhardt et al., 2013). The stratum fibrosum marginale (sfm) is located underneath the pia mater and glia limitans and the stratum opticum (so) is directly below it. The sfm is a plexiform-type layer containing a dense assortment of axons, axon terminals and dendrites, whereas the so is formed of optic nerve terminal bundles (Corbo et al., 2012). Reln is also found in the torus longitudinalis (TL), a ray-finned fish-specific paired longitudinal eminence of granule cells located at the medial margins of the optic tectum. The granule cells of the torus longitudinalis project unmyelinated axons through the contralateral sfm of the optic tectum to synapse upon pyramidal cells. The torus longitudinalis is thought to be involved in learning complex visual scenes (Northmore, 2017). In the isthmic tegmentum, Reln is found in a few cells in the interpeduncular nucleus (nin), a structure that receives projections from the dorsal habenula and may be involved in fear conditioning (Amo et al., 2010). In the hindbrain, granule cells of the corpus cerebelli (CCe) send their axons to Purkinje cells in the molecular layer of the cerebellum, whereas the granule cells of the caudal lobe of the cerebellum (LCa) project to crest cells in the crista cerebellaris (CC; Takeuchi et al., 2015). Therefore, the hindbrain areas that contain Reln are all linked to each other functionally. Scattered Reln-positive cells are also present in the intermediate and inferior part of the reticular formation, an intricate network of excitatory and inhibitory neurons and diffuse nuclei extending from the spinal cord through the medulla oblongata to the mesencephalon.

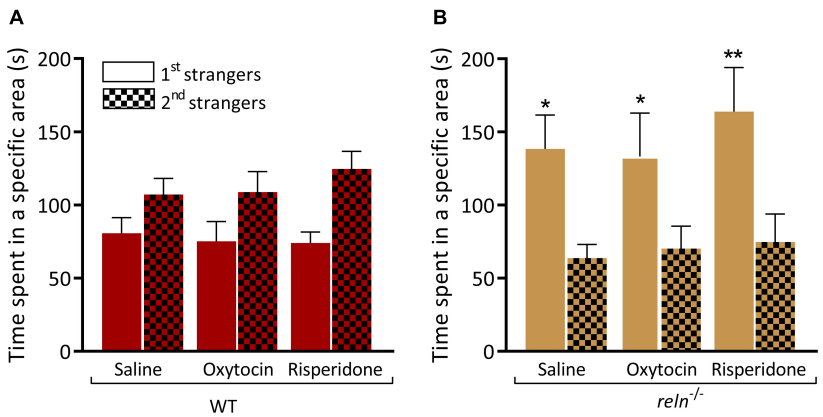

FIGURE 8 | Oxytocin and risperidone do not rescue preference for social novelty. **(A)** WT treated with saline ($p = 0.57$), oxytocin ($p = 0.53$), and risperidone ($p = 0.14$) spend equal time near the two groups of unfamiliar fish. **(B)** Neither oxytocin ($p = 0.048$) nor risperidone ($p = 0.0023$) treatment rescues the impaired preference for social novelty of *reln*$^{-/-}$ zebrafish (saline control, $p = 0.014$). Three-way ANOVA followed by Sidak's *post hoc* for oxytocin, genotype factor: $F(1,64) = 0.3928$, $p = 0.53$, stranger factor: $F(1,64) = 2.133$, $p = 0.15$, treatment factor: $F(1,64) = 0.0143$, $p = 0.90$, interaction genotype × stranger: $F(1,64) = 17.44$, $p < 0.0001$, interaction genotype × treatment: $F(1,64) = 0.0282$, $p = 0.87$, interaction stranger × treatment: $F(1,64) = 0.0707$, $p = 0.79$, interaction stranger × genotype × treatment: $F(1,64) = 0.04759$, $p = 0.83$. Three-way ANOVA followed by Sidak's *post hoc* for risperidone, genotype factor: $F(1,64) = 1.073$, $p = 0.30$, stranger factor: $F(1,64) = 2.573$, $p = 0.11$, treatment factor: $F(1,64) = 0.8058$, $p = 0.37$, interaction genotype × stranger: $F(1,64) = 25.65$, $p < 0.0001$, interaction genotype × treatment: $F(1,64) = 0.3363$, $p = 0.56$, interaction stranger × treatment: $F(1,64) = 0.01244$, $p = 0.91$, interaction stranger × genotype × treatment: $F(1,64) = 0.4869$, $p = 0.49$. $n = 9$ WT and $n = 9$ *reln*$^{-/-}$. $^{*}p < 0.05$, $^{**}p < 0.01$. Mean ± SEM.

The presence of Reln in the laminated structures of the optic tectum and cerebellum suggest that this protein may have a conserved role in neuronal migration in some areas of the zebrafish brain. This hypothesis has been confirmed in a study showing synaptic lamination defects in the optic tectum of *reln*$^{-/-}$ larvae (Di Donato et al., 2018). Although the optic tectum of adult zebrafish *reln*$^{-/-}$ mutants does not show patterning defects, in the cerebellum Purkinje cells, eurydendroid cells and Bergmann glia are found in ectopic positions in the absence of hypoplasia (Nimura et al., 2019). The localization of Reln in the zebrafish brain fits with the idea that this protein could play a role in synaptic organization or the integration of sensory afferent information from tectal or diencephalic brain areas to the dorsal telencephalon (Costagli et al., 2002).

Loss of Reln Function Decreases Preference for Social Novelty

The presence of RELN at the peak region of linkage and first autism susceptibility locus (chromosome 7q22) suggested that loss of *reln* function might alter zebrafish social behavior. In a shoaling test, groups of mutants displayed similar social interactions as groups of WT zebrafish including inter-individual distance (**Figure 3A**), polarization (**Figure 3B**) and velocity (**Figure 3C**). Furthermore, in a social preference test, *reln*$^{-/-}$ mutants interacted normally with a first group of conspecifics (**Figure 2A**) suggesting that social interactions occur normally in this mutant line. However, *reln*$^{-/-}$ fail to interact with a second group of animals placed into the same tank demonstrating a reduction in preference for social novelty (**Figure 2B**). Other behavioral measures, including exploration of a large tank (**Figures 3D–F**), anxiety-like behavior (**Figures 3G,H**), and aggression (**Figure 3I**) were not altered.

Homozygous *Reln*$^{-/-}$ mutant mice are not suitable for behavioral studies since they display severe ataxia, likely due to their severe neuronal migration defects. However, heterozygous *reeler* mice (*Reln*$^{+/-}$) display behavioral, cognitive and neuroanatomical defects that are milder than those seen in *Reln*$^{-/-}$. RELN haploinsufficiency causes loss of Purkinje neurons in the cerebellum of *Reln*$^{+/-}$ (Biamonte et al., 2009; Maloku et al., 2010), a phenotype that is similar to the loss of Purkinje cells seen in the cerebellum of some ASD patients (Ritvo et al., 1986). Behavioral characterization of *Reln*$^{+/-}$ has provided ambiguous results. Some studies have reported increased anxiety, impaired executive function, motor impulsivity, abnormal prepulse inhibition, decreased contextual fear conditioning and associative learning impairments in *Reln*$^{+/-}$ mice (Tueting et al., 1999; Tremolizzo et al., 2002; Krueger et al., 2006; Qiu et al., 2006) whereas other groups report that *Reln*$^{+/-}$ display normal locomotor activity, prepulse inhibition, anxiety, coordination, social behavior, spatial learning and transitions in the light–dark test, a measure of anxiety (Podhorna and Didriksen, 2004; Qiu et al., 2006). Regarding social interactions and communication, hallmarks of ASD, *Reln*$^{+/-}$ spend more time engaging in social investigation (Podhorna and Didriksen, 2004) but do not display alterations in social and vocal repertoires during courtship (Michetti et al., 2014). However, deletion of the positively charged carboxy-terminal region of RELN attenuates canonical RELN signaling and leads to decreased social interaction, impaired working memory, hyperactivity and decreased anxiety compared to WT (Kohno et al., 2015; Sakai et al., 2016). The surprising range of different behavioral phenotypes that has been reported could be due to the genetic background of the mutant animals, the age of testing or the behavioral protocol used.

Canonical Reln Signaling Does Not Underpin the Behavioral Phenotype

Reln signals via several downstream pathways including the canonical receptors apolipoprotein E receptor 2 and the very low density lipoprotein receptor (Trommsdorff et al., 1999) both of which lead to Disabled-1 activation (Howell et al., 1997; Sheldon et al., 1997). We investigated the possible contribution of canonical signaling to the phenotype of *reln*$^{-/-}$ zebrafish by characterizing the behavior of *dab1a*$^{-/-}$ and *vldr*$^{-/-}$ mutant lines. Both *dab1a*$^{-/-}$ and *vldlr*$^{-/-}$ displayed different behavioral profiles. *dab1a*$^{-/-}$ fish were hyperactive (**Figure 4F**) and more aggressive (**Figure 4D**) compared to WT without showing alterations to social behavior (**Figure 4**). Conversely, *vldlr*$^{-/-}$ exhibited a selective increase in exploration of an open field tank (**Figure 5D**). Although we did not have access to an *apoer2*$^{-/-}$ mutant line, the essential adaptor protein Dab1a represents a common target for both receptors. Therefore, the lack of phenotypic overlap with *reln*$^{-/-}$ suggests that we can rule out a contribution of canonical signaling to the decreased preference for social novelty. Studies to address this issue could include examining other Reln signaling targets such as the CrK/Rap1, P13K/Akt/mTOR, and MEK/Erk1/2 pathways (Chen et al., 2010). For example, this could include rescuing the social deficit of *reln*$^{-/-}$ mutants by using drugs that stimulate these signaling pathways.

5-HT Signaling Contributes to the Decreased Preference for Social Novelty Observed in *reln*$^{-/-}$

Irregularities in several neurotransmitter pathways, including the monoamine 5-HT, have been implicated in the pathology of ASD. We used high pressure liquid chromatography to measure the monoamines dopamine, 5-HT and their metabolites (**Figure 6**). We observed a significant increase of 5-HT that was restricted to the hindbrain of *reln*$^{-/-}$ (**Figure 6D**), the brain region that contains the raphe nucleus [the largest group of 5-HT producing neurons in zebrafish (Lillesaar et al., 2009) and that expresses the signaling pathways components *tryptophan hydroxylase 2*, *vesicular monoamine transporter* and the 5-HT transporter-encoding gene *solute carrier family 6 member 4a* (Teraoka et al., 2004; Wang et al., 2006; Norton et al., 2008; Wen et al., 2008)]. As well as regulating cell division and differentiation, neurite growth, and synaptogenesis, 5-HT also modulates human behaviors associated with psychiatric disorders (Chugani, 2002). Both hypo- and hyper-serotonemia can occur in ASD patients (Schain and Freedman, 1961; Connors et al., 2006; Yang et al., 2014). We investigated the connection between aberrant 5-HT signaling and social preference by applying the 5-HT$_{1A}$

receptor partial agonist buspirone (Loane and Politis, 2012). Buspirone acts presynaptically to reduce 5-HT levels (Gebauer et al., 2011) and it can have both anxiolytic and pro-social effects in zebrafish (File and Seth, 2003; Bencan et al., 2009; Gould, 2011; Barba-Escobedo and Gould, 2012; Gould et al., 2012; Maaswinkel et al., 2012; Maaswinkel et al., 2013). Although immersion in buspirone increased the interaction of WT with the second group of unfamiliar fish (**Figure 7A**) it did not rescue the mutant phenotype, with *reln*$^{-/-}$ failing to switch social preference following drug treatment (**Figure 7B**). This suggests that the 5-HT signaling does not underpin the lack of preference for social novelty seen in *reln*$^{-/-}$ zebrafish, and further research is required to understand the neurotransmitter basis of this behavioral phenotype.

CONCLUSION

Multiple lines of evidence suggest that RELN is a vulnerability factor for ASD. Characterization of the behavioral phenotype of *reln*$^{-/-}$ mutant zebrafish provided an opportunity to investigate which adult zebrafish behaviors can be linked to ASD-candidate genes. Using a combination of behavioral tests we were able to identify a specific alteration in preference for social novelty without a general change to social behavior. It is difficult to compare this finding to other model species such as mouse because manipulation of Reln signaling leads to such a wide range of different phenotypes (Podhorna and Didriksen, 2004; Qiu et al., 2006). The reduction in preference for social novelty that we observed is surprisingly specific and would fit with the definition of ASD that includes restricted interests and repetitive patterns of behavior that are abnormal in intensity or focus. Arguing against this idea, however, we were unable to rescue this phenotype by applying two drugs that are used to treat ASD: oxytocin and risperidone. One explanation for this result could be that we need to apply these drugs for a longer time period or at higher concentration. For example, oxytocin administration to mouse models of ASD symptoms only rescued social deficits behavior 1–2 weeks following sub-chronic application (Teng et al., 2013). Furthermore, since there are extensive connections between oxytocin and 5-HT neurotransmitter signaling co-application of drugs targeting both these pathways may be required to rescue the behavioral phenotype of *reln*$^{-/-}$.

In summary, the abnormal preference for social novelty displayed by *reln*$^{-/-}$ zebrafish mutants suggest that they may represent a good model to analyze some aspects of ASD, including restricted or repetitive behavior. Further research comparing the simultaneous presentation of different types of stimuli in the visually mediated preference test could be used to investigate this idea in more detail. Creation of novel zebrafish *reln* mutant lines that either harbor mutations associated with ASD in human patients or in different genetic backgrounds might provide further insights into the pleiotropic behavioral phenotypes seen in animals lacking Reln signaling.

DATA AVAILABILITY

The datasets generated for this study are available on request to the corresponding author.

ETHICS STATEMENT

This study was carried out in accordance with the recommendations of the local Animal Welfare and Ethical Review board at the University of Leicester. The protocol was approved by the local Animal Welfare and Ethical Review board at the University of Leicester.

AUTHOR CONTRIBUTIONS

ED designed the experiments, collected and analyzed the data, and wrote a first version of the manuscript. VD created the *reln*$^{-/-}$, *dab1a*$^{-/-}$ and *vldlr*$^{-/-}$ mutant lines. AY helped collect and analyze the HPLC data. FD provided the novel mutant lines. WN analyzed the data and wrote the manuscript. All authors approved the final manuscript before submission.

FUNDING

The research leading to this publication received funding from the European Union's Horizon2020 Research and Innovation Program under grant agreement no 643051.

ACKNOWLEDGMENTS

We are grateful to Carl Breaker and members of the preclinical research facility for zebrafish care, Ceinwen Tilley for technical support and all members of the Norton lab for discussions about this data.

REFERENCES

Amo, R., Aizawa, H., Takahoko, M., Kobayashi, M., Takahashi, R., Aoki, T., et al. (2010). Identification of the zebrafish ventral habenula as a homolog of the mammalian lateral habenula. *J. Neurosci.* 30, 1566–1574. doi: 10.1523/JNEUROSCI.3690-09.2010

Andari, E., Duhamel, J. R., Zalla, T., Herbrecht, E., Leboyer, M., and Sirigu, A. (2010). Promoting social behavior with oxytocin in high-functioning autism spectrum disorders. *Proc. Natl. Acad. Sci. U.S.A.* 107, 4389–4394. doi: 10.1073/pnas.0910249107

Barba-Escobedo, P. A., and Gould, G. G. (2012). Visual social preferences of lone zebrafish in a novel environment: strain and anxiolytic effects. *Genes Brain Behav.* 11, 366–373. doi: 10.1111/j.1601-183X.2012.00770.x

Barr, A. M., Fish, K. N., Markou, A., and Honer, W. G. (2008). Heterozygous reeler mice exhibit alterations in sensorimotor gating but not presynaptic proteins. *Eur. J. Neurosci.* 27, 2568–2574. doi: 10.1111/j.1460-9568.2008.06233.x

Bencan, Z., Sledge, D., and Levin, E. D. (2009). Buspirone, chlordiazepoxide and diazepam effects in a zebrafish model of anxiety. *Pharmacol. Biochem. Behav.* 94, 75–80. doi: 10.1016/j.pbb.2009.07.009

Biamonte, F., Assenza, G., Marino, R., D'amelio, M., Panteri, R., Caruso, D., et al. (2009). Interactions between neuroactive steroids and reelin haploinsufficiency in Purkinje cell survival. *Neurobiol. Dis.* 36, 103–115. doi: 10.1016/j.nbd.2009.07.001

Bock, H. H., and May, P. (2016). Canonical and non-canonical reelin signaling. *Front. Cell. Neurosci.* 10:166. doi: 10.3389/fncel.2016.00166

Bonora, E., Beyer, K. S., Lamb, J. A., Parr, J. R., Klauck, S. M., Benner, A., et al. (2003). Analysis of reelin as a candidate gene for autism. *Mol. Psychiatry* 8, 885–892. doi: 10.1038/sj.mp.4001310

Bufill, E., Roura-Poch, P., Sala-Matavera, I., Antón, S., Lleó, A., Sánchez-Saudinós, B., et al. (2013). Reelin signaling pathway genotypes and alzheimer disease in a spanish population. *Alzheimer Dis. Assoc. Disord.* 29, 169–172. doi: 10.1097/WAD.0000000000000002

Canitano, R., and Scandurra, V. (2008). Risperidone in the treatment of behavioral disorders associated with autism in children and adolescents. *Neuropsychiatr. Dis. Treat.* 4, 723–730.

Carreno Gutierrez, H., Colanesi, S., Cooper, B., Reichmann, F., Young, A. M. J., Kelsh, R. N., et al. (2019). Endothelin neurotransmitter signalling controls zebrafish social behaviour. *Sci. Rep.* 9:3040. doi: 10.1038/s41598-019-39907-7

Carreno Gutierrez, H., O'leary, A., Freudenberg, F., Fedele, G., Wilkinson, R., Markham, E., et al. (2017). Nitric oxide interacts with monoamine oxidase to modulate aggression and anxiety-like behaviour. *Eur. Neuropsychopharmacol.* doi: 10.1016/j.euroneuro.2017.09.004 [Epub ahead of print].

Chen, Y., Durakoglugil, M. S., Xian, X., and Herz, J. (2010). ApoE4 reduces glutamate receptor function and synaptic plasticity by selectively impairing ApoE receptor recycling. *Proc. Natl. Acad. Sci. U.S.A.* 107, 12011–12016. doi: 10.1073/pnas.0914984107

Chugani, D. (2002). Role of altered brain serotonin mechanisms in autism. *Mol. Psychiatry* 7(Suppl. 2), S16–S17.

Connors, S. L., Matteson, K. J., Sega, G. A., Lozzio, C. B., Carroll, R. C., and Zimmerman, A. W. (2006). Plasma serotonin in autism. *Pediatr. Neurol.* 35, 182–186.

Corbo, C. P., Othman, N. A., Gutkin, M. C., Alonso Adel, C., and Fulop, Z. L. (2012). Use of different morphological techniques to analyze the cellular composition of the adult zebrafish optic tectum. *Microsc. Res. Tech.* 75, 325–333. doi: 10.1002/jemt.21061

Costa, E. (2002). The heterozygote reeler mouse as a model for the development of a new generation of antipsychotics. *Curr. Opin. Pharmacol.* 2, 56–62. doi: 10.1016/s1471-4892(01)00121-7

Costagli, A., Kapsimali, M., Wilson, S. W., and Mione, M. (2002). Conserved and divergent patterns of Reelin expression in the zebrafish central nervous system. *J. Comp. Neurol.* 450, 73–93. doi: 10.1002/cne.10292

D'Arcangelo, G. (2005). The reeler mouse: anatomy of a mutant. *Int. Rev. Neurobiol.* 71, 383–417. doi: 10.1016/s0074-7742(05)71016-3

D'Arcangelo, G. (2006). Reelin mouse mutants as models of cortical development disorders. *Epilepsy Behav.* 8, 81–90. doi: 10.1016/j.yebeh.2005.09.005

D'Arcangelo, G. (2014). Reelin in the years: controlling neuronal migration and maturation in the mammalian brain. *Adv. Neurosci.* 2014, 1–19. doi: 10.1155/2014/597395

De Rubeis, S., He, X., Goldberg, A. P., Poultney, C. S., Samocha, K., Cicek, A. E., et al. (2014). Synaptic, transcriptional and chromatin genes disrupted in autism. *Nature* 515, 209–215. doi: 10.1038/nature13772

Di Donato, V., De Santis, F., Albadri, S., Auer, T. O., Duroure, K., Charpentier, M., et al. (2018). An attractive reelin gradient establishes synaptic lamination in the vertebrate visual system. *Neuron* 97, 1049.e6–1062.e6. doi: 10.1016/j.neuron.2018.01.030

Dutta, S., Guhathakurta, S., Sinha, S., Chatterjee, A., Ahmed, S., Ghosh, S., et al. (2006). Reelin gene polymorphisms in the Indian population: a possible paternal 5'UTR-CGG-repeat-allele effect on autism. *Am. J. Med. Genet. Part B Neuropsychiatr. Genet.* 144B, 106–112. doi: 10.1002/ajmg.b.30419

Dutta, S., Sinha, S., Ghosh, S., Chatterjee, A., Ahmed, S., and Usha, R. (2008). Genetic analysis of reelin gene (RELN) SNPs: no association with autism spectrum disorder in the Indian population. *Neurosci. Lett.* 441, 56–60. doi: 10.1016/j.neulet.2008.06.022

Egan, R. J., Bergner, C. L., Hart, P. C., Cachat, J. M., Canavello, P. R., Elegante, M. F., et al. (2009). Understanding behavioral and physiological phenotypes of stress and anxiety in zebrafish. *Behav. Brain Res.* 205, 38–44. doi: 10.1016/j.bbr.2009.06.022

Fatemi, S. H. (2001). Reelin mutations in mouse and man: from reeler mouse to schizophrenia, mood disorders, autism and lissencephaly. *Mol. Psychiatry* 6, 129–133. doi: 10.1038/sj.mp.4000129

Fatemi, S. H., Snow, A. V., Stary, J. M., Araghi-Niknam, M., Reutiman, T. J., Lee, S., et al. (2005). Reelin signaling is impaired inFsample autism. *Biol. Psychiatry* 57, 777–787. doi: 10.1016/j.biopsych.2004.12.018

File, S. E., and Seth, P. (2003). A review of 25 years of the social interaction test. *Eur. J. Pharmacol.* 463, 35–53. doi: 10.1016/s0014-2999(03)01273-1

Folgueira, M., Bayley, P., Navratilova, P., Becker, T. S., Wilson, S. W., and Clarke, J. D. (2012). Morphogenesis underlying the development of the everted teleost telencephalon. *Neural Dev.* 7:32. doi: 10.1186/1749-8104-7-32

Förster, E., Bock, H. H., Herz, J., Chai, X., Frotscher, M., and Zhao, S. (2010). Emerging topics in Reelin function. *Eur. J. Neurosci.* 31, 1511–1518. doi: 10.1111/j.1460-9568.2010.07222.x

Gebauer, D. L., Pagnussat, N., Piato, A. L., Schaefer, I. C., Bonan, C. D., and Lara, D. R. (2011). Effects of anxiolytics in zebrafish: similarities and differences between benzodiazepines, buspirone and ethanol. *Pharmacol. Biochem. Behav.* 99, 480–486. doi: 10.1016/j.pbb.2011.04.021

Gebhardt, C., Baier, H., and Del Bene, F. (2013). Direction selectivity in the visual system of the zebrafish larva. *Front. Neural Circuits* 7:111. doi: 10.3389/fncir.2013.00111

Goffinet, A. M. (1983). The embryonic development of the cerebellum in normal and reeler mutant mice. *Anat. Embryol.* 168, 73–86. doi: 10.1007/bf00305400

Gould, G. G. (2011). "Aquatic light/dark plus maze novel environment for assessing anxious versus exploratory behavior in zebrafish (Danio rerio) and other small teleost fish," in *Zebrafish Neurobehavioral Protocols*, eds A. Kalueff, and J. Cachat, (Totowa, NJ: Humana Press), 99–108. doi: 10.1007/978-1-60761-953-6_8

Gould, G. G., Seillier, A., Weiss, G., Giuffrida, A., Burke, T. F., Hensler, J. G., et al. (2012). Acetaminophen differentially enhances social behavior and cortical cannabinoid levels in inbred mice. *Prog. Neuro Psychopharmacol. Biol. Psychiatry* 38, 260–269. doi: 10.1016/j.pnpbp.2012.04.011

Guastella, A. J., Einfeld, S. L., Gray, K. M., Rinehart, N. J., Tonge, B. J., Lambert, T. J., et al. (2010). Intranasal oxytocin improves emotion recognition for youth with autism spectrum disorders. *Biol. Psychiatry* 67, 692–694. doi: 10.1016/j.biopsych.2009.09.020

He, Y., Xun, G., Xia, K., Hu, Z., Lv, L., Deng, Z., et al. (2011). No significant association between RELN polymorphism and autism in case-control and family-based association study in Chinese Han population. *Psychiatry Res.* 187, 462–464. doi: 10.1016/j.psychres.2010.04.051

Herculano, A. M., and Maximino, C. (2014). Serotonergic modulation of zebrafish behavior: towards a paradox. *Prog. Neuropsychopharmacol. Biol. Psychiatry* 55, 50–66. doi: 10.1016/j.pnpbp.2014.03.008

Herz, J., and Chen, Y. (2006). Reelin, lipoprotein receptors and synaptic plasticity. *Nat. Rev. Neurosci.* 7, 850–859. doi: 10.1038/nrn2009

Hollander, E., Novotny, S., Hanratty, M., Yaffe, R., Decaria, C. M., Aronowitz, B. R., et al. (2003). Oxytocin infusion reduces repetitive behaviors in adults with autistic and Asperger's disorders. *Neuropsychopharmacology* 28, 193–198. doi: 10.1038/sj.npp.1300021

Hong, S. E., Shugart, Y. Y., Huang, D. T., Shahwan, S. A., Grant, P. E., Hourihane, J. O. B., et al. (2000). Autosomal recessive lissencephaly with cerebellar hypoplasia is associated with human RELN mutations. *Nat. Genet.* 26, 93–96. doi: 10.1038/79246

Howell, B. W., Hawkes, R., Soriano, P., and Cooper, J. A. (1997). Neuronal position in the developing brain is regulated by mouse disabled-1. *Nature* 389, 733–737. doi: 10.1038/39607

Iafrati, J., Orejarena, M. J., Lassalle, O., Bouamrane, L., and Chavis, P. (2013). Reelin, an extracellular matrix protein linked to early onset psychiatric diseases, drives postnatal development of the prefrontal cortex via GluN2B-NMDARs and the mTOR pathway. *Mol. Psychiatry* 19, 417–426. doi: 10.1038/mp.2013.66

Idalencio, R., Kalichak, F., Rosa, J. G., De Oliveira, T. A., Koakoski, G., Gusso, D., et al. (2015). Waterborne risperidone decreases stress response in Zebrafish. *PLoS One* 10:e0140800. doi: 10.1371/journal.pone.0140800

Imai, H., Shoji, H., Ogata, M., Kagawa, Y., Owada, Y., Miyakawa, T., et al. (2016). Dorsal forebrain-specific deficiency of Reelin-Dab1 signal causes behavioral abnormalities related to psychiatric disorders. *Cereb. Cortex* 27, 3485–3501. doi: 10.1093/cercor/bhv334

Kilpatrick, I. C., Jones, M. W., and Phillipson, O. T. (1986). A semiautomated analysis method for catecholamines, indoleamines, and some prominent metabolites in microdissected regions of the nervous system: an isocratic HPLC technique employing coulometric detection and minimal sample preparation. *J. Neurochem.* 46, 1865–1876. doi: 10.1111/j.1471-4159.1986.tb08506.x

Kohno, T., Honda, T., Kubo, K.-I., Nakano, Y., Tsuchiya, A., Murakami, T., et al. (2015). Importance of Reelin C-terminal region in the development and maintenance of the postnatal cerebral cortex and its regulation by specific proteolysis. *J. Neurosci.* 35, 4776–4787. doi: 10.1523/JNEUROSCI.4119-14.2015

Koshimizu, E., Miyatake, S., Okamoto, N., Nakashima, M., Tsurusaki, Y., Miyake, N., et al. (2013). Performance comparison of bench-top next generation sequencers using microdroplet PCR-based enrichment for targeted sequencing in patients with autism spectrum disorder. *PLoS One* 8:e74167. doi: 10.1371/journal.pone.0074167

Krebs, M. O., Betancur, C., Leroy, S., Bourdel, M. C., Gillberg, C., and Leboyer, M. (2002). Absence of association between a polymorphic GGC repeat in the 5' untranslated region of the reelin gene and autism. *Mol. Psychiatry* 7, 801–804. doi: 10.1038/sj.mp.4001071

Krueger, D. D., Howell, J. L., Hebert, B. F., Olausson, P., Taylor, J. R., and Nairn, A. C. (2006). Assessment of cognitive function in the heterozygous reeler mouse. *Psychopharmacology* 189, 95–104. doi: 10.1007/s00213-006-0530-0

Kutiyanawalla, A., Promsote, W., Terry, A., and Pillai, A. (2011). Cysteamine treatment ameliorates alterations in GAD67 expression and spatial memory in heterozygous reeler mice. *Int. J. Neuropsychopharmacol.* 15, 1073–1086. doi: 10.1017/S1461145711001180

Lee, G. H., and D'Arcangelo, G. (2016). New insights into Reelin-mediated signaling pathways. *Front. Cell. Neurosci.* 10:122. doi: 10.3389/fncel.2016.00122

Levenson, J. M., Qiu, S., and Weeber, E. J. (2008). The role of reelin in adult synaptic function and the genetic and epigenetic regulation of the reelin gene. *Biochim. Biophys. Acta (BBA) Gene Regul. Mech.* 1779, 422–431. doi: 10.1016/j.bbagrm.2008.01.001

Levy, A. D., Omar, M. H., and Koleske, A. J. (2014). Extracellular matrix control of dendritic spine and synapse structure and plasticity in adulthood. *Front. Neuroanat.* 8:116. doi: 10.3389/fnana.2014.00116

Li, H., Li, Y., Shao, J., Li, R., Qin, Y., Xie, C., et al. (2008). The association analysis of RELN and GRM8 genes with autistic spectrum disorder in chinese han population. *Am. J. Med. Genet. Part B Neuropsychiatr. Genet.* 147B, 194–200. doi: 10.1002/ajmg.b.30584

Li, J., Nguyen, L., Gleason, C., Lotspeich, L., Spiker, D., Risch, N., et al. (2004). Lack of evidence for an association between WNT2 and RELN polymorphisms and autism. *Am. J. Med. Genet.* 126B, 51–57. doi: 10.1002/ajmg.b.20122

Li, W., Guo, X., and Xiao, S. (2015). Evaluating the relationship between reelin gene variants (rs7341475 and rs262355) and schizophrenia: a meta-analysis. *Neurosci. Lett.* 609, 42–47. doi: 10.1016/j.neulet.2015.10.014

Lillesaar, C., Stigloher, C., Tannhauser, B., Wullimann, M. F., and Bally-Cuif, L. (2009). Axonal projections originating from raphe serotonergic neurons in the developing and adult zebrafish, Danio rerio, using transgenics to visualize raphe-specific pet1 expression. *J. Comp. Neurol.* 512, 158–182. doi: 10.1002/cne.21887

Loane, C., and Politis, M. (2012). Buspirone: what is it all about? *Brain Res.* 1461, 111–118. doi: 10.1016/j.brainres.2012.04.032

Maaswinkel, H., Le, X., He, L., Zhu, L., and Weng, W. (2013). Dissociating the effects of habituation, black walls, buspirone and ethanol on anxiety-like behavioral responses in shoaling zebrafish. A 3D approach to social behavior. *Pharmacol. Biochem. Behav.* 108, 16–27. doi: 10.1016/j.pbb.2013.04.009

Maaswinkel, H., Zhu, L., and Weng, W. (2012). The immediate and the delayed effects of buspirone on zebrafish (Danio rerio) in an open field test: a 3-D approach. *Behav. Brain Res.* 234, 365–374. doi: 10.1016/j.bbr.2012.07.014

Maloku, E., Covelo, I. R., Hanbauer, I., Guidotti, A., Kadriu, B., Hu, Q., et al. (2010). Lower number of cerebellar Purkinje neurons in psychosis is associated with reduced reelin expression. *Proc. Natl. Acad. Sci. U.S.A.* 107, 4407–4411. doi: 10.1073/pnas.0914483107

Michetti, C., Romano, E., Altabella, L., Caruso, A., Castelluccio, P., Bedse, G., et al. (2014). Mapping pathological phenotypes in reelin mutant mice. *Front. Pediatr.* 2:95. doi: 10.3389/fped.2014.00095

Miyata, T., Nakajima, K., Mikoshiba, K., and Ogawa, M. (1997). Regulation of Purkinje cell alignment by reelin as revealed with CR-50 antibody. *J. Neurosci.* 17, 3599–3609. doi: 10.1523/jneurosci.17-10-03599.1997

Mueller, T. (2011). The conserved bauplan of the teleostean telencephalon. *Brain Behav. Evol.* 78, 259–260. doi: 10.1159/000331869

Neale, B. M., Kou, Y., Liu, L., Ma'ayan, A., Samocha, K. E., Sabo, A., et al. (2012). Patterns and rates of exonic de novo mutations in autism spectrum disorders. *Nature* 485, 242–245. doi: 10.1038/nature11011

Nieuwenhuys, R. (1994). The neocortex. An overview of its evolutionary development, structural organization and synaptology. *Anat. Embryol.* 190, 307–337.

Nimura, T., Itoh, T., Hagio, H., Hayashi, T., Di Donato, V., Takeuchi, M., et al. (2019). Role of reelin in cell positioning in the cerebellum and the cerebellum-like structure in zebrafish. *Dev. Biol.* doi: 10.1016/j.ydbio.2019.07.010 [Epub ahead of print].

Northmore, D. P. (2017). Holding visual attention for 400millionyears: a model of tectum and torus longitudinalis in teleost fishes. *Vision Res.* 131, 44–56. doi: 10.1016/j.visres.2016.12.001

Norton, W. H., Folchert, A., and Bally-Cuif, L. (2008). Comparative analysis of serotonin receptor (HTR1A/HTR1B families) and transporter (slc6a4a/b) gene expression in the zebrafish brain. *J. Comp. Neurol.* 511, 521–542. doi: 10.1002/cne.21831

Norton, W. H., Stumpenhorst, K., Faus-Kessler, T., Folchert, A., Rohner, N., Harris, M. P., et al. (2011). Modulation of Fgfr1a signaling in zebrafish reveals a genetic basis for the aggression-boldness syndrome. *J. Neurosci.* 31, 13796–13807. doi: 10.1523/JNEUROSCI.2892-11.2011

Norton, W. H. J., Manceau, L., and Reichmann, F. (2019). The visually mediated social preference test: a novel technique to measure social behavior and behavioral disturbances in Zebrafish. *Methods Mol. Biol.* 2011, 121–132. doi: 10.1007/978-1-4939-9554-7_8

Ovadia, G., and Shifman, S. (2011). The genetic variation of RELN expression in schizophrenia and bipolar disorder. *PLoS One* 6:e19955. doi: 10.1371/journal.pone.0019955

Parker, M. O., Brock, A. J., Millington, M. E., and Brennan, C. H. (2013). Behavioral phenotyping of *casper* mutant and 1-pheny-2-thiourea treated adult zebrafish. *Zebrafish* 10, 466–471. doi: 10.1089/zeb.2013.0878

Persico, A. M., D'agruma, L., Maiorano, N., Totaro, A., Militerni, R., Bravaccio, C., et al. (2001). Reelin gene alleles and haplotypes as a factor predisposing to autistic disorder. *Mol. Psychiatry* 6, 150–159. doi: 10.1038/sj.mp.4000850

Pesold, C., Impagnatiello, F., Pisu, M., Uzunov, D., Costa, E., Guidotti, A., et al. (1998). Reelin is preferentially expressed in neurons synthesizing γ-aminobutyric acid in cortex and hippocampus of adult rats. *Proc. Natl. Acad. Sci. U.S.A.* 95, 3221–3226. doi: 10.1073/pnas.95.6.3221

Podhorna, J., and Didriksen, M. (2004). The heterozygous reeler mouse: behavioural phenotype. *Behav. Brain Res.* 153, 43–54. doi: 10.1016/j.bbr.2003.10.033

Popova, N. K. (2008). From gene to aggressive behavior: the role of brain serotonin. *Neurosci. Behav. Physiol.* 38, 471–475. doi: 10.1007/s11055-008-9004-7

Qiu, S., Korwek, K. M., Pratt-Davis, A. R., Peters, M., Bergman, M. Y., and Weeber, E. J. (2006). Cognitive disruption and altered hippocampus synaptic function in Reelin haploinsufficient mice. *Neurobiol. Learn. Mem.* 85, 228–242. doi: 10.1016/j.nlm.2005.11.001

Rakic, P. (2009). Evolution of the neocortex: a perspective from developmental biology. *Nat. Rev. Neurosci.* 10, 724–735. doi: 10.1038/nrn2719

Ritvo, E. R., Freeman, B., Scheibel, A. B., Duong, T., Robinson, H., Guthrie, D., et al. (1986). Lower Purkinje cell counts in the cerebella of four autistic subjects: initial findings of the UCLA-NSAC research report. *Am. J. Psychiatry* 143, 862–866. doi: 10.1176/ajp.143.7.862

Ruhl, N., Mcrobert, S. P., and Currie, W. J. (2009). Shoaling preferences and the effects of sex ratio on spawning and aggression in small laboratory populations of zebrafish (Danio rerio). *Lab. Anim.* 38, 264–269. doi: 10.1038/laban0809-264

Sakai, K., Shoji, H., Kohno, T., Miyakawa, T., and Hattori, M. (2016). Mice that lack the C-terminal region of Reelin exhibit behavioral abnormalities related to neuropsychiatric disorders. *Sci. Rep.* 6:28636. doi: 10.1038/srep28636

Schain, R. J., and Freedman, D. X. (1961). Studies on 5-hydroxyindole metabolism in autistic and other mentally retarded children. *J. Pediatr.* 58, 315–320. doi: 10.1016/s0022-3476(61)80261-8

Serajee, F. J., Zhong, H., and Mahbubul Huq, A. H. M. (2006). Association of Reelin gene polymorphisms with autism. *Genomics* 87, 75–83. doi: 10.1016/j.ygeno.2005.09.008

Sheldon, M., Rice, D. S., D'arcangelo, G., Yoneshima, H., Nakajima, K., Mikoshiba, K., et al. (1997). Scrambler and yotari disrupt the disabled gene and produce a reeler-like phenotype in mice. *Nature* 389, 730–733. doi: 10.1038/39601

Takeuchi, M., Matsuda, K., Yamaguchi, S., Asakawa, K., Miyasaka, N., Lal, P., et al. (2015). Establishment of Gal4 transgenic zebrafish lines for analysis of development of cerebellar neural circuitry. *Dev. Biol.* 397, 1–17. doi: 10.1016/j.ydbio.2014.09.030

Teixeira, C. M., Martín, E. D., Sahún, I., Masachs, N., Pujadas, L., Corvelo, A., et al. (2011). Overexpression of Reelin prevents the manifestation of behavioral phenotypes related to schizophrenia and bipolar disorder. *Neuropsychopharmacology* 36, 2395–2405. doi: 10.1038/npp.2011.153

Teng, B. L., Nonneman, R. J., Agster, K. L., Nikolova, V. D., Davis, T. T., Riddick, N. V., et al. (2013). Prosocial effects of oxytocin in two mouse models of autism spectrum disorders. *Neuropharmacology* 72, 187–196. doi: 10.1016/j.neuropharm.2013.04.038

Teraoka, H., Russell, C., Regan, J., Chandrasekhar, A., Concha, M. L., Yokoyama, R., et al. (2004). Hedgehog and Fgf signaling pathways regulate the development of tphR-expressing serotonergic raphe neurons in zebrafish embryos. *J. Neurobiol.* 60, 275–288. doi: 10.1002/neu.20023

Tremolizzo, L., Carboni, G., Ruzicka, W., Mitchell, C., Sugaya, I., Tueting, P., et al. (2002). An epigenetic mouse model for molecular and behavioral neuropathologies related to schizophrenia vulnerability. *Proc. Natl. Acad. Sci. U.S.A.* 99, 17095–17100. doi: 10.1073/pnas.262658999

Trommsdorff, M., Gotthardt, M., Hiesberger, T., Shelton, J., Stockinger, W., and Nimpf, J. (1999). Reeler/Disabled-like disruption of neuronal migration in knockout mice lacking the VLDL receptor and ApoE receptor 2. *Cell* 97, 689–701. doi: 10.1016/S0092-8674(00)80782-5

Tueting, P., Costa, E., Dwivedi, Y., Guidotti, A., Impagnatiello, F., Manev, R., et al. (1999). The phenotypic characteristics of heterozygous reeler mouse. *Neuro Rep.* 10, 1329–1334. doi: 10.1097/00001756-199904260-00032

Wang, Y., Takai, R., Yoshioka, H., and Shirabe, K. (2006). Characterization and expression of serotonin transporter genes in zebrafish. *Tohoku J. Exp. Med.* 208, 267–274. doi: 10.1620/tjem.208.267

Wang, Z., Hong, Y., Zou, L., Zhong, R., Zhu, B., Shen, N., et al. (2014). Reelin gene variants and risk of autism spectrum disorders: an integrated meta-analysis. *Am. J. Med. Genet. B Neuropsychiatr. Genet.* 165B, 192–200. doi: 10.1002/ajmg.b.32222

Weeber, E. J., Beffert, U., Jones, C., Christian, J. M., Förster, E., Sweatt, J. D., et al. (2002). Reelin and ApoE receptors cooperate to enhance hippocampal synaptic plasticity and learning. *J. Biol. Chem.* 277, 39944–39952. doi: 10.1074/jbc.m205147200

Wen, L., Wei, W., Gu, W., Huang, P., Ren, X., Zhang, Z., et al. (2008). Visualization of monoaminergic neurons and neurotoxicity of MPTP in live transgenic zebrafish. *Dev. Biol.* 314, 84–92. doi: 10.1016/j.ydbio.2007.11.012

Yang, C.-J., Tan, H.-P., and Du, Y.-J. (2014). The developmental disruptions of serotonin signaling may involved in autism during early brain development. *Neuroscience* 267, 1–10. doi: 10.1016/j.neuroscience.2014.02.021

Yuen, R. K. C., Thiruvahindrapuram, B., Merico, D., Walker, S., Tammimies, K., Hoang, N., et al. (2015). Whole-genome sequencing of quartet families with autism spectrum disorder. *Nat. Med.* 21, 185–191. doi: 10.1038/nm.3792

Zhang, H., Liu, X., Zhang, C., Mundo, E., Macciardi, F., Grayson, D. R., et al. (2002). Reelin gene alleles and susceptibility to autism spectrum disorders. *Mol. Psychiatry* 7, 1012–1017. doi: 10.1038/sj.mp.4001124

Zhang, Y., Kong, W., Gao, Y., Liu, X., Gao, K., Xie, H., et al. (2015). Gene mutation analysis in 253 Chinese children with unexplained epilepsy and intellectual/developmental disabilities. *PLoS One* 10:e0141782. doi: 10.1371/journal.pone.0141782

Zimmermann, F. F., Gaspary, K. V., Siebel, A. M., and Bonan, C. D. (2016). Oxytocin reversed MK-801-induced social interaction and aggression deficits in zebrafish. *Behav. Brain Res.* 311, 368–374. doi: 10.1016/j.bbr.2016.05.059

Conflict of Interest Statement: The authors declare that the research was conducted in the absence of any commercial or financial relationships that could be construed as a potential conflict of interest.

frontiers in Behavioral Neuroscience

MINI REVIEW
published: 21 January 2020
doi: 10.3389/fnbeh.2019.00287

Contributions of Interleukin-1 Receptor Signaling in Traumatic Brain Injury

*Jason G. Thome[1], Evan L. Reeder[2], Sean M. Collins[2], Poornima Gopalan[2] and Matthew J. Robson[2]**

[1] Department of Anesthesia and Critical Care, Division of Biological Sciences, College of Medicine, University of Chicago, Chicago, IL, United States, [2] Division of Pharmaceutical Sciences, James L. Winkle College of Pharmacy, University of Cincinnati, Cincinnati, OH, United States

Traumatic brain injury (TBI) in various forms affects millions in the United States annually. There are currently no FDA-approved therapies for acute injury or the chronic comorbidities associated with TBI. Acute phases of TBI are characterized by profound neuroinflammation, a process that stimulates the generation and release of proinflammatory cytokines including interleukin-1α (IL-1α) and IL-1β. Both forms of IL-1 initiate signaling by binding with IL-1 receptor type 1 (IL-1R1), a receptor with a natural, endogenous antagonist dubbed IL-1 receptor antagonist (IL-1Ra). The recombinant form of IL-1Ra has gained FDA approval for inflammatory conditions such as rheumatoid arthritis, prompting interest in repurposing these pharmacotherapies for other inflammatory diseases/injury states including TBI. This review summarizes the currently available preclinical and clinical literature regarding the therapeutic potential of inhibiting IL-1-mediated signaling in the context of TBI. Additionally, we propose specific research areas that would provide a greater understanding of the role of IL-1 signaling in TBI and how these data may be beneficial for the development of IL-1-targeted therapies, ushering in the first FDA-approved pharmacotherapy for acute TBI.

Keywords: traumatic brain injury, interleukin-1, interleukin-1 receptor, cytokine, microglia, astrocyte

OPEN ACCESS

Edited by:
Gregg Stanwood, Florida State University, United States

Reviewed by:
Sandy R. Shultz, Monash University, Australia
Stuart McRae Allan, The University of Manchester, United Kingdom

***Correspondence:**
Matthew J. Robson
Matthew.Robson@uc.edu

Specialty section:
This article was submitted to Pathological Conditions, a section of the journal Frontiers in Behavioral Neuroscience

Received: *15 October 2019*
Accepted: *16 December 2019*
Published: *21 January 2020*

Citation:
Thome JG, Reeder EL, Collins SM, Gopalan P and Robson MJ (2020) Contributions of Interleukin-1 Receptor Signaling in Traumatic Brain Injury. Front. Behav. Neurosci. 13:287. doi: 10.3389/fnbeh.2019.00287

INTRODUCTION

Traumatic brain injury (TBI) is a significant clinical health problem. TBI is currently a leading cause of death and disability within the United States (US) (Centers for Disease Control and Prevention, 2014) translating to an annual economic cost of $76.5 billion (Centers for Disease Control and Prevention, 2019). Compounding this problem is the lack of FDA-approved treatments for acute injury, consequentially driving long-term costs due to the chronic effects of TBI. These chronic effects can include epileptogenesis, cognitive deficits, and neuropsychiatric conditions (McIntosh et al., 1996; Bombardier et al., 2010; Hart et al., 2011, 2016).

Depression is the most frequent neuropsychiatric disorder post-TBI, its incidence unrelated to degree of injury severity (Fann et al., 2013). Depression is linked to the high suicide rates following TBI, three to four times that of the general population (Fleminger, 2008; Alway et al., 2016; Ouellet et al., 2018). Cognitive deficits are inherent in TBI, including deficits in attention, working memory, and processing speed, among other issues (Cicerone, 1996; McAllister et al., 1999; McAllister et al., 2001; Chan, 2002). Post-traumatic epilepsy (PTE) is common following TBI

(Fleminger, 2008), with an incidence rate between 10 and 35%, an effect positively correlated with severity of injury, and negatively correlated with age at insult (Appleton and Demellweek, 2002; Frey, 2003; Ates et al., 2006; Statler et al., 2009; Arndt et al., 2013). Management of PTE has proven difficult due to a lack of therapies for prevention/occurrence of PTE following neurotrauma (Barlow et al., 2000). It is possible that targeting acute molecular processes of TBI may prove an effective strategy for minimizing the emergence of depression, cognitive decline, and PTE post-TBI, thereby circumventing the lack of currently available treatments for these conditions.

The acute phases of TBI are characterized by profound neuroinflammation, increased glial cell reactivity, cytokine generation/release, and neural degeneration. Inflammatory cytokines, including interleukin-1α (IL-1α) and IL-1β, are the primary orchestrators of neuroinflammatory cascades, and many utilize receptors in a cell heterologous and/or autonomous fashion. The IL-1 receptor type 1 (IL-1R1) is the primary functional target of three endogenous ligands, IL-1α, IL-1β, and IL-1 receptor antagonist (IL-1Ra) (Symons et al., 1995). Upon activation, IL1-R1 recruits IL-1 receptor accessory chain protein (IL-1RAcP), also known as IL-1R3, forming a heterotrimeric complex with IL-1R1 and the bound ligand (Casadio et al., 2001). Toll/IL-1 receptor (TIR) domains within the cytoplasm form a complex with the myeloid differentiation primary response gene 88 (MYD88) adapter protein, subsequently recruiting IL-1 receptor-associated kinase 4 (IRAK4) (Burns et al., 1998; Xu et al., 2000; De Nardo et al., 2018). Once recruited, IRAK4 trans-autophosphorylates, recruiting and phosphorylating IRAK1, and forming a complex with tumor necrosis factor receptor-associated factor 6 (TRAF6) (Ye et al., 2002; Burns et al., 2003; Ferrao et al., 2014; Vollmer et al., 2017). The IRAK1/TRAF6 complex initiates phosphorylation of membrane-bound transforming growth factor beta-activated kinase 1 (TAK-1), leading to downstream activation of the transcription factors nuclear factor-kappa B (NF-κB) and activator protein 1 (AP-1) (Lee et al., 2002; Shim et al., 2005; **Figure 1**). Together, these transcription factors promote the production of a myriad of proinflammatory cytokines involved in neuroinflammation, including IL-6 and IL-1β (Collart et al., 1990; Sung et al., 1992; Serkkola and Hurme, 1993; Jeon et al., 2000; Roman et al., 2000).

The regulatory role of IL-1R1 in innate immune system activation renders it an ideal candidate to block downstream effects of the IL-1 pathway. Beneficial effects in inflammatory diseases, such as rheumatoid arthritis, have led to FDA approval of the recombinant form of IL-1Ra, Anakinra. The availability of this treatment has fueled interest in IL-1R1-mediated signaling for various disease states/disorders with an inflammatory component. IL-1Ra administration in animal models of cerebral ischemia, for example, has been demonstrated to provide neuroprotective effects (Banwell et al., 2009; Becker et al., 2014; Girard et al., 2014; Clausen et al., 2016; Pradillo et al., 2017), with Anakinra advancing to clinical trials for this indication (Emsley et al., 2005; Galea et al., 2018; Smith et al., 2018). Further, recent studies have aimed to delineate the role of IL-1R1 signaling within the central nervous system (CNS) following neurotrauma using pharmacologic and genetic means. Recent studies, emerging clinical trials, and potential future directions specific to IL-1R1 signaling in the context of TBI are the primary focus of this review.

IL-1R1 LOCALIZATION IN THE CNS

While expression of IL-1R1 is ubiquitous throughout the brain, there are regions of dense expression that provide insight to abnormal behaviors believed to be associated with IL-1R1-mediated signaling. Autoradiography labeling of IL-1α and IL-1β in the mouse brain resulted in concentrated labeling of the granule cell layer of the hippocampus, choroid plexus, and pituitary gland (Takao et al., 1990; Ban et al., 1991). These studies have been corroborated via regional *in situ* hybridization of IL-1R1 mRNA within the dentate region of the hippocampus, choroid plexus, and pituitary gland, as well as in the raphe nuclei (Cunningham et al., 1991, 1992).

Functional IL-1R1 expression has been demonstrated in astrocytes, microglia, neurons, and endothelial cells (Liu et al., 2019). IL-1R1 mRNA is expressed at high levels in cultured astrocytes, and radiolabeled IL-1α has been demonstrated to bind to primary astrocyte cultures (Ban et al., 1993; Tomozawa et al., 1995; Pinteaux et al., 2002), implying expression of functional IL-1R1. Further evidence of functional IL-1R1 expression in astrocytes is the release of proinflammatory factors such as IL-6 post-stimulation (Gottschall et al., 1994). IL-1R1 expression is present within microglial populations; however, expression levels are substantially lower compared to astrocytes (Pinteaux et al., 2002). IL-1R1 appears to be expressed in microglial populations *in vivo*, as confocal microscopy analyses have demonstrated colocalization of IL-1R1 with OX-42-labeled microglia in the spinal cord (Wang et al., 2006). Binding sites for IL-1α, presumed to be IL-1R1, have also been localized to hippocampal neurons (Takao et al., 1990; Ban et al., 1991). Finally, IL-1R1 is localized to endothelial cells within the brain with activation leading to hyperthermia and cytokine signaling (Cao et al., 2001; Liu et al., 2015). The diverse localization of IL-1R1 expression within the CNS suggests a myriad of roles in the regulation of the innate immune system following neurotrauma.

PRECLINICAL TARGETING OF IL-1R1

IL-1Ra

Much of the preclinical work aimed at delineating the roles of IL-1R1-mediated signaling in neurotrauma has utilized recombinant human IL-1Ra. IL-1Ra competitively binds to IL-1R1, thereby impeding the ability of IL-1β and IL-1α to bind to and signal through the receptor. These pharmacologic studies are significant due to their potential to repurpose an already FDA-approved therapy (Anakinra or Kineret). In a rat fluid percussion injury (FPI) model, IL-1Ra administration was shown to rescue cognitive impairment as assessed in the Morris water maze (MWM) (Sanderson et al., 1999).

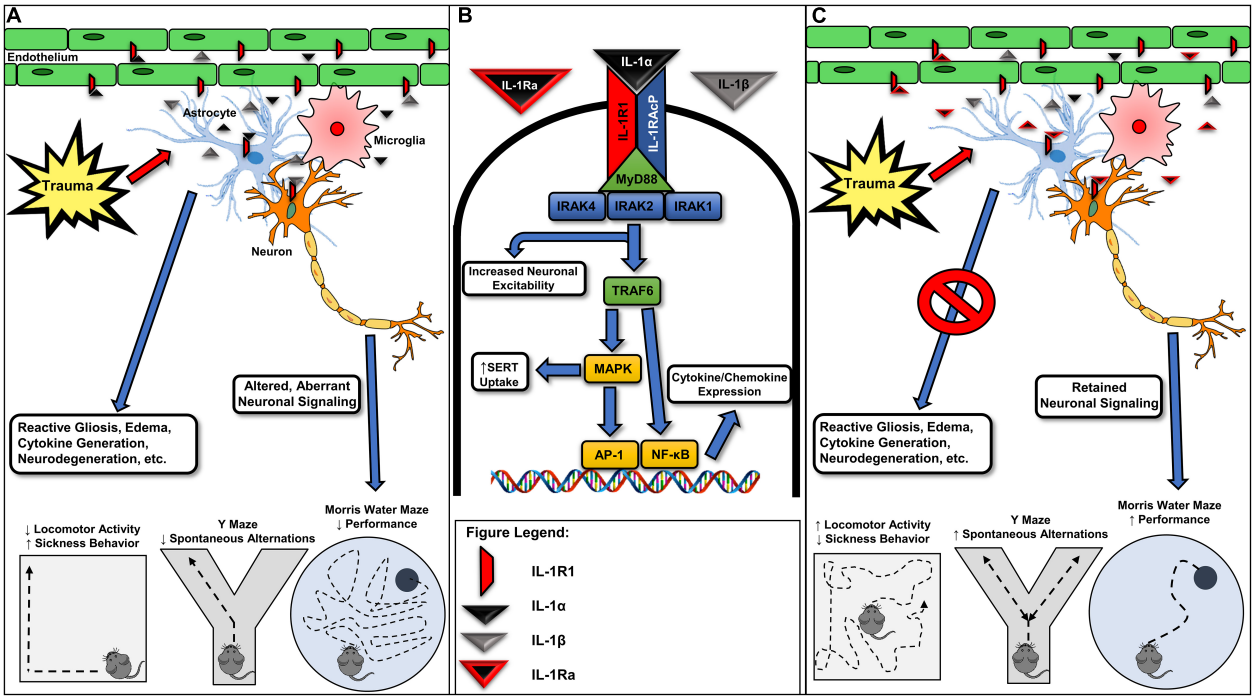

FIGURE 1 | Various forms of neurotrauma induce interleukin-1 receptor-mediated signaling in the CNS. **(A)** Interleukin-1 receptor (IL-1R1) activation occurring from IL-1α or IL-1β binding in various glial cells, endothelial cells, and neuronal populations is associated with reactive gliosis, the further generation and release of inflammatory cytokines/chemokines, neurodegeneration, and ultimately, alterations in behavior. **(B)** Acute molecular signaling associated with IL-1R1 activation in various cell types of the CNS. Binding of IL-1α and/or IL-1β to IL-1R1 acts to increase gene transcription of several inflammatory mediators including IL-6 and a feed-forward loop increasing the expression of IL-1β through an activation of NF-κB and AP-1. Several proteins, including IL-1 receptor associated kinase-1 (IRAK1) and IL-1 receptor associated kinase 4 (IRAK4), are required for IL-1R1-mediated signaling and may provide further drug targets for pharmacotherapy development. IL-1-mediated activation of IL-1R1 is known to rapidly increase neuronal excitability and serotonin transporter (SERT)-mediated serotonin clearance, effects contributing to seizure susceptibility and despair-like behaviors, respectively. **(C)** Recombinant IL-1Ra (Anakinra) administration has been shown in preclinical models for neurotrauma to mitigate trauma-elicited astrogliosis, edema, and cytokine generation. Further, blockade of trauma-associated IL-1R1-mediated signaling provides cognitive-sparing effects in the Y Maze and Morris water maze behavioral assays. Given promising preclinical data and the previous FDA approval of recombinant IL-1Ra, targeting IL-1R1-mediated signaling may represent a viable avenue for the pursuit of the first FDA-approved pharmacotherapy for acute TBI. IRAK2, interleukin-1 receptor associated kinase-1; IL-1RAcP, interleukin-1 receptor accessory protein; TRAF6, tumor necrosis factor receptor associated factor 6; MAPK, mitogen-activated protein kinase; AP-1, activator protein-1; NF-κB, nuclear factor kappa-light-chain-enhancer of activated B cells; MyD88, myeloid differentiation primary response protein.

Acute IL-1Ra administration reduces pentylenetetrazol (PTZ)-evoked seizure hypersensitivity in a pediatric model for TBI, providing evidence that IL-1R1 blockade may be a promising avenue for preventing PTE (Semple et al., 2017; Webster et al., 2017). Similarly, the effects of IL-1Ra overexpression on the effects of TBI have been explored. Transgenic mice overexpressing IL-1Ra demonstrated significantly higher neurological recovery; evaluated by neurological severity score (NSS), a task which assesses performance on motor and behavioral tasks, in a closed head injury (CHI) model of TBI (Tehranian et al., 2002).

Polytrauma is common in the context of TBI and leads to profound peripheral inflammatory responses that may exacerbate neuroinflammation. Clinically, patients with polytrauma exhibit increased mortality rates compared to TBI alone: 21.8–11.1%, respectively (Wilson and Tyburski, 2001; McDonald et al., 2016; Sun et al., 2018). Controlled cortical impact (CCI) in combination with tibial injury increases brain levels of IL-1β in mice receiving both injuries compared to those receiving only TBI (Yang et al., 2016). Additionally, FPI in combination with tibial injury corroborates these results, acutely increasing brain levels of IL-1β in mice receiving polytrauma compared to TBI-only controls (Shultz et al., 2015), an effect that may arise from increased peripheral IL-1 expression and transport across the blood–brain barrier (Banks et al., 1993; Plotkin et al., 1996; Sadowska et al., 2015). Polytrauma-induced increases in IL-1β are time dependent however as after 48 h the levels of IL-1β decrease compared to TBI-only controls (Maegele et al., 2007). Sustained inhibition of polytrauma-elicited increases in IL-1 signaling using IL-1Ra reduces cortical neutrophil infiltration, cerebral edema, and brain atrophy following a CHI weight-drop model with concomitant tibial fracture (Sun et al., 2017). It should be noted, however, that IL-1R1 administration did not mitigate behavioral deficits in the MWM, Crawley three-chamber sociability task, open field, or rotarod test (Sun et al., 2017).

The caveat of studies utilizing IL-1Ra lies in the poor ability of IL-1Ra to cross the BBB and the high doses needed to see an effect. Previous preclinical studies have found no

changes with low dose, 190 mg/kg IL-1Ra, but did see effects when subjects are administered a high dose of 1900 mg/kg, administered over 7 days (Sanderson et al., 1999). The authors acknowledged that giving nearly 2 g/kg of IL-1Ra is likely to supply large colloid protein load, potentially influencing brain water volumes. Thus, shear amounts of protein could be eliciting an effect independently of IL-1R1 blockade. Pharmacokinetic assessments of IL-1Ra have indicated that brain concentrations are approximately 1% of the plasma concentration at any given time, with a maximum of 2% (Greenhalgh et al., 2010).

If the IL-1Ra therapeutic intervention is pursued, one particular area of importance will be the ability for the molecule to cross the BBB. In fact, some studies have already experimented with modification of the IL-1Ra molecule to enhance its penetration of the BBB. Researchers conducting these studies fused the cell penetrating peptide PEP-1 with IL-1Ra in order to create the novel IL-1Ra–PEP fusion protein. The results of these studies found that the novel fusion protein improved delivery of IL-1Ra due to the molecule's increased permeability to the BBB compared to unmodified IL-1Ra under the same conditions (Zhang et al., 2017, 2018). Furthermore, modification of the protein did not alter protein function, as evidenced by a significant reduction of inflammatory markers after administration of the fusion protein (Zhang et al., 2017), as well as alleviation of BBB disruption caused by initial injury (Zhang et al., 2018). While these studies focused on treating injuries caused by ischemia–reperfusion, TBIs share many of the negative effects ameliorated by the administration of IL-1Ra–PEP, which suggests that IL-1Ra–PEP would also prove useful for treating the negative effects caused by TBIs. Additionally, since increased permeability of IL-1Ra–PEP across the BBB was shown to occur whether or not the BBB was disrupted, modification of IL-1Ra would address any issues of decreased efficacy in the unmodified therapeutic due to a decrease in permeability after amelioration of the disrupted BBB.

Genetic KO Models

The role of IL-1R1 has been investigated utilizing genetic knockout models of the receptor. Early experiments involved mice with a global IL-1R1 knockout (Chung et al., 2018). Knockout mice showed increased performance on some behavioral tests in a CHI and a CCI model compared to their WT counterparts. In a CHI model, constitutive, global elimination of IL-1R1 resulted in a normalization of TBI-induced memory deficits in hidden and visible MWM platform trials, resulting in performance comparable to that of the WT sham mice (Chung et al., 2018). In a Y-Maze study, WT CHI mice had a decrease in alternating decisions compared to their respective sham counterparts, whereas IL-1R1 KO mice performed similarly to WT sham subjects (Chung et al., 2018). No overt effects of IL-1R1 elimination alone were found in any of the behavioral paradigms (Chung et al., 2018), providing evidence that inflammatory signaling mediated by IL-1R1 is involved in spatial and working memory deficits following CHI. It should be noted that due to the constitutive nature of IL-1R1 elimination in these subjects the temporal requirements for IL-1R1-mediated signaling in driving these effects are currently unknown.

Subsequent studies have focused on the role of IL-1R1 in various cell types by utilizing a genetic restoration strategy (IL-1R1 Restore mice) (Liu et al., 2015), which is able to selectively restore the expression of IL-1R1 in a cell-specific manner. Global knockout of IL-1R1 and selective restoration to microglia revealed mitigation of IL-1-driven microglial activation following intracerebroventricular (ICV) IL-1β injections (Zhu et al., 2019). Selective deletion of IL-1R1 in microglia had no effect on this process, showing an IL-1-driven microglial activation independent of microglial IL-1R1 (Zhu et al., 2019). In mice expressing IL-1R1 only in endothelial cells, mRNA expression of microglial cytokines, including IL-1β, is increased compared to WT controls (Liu et al., 2019). In a mouse model of cerebral ischemia, pan-neuronal, and brain endothelial-specific IL-1R1 deletion showed reduced infarct volume, with endothelial elimination attenuating BBB permeability and improving neurological function (Wong et al., 2019). Elimination of IL-1R1 in cholinergic neurons also improved functional outcomes and reduced infarct size, providing evidence that specific neuronal populations may be required for IL-1R1-mediated effects within the CNS (Wong et al., 2019). Another notable feature of IL-1-mediated signaling is the ability to drive sickness behaviors. Endothelial IL-1R1 expression has been found to be both necessary and sufficient to induce IL-1-driven sickness behavior in mice (Liu et al., 2019). Combined, these data have begun elucidating the role of IL-1R1 in various cell types of the CNS; however, further experiments are needed utilizing these genetic models in conjunction with models of TBI.

IL-1β and IL-1α Neutralization

Another strategy commonly employed when targeting immunologic targets is the direct inhibition of cytokine and/or chemokines through the use of antibodies aimed at these respective immunologic signaling components. In the context of neurologic disorders, it is possible that this strategy may exert similar effects as IL-1Ra administration while circumventing the issues surrounding IL-1Ra and minimal BBB permeability. With regard to TBI specifically, preclinical attempts to neutralize the actions of IL-1β using anti-IL-1β antibodies in order to mitigate IL-1R1 binding have been made. One TBI study using the CCI model used continuous ICV-delivered anti-IL-1β via osmotic pump at a rate of 0.375 ng/h to its experimental group; treatment began at 5 min post-injury and continued for up to 14 days thereafter (Clausen et al., 2009). When measured at 1–7 days post-injury, IL-1β neutralization was found to attenuate the CCI-induced cortical and hippocampal microglial activation, as well as cortical infiltration of neutrophils and activated T cells (Clausen et al., 2009). Moreover, lesion volume and hemispheric tissue loss evaluated 18 days post-injury were further reduced by IL-1β neutralization (Clausen et al., 2009). MWM evaluation also demonstrated that IL-1β neutralization reduced the significant deficits in neurological cognitive function induced by CCI, though evaluation by the rotarod and cylinder tests showed no significant reduction in induced neurological motor deficits (Clausen et al., 2009).

While the previous study explores the effects of long-term ICV delivery of anti-IL-1β on the effects of TBI, a follow-up

study conducted by the same research group delivered a single 4 μg dose of anti-IL-1β intraperitoneally, first at 30 min post-injury, and again at 7 days post-injury (Clausen et al., 2011). Although measurements at 48 h post-CCI found that anti-IL-1β attenuated the TBI-induced hemispheric edema, it did not improve post-injury memory deficits evaluated by the MWM (Clausen et al., 2011). However, up to 20 days post-injury, anti-IL-1β was found to improve visuospatial learning as evaluated by the MWM, as well as to reduce hemispheric tissue loss and to attenuate TBI-induced microglial activation (Clausen et al., 2011). Taken together, these results suggest a temporal dependence for inhibition of IL-1 signaling to attenuate certain memory-associated deficits. With regards to motor function, this study corroborates the results of the group's previous study, finding that anti-IL-1β had no significant effect on neurological motor deficits as evaluated by the rotarod and cylinder tests (Clausen et al., 2011).

The particular method used in these studies to explore the effects of IL-1 signaling on TBI-induced deficits, nonetheless, has its limits. First, the use of anti-IL-1β antibody relies on increased permeability of the BBB for the antibody to reach the brain and exert its therapeutic effects. If the body's initial response to the antibody is attenuation of the disrupted BBB while neuroinflammation persists, then further administration of the antibody will fail to exert the desired effect on brain inflammation. Additionally, the anti-IL-1β antibody targets specifically IL-1β; however, freely available IL-1α can still signal through IL-1R1 and exert proinflammatory effects (Brough and Denes, 2015). This unaccounted signaling could confound the results of studies exploring the relationship among IL-1 proinflammatory signaling, secondary physiological effects, and cognitive/behavioral deficits resulting from TBI.

CLINICAL STUDIES

IL-1Ra

Due to the promising results in many preclinical studies showing the potential benefits of IL-1Ra treatment post-TBI, clinical trials aimed at determining a potential benefit in heterogeneous clinical populations have been initiated (Helmy et al., 2014, 2016). To date, one clinical trial has been conducted aiming to delineate whether IL-1Ra administration may provide beneficial effects in a clinical neurotrauma cohort. Briefly, 20 patients with severe TBI were recruited within 24 h post-injury and given either IL-1Ra or placebo. Shortly after treatment, the IL-1Ra treatment group showed large increases in IL-1Ra in the brain and in blood plasma compared to the placebo group (Helmy et al., 2016). These results indicate that there is some ability for IL-1Ra to cross the BBB; however, even the infiltration of large doses may be limited.

Initial clinical trials have provided evidence that IL-1Ra treatment results in an increase of pro-inflammatory M1-type macrophages, characterized by increased GM-CSF and IL-1β cytokine levels, whereas levels of IL-4, IL-10, and MDC – the cytokines associated with anti-inflammatory M2-type macrophages – are reduced (Helmy et al., 2016). These results counter previous studies showing decreases in IL-1β levels in treated groups (Sun et al., 2017). The classical view is that M1-differentiated cells induce pro-inflammatory responses and M2 macrophages antagonize pro-inflammatory responses (Martinez and Gordon, 2014); however, this view has recently come under increased scrutiny as microglia and/or macrophages exhibit a wide range of phenotypes that may be induced through a variety of insults.

It is important to note that all data involved with this particular clinical trial are from within the first 48 h of treatment, thus the long-term effects of IL-1Ra treatment post-injury must still be studied. Current trials in stage II are reportedly investigating dose effects, and while initial studies have validated the safety profile of IL-1Ra administration post-injury, a great deal of work remains in order to fully assess IL-1Ra efficacy as a clinical therapeutic for TBI.

DISCUSSION

Currently, it is clear that targeting components of IL-1 signaling post-injury results in favorable outcomes in preclinical rodent models. Initial clinical studies have also shown currently available therapies to be safe for use in TBI populations, but there is currently a lack of data regarding their efficacy. We posit here that further work in the preclinical and clinical arenas is warranted, as each will provide crucial information required to further the potential use of pharmacotherapies targeting IL-1-mediated signaling. We also believe that recently developed molecular tools aimed at delineating the roles of IL-1 signaling, such as IL-1R1$^{loxP/loxP}$ mice and IL-1R1 Restore mice, will prove useful for determining the specific cell types and timelines critical for targeting IL-1 signaling post-TBI, similar to efforts in preclinical models for ischemia (Liu et al., 2015; Robson et al., 2016; Wong et al., 2019). Although IL-1-targeted therapies have been shown to be safe in clinical populations post-injury, the temporal requirements for targeting IL-1 signaling are important, and the optimization of timing post-injury should be analyzed thoroughly for studies moving forward. Concerted efforts between clinical and preclinical researchers will certainly aid in the further development of IL-1-targeted therapies, and as evidenced by studies discussed above, they may result in the first FDA-approved pharmacotherapies for acute TBI.

AUTHOR CONTRIBUTIONS

JT and ER contributed by selecting and summarizing the relevant studies. JT, ER, SC, PG, and MR wrote the original sections of the current manuscript. ER and PG created the figure included in the review article.

FUNDING

Portions of this work were supported by a Brain and Behavior Research Foundation NARSAD YI Award (MR), a PhRMA Foundation Research Starter Grant (MR), and the University of Cincinnati.

REFERENCES

Alway, Y., Gould, K. R., Johnston, L., McKenzie, D., and Ponsford, J. (2016). A prospective examination of Axis I psychiatric disorders in the first 5 years following moderate to severe traumatic brain injury. *Psychol. Med.* 46, 1331–1341. doi: 10.1017/S0033291715002986

Appleton, R. E., and Demellweek, C. (2002). Post-traumatic epilepsy in children requiring inpatient rehabilitation following head injury. *J. Neurol. Neurosurg. Psychiatry* 72, 669–672. doi: 10.1136/jnnp.72.5.669

Arndt, D. H., Lerner, J. T., Matsumoto, J. H., Madikians, A., Yudovin, S., Valino, H., et al. (2013). Subclinical early posttraumatic seizures detected by continuous EEG monitoring in a consecutive pediatric cohort. *Epilepsia* 54, 1780–1788. doi: 10.1111/epi.12369

Ates, O., Ondul, S., Onal, C., Buyukkiraz, M., Somay, H., Cayli, S. R., et al. (2006). Post-traumatic early epilepsy in pediatric age group with emphasis on influential factors. *Childs Nerv. Syst.* 22, 279–284.

Ban, E., Milon, G., Prudhomme, N., Fillion, G., and Haour, F. (1991). Receptors for interleukin-1 (alpha and beta) in mouse brain: mapping and neuronal localization in hippocampus. *Neuroscience* 43, 21–30. doi: 10.1016/0306-4522(91)90412-h

Ban, E. M., Sarlieve, L. L., and Haour, F. G. (1993). Interleukin-1 binding sites on astrocytes. *Neuroscience* 52, 725–733. doi: 10.1016/0306-4522(93)90421-b

Banks, W. A., Kastin, A. J., and Gutierrez, E. G. (1993). Interleukin-1 alpha in blood has direct access to cortical brain cells. *Neurosci. Lett.* 163, 41–44. doi: 10.1016/0304-3940(93)90224-9

Banwell, V., Sena, E. S., and Macleod, M. R. (2009). Systematic review and stratified meta-analysis of the efficacy of interleukin-1 receptor antagonist in animal models of stroke. *J. Stroke Cerebrovasc. Dis.* 18, 269–276. doi: 10.1016/j.jstrokecerebrovasdis.2008.11.009

Barlow, K. M., Spowart, J. J., and Minns, R. A. (2000). Early posttraumatic seizures in non-accidental head injury: relation to outcome. *Dev. Med. Child. Neurol.* 42, 591–594. doi: 10.1111/j.1469-8749.2000.tb00363.x

Becker, K. J., Dankwa, D., Lee, R., Schulze, J., Zierath, D., Tanzi, P., et al. (2014). Stroke, IL-1ra, IL1RN, infection and outcome. *Neurocrit. Care* 21, 140–146. doi: 10.1007/s12028-013-9899-x

Bombardier, C. H., Fann, J. R., Temkin, N. R., Esselman, P. C., Barber, J., and Dikmen, S. S. (2010). Rates of major depressive disorder and clinical outcomes following traumatic brain injury. *JAMA* 303, 1938–1945. doi: 10.1001/jama.2010.599

Brough, D., and Denes, A. (2015). Interleukin-1alpha and brain inflammation. *IUBMB Life* 67, 323–330. doi: 10.1002/iub.1377

Burns, K., Janssens, S., Brissoni, B., Olivos, N., Beyaert, R., and Tschopp, J. (2003). Inhibition of interleukin 1 receptor/Toll-like receptor signaling through the alternatively spliced, short form of MyD88 is due to its failure to recruit IRAK-4. *J. Exp. Med.* 197, 263–268. doi: 10.1084/jem.20021790

Burns, K., Martinon, F., Esslinger, C., Pahl, H., Schneider, P., Bodmer, J. L., et al. (1998). MyD88, an adapter protein involved in interleukin-1 signaling. *J. Biol. Chem.* 273, 12203–12209. doi: 10.1074/jbc.273.20.12203

Cao, C., Matsumura, K., Shirakawa, N., Maeda, M., Jikihara, I., Kobayashi, S., et al. (2001). Pyrogenic cytokines injected into the rat cerebral ventricle induce cyclooxygenase-2 in brain endothelial cells and also upregulate their receptors. *Eur. J. Neurosci.* 13, 1781–1790. doi: 10.1046/j.0953-816x.2001.01551.x

Casadio, R., Frigimelica, E., Bossu, P., Neumann, D., Martin, M. U., Tagliabue, A., et al. (2001). Model of interaction of the IL-1 receptor accessory protein IL-1RAcP with the IL-1beta/IL-1R(I) complex. *FEBS Lett.* 499, 65–68. doi: 10.1016/s0014-5793(01)02515-7

Centers for Disease Control and Prevention, (2014). *TBI Data and Statistics | Concussion | Traumatic Brain Injury | CDC Injury Center*. Atlanta, GA: Centers for Disease Control and Prevention.

Centers for Disease Control and Prevention, (2019). *Surveillance Report of Traumatic Brain Injury-related Emergency Department Visits, Hospitalizations, and Deaths—United States,2014*. Atlanta, GA: Centers for Disease Control and Prevention.

Chan, R. C. (2002). Attentional deficits in patients with persisting postconcussive complaints: a general deficit or specific component deficit? *J. Clin. Exp. Neuropsychol.* 24, 1081–1093. doi: 10.1076/jcen.24.8.1081.8371

Chung, J. Y., Krapp, N., Wu, L., Lule, S., McAllister, L. M., Edmiston, W. J. III, et al. (2018). Interleukin-1 receptor 1 deletion in focal and diffuse experimental traumatic brain injury in mice. *J. Neurotrauma* 36, 370–379. doi: 10.1089/neu.2018.5659

Cicerone, K. D. (1996). Attention deficits and dual task demands after mild traumatic brain injury. *Brain Inj.* 10, 79–89.

Clausen, B. H., Lambertsen, K. L., Dagnaes-Hansen, F., Babcock, A. A., von Linstow, C. U., Meldgaard, M., et al. (2016). Cell therapy centered on IL-1Ra is neuroprotective in experimental stroke. *Acta Neuropathol.* 131, 775–791. doi: 10.1007/s00401-016-1541-5

Clausen, F., Hanell, A., Bjork, M., Hillered, L., Mir, A. K., Gram, H., et al. (2009). Neutralization of interleukin-1beta modifies the inflammatory response and improves histological and cognitive outcome following traumatic brain injury in mice. *Eur. J. Neurosci.* 30, 385–396. doi: 10.1111/j.1460-9568.2009.06820.x

Clausen, F., Hanell, A., Israelsson, C., Hedin, J., Ebendal, T., Mir, A. K., et al. (2011). Neutralization of interleukin-1beta reduces cerebral edema and tissue loss and improves late cognitive outcome following traumatic brain injury in mice. *Eur. J. Neurosci.* 34, 110–123. doi: 10.1111/j.1460-9568.2011.07723.x

Collart, M. A., Baeuerle, P., and Vassalli, P. (1990). Regulation of tumor necrosis factor alpha transcription in macrophages: involvement of four kappa B-like motifs and of constitutive and inducible forms of NF-kappa B. *Mol. Cell. Biol.* 10, 1498–1506. doi: 10.1128/mcb.10.4.1498

Cunningham, E. T. Jr., Wada, E., Carter, D. B., Tracey, D. E., Battey, J. F., and De Souza, E. B. (1991). Localization of interleukin-1 receptor messenger RNA in murine hippocampus. *Endocrinology* 128, 2666–2668. doi: 10.1210/endo-128-5-2666

Cunningham, E. T. Jr., Wada, E., Carter, D. B., Tracey, D. E., Battey, J. F., and De Souza, E. B. (1992). In situ histochemical localization of type I interleukin-1 receptor messenger RNA in the central nervous system, pituitary, and adrenal gland of the mouse. *J. Neurosci.* 12, 1101–1114. doi: 10.1523/jneurosci.12-03-01101.1992

De Nardo, D., Balka, K. R., Cardona Gloria, Y., Rao, V. R., Latz, E., and Masters, S. L. (2018). Interleukin-1 receptor-associated kinase 4 (IRAK4) plays a dual role in myddosome formation and Toll-like receptor signaling. *J. Biol. Chem.* 293, 15195–15207. doi: 10.1074/jbc.RA118.003314

Emsley, H. C., Smith, C. J., Georgiou, R. F., Vail, A., Hopkins, S. J., Rothwell, N. J., et al. (2005). A randomised phase II study of interleukin-1 receptor antagonist in acute stroke patients. *J. Neurol. Neurosurg. Psychiatry* 76, 1366–1372. doi: 10.1136/jnnp.2004.054882

Fann, J., Hart, T., and University, C. (2013). of Washington model systems knowledge translation, depression after traumatic brain injury. *Arch. Phys. Med. Rehabil.* 94, 801–802.

Ferrao, R., Zhou, H., Shan, Y., Liu, Q., Li, Q., Shaw, D. E., et al. (2014). IRAK4 dimerization and trans-autophosphorylation are induced by Myddosome assembly. *Mol. cell* 55, 891–903. doi: 10.1016/j.molcel.2014.08.006

Fleminger, S. (2008). Long-term psychiatric disorders after traumatic brain injury. *Eur. J. Anaesthesiol. Suppl.* 42, 123–130. doi: 10.1017/S0265021507003250

Frey, L. C. (2003). Epidemiology of posttraumatic epilepsy: a critical review. *Epilepsia* 44(Suppl 10), 11–17. doi: 10.1046/j.1528-1157.44.s10.4.x

Galea, J., Ogungbenro, K., Hulme, S., Patel, H., Scarth, S., Hoadley, M., et al. (2018). Reduction of inflammation after administration of interleukin-1 receptor antagonist following aneurysmal subarachnoid hemorrhage: results of the Subcutaneous Interleukin-1Ra in SAH (SCIL-SAH) study. *J. Neurosurg.* 128, 515–523. doi: 10.3171/2016.9.JNS16615

Girard, S., Murray, K. N., Rothwell, N. J., Metz, G. A., and Allan, S. M. (2014). Long-term functional recovery and compensation after cerebral ischemia in rats. *Behav. Brain Res.* 270, 18–28. doi: 10.1016/j.bbr.2014.05.008

Gottschall, P. E., Tatsuno, I., and Arimura, A. (1994). Regulation of interleukin-6 (IL-6) secretion in primary cultured rat astrocytes: synergism of interleukin-1 (IL-1) and pituitary adenylate cyclase activating polypeptide (PACAP). *Brain Res.* 637, 197–203. doi: 10.1016/0006-8993(94)91233-5

Greenhalgh, A. D., Galea, J., Dénes, A., Tyrrell, P. J., and Rothwell, N. J. (2010). Rapid brain penetration of interleukin-1 receptor antagonist in rat cerebral ischaemia: pharmacokinetics, distribution, protection. *Br. J. Pharmacol.* 160, 153–159. doi: 10.1111/j.1476-5381.2010.00684.x

Hart, T., Brenner, L., Clark, A. N., Bogner, J. A., Novack, T. A., Chervoneva, I., et al. (2011). Major and minor depression after traumatic brain injury. *Arch. Phys. Med. Rehabil.* 92, 1211–1219. doi: 10.1016/j.apmr.2011.03.005

Hart, T., Fann, J. R., Chervoneva, I., Juengst, S. B., Rosenthal, J. A., Krellman, J. W., et al. (2016). Prevalence, risk factors, and correlates of anxiety at 1 year

after moderate to severe traumatic brain injury. *Arch. Phys. Med. Rehabil.* 97, 701–707. doi: 10.1016/j.apmr.2015.08.436

Helmy, A., Guilfoyle, M. R., Carpenter, K. L., Pickard, J. D., Menon, D. K., and Hutchinson, P. J. (2014). Recombinant human interleukin-1 receptor antagonist in severe traumatic brain injury: a phase ii randomized control trial. *J. Cereb. Blood Flow Metab.* 34, 845–851. doi: 10.1038/jcbfm.2014.23

Helmy, A., Guilfoyle, M. R., Carpenter, K. L. H., Pickard, J. D., Menon, D. K., and Hutchinson, P. J. (2016). Recombinant human interleukin-1 receptor antagonist promotes M1 microglia biased cytokines and chemokines following human traumatic brain injury. *J. Cereb. Blood Flow Metab.* 36, 1434–1448. doi: 10.1177/0271678X15620204

Jeon, Y. J., Han, S. H., Lee, Y. W., Lee, M., Yang, K. H., and Kim, H. M. (2000). Dexamethasone inhibits IL-1 beta gene expression in LPS-stimulated RAW 264.7 cells by blocking NF-kappa B/Rel and AP-1 activation. *Immunopharmacology* 48, 173–183. doi: 10.1016/s0162-3109(00)00199-5

Lee, S. W., Han, S. I., Kim, H. H., and Lee, Z. H. (2002). TAK1-dependent activation of AP-1 and c-Jun N-terminal kinase by receptor activator of NF-kappaB. *J. Biochem. Mol. Biol.* 35, 371–376. doi: 10.5483/bmbrep.2002.35.4.371

Liu, X., Nemeth, D. P., McKim, D. B., Zhu, L., DiSabato, D. J., Berdysz, O., et al. (2019). Cell-type-specific interleukin 1 receptor 1 signaling in the brain regulates distinct neuroimmune activities. *Immunity* 50, 764–766. doi: 10.1016/j.immuni.2019.02.012

Liu, X., Yamashita, T., Chen, Q., Belevych, N., McKim, D. B., Tarr, A. J., et al. (2015). Interleukin 1 type 1 receptor restore: a genetic mouse model for studying interleukin 1 receptor-mediated effects in specific cell types. *J. Neurosci.* 35, 2860–2870. doi: 10.1523/JNEUROSCI.3199-14.2015

Maegele, M., Sauerland, S., Bouillon, B., Schafer, U., Trubel, H., Riess, P., et al. (2007). Differential immunoresponses following experimental traumatic brain injury, bone fracture and "two-hit"-combined neurotrauma. *Inflamm. Res.* 56, 318–323. doi: 10.1007/s00011-007-6141-3

Martinez, F. O., and Gordon, S. (2014). The M1 and M2 paradigm of macrophage activation: time for reassessment. *F1000prime Rep.* 6:13. doi: 10.12703/P6-13

McAllister, T. W., Saykin, A. J., Flashman, L. A., Sparling, M. B., Johnson, S. C., Guerin, S. J., et al. (1999). Brain activation during working memory 1 month after mild traumatic brain injury: a functional MRI study. *Neurology* 53, 1300–1308.

McAllister, T. W., Sparling, M. B., Flashman, L. A., Guerin, S. J., Mamourian, A. C., and Saykin, A. J. (2001). Differential working memory load effects after mild traumatic brain injury. *Neuroimage* 14, 1004–1012. doi: 10.1006/nimg.2001.0899

McDonald, S. J., Sun, M., Agoston, D. V., and Shultz, S. R. (2016). The effect of concomitant peripheral injury on traumatic brain injury pathobiology and outcome. *J. Neuroinflam.* 13:90. doi: 10.1186/s12974-016-0555-1

McIntosh, T. K., Smith, D. H., Meaney, D. F., Kotapka, M. J., Gennarelli, T. A., and Graham, D. I. (1996). Neuropathological sequelae of traumatic brain injury: relationship to neurochemical and biomechanical mechanisms. *Lab. Invest.* 74, 315–342.

Ouellet, M. C., Beaulieu-Bonneau, S., Sirois, M. J., Savard, J., Turgeon, A. F., Moore, L., et al. (2018). Depression in the first year after traumatic brain injury. *J. Neurotrauma* 35, 1620–1629. doi: 10.1089/neu.2017.5379

Pinteaux, E., Parker, L. C., Rothwell, N. J., and Luheshi, G. N. (2002). Expression of interleukin-1 receptors and their role in interleukin-1 actions in murine microglial cells. *J. Neurochem.* 83, 754–763. doi: 10.1046/j.1471-4159.2002.01184.x

Plotkin, S. R., Banks, W. A., and Kastin, A. J. (1996). Comparison of saturable transport and extracellular pathways in the passage of interleukin-1 alpha across the blood-brain barrier. *J. Neuroimmunol.* 67, 41–47. doi: 10.1016/s0165-5728(96)00036-7

Pradillo, J. M., Murray, K. N., Coutts, G. A., Moraga, A., Oroz-Gonjar, F., Boutin, H., et al. (2017). Reparative effects of interleukin-1 receptor antagonist in young and aged/co-morbid rodents after cerebral ischemia. *Brain Behav. Immun.* 61, 117–126. doi: 10.1016/j.bbi.2016.11.013

Robson, M. J., Zhu, C. B., Quinlan, M. A., Botschner, D. A., Baganz, N. L., Lindler, K. M., et al. (2016). Generation and characterization of mice expressing a conditional allele of the interleukin-1 receptor type 1. *PLoS One* 11:e0150068. doi: 10.1371/journal.pone.0150068

Roman, J., Ritzenthaler, J. D., Fenton, M. J., Roser, S., and Schuyler, W. (2000). Transcriptional regulation of the human interleukin 1beta gene by fibronectin: role of protein kinase C and activator protein 1 (AP-1). *Cytokine* 12, 1581–1596. doi: 10.1006/cyto.2000.0759

Sadowska, G. B., Chen, X., Zhang, J., Lim, Y. P., Cummings, E. E., Makeyev, O., et al. (2015). Interleukin-1beta transfer across the blood-brain barrier in the ovine fetus. *J. Cereb. Blood Flow Metab.* 35, 1388–1395. doi: 10.1038/jcbfm.2015.134

Sanderson, K. L., Raghupathi, R., Saatman, K. E., Martin, D., Miller, G., and McIntosh, T. K. (1999). Interleukin-1 receptor antagonist attenuates regional neuronal cell death and cognitive dysfunction after experimental brain injury. *J. Cereb. Blood Flow Metab.* 19, 1118–1125. doi: 10.1097/00004647-199910000-00008

Semple, B. D., O'Brien, T. J., Gimlin, K., Wright, D. K., Kim, S. E., Casillas-Espinosa, P. M., et al. (2017). Interleukin-1 receptor in seizure susceptibility after traumatic injury to the pediatric brain. *J. Neurosci.* 37, 7864–7877. doi: 10.1523/JNEUROSCI.0982-17.2017

Serkkola, E., and Hurme, M. (1993). Synergism between protein-kinase C and cAMP-dependent pathways in the expression of the interleukin-1 beta gene is mediated via the activator-protein-1 (AP-1) enhancer activity. *Eur. J. Biochem.* 213, 243–249. doi: 10.1111/j.1432-1033.1993.tb17754.x

Shim, J. H., Xiao, C., Paschal, A. E., Bailey, S. T., Rao, P., Hayden, M. S., et al. (2005). TAK1, but not TAB 1 or TAB 2, plays an essential role in multiple signaling pathways in vivo. *Genes Dev.* 19, 2668–2681. doi: 10.1101/gad.1360605

Shultz, S. R., Sun, M., Wright, D. K., Brady, R. D., Liu, S., Beynon, S., et al. (2015). Tibial fracture exacerbates traumatic brain injury outcomes and neuroinflammation in a novel mouse model of multitrauma. *J. Cereb. Blood Flow Metab.* 35, 1339–1347. doi: 10.1038/jcbfm.2015.56

Smith, C. J., Hulme, S., Vail, A., Heal, C., Parry-Jones, A. R., Scarth, S., et al. (2018). SCIL-STROKE (Subcutaneous interleukin-1 receptor antagonist in ischemic stroke): a randomized controlled phase 2 trial. *Stroke* 49, 1210–1216. doi: 10.1161/STROKEAHA.118.020750

Statler, K. D., Scheerlinck, P., Pouliot, W., Hamilton, M., White, H. S., and Dudek, F. E. (2009). A potential model of pediatric posttraumatic epilepsy. *Epilepsy Res.* 86, 221–223. doi: 10.1016/j.eplepsyres.2009.05.006

Sun, M., Brady, R. D., Wright, D. K., Kim, H. A., Zhang, S. R., Sobey, C. G., et al. (2017). Treatment with an interleukin-1 receptor antagonist mitigates neuroinflammation and brain damage after polytrauma. *Brain Behav. Immun.* 66, 359–371. doi: 10.1016/j.bbi.2017.08.005

Sun, M., McDonald, S. J., Brady, R. D., O'Brien, T. J., and Shultz, S. R. (2018). The influence of immunological stressors on traumatic brain injury. *Brain Behav. Immun.* 69, 618–628. doi: 10.1016/j.bbi.2018.01.007

Sung, S. J., Walters, J. A., and Fu, S. M. (1992). Stimulation of tumor necrosis factor alpha production in human monocytes by inhibitors of protein phosphatase 1 and 2A. *J. Exp. Med.* 176, 897–901. doi: 10.1084/jem.176.3.897

Symons, J. A., Young, P. R., and Duff, G. W. (1995). Soluble type II interleukin 1 (IL-1) receptor binds and blocks processing of IL-1 beta precursor and loses affinity for IL-1 receptor antagonist. *Proc. Natl. Acad. Sci. U.S.A.* 92, 1714–1718. doi: 10.1073/pnas.92.5.1714

Takao, T., Tracey, D. E., Mitchell, W. M., and De Souza, E. B. (1990). Interleukin-1 receptors in mouse brain: characterization and neuronal localization. *Endocrinology* 127, 3070–3078. doi: 10.1210/endo-127-6-3070

Tehranian, R., Andell-Jonsson, S., Beni, S. M., Yatsiv, I., Shohami, E., Bartfai, T., et al. (2002). Improved recovery and delayed cytokine induction after closed head injury in mice with central overexpression of the secreted isoform of the Interleukin-1 receptor antagonist. *J. Neurotrauma* 19, 939–951. doi: 10.1089/089771502320317096

Tomozawa, Y., Inoue, T., and Satoh, M. (1995). Expression of type I interleukin-1 receptor mRNA and its regulation in cultured astrocytes. *Neurosci. Lett.* 195, 57–60. doi: 10.1016/0304-3940(95)11781-q

Vollmer, S., Strickson, S., Zhang, T., Gray, N., Lee, K. L., Rao, V. R., et al. (2017). The mechanism of activation of IRAK1 and IRAK4 by interleukin-1 and Toll-like receptor agonists. *Biochem. J.* 474, 2027–2038. doi: 10.1042/BCJ20170097

Wang, X. F., Huang, L. D., Yu, P. P., Hu, J. G., Yin, L., Wang, L., et al. (2006). Upregulation of type I interleukin-1 receptor after traumatic spinal cord injury in adult rats. *Acta Neuropathol.* 111, 220–228. doi: 10.1007/s00401-005-0016-x

Webster, K. M., Sun, M., Crack, P., O'Brien, T. J., Shultz, S. R., and Semple, B. D. (2017). Inflammation in epileptogenesis after traumatic brain injury. *J. Neuroinflam.* 14:10. doi: 10.1186/s12974-016-0786-1

Wilson, R. F., and Tyburski, J. G. (2001). Management of patients with head injuries and multiple other trauma. *Neurol. Res.* 23, 117–120. doi: 10.1179/016164101101198415

Wong, R., Lenart, N., Hill, L., Toms, L., Coutts, G., Martinecz, B., et al. (2019). Interleukin-1 mediates ischaemic brain injury via distinct actions on endothelial cells and cholinergic neurons. *Brain Behav. Immun.* 76, 126–138. doi: 10.1016/j.bbi.2018.11.012

Xu, Y., Tao, X., Shen, B., Horng, T., Medzhitov, R., Manley, J. L., et al. (2000). Structural basis for signal transduction by the Toll/interleukin-1 receptor domains. *Nature* 408, 111–115. doi: 10.1038/35040600

Yang, L., Guo, Y., Wen, D., Yang, L., Chen, Y., Zhang, G., et al. (2016). Bone fracture enhances trauma brain injury. *Scand. J. Immunol.* 83, 26–32. doi: 10.1111/sji.12393

Ye, H., Arron, J. R., Lamothe, B., Cirilli, M., Kobayashi, T., Shevde, N. K., et al. (2002). Distinct molecular mechanism for initiating TRAF6 signalling. *Nature* 418, 443–447. doi: 10.1038/nature00888

Zhang, D. D., Jin, C., Zhang, Y. T., Gan, X. D., Zou, M. J., Wang, Y. Y., et al. (2018). A novel IL-1RA-PEP fusion protein alleviates blood-brain barrier disruption after ischemia-reperfusion in male rats. *J. Neuroinflam.* 15:16. doi: 10.1186/s12974-018-1058-z

Zhang, D. D., Zou, M. J., Zhang, Y. T., Fu, W. L., Xu, T., Wang, J. X., et al. (2017). A novel IL-1RA-PEP fusion protein with enhanced brain penetration ameliorates cerebral ischemia-reperfusion injury by inhibition of oxidative stress and neuroinflammation. *Exp. Neurol.* 297, 1–13. doi: 10.1016/j.expneurol.2017.06.012

Zhu, L., Liu, X., Nemeth, D. P., DiSabato, D. J., Witcher, K. G., McKim, D. B., et al. (2019). Interleukin-1 causes CNS inflammatory cytokine expression via endothelia-microglia bi-cellular signaling. *Brain Behav. Immun.* doi: 10.1016/j.bbi.2019.06.026 [Epub ahead print].

Conflict of Interest: The authors declare that the research was conducted in the absence of any commercial or financial relationships that could be construed as a potential conflict of interest.

frontiers in Behavioral Neuroscience

ORIGINAL RESEARCH
published: 03 June 2020
doi: 10.3389/fnbeh.2020.00070

Wistar Kyoto Rats Display Anhedonia In Consumption but Retain Some Sensitivity to the Anticipation of Palatable Solutions

Rebecca L. Wright[1], *Gary Gilmour*[2] *and Dominic M. Dwyer*[1]*

[1]School of Psychology, Cardiff University, Cardiff, United Kingdom, [2]Lilly Research Centre, Eli Lilly & Co. Ltd., Erl Wood Manor, United Kingdom

The Wistar Kyoto (WKY) rat has been proposed as a model of depression-like symptoms. However, anhedonia—a reduction in the response to normatively rewarding events—as a central depression symptom has yet to be fully assessed in this model. We compared WKY rats and Wistar controls, with stress-susceptibility examined by applying mild unpredictable stress to a subset of each group. Anhedonia-like behavior was assessed using microstructural analysis of licking behavior, where mean lick cluster size reflects hedonic responses. This was combined with tests of anticipatory contrast, where the consumption of a moderately palatable solution (4% sucrose) is suppressed in anticipation of a more palatable solution (32% sucrose). WKY rats displayed greatly attenuated hedonic reactions to sucrose overall, although their reactions retained some sensitivity to differences in sucrose concentration. They displayed normal reductions in consumption in anticipatory contrast, although the effect of contrast on hedonic reactions was greatly blunted. Mild stress produced overall reductions in sucrose consumption, but this was not exacerbated in WKY rats. Moreover, mild stress did not affect hedonic reactions or the effects of contrast. These results confirm that the WKY substrain expresses a direct behavioral analog of anhedonia, which may have utility for increasing mechanistic understanding of depression symptoms.

Keywords: WKY, depression, anhedonia, consummatory, anticipatory, contrast

OPEN ACCESS

Edited by:
Christian P. Müller, University of Erlangen Nuremberg, Germany

Reviewed by:
Kevin Pang, VA New Jersey Health Care System, United States
Carla Gambarana, University of Siena, Italy

***Correspondence:**
Dominic M. Dwyer
dwyerdm@cardiff.ac.uk

Specialty section:
This article was submitted to Pathological Conditions, a section of the journal Frontiers in Behavioral Neuroscience

Received: *23 December 2019*
Accepted: *17 April 2020*
Published: *03 June 2020*

Citation:
Wright RL, Gilmour G and Dwyer DM (2020) Wistar Kyoto Rats Display Anhedonia In Consumption but Retain Some Sensitivity to the Anticipation of Palatable Solutions. Front. Behav. Neurosci. 14:70. doi: 10.3389/fnbeh.2020.00070

INTRODUCTION

Depression is a highly debilitating disorder with symptoms that manifest at the psychological, behavioral and physiological levels. With higher prevalence than other psychiatric disorders, it has been reported that approximately 16% of people will develop depression at some point over their lifetime (Kessler et al., 2003), and is currently a leading global cause of disability (WHO, 2020). While the presentation of depression is varied, a central symptom is an anhedonia (American Psychiatric Association, 2013)—a reduction in the response to normatively rewarding events (Ribot, 1897; Gorwood, 2008), including both consummatory (in the moment pleasure) and anticipatory (expected pleasure) deficits (Gard et al., 2006; Rizvi et al., 2016). Although pharmacotherapy is typically the first-line treatment for depression, current antidepressant drugs are only partially effective (approximately 20% better recovery rates than no-treatment controls), with a slow onset of action (4-6 weeks), and with few genuinely

new compounds recently introduced clinically (Belzung, 2014; Willner and Belzung, 2015). Valid animal models play a central role in the investigation of basic pathology and the development of novel therapeutic techniques (Overstreet, 2012; Willner and Belzung, 2015). Much of the animal modeling of depression has focused on the application of stress (e.g., the chronic mild stress procedure), but applying this to genetically "normal" animals does not account for the evidence that there are material differences between individuals in the risk of depression and thus that considering dispositional factors is vital in a truly valid modeling approach (Willner and Belzung, 2015; Wang et al., 2017). A variety of rodent modes of susceptibility to depression, stress, and/or anxiety have been proposed, amongst these the Wistar-Kyoto (WKY) rat is becoming increasingly recognized for its promise in reflecting key aspects of depression (Overstreet, 2012; Nam et al., 2014; Willner and Belzung, 2015; Wang et al., 2017).

Originally bred as controls for the Spontaneously Hypertensive Rat (Louis and Howes, 1990), WKY animals were soon noted as having high susceptibility to stress-ulceration (e.g., Paré, 1989b; Paré and Redei, 1993; Paré and Kluczynski, 1997), and subsequent research revealed greater expression of behavioral markers in rodent depression studies (e.g., Paré, 1989a,b; Paré and Redei, 1993; Paré and Kluczynski, 1997; Rittenhouse et al., 2002), as well as deficits on other tests relating to anxiety and/or depression (e.g., Paré, 1994; Solberg et al., 2001; Pardon et al., 2002; De La Garza and Mahoney, 2004; Ferguson and Gray, 2005; Shepard and Myers, 2008; D'Souza and Sadananda, 2017). Moreover, the WKY rat appears to be insensitive to some common antidepressant compounds (e.g., Lahmame et al., 1997; López-Rubalcava and Lucki, 2000; Tejani-Butt et al., 2003), suggesting it may be particularly suitable as a model of treatment-resistant depression. Despite this promising literature, the key question of whether WKY rats truly display anhedonia remains to be answered: partially because of some inconsistencies between reported results and because of the nature of the testing methods used.

In assessing anhedonia, traditional tests have relied on the consumption of (or preference for) sweetened solutions such as sucrose or saccharin, on the assumption that a lowered hedonic response to palatable sweet flavors would be directly analogous to anhedonia (Willner et al., 1987; Papp et al., 1991; Muscat and Willner, 1992; Forbes et al., 1996). But while palatability certainly can influence consumption, a great many other factors will also produce consumption changes, including differences in motivation and physiological need, post ingestive effects, and satiety (Booth et al., 1972; Warwick and Weingarten, 1996; Brennan et al., 2001; Dwyer, 2012; Lewis et al., 2019). Thus, reductions in the consumption or preference for sweet flavors are not uniquely consistent with anhedonia and assuming consumption changes reflect hedonic responses is problematic. Moreover, direct intake measures only address the consummatory aspects of anhedonia and not anticipatory anhedonia. Also, although there are several reports that WKY rats display deficits in sweet flavor consumption or preference (e.g., Malkesman et al., 2005; Luo et al., 2015; Burke et al., 2016; Shoval et al., 2016; D'Souza and Sadananda, 2017; Fragale et al., 2017) others report no such deficits and even enhancements of consumption/preference (e.g., Nam et al., 2014; Mileva and Bielajew, 2015).

In response to the fact that consumption-only measures do not directly assess hedonic reactions, more sensitive assays of hedonic behavior have been developed. For example, orofacial reactivity tests (Grill and Norgren, 1978) use the fact that responses to intra-orally infused solutions can be separated into appetitive and aversive behavior patterns. This measure has been extensively used in the context of separating hedonic and other components of reward processing and their biological basis (e.g., Berridge, 1996; Berridge and Robinson, 1998; Castro and Berridge, 2014). While they have been used in a highly productive manner, orofacial reactivity tests have some practical limitations, particularly concerning the effective life of implanted oral cannula and the separation of voluntary consumption from the reactions to infused solutions. An alternative approach to assessing hedonic responses relies on the analysis of the microstructure of voluntary consumption—rodents typically produce clusters of licks separated by pauses, and the mean number of licks per cluster displays a positive monotonic relationship with the concentration of palatable sucrose solution (e.g., Davis and Smith, 1992; Davis and Perez, 1993; Spector et al., 1998), a negative relationship with an unpalatable solution such as quinine (Hsiao and Fan, 1993; Spector and St John, 1998), as well as being sensitive to pharmacological interventions known to affect palatability in humans (Asin et al., 1992; Higgs and Cooper, 1998). Critically, lick cluster size is not simply a proxy for consumption: although cluster size increases with increased sucrose concentration, the amount consumed decreases at high concentrations due to satiety (e.g., Ernits and Corbit, 1973); while studies of conditioned taste aversion and preference have also shown that palatability and consumption can dissociate (e.g., Dwyer et al., 2008, 2009, 2012, 2013; Dwyer, 2009). Thus, in the present experiments, we used the analysis of lick cluster size to provide a means of selectively assessing palatability responses. We have previously used this method to demonstrate the presence of an anhedonic profile in animals subject to social- (Dwyer, 2012) or handling-stress (Clarkson et al., 2018), as well as in a genetic model for Silver Russell Syndrome (McNamara et al., 2016) while ruling out a hedonic disturbance in a model for Prader-Willi syndrome (Davies et al., 2015) and NMDA antagonist models for psychosis (Lydall et al., 2010).

As previously mentioned, anhedonia in depression can separate between consummatory and anticipatory deficits (Gard et al., 2006; Rizvi et al., 2016). Moreover, there is evidence from patient studies that both consummatory and anticipatory hedonic deficits are present in depression (McFarland and Klein, 2009; Liu et al., 2011). To address both anticipatory and consummatory aspects of anhedonia in WKY rats we used an anticipatory contrast procedure (e.g., Flaherty and Rowan, 1985; Flaherty, 1996). This involves giving rats access to two solutions each day when the first solution is of a lower concentration than the second (e.g., 4% then 32% sucrose), both consumption of, and the lick cluster size for, the initial solution is suppressed compared to when the two solutions are of equal concentration (Arthurs et al., 2012; Wright et al., 2013). Thus, anticipatory

contrast involves the downregulation of the current hedonic experience based on the expectation of a future event of high value and reflects anticipatory aspects of hedonic responses. We complemented this anticipatory test with the analysis of licking microstructure during the simple consumption of a range of sucrose concentrations to examine consummatory hedonic responses.

Also, it is uncertain whether the deficits seen with WKY rats are exacerbated by external stressors (compare Paré and Kluczynski, 1997; Nam et al., 2014 with Malkesman et al., 2006; Sterley et al., 2011). Thus we used a factorial design whereby both WKY and Wistar control groups were divided and an attenuated chronic mild stress procedure (Willner et al., 1987, 1992) was applied to half of the rats in each group. The stressor involved exposures to a brief swimming event, and thus also provided an opportunity to confirm that the typical WKY deficit on this task was present in the current cohort of animals. Importantly, the frequency of the stressor application was reduced compared to the typical chronic mild stress procedure (3 per week as opposed to daily treatments) to test whether WKY animals would be susceptible to a lower level of stress than that required to produce effects in control animals.

MATERIALS AND METHODS

Animals

Male Wistar (N = 24) and Wistar Kyoto (WKY, N = 24) rats were used. Both were from Charles River (UK) breeding stocks and were delivered to Cardiff University at approximately 11 weeks of age. On arrival, both Wistar and WKY rats were split into two weight-matched groups of twelve into either a "No-stress" or a "Stress" condition [Mean Weights (±SEM): Wistar No-Stress 177.8 g (±3.9); Wistar Stress 182 g (±6.8); WKY No-stress 182.3 g (±4.2); WKY Stress 178.4 g (±7.9)]. No-stress rats were housed in pairs and their home cages included standard environmental enrichment (tubes and gnawing sticks). Stress rats were singly housed in a separate room and no environmental enrichment was provided. Before the start of experimental work, all animals were placed on a food-restricted diet, which maintained them between 85 to 95% of their free-feeding weights (this was matched to the expected growth rate of free-feeding animals, and thus weights during the experimental periods exceeded the original free-feeding weights). Their food ration was given in their home cage approximately 30 min after behavioral procedures (or around 5 pm if there were no procedures on that day). Careful monitoring was employed throughout to ensure that rat weights, as a percentage of free-feeding weights, did not differ significantly between the two strain and stress conditions. Animal weight data during the experimental periods and its analysis can be found in **Supplementary Table S3** (for the Anticipatory Contrast study) and **Supplementary Table S4** (for the Consumption study). Food restriction was performed to motivate the consumption of the caloric sugar solutions and also allowed for the motivational state of the stressed and non-stressed animals to be matched in case the stress procedures created a difference in energy demands between conditions. While food restriction may affect lick cluster size (compare Davis and Perez, 1993 with Spector et al., 1998) this is unlikely to have a material effect on the results obtained here because the food restriction was applied to all animals and groups were equivalent in terms of the effects of restriction on body weight as a percentage of free-feeding weights (see **Supplementary Tables S3, S4**). Unless otherwise specified, rats were held under a 12-h light/dark cycle. Experimental sessions were performed during the light phase, beginning at approximately 11 am, and were conducted 6 to 7 days per week. Due to the provision of food rations and application of stress procedures (or handling in the No-stress conditions) during the light phase, rats had 2 weeks to adapt to procedures occurring in this phase, thus minimizing the impact of testing normally nocturnal animals during the day. This project was considered and approved by the Cardiff University Animal Welfare and Ethical Review Board (AWERB) and all experiments were conducted following the United Kingdom Animals Scientific Procedures Act, 1986.

Mild Stressor Tests

Rats in the Stress condition underwent a series of mild social and environmental stressors which commenced a week before testing. This continued throughout these experiments. Each week, rats in the stress group were exposed to three of five possible stressors: wet bedding, overnight illumination, cage swap with an unfamiliar rat, pair-up with an unfamiliar rat, and a brief swim test. Details of the stress procedures, including the relationship to other experimental manipulations, are shown in the Supplementary Materials (see **Supplementary Tables S1, S2**). The identity of the stressor was randomly allocated, as was the day on which it was given. When stress manipulations were to occur on the same day as an experimental session, the stressor was applied after the training or test session had been carried out. Rats in the No-stress condition were gently handled on the same days as stress procedures were applied.

During brief swim tests, the rats' behavior was recorded *via* a camcorder mounted above the water cylinders. Data were scored using a time sampling technique, whereby the rats' predominant behavior was noted every 2 s across the 120 s test. Recording commenced as soon as the rats had entered the water. Their behavior was scored as either "Active," "Escape" or "Immobile." Active behavior was recorded when the rat was swimming, climbing or diving. Thus, rats would be considered "active" if they made upward-directed movements of the forepaws, horizontal movements across the cylinder (including rapid changes in the rat's direction) or dived to the bottom of the cylinder before resurfacing. Immobile behavior was recorded if rats were floating in the water without any signs of struggling. Small movements of the back limbs were permitted in this category if they served only to keep the animals head out of the water. Escape behavior was recorded if the rat was able to leave the cylinder. This would be considered as one escape. For every subsequent 2 s period where the rat was out of the water, an "X" would be recorded so that it was not included in subsequent analysis. The percentage of time spent active, immobile or escaping was then calculated for each animal.

As the primary observer was not blind to rat strain, a single session, chosen at random, was re-scored by a secondary observer (who was blind to the strain) using the criterion outlined above. Inter-rater reliability assessment revealed a strong positive correlation between the two observers' immobility scores, $r_{(22)} = 0.975$, $p < 0.001$.

Negative Anticipatory Contrast

Apparatus

Testing was conducted in six automated drinking chambers (Med Associates Inc., St Albans, VT, USA), measuring 30 × 24 × 21 cm, and comprised of two clear Perspex and two aluminum walls. The chamber floor consisted of 19 steel rods, 4.8 mm in diameter and 16 mm apart. Approximately 5 cm above the grid floor, two holes each of 1 cm diameter were positioned on each side of one aluminum wall to allow the rat access to the solutions. Solutions were delivered through the right and left access holes by 50 ml cylinders with ball-bearing metal drinking-spouts. These were mounted to the cage *via* motorized holders that held the spout flush with the outside of the chamber and retracted it as required. Contact sensitive lickometers registered the timing of each lick made by the animal to the nearest 0.01 s, and a computer running MED-PC software controlled the equipment and recorded the data. The solutions used were 4% and 32% (wt/wt) sucrose formulated using commercial-grade cane sugar and deionized water.

Procedure

All rats were habituated to the drinking boxes for 10 min each day for 3 days before the pre-training phase of the experiment. This was to overcome stress effects caused by a novel environment that may have differentially affected the potentially stress-sensitive WKY rats. No solutions were made available during this habituation. During pre-training, rats were water restricted for 22 h and then given access to water for 10 min from both the left- and right-hand side of the drinking chamber. Only one pre-training day was given, after which rats were returned to *ad libitum* water and remained so for the duration of the experiment. During initial training, drinking spouts were positioned inside the chamber to allow for easy detection by the rats, spouts were gradually moved back to be flush with the outside of the chamber across the first 3 days of training.

On each subsequent training day, the solution pairings were manipulated within subjects. Rats were presented with either a 4% sucrose solution followed by more 4% sucrose (the 4–4 condition) or a 4% sucrose solution followed by a 32% sucrose solution (the 4–32 condition). These daily solution pairings were presented in double alternation (e.g., ABBAABBA) and different contextual cues were used to signal which of the two solution pairings was in operation each day. There were thus 32 total testing days, with 16 days in each of the 4–4 and 4–32 conditions. For half the animals, context 1 (consisting of bright light and normal grid floor) was paired with the 4–4 condition, and context 2 (consisting of dim light provided by a table lamp and a wire mesh floor insert) was paired with the 4–32 condition. The remaining subjects had the opposite pairings. The first solution in the pair was made available for 3 min on the left-hand side of the chamber. Following a 4-s inter-solution interval, the second solution was then made available for 6 min on the right-hand side of the chamber. The apparatus and procedures are the same we have reported previously (Wright et al., 2013).

Consumption and Lick Cluster Size Analysis

Consumption was assessed by weighing the bottle before and after each experimental run. Lick cluster size (defined as the mean number of licks per cluster) was extracted from the MED-PC data. As in our lab's previous experiments using these general methods and equipment (e.g., Lydall et al., 2010; Dwyer et al., 2011, 2018; Wright et al., 2013), a cluster was defined as series of licks, with each lick separated by no more than a 0.5 s interval. The same criterion had been adopted by Davis and his colleagues (e.g., Davis, 1989; Davis and Smith, 1992; Davis and Perez, 1993). Drinking data were collated into 2-session blocks.

Sucrose Consumption

The same animals were re-tested to examine sucrose consumption across a range of concentrations without contrast. The solutions used were 2, 8 and 24% (wt/wt) sucrose made daily with deionized water and the apparatus was as described previously. Because rats had already undergone anticipatory contrast testing involving multiple drinking sessions no pre-training or habituation was necessary.

Rats were given access to one of the three sucrose concentrations which were always made available from the left-hand side of the drinking chamber. Each concentration was given for three consecutive days and the order of sucrose presentations was counterbalanced so that half of the rats received the sucrose in order of increasing concentration (2–8–24) and the other half received them in order of decreasing (24–8–2) concentration. A two-day rest was given before the next concentration in the sequence was presented. All solutions were made available for 10 min each day.

Consumption and lick cluster size analyses were conducted using the same parameters described for anticipatory contrast. To minimize any effects of transition between concentration, data were analyzed across the last 2 days of exposure for each solution concentration. One animal (a WKY No-stress rat) was excluded from the descriptive and inferential statistics reported for the sucrose consumption phase. This was due to abnormally high lick cluster size displayed by this animal for 32% sucrose, more than 3.5 standard deviations above the group mean[1].

Data Analysis

Immobility data in the brief swim test was analyzed with mixed ANOVA with a within-subject factor of the sessions (1–5), and a between-subject factor of strain (Wistar vs. WKY). Data from anticipatory contrast and consumption phases were analyzed with mixed ANOVAs with between-subject factors of strain (Wistar vs. WKY) and stress (Stress vs. No stress), plus within-subject factors appropriate for each experiment: For the

[1]The removal of this animal does not impact on the significance (or otherwise) of main effects of strain, stress, or the interaction between them any analysis presented below.

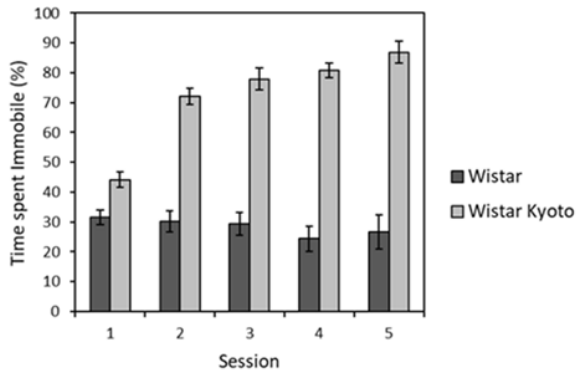

FIGURE 1 | Mean percentage of time immobile (±SEM) during 2 min brief swim sessions for animals subjected to mild stressor protocols (Wistar: dark bars; WKY: light bars). WKY rats were significantly more immobile than Wistar rats, and the levels of immobility significantly increased across sessions in WKY but not Wistar rats (see "Stress Manipulation and Brief Swim" section, for details). See **Supplementary Table S2** for the timing of these sessions relative to the other experimental procedures.

anticipatory contest, there were within-subject factors of the block (1–8) and contrast condition (4–4 or control condition vs. 4–32 or contrast condition); for consumption, there was a within-subject factor of concentration (2, 8, 24%). An alpha level of 0.05 was adopted as the level of significance throughout and Greenhouse-Geisser corrections for violations of the assumption of sphericity applied as appropriate.

RESULTS

Stress Manipulation and Brief Swim

Repeated swim test exposures occurring throughout the stressor protocol were analyzed over time (see **Supplementary Table S2** for the relationship between brief swim tests and other stressor events). It was found that WKY rats spent more time immobile compared to their Wistar counterparts across all sessions (**Figure 1**). Time spent immobile also generally increased across sessions for WKY animals, unlike for the Wistar strain. ANOVA yielded main effects of session ($F_{(4,88)} = 10.8$, $p < 0.001$, $\eta_p^2 = 0.33$) and strain ($F_{(1,22)} = 187.7$, $p < 0.001$, $\eta^2 = 0.90$), as well as a session × strain interaction ($F_{(4,88)} = 14.5$, $p < 0.001$, $\eta_p^2 = 0.45$). Further inspection of the interaction revealed that that immobility significantly increased across sessions for WKY rats ($F_{(4,44)} = 36.9$, $p < 0.001$, $\eta^2 = 0.77$) but not Wistar rats ($F < 1$). Thus, the typical pattern of enhanced immobility for WKY animals in swim tests was replicated here.

Negative Anticipatory Contrast

First Solution Consumption—Anticipatory Contrast

Figure 2 depicts consumption of the initially presented 4% sucrose solution across training blocks. In general, WKY rats consumed significantly less than Wistars did (main effect of strain: $F_{(1,44)} = 13.8$, $p < 0.001$, $\eta_p^2 = 0.24$), and stressed rats consumed less than non-stressed rats (main effect of stress: $F_{(1,44)} = 6.1$, $p = 0.018$, $\eta_p^2 = 0.12$), although no significant interaction was found between these factors (strain × stress: $F < 1$). These effects significantly varied across training blocks (main effect of block: $F_{(4.6,199.0)} = 59.9$, $p < 0.001$, $\eta_p^2 = 0.58$), with strain and stressor effects increasing in effect size across blocks (block × strain: $F_{(4.6,199.0)} = 3.4$, $p = 0.008$, $\eta_p^2 = 0.07$; block × stress: $F_{(4.6,199.0)} = 3.2$, $p = 0.010$, $\eta_p^2 = 0.07$); block × strain × stress: $F_{(4.6, 199.0)} = 2.6$, $p = 0.029$, $\eta_p^2 = 0.06$).

Importantly, a significant anticipatory contrast effect was evident (main effect of contrast: $F_{(1,44)} = 28.4$, $p < 0.001$, $\eta_p^2 = 0.39$) where consumption of the initially presented 4% sucrose solution was lower when followed by the more palatable 32% sucrose compared to when followed by a second presentation of 4% sucrose. Critically, this anticipatory contrast effect did not differ significantly between strains and did not significantly interact with stress (contrast × strain, contrast × stress, contrast × strain × stress interactions: Fs < 1). Consistent with anticipatory contrast effects emerging as a function of learning over training blocks, a significant block × contrast interaction was found ($F_{(4.0,175.8)} = 4.0$, $p = 0.004$, $\eta_p^2 = 0.08$). This learning function did not significantly interact with strain or stress (block × contrast × strain, block × contrast × stress (Fs < 1), block × contrast × strain × stress ($F_{(4.0,175.8)} = 2.0$, $p = 0.097$, $\eta_p^2 = 0.04$)[2].

First Solution Lick Cluster Size—Anticipatory Contrast

Figure 3 depicts mean lick cluster size (LCS) during consumption of the initially presented 4% sucrose solution across training blocks. Overall, WKY rats produced fewer licks per cluster compared to Wistar rats (main effect of strain ($F_{(1,44)} = 17.2$, $p < 0.001$, $\eta_p^2 = 0.28$). Stress did not significantly affect lick cluster size (Main effect of stress; stress × strain interaction, Fs < 1). As with consumption, significant anticipatory contrast effects were evident for lick cluster size (Main effect of contrast: $F_{(1,44)} = 9.4$, $p = 0.004$, $\eta_p^2 = 0.18$), with lick cluster size for the initially presented 4% sucrose solution lower when followed by the more palatable 32% sucrose compared to when followed by a second presentation of 4% solution. Critically, this contrast effect was significantly smaller in WKY than Wistar rats (contrast × strain: $F_{(1,44)} = 4.4$, $p = 0.041$, $\eta_p^2 = 0.09$). The contrast effect was not influenced by stress (contrast × stress, contrast × strain × stress, Fs < 1). Consistent with the emergence of effects over training, there was a main effect of block ($F_{(3.6,156.4)} = 7.5$, $p < 0.001$, $\eta_p^2 = 0.15$), and a block × contrast interaction ($F_{(4.0,175.8)} = 3.0$, $p = 0.020$, $\eta_p^2 = 0.06$). There was also a block × strain interaction ($F_{(3.6,156.4)} = 6.1$, $p < 0.001$, $\eta_p^2 = 0.12$), but

[2]Although the test consumption of sucrose represents only a fraction of the rats overall energy intake, the caloric requirements of animals generally scale such that they relate to weight (Kleiber, 1947). If this scaling is applied to the consumption tests described above, the main effect of rat strain is removed ($F < 1$), but the remaining features of the analysis are unaffected (with the exception of the 4-way block × contrast × strain × stress interaction that becomes significant ($F_{(3.9,169.8)} = 2.5$, $p = 0.049$, $\eta_p^2 = 0.05$). Therefore, differences in bodyweight may have contributed to the lower overall consumption exhibited by WKY rats. This, together with the dissociation between stress effects on consumption and lick cluster size measures, reinforces the idea that consumption measures alone can be ambiguous indicators of hedonic responses.

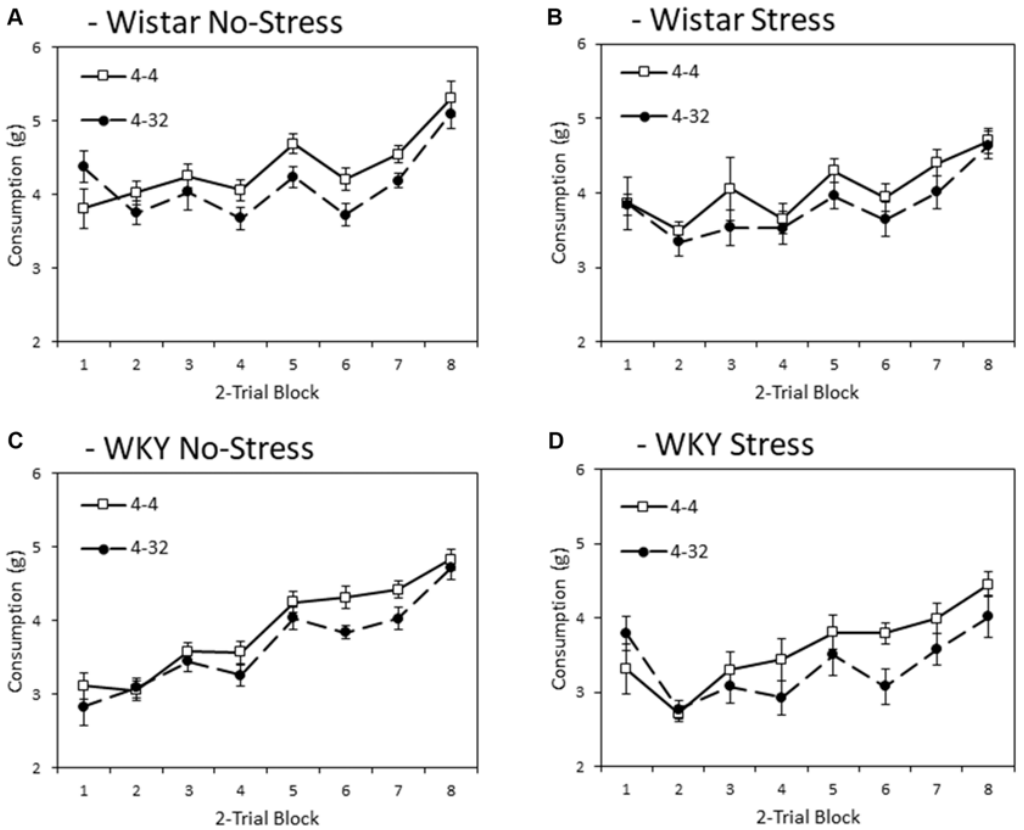

FIGURE 2 | Anticipatory contrast in mean consumption (±SEM) of the initially presented 4% sucrose solution as a function of whether it was followed by either 4% sucrose (open symbols) or 32% sucrose (filled symbols), separated by strain (Wistar: Panels **A,B**; WKY: Panels **C,D**) and stress groups (No-Stress: Panels **A,C**; Stress: Panels **B,D**). The data presented is averaged over two-day blocks. The solution was available for 3 min per day. WKY rats consumed significantly less than Wistar rats, and stressed rats consumed significantly less than no-stress rats, and these effects did not interact. Critically, there was an anticipatory contrast effect (consumption of 4% sucrose was significantly lower when followed by 32% sucrose than 4% sucrose) and this effect did not interact with strain or stress manipulations (see "First Solution Consumption—Anticipatory Contrast" section for details).

not block × stress ($F_{(3.6,156.4)}$ = 2.1, p = 0.091, η_p^2 = 0.05), nor block × strain × stress ($F_{(3.6,156.4)}$ = 1.264, p = 0.228, η_p^2 = 0.03). There were no significant interactions between block × contrast × strain, block × contrast × stress (Fs < 1), or block × contrast × strain × stress ($F_{(4.0,175.8)}$ = 1.4, p = 0.194, η_p^2 = 0.03).

To aid interpretation, the critical contrast × strain interaction was explored further with separate ANOVAs conducted on each strain with factors of block and contrast condition. Wistar rats showed significant main effects of contrast ($F_{(1,23)}$ = 7.5, p = 0.012, η_p^2 = 0.25) and block ($F_{(3.1,72.0)}$ = 7.6, p < 0.001, η_p^2 = 0.25), but no contrast × block interaction ($F_{(3.4,79.3)}$ = 1.7, p = 0.122, η_p^2 = 0.07). WKY rats presented with a different pattern of findings, where there was no significant main effect of contrast ($F_{(1,23)}$ = 2.9, p = 0.103, η_p^2 = 0.11) or block ($F_{(2.8,63.7)}$ = 1.776, p = 0.165, η_p^2 = 0.07), but there was a significant contrast × block interaction ($F_{(3.8,88.1)}$ = 2.9, p = 0.008, η_p^2 = 0.11). These results suggest that lick cluster size in WKY rats did show some sensitivity to contrast as training progressed, but far less than the Wistar controls, possibly due to the generally low levels of hedonic response seen in the WKY animals overall. While the anticipatory contrast effect was attenuated for WKY No-stress and Stress rats with a lower lick cluster size difference for first presentation 4% sucrose solution between the two contrast conditions than for the Wistar controls, a contrast effect in WKY animals was apparent by the end of the experiment, most obviously for the No-stress group.

Second Solution Consumption—Low vs. High Sucrose Concentration

Figure 4 depicts consumption of second presentation solution (4% or 32% sucrose) across training blocks. Note that consumption levels were larger than for first presentation because the first bottle was only made available for 3 min and the second bottle for 6 min. Like the first presentation data, WKY rats generally consumed less during second presentation compared to Wistars (main effect of strain: $F_{(1,44)}$ = 65.2, p < 0.001, η_p^2 = 0.60), and stressed animals consumed less than non-stressed animals (main effect of stress: $F_{(1,44)}$ = 8.1, p = 0.007, η_p^2 = 0.16), again in the absence of a significant stain × stress

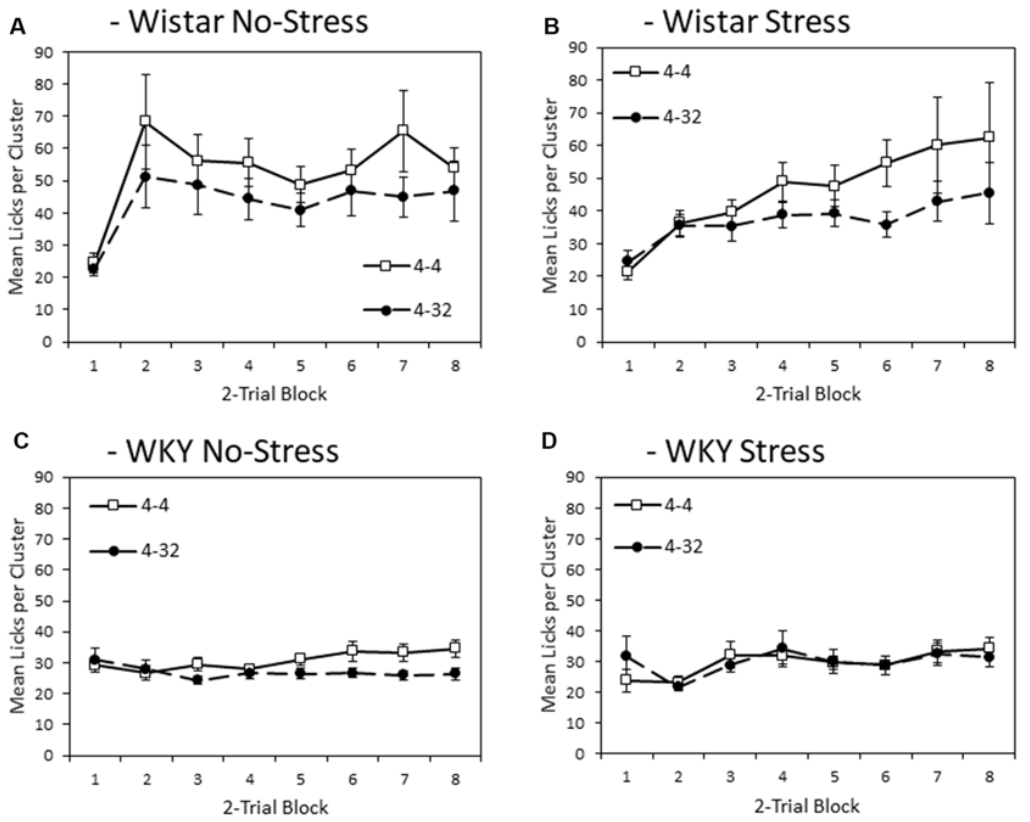

FIGURE 3 | Anticipatory contrast in mean lick cluster size (LCS: ±SEM) of the initially presented 4% sucrose solution as a function of whether it was followed by either 4% sucrose (open symbols) or 32% sucrose (filled symbols), separated by strain (Wistar: Panels **A,B**; WKY: Panels **C,D**) and stress groups (No-Stress: Panels **A,C**; Stress: Panels **B,D**). The data presented is averaged over two-day blocks. The solution was available for 3 min per day. WKY rats displayed a significantly lower mean lick cluster size than Wistar rats, but there was no effect of stress or stress × strain interaction. Critically, there was an anticipatory contrast effect (lick cluster size, indicating hedonic responses, for 4% sucrose was significantly lower when followed by 32% sucrose than 4% sucrose) and this effect was significantly reduced in WKY compared to Wistar rats (see "First Solution Lick Cluster Size—Anticipatory Contrast" section for details). Differential lick cluster sizes for the 4% solution depending on the subsequent concentration of sucrose solution offers a potential measure of anticipatory anhedonia.

interaction ($F < 1$). In general, there was higher consumption of the more palatable 32% sucrose solution compared with the moderately palatable 4% sucrose solution (main effect of solution concentration: $F_{(1,44)} = 23.8$, $p < 0.001$, $\eta_p^2 = 0.35$). The differential consumption of the 4% and 32% sucrose solutions was not significantly impacted by factors of strain or stress (concentration × strain: $F_{(1,44)} = 1.1$, $p = 0.294$, $\eta_p^2 = 0.03$, concentration × stress, concentration × strain × stress, Fs < 1). Consistent with the progressive increase in consumption as a function of training, there was a main effect of block ($F_{(3.3,145.5)} = 91.8$, $p < 0.001$, $\eta_p^2 = 0.68$), which was not significantly impacted by factors of strain, stress or solution concentration (block × strain: $F_{(3.3,145.5)} = 1.0$, $p = 0.385$, $\eta_p^2 = 0.02$; block × stress: $F_{(3.3,145.5)} = 2.5$, $p = 0.058$, $\eta_p^2 = 0.05$; block × strain × stress, $F < 1$; block × concentration: $F_{(2.8,123.2)} = 1.689$, $p = 0.176$, $\eta_p^2 = 0.04$; block × concentration × strain; block × concentration × stress; or block × concentration × strain × stress, Fs < 1)[3].

Second Solution Lick Cluster Size—Low vs. High Sucrose Concentration

Figure 5 depicts mean lick cluster size (LCS) during consumption of second presentation solution (4% or 32% sucrose) across training blocks. Overall, WKY rats exerted significantly fewer licks per cluster compared with Wistar animals (main effect of strain: $F_{(1,44)} = 18.6$, $p < 0.001$, $\eta_p^2 = 0.30$). Lick cluster size was not significantly influenced by the application of an external stressor (main effect of stress; stress × strain interaction, Fs < 1). As for consumption, lick cluster size was significantly greater for 32% sucrose solution compared to 4% sucrose (main effect of concentration ($F_{(1,44)} = 9.4$, $p < 0.001$, $\eta_p^2 = 0.32$). Critically, this effect significantly varied with strain (concentration × strain interaction ($F_{(1,44)} = 5.817$, $p = 0.020$, $\eta_p^2 = 0.12$), but not with stress (concentration × stress, or concentration × strain × stress interactions (Fs < 1). In addition, lick cluster size for the second presented solution was also subject to significant change

[3]If the bodyweight scaling described previously is applied to the consumption tests reported here the main effect of rat strain is greatly reduced in effect size but remains significant ($F_{(1,44)} = 212$, $p < 0.001$, $\eta_p^2 = 0.33$). The remaining features of the analysis are unaffected by normalization. Therefore, differences in bodyweight may have contributed to the lower overall consumption exhibited by WKY rats.

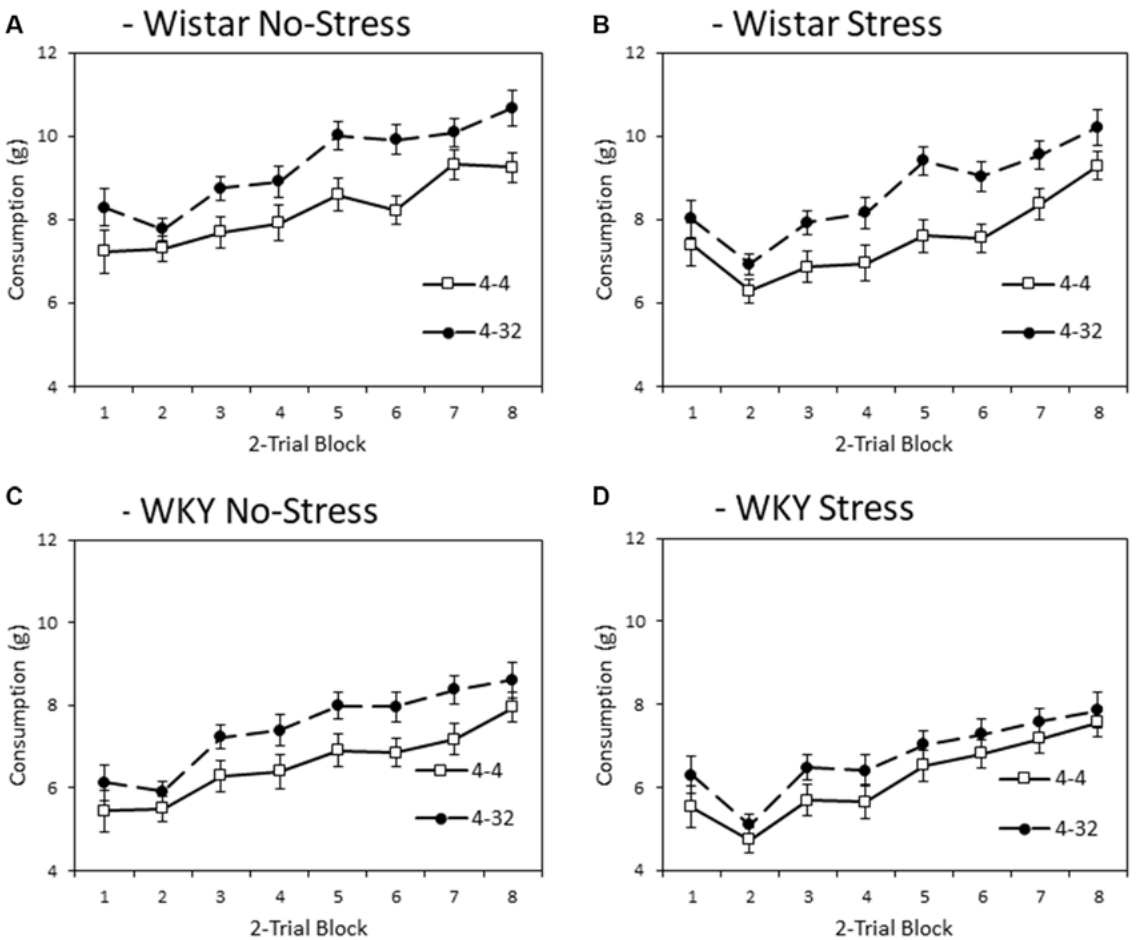

FIGURE 4 | Mean consumption (±SEM) of the second presentation solution made available each day as a factor of strain (Wistar: Panels **A,B**; WKY: Panels **C,D**) and stress (No-Stress: Panels **A,C** ; Stress: Panels **B,D**). Open symbols represent the consumption of 4% sucrose in the second bottle and filled symbols represent the consumption of 32% sucrose in the second bottle. Data presented is averaged across 2-session blocks. Solutions in the second bottle were made available for 6 min. WKY rats consumed significantly less than Wistar rats, and stressed rats consumed significantly less than no-stress rats, but these effects did not interact. Also, consumption of 32% sucrose was higher than that of 4% sucrose, but this difference was not significantly influenced by strain or stress (see "Second Solution Consumption—Low vs. High Sucrose Concentration" section for details).

over training (main effect of block: $F_{(3.4,149.9)} = 7.8$, $p < 0.001$, $\eta_p^2 = 0.15$). While there was no significant block × concentration interaction ($F_{(3.5,153.5)} = 1.2$, $p = 0.326$, $\eta_p^2 = 0.03$), there were both significant block × strain ($F_{(3.4,149.9)} = 12.1$, $p < 0.001$, $\eta_p^2 = 0.22$), and block × concentration × strain ($F_{(3.5,153.5)} = 5.6$, $p < 0.001$, $\eta_p^2 = 0.11$) interactions. The factor of stress did not significantly interact with any statistical comparison involving the factor of block (block × stress, $F < 1$; block × strain × stress: $F_{(3.4,\ 149.9)} = 2.2$, $p = 0.082$, $\eta_p^2 = 0.05$; block × concentration × stress, $F < 1$; block × concentration × strain × stress: $F_{(3.5,153.5)} = 1.8$, $p = 0.150$, $\eta_p^2 = 0.04$).

Further exploration of the critical concentration × strain interaction described above revealed that, although the difference in lick cluster size between 4% and 32% sucrose was smaller in WKY than Wistar rats, it was nevertheless significant in both groups (WKY, main effect of concentration: $F_{(1,23)} = 4.7$, $p = 0.040$, $\eta_p^2 = 0.17$; Wistar, main effect of concentration: $F_{(1,23)} = 16.9$, $p < 0.001$, $\eta_p^2 = 0.42$). In summary, for Wistar rats, irrespective of stress, lick cluster sizes elicited during consumption of the 32% solution were higher compared with when the 4% solution was consumed, reflecting the greater palatability of this solution. Likewise for WKY rats, lick cluster size was also marginally higher for the 32% sucrose solution than for the 4% sucrose solution, at least early in training. This suggests that, while the hedonic reaction of WKY rats to palatable sucrose is materially blunted, it is not entirely absent.

Sucrose Consumption

Consumption of 2, 8, and 32% Sucrose

Figures 6A,C depict the mean consumption of the three sucrose concentrations (2, 8 and 24%) for Wistar and WKY

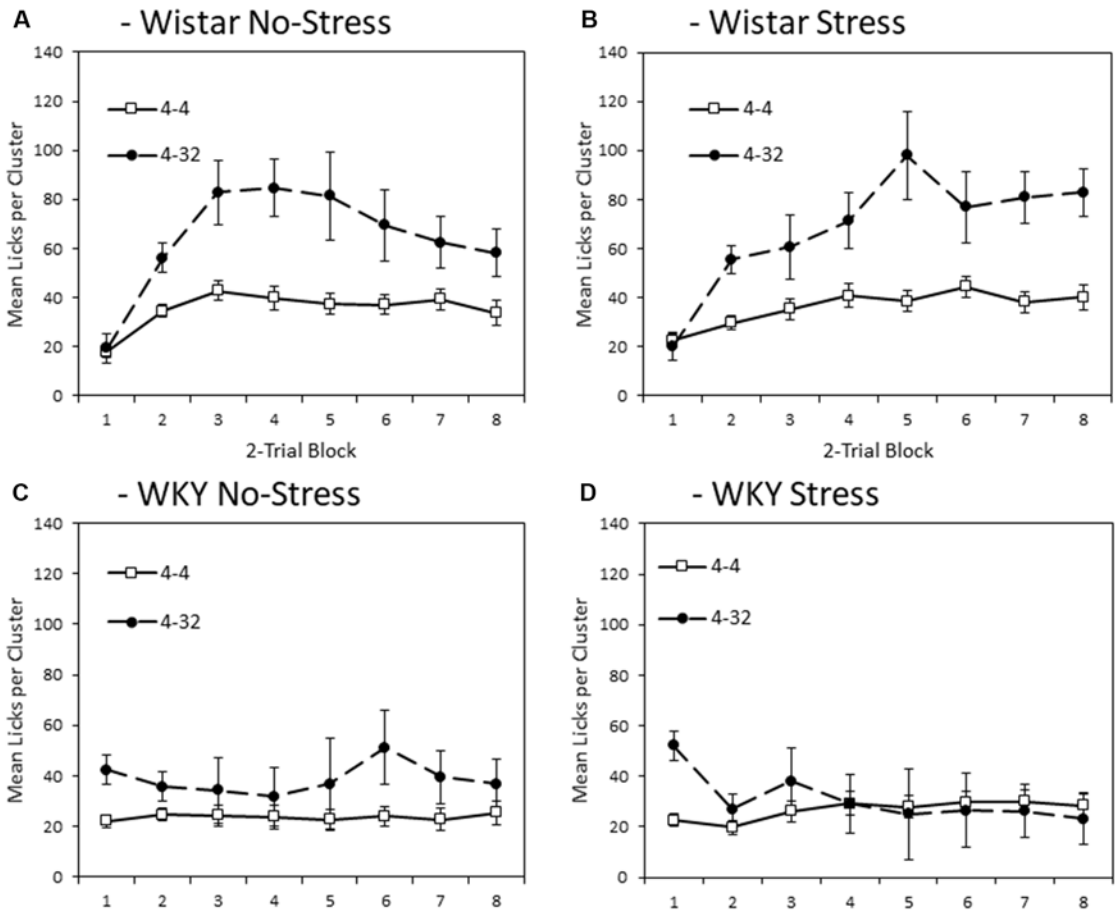

FIGURE 5 | Mean lick cluster size (LCS: ±SEM) for the second solution available each day (4% vs. 32% sucrose) separated by strain (Wistar: Panels **A,B**; WKY: Panels **C,D**) and stress groups (No-Stress: Panels **A,C**; Stress: Panels **B,D**). Open symbols represent responses to the 4% sucrose solution, the filled symbols represent responses to the 32% sucrose solution made available in the second bottle. Data presented is averaged across 2-session blocks. While both WKY and Wistar rats showed significantly higher lick cluster size for 32% than 4% sucrose (reflecting its higher palatability), this difference was significantly smaller in WKY rats and mean lick cluster size overall was significantly lower in WKY rats, indicating a blunted hedonic response (see "Second Solution Lick Cluster Size—Low vs. High Sucrose Concentration" section for details).

rats, separated into Stress and No-stress groups. Sucrose concentration influenced total consumption, with the moderate (8%) solution instead eliciting the highest intake across animals (main effect of concentration: $F_{(1.6,67.6)} = 194.2$, $p < 0.001$, $\eta_p^2 = 0.82$). Regardless of concentration, WKY rats consumed significantly less than their Wistar counterparts (main effect of strain: $F_{(1,43)} = 15.2$, $p < 0.001$, $\eta_p^2 = 0.26$) and stressed rats consumed significantly less than non-stressed rats (main effect of stress: $F_{(1,43)} = 7.0931$, $p = 0.011$, $\eta_p^2 = 0.14$). There was no significant strain × stress interaction ($F < 1$), indicating that stress did not differentially affect intake levels across the Wistar and WKY strains. There was also no strain × concentration ($F < 1$), stress × concentration ($F_{(1.6,67.6)} = 1.1$, $p = 0.307$ $\eta_p^2 = 0.03$), or strain × stress × concentration interactions ($F < 1$)[4].

Lick Cluster Size for 2, 8, and 32% Sucrose

Figures 6B,D depict the mean lick cluster size (LCS) elicited by Wistar and WKY rats, separated into the two stress conditions, when consuming each of the three sucrose concentrations. While overall there was a significant concentration-dependent increase in lick cluster size (main effect of solution concentration: $F_{(1.5,64.4)} = 49.9$, $p < 0.001$, $\eta_p^2 = 0.54$), Wistar rats in general displayed significantly greater lick cluster size than WKY rats (main effect of strain: $F_{(1,43)} = 30.7$, $p < 0.001$, $\eta_p^2 = 0.42$) indicating a deficit in hedonic reactions to sucrose. In addition, a significant strain × concentration interaction was evident ($F_{(1.5,64.3784)} = 17.9$, $p < 0.001$, $\eta_p^2 = 0.29$), but stress did not significantly influence effects of other factors on lick cluster size (main effect of stress; strain × stress interaction;

[4]If the bodyweight scaling described previously is applied to the consumption tests reported here the main effect of rat strain is removed ($F < 1$), but the remaining features of the analysis are unaffected. Therefore, differences in bodyweight may have contributed to the lower overall consumption exhibited by WKY rats.

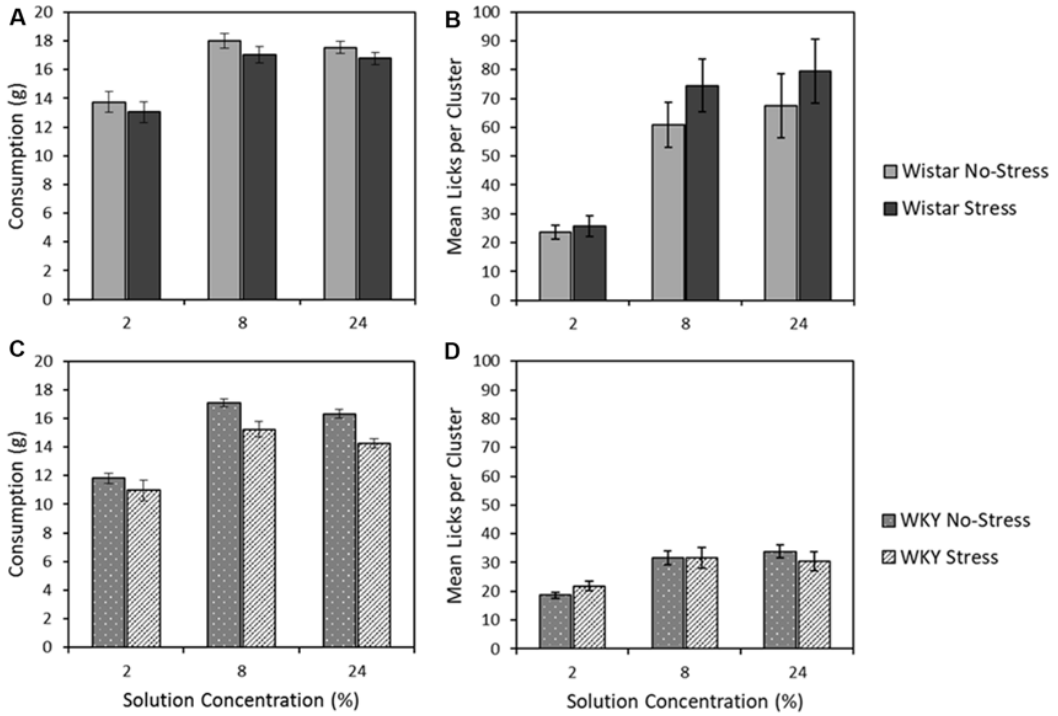

FIGURE 6 | Mean consumption (±SEM]; panels **A,C**) and mean lick cluster size [LCS: panels **B,D** (±SEM) as a function of concentration. This test involves single solution presentations only and thereby removes the anticipatory element of the previous contrast studies. Wistar rats are shown in the upper panels **(A,B)**, WKY rats in the lower panels **(C,D)**. For consumption, WKY rats drank significantly less than Wistar rats, and stressed rats consumed significantly less than no-stress rats, but these factors did not interact (see "Consumption of 2, 8, and 32% Sucrose" section for details). While both WKY and Wistar rats displayed increasing lick cluster size with concentration increases (reflecting the higher palatability of more concentrated solutions), these effects were significantly smaller in WKY rats, which also displayed lower lick cluster size overall: a pattern of effects that is consistent with a partially preserved but extremely blunted hedonic responses in WKY rats (see "Lick Cluster Size for 2, 8, and 32% Sucrose" section for details).

stress × concentration; concentration × strain × stress interactions, Fs < 1).

Further exploration of the critical concentration × strain interaction was explored by performing separate ANOVA analyses for WKY and Wistar rats. In each analysis rats, a significant main effect of concentration (Wistar: $F_{(2,44)} = 36.0$, $p < 0.001$, $\eta_p^2 = 0.62$; WKY: $F_{(2,42)} = 26.9$, $p < 0.001$, $\eta_p^2 = 0.56$) was found, while there was no main effect of stress (Wistar: $F_{(1,22)} = 1.0$, $p = 0.486$, $\eta_p^2 = 0.02$; WKY: $F < 1$), and no stress × concentration interaction (Wistar: $F < 1$; WKY: $F_{(2,42)} = 1.5$, $p = 0.228$, $\eta_p^2 = 0.07$). Thus, irrespective of stress, Wistar and WKY rats both increased the size of their licking clusters as the solution consumed increased in concentration. While lick cluster size increased concentration in WKY rats, their overall affective response to each solution appeared greatly reduced relative to Wistars. This confirms the suggestion from the anticipatory contrast tests that, while the hedonic reaction of WKY rats to palatable sucrose is materially blunted, it is not entirely absent.

DISCUSSION

The present study highlighted how from the perspective of potential stress-diathesis animal modeling of depression that the application of a mild stressor sequence results in qualitatively different effects to those exhibited by WKY rats in tests of anticipatory and consummatory anhedonia. Stress did not significantly exacerbate any behavioral differences exhibited by WKY rats. These results suggest the potential utility of WKY rats in modeling aspects of depressive symptomatology, but a caution for a more nuanced interpretation of the biological factors driving alterations in hedonic behavior. Measures of total consumption should not be considered biologically equivalent to other measures of palatability, and anticipatory and consummatory phases of hedonic responses can be behaviorally and biologically dissociated.

Consumptive behavior during the sucrose preference test has been the most frequently used approach to infer potential impairments in hedonic response in several animal models of depression (e.g., unpredictable chronic mild stress, olfactory bulbectomy, social defeat, as evidenced by Romeas et al., 2009; Burstein and Doron, 2018; Iñiguez et al., 2018; Antoniuk et al., 2019). While the present study indicated the presence of decreased consumptive behavior of sucrose solution in WKY rats, as indexed by the total amount of solution ingested, a potential confound arises from the fact that WKY rats were of lower overall bodyweight than their age-matched Wistar counterparts. When bodyweight is corrected for, the differences

between WKY and Wistar rats were removed or greatly reduced. Previous findings have been somewhat mixed here, where for instance marked increases in sucrose consumption have been observed in WKY rats (Papacostas-Quintanilla et al., 2017). Other previous studies have not included a comparator strain as a control (e.g., Tacchi et al., 2008), while others have found increased bodyweight of WKY rats compared to Wistars (Dommett and Rostron, 2013). These discrepancies should be borne in mind when considering the reliability of consumptive measures in this context and overall interpretation of such literature.

Beyond overall consumption, the most general difference observed between WKY and Wistar rats was the far lower levels of lick cluster size seen in the WKY animals when consuming sucrose. Importantly, this difference in the lick cluster size measure of hedonic response is unlikely to be a product of either the differences in the amounts of the solutions consumed—because lick cluster size and consumption vary independently (Davis and Smith, 1992; Spector et al., 1998; Dwyer, 2012), as they do here concerning the effects of stress—or the differences in body weight. We are aware of no reports that bodyweight influences lick cluster size and in the current experiments there was no relationship between weight and lick cluster size[5]. Because lick cluster size is a direct indication of the palatability or hedonic response to the solution being consumed, this measure can be considered a clear analog of consummatory anhedonia as seen in depression (Rizvi et al., 2016; Wu et al., 2017). In the sucrose consumption test involving single solution presentations of different concentrations of sucrose, WKY rats remained somewhat sensitive to the difference between sucrose concentrations, exhibiting larger lick cluster sizes for higher concentrations. Thus, consummatory hedonic responses were not entirely absent in WKY rats, but very markedly blunted. In addition to deficits in consummatory pleasure, anticipatory hedonic responses are also reported to be significantly diminished in depressed patients (Bylsma et al., 2008; Sherdell et al., 2012) and may relate to impairments in episodic future thinking related to hedonic responses (Hallford et al., 2020). Results from the anticipatory contrast test conducted suggested that WKY rats were able to learn the contingencies in force during this study—displaying lower consumption of 4% sucrose in the context where 32% sucrose was anticipated later in the session. This finding is in line with the previously reported findings of sensitivity to positive and negative contrast in WKY rats (Dommett and Rostron, 2013). In the present study, negative anticipatory contrast effects on the lick cluster size measure displayed a different temporal profile to that of contrast effects on consumption and were only reduced for the 4% solution by the end of the contrast training period. While the size of this anticipatory hedonic effect was far smaller than in Wistar controls, mean lick cluster sizes in WKY rats were low overall. There was a clear possibility that floor effects could limit the opportunity for WKY rats to display contrast effects on lick cluster size. Previous evidence is consistent with consumption and hedonic changes being independent effects of contrast, or with the consumption changes being the result of hedonic devaluation (Wright et al., 2013). Such measures may be very important from a translational perspective, as the presentation of anhedonic symptoms has been related to poorer prognosis and treatment sensitivity (e.g., Moos and Cronkite, 1999; McMakin et al., 2012).

The impact of a sequence of stressful events on sucrose solution ingestive behavior was quite distinct to the baseline differences observed in WKY rats. The stressors applied in the present study did result in generally lower levels of consumption across both the anticipatory and consumption phases of the experiment, an effect that survived bodyweight correction. Many prior studies have inferred hedonic deficits from reduction in sucrose consumption and/or preference. This has been particularly common in the case of the chronic mild stress model for depression (e.g., Willner et al., 1987; Papp et al., 1991; Muscat and Willner, 1992; Forbes et al., 1996). The current results reflect prior reports that chronic mild stress can reduce sucrose consumption, but the effects of stress did not extend to the more direct measure of hedonic reactions through the analysis of lick cluster size. That is not to suggest that chronic stress cannot produce hedonic deficits (indeed, see Dwyer, 2012; Clarkson et al., 2018; for reports of just such effects), especially because the current stress protocol was deliberately chosen to be less intense than those typically used. Instead, the present study serves as a reminder that stress effects on consumptive and hedonic behaviors are not always overlapping in animal models, and that other non-hedonic influences may drive changes in consumptive behavior in such contexts.

It is, however, noteworthy that the stress procedures applied in the present study did not exacerbate the hedonic deficits indicated by low lick cluster sizes seen in WKY rats, suggesting that this combination of parameters is not a viable stress-diathesis model. While this finding is consistent with some prior reports (e.g., Paré and Kluczynski, 1997; Nam et al., 2014) possibly the large endogenous deficit seen in the non-stressed WKY animals produced a floor effect which could obscure any additional stress effect. However, this explanation is challenged by the fact that stress effects on consumption *per se* were not so obviously affected by potential floor effects and there was no stress-induced enhancement of the WKY response for consumption. It is interesting to consider that a stressor paradigm that induced a deficit *per se* could not exacerbate a qualitatively distinct deficit in WKY rats. The present results suggest that translation of the complexity of experiences of depression-precipitating stressful events in humans to stress-diathesis models in rats may require considerably more effort to validate (Willner and Belzung, 2015).

Despite the lack of findings of stress-induced exacerbation on sucrose ingestive behavior in WKY rats, there was a strong effect of the repeated exposure to the brief swim test in these animals. The finding of generally greater immobility for WKY rats along with the fact WKY show greater increases

[5]For the negative anticipatory contrast experiment, the correlation closest to being significant was that between weight and lick cluster size for 4% sucrose in the 4–4 condition in Wistar rats, $r_{(24)} = -0.301$, $p = 0.153$. For the consumption experiment, the correlation closest to being significant was that between weight and lick cluster size for 8% sucrose in Wistar rats, $r_{(24)} = -0.287$, $p = 0.174$.

in immobility across tests is consistent with previous results (e.g., Paré, 1989a,b; Paré and Redei, 1993; Paré and Kluczynski, 1997; López-Rubalcava and Lucki, 2000; Rittenhouse et al., 2002; Nam et al., 2014). Because most swim test paradigms previously reported in the literature are far longer (e.g., involving a 15 min pre-test and a 5 min test period) than the 2 min sessions used here, the current results are novel in showing significant differences between Wistar and WKY rats despite a significantly reduced swim time. This has an important welfare implication in that reliable WKY deficits, and by implication, other swim test effects can be identified while reducing the overall exposure to the stressful environment of the test. Progressive increases in immobility of WKY rats with repeated exposure to swim tests potentially demonstrate that different behavioral parameters are differentially sensitive to stressors in these animals. However, there are two important limitations to this finding. First, the brief swim test was only administered within the context of a broader chronic mild stress paradigm, and future studies should consider whether such brief swim procedures are sensitive to WKY vs. Control differences in the absence of additional stressors. The second limitation relates to the interpretation of the translational relevance of changes in swim test behavior in the context of depression. Some authors elegantly argue that swim testing in rodents has little construct validity concerning depression symptoms in humans (Commons et al., 2017), but may more accurately index the ability of an animal to cope with stress. From this perspective, it could be speculated that WKY rats did not cope with the chronic mild stress paradigm as well as Wistar rats did, but that this differential sensitivity to stress did not manifest at the level of hedonic responding.

A final very important limitation to acknowledge regarding this study was the focus on male rats, an unfortunate consequence of resource limitation. It has long been proposed that there is a female bias in the incidence of depression (Weissman et al., 1993) and that there are sex-dependent differences in the expression of depressive symptoms (Cavanagh et al., 2017). Differential sex effects can also be observed concerning stress vulnerability (Bangasser and Valentino, 2014; Bangasser and Wicks, 2017; Bangasser and Wiersielis, 2018; Bangasser et al., 2018; Wellman et al., 2018) and thereby the potential ability of stress to modulate ongoing depressive symptoms. In animal studies, sex is an important variable in the expression of sucrose binging-like behavior in WKY rats (Papacostas-Quintanilla et al., 2017). Other work suggests that female WKY rats exhibit less anhedonia than male WKY rats (Burke et al., 2016), although direct non-consumptive measures of anhedonia were not employed in this study. Future work should more thoroughly test the effect of sex of WKY rats on stress-induced exacerbation of hedonic responses.

A greater appreciation of the heterogeneity of depressive symptoms and neurobiological substrates underpinning these effects makes discussion of the "best" animal models of depression somewhat superficial, especially in the context of the hedonic tests applied here, that have been rarely reported in the previous literature. However, understanding the behavioral profiles of animal models with greater resolution will greatly help in consideration of their translational relevance, and which systems and circuits might be involved in the expression of these effects. WKY rats were found to be sensitive to some degree to differences between the present and anticipated sucrose solution in a contrast study, but show greatly attenuated hedonic reactions to them. Thus, WKY animals display a specific hedonic deficit rather than a general insensitivity to reward. Further, a mild stress paradigm did not exacerbate the effects on hedonic reactions in WKY rats. Altogether, the current results are consistent with previous proposals that WKY rats are a promising laboratory model for the study of hedonic aspects of depression (Overstreet, 2012; Nam et al., 2014; Willner and Belzung, 2015; Wang et al., 2017) but further work will be needed to establish a reliable diathesis-stress procedure.

DATA AVAILABILITY STATEMENT

The raw data supporting the conclusions of this article will be made available by the authors, without undue reservation, to any qualified researcher.

ETHICS STATEMENT

The animal study was reviewed and approved by the Cardiff University Animal Welfare and Ethical Review Board (AWERB) and all experiments were conducted in accordance with the United Kingdom Animals Scientific Procedures Act, 1986.

AUTHOR CONTRIBUTIONS

All authors contributed to the overall design of the studies, with RW and DD determining the exact schedule of testing. RW performed the experiments and collated the data for analysis. RW and DD performed the statistical analysis. These experiments were initially prepared for inclusion in her Ph.D. thesis by RW, and the initial draft of the article written by DD and GG. All authors contributed to and approved the final draft of the article.

FUNDING

This research was supported by a BBSRC CASE studentship awarded to RW (BB/I015639/1), and co-funded by Eli Lilly & Co.

ACKNOWLEDGMENTS

The work presented here was performed as part of the RW's Ph.D. and has been reported in her thesis (Wright, 2015).

SUPPLEMENTARY MATERIAL

The Supplementary Material for this article can be found online at: https://www.frontiersin.org/articles/10.3389/fnbeh.2020.00070/full#supplementary-material.

REFERENCES

Antoniuk, S., Bijata, M., Ponimaskin, E., and Wlodarczyk, J. (2019). Chronic unpredictable mild stress for modeling depression in rodents: meta-analysis of model reliability. *Neurosci. Biobehav. Rev.* 99, 101–116. doi: 10.1016/j.neubiorev.2018.12.002

Arthurs, J., Lin, J.-Y., Amodeo, L. R., and Reilly, S. (2012). Reduced palatability in drug-induced taste aversion: II. Aversive and rewarding unconditioned stimuli. *Behav. Neurosci.* 126, 433–444. doi: 10.1037/a0027676

Asin, K. E., Davis, J. D., and Bednarz, L. (1992). Differential-effects of serotonergic and catecholaminergic drugs on ingestive behavior. *Psychopharmacology* 109, 415–421. doi: 10.1007/bf02247717

American Psychiatric Association (2013). *Diagnostic and Statistical Manual of Mental Disorders, Fifth Edition.* Arlington, VA: American Psychiatric Association.

Bangasser, D. A., Eck, S. R., Telenson, A. M., and Salvatore, M. (2018). Sex differences in stress regulation of arousal and cognition. *Physiol. Behav.* 187, 42–50. doi: 10.1016/j.physbeh.2017.09.025

Bangasser, D. A., and Valentino, R. J. (2014). Sex differences in stress-related psychiatric disorders: neurobiological perspectives. *Front. Neuroendocrinol.* 35, 303–319. doi: 10.1016/j.yfrne.2014.03.008

Bangasser, D. A., and Wicks, B. (2017). Sex-specific mechanisms for responding to stress. *J. Neurosci. Res.* 95, 75–82. doi: 10.1002/jnr.23812

Bangasser, D. A., and Wiersielis, K. R. (2018). Sex differences in stress responses: a critical role for corticotropin-releasing factor. *Hormones* 17, 5–13. doi: 10.1007/s42000-018-0002-z

Belzung, C. (2014). Innovative drugs to treat depression: did animal models fail to be predictive or did clinical trials fail to detect effects? *Neuropsychopharmacology* 39, 1041–1051. doi: 10.1038/npp.2013.342

Berridge, K. C. (1996). Food reward: brain substrates of wanting and liking. *Neurosci. Biobehav. Rev.* 20, 1–25. doi: 10.1016/0149-7634(95)00033-b

Berridge, K. C., and Robinson, T. E. (1998). What is the role of dopamine in reward: hedonic impact, reward learning, or incentive salience? *Neurosci. Biobehav. Rev.* 28, 309–369. doi: 10.1016/s0165-0173(98)00019-8

Booth, D. A., Lovett, D., and McSherry, G. M. (1972). Postingestive modulation of the sweetness preference gradient in the rat. *J. Comp. Physiol. Psychol.* 78, 485–512. doi: 10.1037/h0092970

Brennan, K., Roberts, D. C. S., Anisman, H., and Merali, Z. (2001). Individual differences in sucrose consumption in the rat: motivational and neurochemical correlates of hedonia. *Psychopharmacology* 157, 269–276. doi: 10.1007/s002130100805

Burke, N. N., Coppinger, J., Deaver, D. R., Roche, M., Finn, D. P., and Kelly, J. (2016). Sex differences and similarities in depressive-and anxiety-like behaviour in the Wistar-Kyoto rat. *Physiol. Behav.* 167, 28–34. doi: 10.1016/j.physbeh.2016.08.031

Burstein, O., and Doron, R. (2018). The unpredictable chronic mild stress protocol for inducing anhedonia in mice. *J. Vis. Exp.* 140:e58184. doi: 10.3791/58184

Bylsma, L. M., Morris, B. H., and Rottenberg, J. (2008). A meta-analysis of emotional reactivity in major depressive disorder. *Clin. Psychol. Rev.* 28, 676–691. doi: 10.1016/j.cpr.2007.10.001

Castro, D. C., and Berridge, K. C. (2014). Advances in the neurobiological bases for food 'liking' versus 'wanting'. *Physiol. Behav.* 136, 22–30. doi: 10.1016/j.physbeh.2014.05.022

Cavanagh, A., Wilson, C. J., Kavanagh, D. J., and Caputi, P. (2017). Differences in the expression of symptoms in men versus women with depression: a systematic review and meta-analysis. *Harv. Rev. Psychiatry* 25, 29–38. doi: 10.1097/hrp.0000000000000128

Clarkson, J. M., Dwyer, D. M., Flecknell, P. A., Leach, M. C., and Rowe, C. (2018). Handling method alters the hedonic value of reward in laboratory mice. *Sci. Rep.* 8:2448. doi: 10.1038/s41598-018-20716-3

Commons, K. G., Cholanians, A. B., Babb, J. A., and Ehlinger, D. G. (2017). The rodent forced swim test measures stress-coping strategy, not depression-like behavior. *ACS Chem. Neurosci.* 8, 955–960. doi: 10.1021/acschemneuro.7b00042

Davies, J. R., Humby, T., Dwyer, D. M., Garfield, A. S., Furby, H., Wilkinson, L. S., et al. (2015). Calorie seeking, but not hedonic response, contributes to hyperphagia in a mouse model for Prader-Willi syndrome. *Eur. J. Neurosci.* 42, 2105–2113. doi: 10.1111/ejn.12972

Davis, J. D. (1989). The microstructure of ingestive behavior. *Ann. N Y Acad. Sci.* 575, 106–121. doi: 10.1111/j.1749-6632.1989.tb53236.x

Davis, J. D., and Perez, M. C. (1993). Food deprivation-induced and palatability-induced microstructural changes in ingestive behavior. *Am. J. Physiol.* 264, R97–R103. doi: 10.1152/ajpregu.1993.264.1.r97

Davis, J. D., and Smith, G. P. (1992). Analysis of the microstructure of the rhythmic tongue movements of rats ingesting maltose and sucrose solutions. *Behav. Neurosci.* 106, 217–228. doi: 10.1037/0735-7044.106.1.217

De La Garza, R., and Mahoney, J. J. III. (2004). A distinct neurochemical profile in WKY rats at baseline and in response to acute stress: implications for animal models of anxiety and depression. *Brain Res.* 1021, 209–218. doi: 10.1016/j.brainres.2004.06.052

Dommett, E. J., and Rostron, C. L. (2013). Appetitive and consummative responding for liquid sucrose in the spontaneously hypertensive rat model of attention deficit hyperactivity disorder. *Behav. Brain Res.* 238, 232–242. doi: 10.1016/j.bbr.2012.10.025

D'Souza, D., and Sadananda, M. (2017). Anxiety- and depressive-like profiles during early- and mid-adolescence in the female Wistar Kyoto rat. *Int. J. Dev. Neurosci.* 56, 18–26. doi: 10.1016/j.ijdevneu.2016.11.003

Dwyer, D. M. (2009). Microstructural analysis of ingestive behaviour reveals no contribution of palatability to the incomplete extinction of a conditioned taste aversion. *Q. J. Exp. Psychol.* 62, 9–17. doi: 10.1080/17470210802215152

Dwyer, D. M. (2012). Licking and liking: the assessment of hedonic responses in rodents. *Q. J. Exp. Psychol.* 65, 371–394. doi: 10.1080/17470218.2011.652969

Dwyer, D. M., Boakes, R. A., and Hayward, A. J. (2008). Reduced palatability in lithium- and activity-based, but not in amphetamine-based, taste aversion learning. *Behav. Neurosci.* 122, 1051–1060. doi: 10.1037/a0012703

Dwyer, D. M., Burgess, K. V., and Honey, R. C. (2012). Avoidance but not aversion following sensory preconditioning with flavors: a challenge to stimulus substitution. *J. Exp. Psychol. Anim. Behav. Process.* 38, 359–368. doi: 10.1037/a0029784

Dwyer, D. M., Figueroa, J., Gasalla, P., and López, M. (2018). Reward adaptation and the mechanisms of learning: contrast changes reward value in rats and drives learning. *Psychol. Sci.* 29, 219–227. doi: 10.1177/0956797617729825

Dwyer, D. M., Gasalla, P., and López, M. (2013). Nonreinforced flavor exposure attenuates the effects of conditioned taste aversion on both flavor consumption and cue palatability. *Learn. Behav.* 41, 390–401. doi: 10.3758/s13420-013-0114-x

Dwyer, D. M., Lydall, E. S., and Hayward, A. J. (2011). Simultaneous contrast: evidence from licking microstructure and cross-solution comparisons. *J. Exp. Psychol. Anim. Behav. Process.* 37, 200–210. doi: 10.1037/a0021458

Dwyer, D. M., Pincham, H. L., Thein, T., and Harris, J. A. (2009). A learned flavor preference persists despite the extinction of conditioned hedonic reactions to the cue flavors. *Learn. Behav.* 37, 305–310. doi: 10.3758/lb.37.4.305

Ernits, T., and Corbit, J. D. (1973). Taste as a dipsogenic stimulus. *J. Comp. Physiol. Psychol.* 83, 27–31. doi: 10.1037/h0034258

Ferguson, S. A., and Gray, E. P. (2005). Aging effects on elevated plus maze behavior in spontaneously hypertensive, Wistar-Kyoto and Sprague-Dawley male and female rats. *Physiol. Behav.* 85, 621–628. doi: 10.1016/j.physbeh.2005.06.009

Flaherty, C. F. (1996). *Incentive Relativity*. New York, NY: Cambridge University Press.

Flaherty, C. F., and Rowan, G. A. (1985). Anticipatory contrast: within-subjects analysis. *Anim. Learn. Behav.* 13, 2–5. doi: 10.3758/bf03213357

Forbes, N. F., Stewart, C. A., Matthews, K., and Reid, I. C. (1996). Chronic mild stress and sucrose consumption: validity as a model of depression. *Physiol. Behav.* 60, 1481–1484. doi: 10.1016/s0031-9384(96)00305-8

Fragale, J. E. C., Beck, K. D., and Pang, K. C. H. (2017). Use of the exponential and exponentiated demand equations to assess the behavioral economics of negative reinforcement. *Front. Neurosci.* 11:376. doi: 10.3389/fnins.2017.00376

Gard, D. E., Gard, M. G., Kring, A. M., and John, O. P. (2006). Anticipatory and consummatory components of the experience of pleasure: a scale development study. *J. Res. Pers.* 40, 1086–1102. doi: 10.1016/j.jrp.2005.11.001

Gorwood, P. (2008). Neurobiological mechanisms of anhedonia. *Dialogues Clin. Neurosci.* 10, 291–299.

Grill, H. J., and Norgren, R. (1978). Taste reactivity test. I. mimetic responses to gustatory stimuli in neurologically normal rats. *Brain Res.* 143, 263–279. doi: 10.1016/0006-8993(78)90568-1

Hallford, D. J., Barry, T. J., Austin, D. W., Raes, F., Takano, K., and Klein, B. (2020). Impairments in episodic future thinking for positive events and anticipatory pleasure in major depression. *J. Affect. Disord.* 260, 536–543. doi: 10.1016/j.jad.2019.09.039

Higgs, S., and Cooper, S. J. (1998). Effects of benzodiazepine receptor ligands on the ingestion of sucrose, intralipid and maltodextrin: an investigation using a microstructural analysis of licking behavior in a brief contact test. *Behav. Neurosci.* 112, 447–457. doi: 10.1037//0735-7044.112.2.447

Hsiao, S., and Fan, R. J. (1993). Additivity of taste-specific effects of sucrose and quinine—microstructural analysis of ingestive behavior in rats. *Behav. Neurosci.* 107, 317–326. doi: 10.1037/0735-7044.107.2.317

Iñiguez, S. D., Flores-Ramirez, F. J., Riggs, L. M., Alipio, J. B., Garcia-Carachure, I., Hernandez, M. A., et al. (2018). Vicarious social defeat stress induces depression-related outcomes in female mice. *Biol. Psychiatry* 83, 9–17. doi: 10.1016/j.biopsych.2017.07.014

Kessler, R. C., Berglund, P., Demler, O., Jin, R., Koretz, D., Merikangas, K. R., et al. (2003). The epidemiology of major depressive disorder—results from the National Comorbidity Survey Replication (NCS-R). *JAMA* 289, 3095–3105. doi: 10.1001/jama.289.23.3095

Kleiber, M. (1947). Body size and metabolic rate. *Physiol. Rev.* 27, 511–541. doi: 10.1152/physrev.1947.27.4.511

Lahmame, A., del Arco, C., Pazos, A., Yritia, M., and Armario, A. (1997). Are Wistar-Kyoto rats a genetic animal model of depression resistant to antidepressants? *Eur. J. Pharmacol.* 337, 115–123. doi: 10.1016/s0014-2999(97)01276-4

Lewis, L. R., Benn, A., Dwyer, D. M., and Robinson, E. S. J. (2019). Affective biases and their interaction with other reward-related deficits in rodent models of psychiatric disorders. *Behav. Brain Res.* 372:112051. doi: 10.1016/j.bbr.2019.112051

Liu, W. H., Chan, R. C. K., Wang, L. Z., Huang, J., Cheung, E. F. C., Gong, Q. Y., et al. (2011). Deficits in sustaining reward responses in subsyndromal and syndromal major depression. *Prog. Neuropsychopharmacol. Biol. Psychiatry* 35, 1045–1052. doi: 10.1016/j.pnpbp.2011.02.018

López-Rubalcava, C., and Lucki, I. (2000). Strain differences in the behavioral effects of antidepressant drugs in the rat forced swimming test. *Neuropsychopharmacology* 22, 191–199. doi: 10.1016/s0893-133x(99)00100-1

Louis, W. J., and Howes, L. G. (1990). Genealogy of the spontaneously hypertensive rat and Wistar-Kyoto rat strains: implications for studies of inherited hypertension. *J. Cardiovasc. Pharmacol.* 16, S1–S5. doi: 10.1097/00005344-199000167-00002

Luo, J., Min, S., Wei, K., Cao, J., Wang, B., Li, P., et al. (2015). Behavioral and molecular responses to electroconvulsive shock differ between genetic and environmental rat models of depression. *Psychiatry Res.* 226, 451–460. doi: 10.1016/j.psychres.2014.12.068

Lydall, E. S., Gilmour, G., and Dwyer, D. M. (2010). Analysis of licking microstructure provides no evidence for a reduction in reward value following acute or sub-chronic phencyclidine administration. *Psychopharmacology* 209, 153–162. doi: 10.1007/s00213-010-1779-x

Malkesman, O., Braw, Y., Zagoory-Sharon, O., Golan, O., Lavi-Avnon, Y., Schroeder, M., et al. (2005). Reward and anxiety in genetic animal models of childhood depression. *Behav. Brain Res.* 164, 1–10. doi: 10.1016/j.bbr.2005.04.023

Malkesman, O., Maayan, R., Weizman, A., and Weller, A. (2006). Aggressive behavior and HPA axis hormones after social isolation in adult rats of two different genetic animal models for depression. *Behav. Brain Res.* 175, 408–414. doi: 10.1016/j.bbr.2006.09.017

McFarland, B. R., and Klein, D. N. (2009). Emotional reactivity in depression: diminished responsiveness to anticipated reward but not to anticipated punishment or to nonreward or avoidance. *J. Neurol.* 26, 117–122. doi: 10.1002/da.20513

McMakin, D. L., Olino, T. M., Porta, G., Dietz, L. J., Emslie, G., Clarke, G., et al. (2012). Anhedonia predicts poorer recovery among youth with selective serotonin reuptake inhibitor treatment-resistant depression. *J. Am. Acad. Child Adolesc. Psychiatry* 51, 404–411. doi: 10.1016/j.jaac.2012.01.011

McNamara, G. I., Davis, B. A., Dwyer, D. M., John, R. M., and Isles, A. R. (2016). Behavioural abnormalities in a novel mouse model for Silver Russell Syndrome. *Hum. Mol. Genet.* 25, 5407–5417. doi: 10.1093/hmg/ddw357

Mileva, G. R., and Bielajew, C. (2015). Environmental manipulation affects depressive-like behaviours in female Wistar-Kyoto rats. *Behav. Brain Res.* 293, 208–216. doi: 10.1016/j.bbr.2015.07.035

Moos, R. H., and Cronkite, R. C. (1999). Symptom-based predictors of a 10-year chronic course of treated depression. *J. Nerv. Ment. Dis.* 187, 360–368. doi: 10.1097/00005053-199906000-00005

Muscat, R., and Willner, P. (1992). Suppression of sucrose drinking by chronic mild unpredictable stress: a methodoligocal analysis. *Neurosci. Biobehav. Rev.* 16, 507–517. doi: 10.1016/s0149-7634(05)80192-7

Nam, H., Clinton, S. M., Jackson, N. L., and Kerman, I. A. (2014). Learned helplessness and social avoidance in the Wistar-Kyoto rat. *Front. Behav. Neurosci.* 8:109. doi: 10.3389/fnbeh.2014.00109

Overstreet, D. H. (2012). "Modeling depression in animal models" in *Psychiatric Disorder: Methods and Protocols*, ed. F. H. Kobeissy (Vol. 829), (New York, NY: Humana Press), 125–144. doi: 10.1007/978-1-61779-458-2_7

Papacostas-Quintanilla, H., Ortiz-Ortega, V. M., and López-Rubalcava, C. (2017). Wistar-Kyoto female rats are more susceptible to develop sugar binging: a comparison with wistar rats. *Front. Nutr.* 4:15. doi: 10.3389/fnut.2017.00015

Papp, M., Willner, P., and Muscat, R. (1991). An animal model of anhedonia: attenuation of sucrose consumption and place preference conditioning by chronic unpredictable mild stress. *Psychopharmacology* 104, 255–259. doi: 10.1007/bf02244188

Pardon, M. C., Gould, G. G., Garcia, A., Phillips, L., Cook, M. C., Miller, S. A., et al. (2002). Stress reactivity of the brain noradrenergic system in three rat strains differing in their neuroendocrine and behavioral responses to stress: implications for susceptibility to stress-related neuropsychiatric disorders. *Neuroscience* 115, 229–242. doi: 10.1016/s0306-4522(02)00364-0

Paré, W. P. (1989a). "Behavioural dispair" test predicts stress-ulcer in WKY rats. *Physiol. Behav.* 46, 483–487. doi: 10.1016/0031-9384(89)90025-5

Paré, W. P. (1989b). Stress-ulcer susceptibility and depression in Wistar-Kyoto (WKY) rats. *Physiol. Behav.* 46, 993–998. doi: 10.1016/0031-9384(89)90203-5

Paré, W. P. (1994). Open-field, learned-helplessness, conditioned defensive burying, and forced-swim tests in WKY rats. *Physiol. Behav.* 55, 433–439. doi: 10.1016/0031-9384(94)90097-3

Paré, W. P., and Kluczynski, J. (1997). Developmental factors modify stress ulcer incidence in a stress-susceptible rat strain. *J. Physiol. Paris* 91, 105–111. doi: 10.1016/s0928-4257(97)89473-9

Paré, W. P., and Redei, E. (1993). Depressive behavior and stress-ulcer in Wistar-Kyoto rats. *J. Physiol. Paris* 87, 229–238. doi: 10.1016/0928-4257(93)90010-q

Ribot, T. (1897). *The Psychology of Emotions.* London: Walter Scott Publishing.

Rittenhouse, P. A., López-Rubalcava, C., Stanwood, G. D., and Lucki, I. (2002). Amplified behavioral and endocrine responses to forced swim stress in the Wistar-Kyoto rat. *Psychoneuroendocrinology* 27, 303–318. doi: 10.1016/s0306-4530(01)00052-x

Rizvi, S. J., Pizzagalli, D. A., Sproule, B. A., and Kennedy, S. H. (2016). Assessing anhedonia in depression: potentials and pitfalls. *Neurosci. Biobehav. Rev.* 65, 21–35. doi: 10.1016/j.neubiorev.2016.03.004

Romeas, T., Morissette, M. C., Mnie-Filali, O., Piñeyro, G., and Boye, S. M. (2009). Simultaneous anhedonia and exaggerated locomotor activation in an animal model of depression. *Psychopharmacology* 205, 293–303. doi: 10.1007/s00213-009-1539-y

Shepard, J. D., and Myers, D. A. (2008). Strain differences in anxiety-like behavior: association with corticotropin-releasing factor. *Behav. Brain Res.* 186, 239–245. doi: 10.1016/j.bbr.2007.08.013

Sherdell, L., Waugh, C. E., and Gotlib, I. H. (2012). Anticipatory pleasure predicts motivation for reward in major depression. *J. Abnorm. Psychol.* 121, 51–60. doi: 10.1037/a0024945

Shoval, G., Shbiro, L., Hershkovitz, L., Hazut, N., Zalsrnan, G., Mechoulam, R., et al. (2016). Prohedonic effect of cannabidiol in a rat model of depression. *Neuropsychobiology* 73, 123–129. doi: 10.1159/000443890

Solberg, L. C., Olson, S. L., Turek, F. W., and Redei, E. (2001). Altered hormone levels and circadian rhythm of activity in the WKY rat, a putative animal model

of depression. *Am. J. Physiol. Regul. Integr. Comp. Physiol.* 281, R786–R794. doi: 10.1152/ajpregu.2001.281.3.r786

Spector, A. C., Klumpp, P. A., and Kaplan, J. M. (1998). Analytical issues in the evaluation of food deprivation and sucrose concentration effects on the microstructure of licking behavior in the rat. *Behav. Neurosci.* 112, 678–694. doi: 10.1037/0735-7044.112.3.678

Spector, A. C., and St John, S. J. (1998). Role of taste in the microstructure of quinine ingestion by rats. *Am. J. Physiol.* 274, 1687–1703. doi: 10.1152/ajpregu.1998.274.6.r1687

Sterley, T. L., Howells, F. M., and Russell, V. A. (2011). Effects of early life trauma are dependent on genetic predisposition: a rat study. *Behav. Brain Funct.* 7:11. doi: 10.1186/1744-9081-7-11

Tacchi, R., Ferrari, A., Loche, A., and Bertolini, A. (2008). Sucrose intake: increase in non-stressed rats and reduction in chronically stressed rats are both prevented by the γ-hydroxybutyrate (GHB) analogue, GET73. *Pharmacol. Res.* 57, 464–468. doi: 10.1016/j.phrs.2008.05.004

Tejani-Butt, S., Kluczynski, J., and Pare, W. P. (2003). Strain-dependent modification of behavior following antidepressant treatment. *Prog. Neuropsychopharmacol. Biol. Psychiatry* 27, 7–14. doi: 10.1016/s0278-5846(02)00308-1

Wang, Q. Z., Timberlake, M. A. II., Prall, K., and Dwivedi, Y. (2017). The recent progress in animal models of depression. *Prog. Neuropsychopharmacol. Biol. Psychiatry* 77, 99–109. doi: 10.1016/j.pnpbp.2017.04.008

Warwick, Z. S., and Weingarten, H. P. (1996). Flavor-postingestive consequence associations incorporate the behaviorally opposing effects of positive reinforcement and anticipated satiety: implications for interpreting two-bottle tests. *Physiol. Behav.* 60, 711–715. doi: 10.1016/0031-9384(96)00087-x

Weissman, M. M., Bland, R., Joyce, P. R., Newman, S., Wells, J. E., and Wittchen, H. U. (1993). Sex differences in rates of depression: cross national perspectives. *J. Affect. Disord.* 29, 77–84. doi: 10.1016/0165-0327(93)90025-f

Wellman, C. L., Bangasser, D. A., Bollinger, J. L., Coutellier, L., Logrip, M. L., Moench, K. M., et al. (2018). Sex differences in risk and resilience: stress effects on the neural substrates of emotion and motivation. *J. Neurosci.* 38, 9423–9432. doi: 10.1523/JNEUROSCI.1673-18.2018

WHO. (2020). *Depression: World Health Organization [Fact Sheet]*. World Health Organization. Available online at: https://www.who.int/news-room/fact-sheets/detail/depression Accessed May 3, 2020.

Willner, P., and Belzung, C. (2015). Treatment-resistant depression: are animal models of depression fit for purpose? *Psychopharmacology* 232, 3473–3495. doi: 10.1007/s00213-015-4034-7

Willner, P., Muscat, R., and Papp, M. (1992). Chronic mild stress-induced anhedonia: a realistic animal-model of depression. *Neurosci. Biobehav. Rev.* 16, 525–534. doi: 10.1016/s0149-7634(05)80194-0

Willner, P., Towell, A., Sampson, D., Sophokleous, S., and Muscat, R. (1987). Reduction of sucrose preference by chronic unpredictable mild stress and its restoration by a tricyclic antidepressant. *Psychopharmacology* 93, 358–364. doi: 10.1007/bf00187257

Wright, R. L. (2015). *Anhedonia and Other Reward-Related Deficits in Animal Models of Psychiatric Disorder*. Cardiff University. Available online at: http://orca.cf.ac.uk/90987/1/2016WrightPhd.pdf.

Wright, R. L., Gilmour, G., and Dwyer, D. M. (2013). Microstructural analysis of negative anticipatory contrast: a reconsideration of the devaluation account. *Learn. Behav.* 41, 353–359. doi: 10.3758/s13420-013-0110-1

Wu, H., Mata, J., Furman, D. J., Whitmer, A. J., Gotlib, I. H., and Thompson, R. J. (2017). Anticipatory and consummatory pleasure and displeasure in major depressive disorder: an experience sampling study. *J. Abnorm. Psychol.* 126, 149–159. doi: 10.1037/abn0000244

Conflict of Interest: RW received a BBSRC CASE studentship cofunded by Eli Lilly & Co., DD has supervised two PhD students cofunded by Eli Lilly & Co., and GG is employed by Eli Lilly & Co. The authors declare that they have no other potential conflicts of interest, financial or otherwise, related to this work.

frontiers in Behavioral Neuroscience

ORIGINAL RESEARCH
published: 30 September 2020
doi: 10.3389/fnbeh.2020.00160

Blast-Related Mild TBI Alters Anxiety-Like Behavior and Transcriptional Signatures in the Rat Amygdala

Jennifer Blaze[1,2], *Inbae Choi*[3], *Zhaoyu Wang*[1,2], *Michelle Umali*[1,2], *Natalia Mendelev*[1,2], *Anna E. Tschiffely*[4], *Stephen T. Ahlers*[4], *Gregory A. Elder*[2,5,6,7], *Yongchao Ge*[6] *and Fatemeh Haghighi*[1,2,3,5]*

[1]*Department of Neuroscience, Icahn School of Medicine at Mount Sinai, New York, NY, United States,* [2]*Friedman Brain Institute, Icahn School of Medicine at Mount Sinai, New York, NY, United States,* [3]*Research and Development Service, James J. Peters Veterans Affairs Medical Center, Bronx, NY, United States,* [4]*Department of Neurotrauma, Operational and Undersea Medicine Directorate, Naval Medical Research Center, Silver Spring, MD, United States,* [5]*Department of Psychiatry, Icahn School of Medicine at Mount Sinai, New York, NY, United States,* [6]*Department of Neurology, Icahn School of Medicine at Mount Sinai, New York, NY, United States,* [7]*Neurology Service, James J. Peters Veterans Affairs Medical Center, Bronx, NY, United States*

OPEN ACCESS

Edited by:
Tamas Kozicz,
Mayo Clinic, United States

Reviewed by:
Balazs Gaszner,
University of Pécs, Hungary
Michael Shaughness,
Uniformed Services University of the Health Sciences, United States

***Correspondence:**
Fatemeh Haghighi
fatemeh.haghighi@mssm.edu

***Specialty section**:*
This article was submitted to Pathological Conditions, a section of the journal Frontiers in Behavioral Neuroscience

Received: *22 May 2020*
Accepted: *11 August 2020*
Published: *30 September 2020*

Citation:
Blaze J, Choi I, Wang Z, Umali M, Mendelev N, Tschiffely AE, Ahlers ST, Elder GA, Ge Y and Haghighi F (2020) Blast-Related Mild TBI Alters Anxiety-Like Behavior and Transcriptional Signatures in the Rat Amygdala. Front. Behav. Neurosci. 14:160. doi: 10.3389/fnbeh.2020.00160

The short and long-term neurological and psychological consequences of traumatic brain injury (TBI), and especially mild TBI (mTBI) are of immense interest to the Veteran community. mTBI is a common and detrimental result of combat exposure and results in various deleterious outcomes, including mood and anxiety disorders, cognitive deficits, and post-traumatic stress disorder (PTSD). In the current study, we aimed to further define the behavioral and molecular effects of blast-related mTBI using a well-established (3 × 75 kPa, one per day on three consecutive days) repeated blast overpressure (rBOP) model in rats. We exposed adult male rats to the rBOP procedure and conducted behavioral tests for anxiety and fear conditioning at 1–1.5 months (sub-acute) or 12–13 months (chronic) following blast exposure. We also used next-generation sequencing to measure transcriptome-wide gene expression in the amygdala of sham and blast-exposed animals at the sub-acute and chronic time points. Results showed that blast-exposed animals exhibited an anxiety-like phenotype at the sub-acute timepoint but this phenotype was diminished by the chronic time point. Conversely, gene expression analysis at both sub-acute and chronic timepoints demonstrated a large treatment by timepoint interaction such that the most differentially expressed genes were present in the blast-exposed animals at the chronic time point, which also corresponded to a *Bdnf*-centric gene network. Overall, the current study identified changes in the amygdalar transcriptome and anxiety-related phenotypic outcomes dependent on both blast exposure and aging, which may play a role in the long-term pathological consequences of mTBI.

Keywords: mTBI, amygdala, blast, anxiety, transcriptome

INTRODUCTION

Traumatic brain injury (TBI) affects 1.7 million Americans each year according to the Centers for Disease Control and Prevention (Faul et al., 2010). Between 2000 and 2019 over 300,000 members of the United States Armed Forces were diagnosed with TBI, and of these 82.8% were diagnosed with mild TBI (mTBI; Defense and Veterans Brain Injury Center, 2019). It has also been suggested that these injury rates are likely to be underestimated (Chase and Nevin, 2014). The modes of injury that can result in mTBI vary from exposure to improvised explosive devices to closed head injuries. Of particular interest to the Veteran population are the long-term sequelae of mTBI, which can include mood and anxiety disorders, posttraumatic stress disorder, heightened suicidality, and diminished cognitive capacity with deficits in attention and memory. Also, there is a growing concern for the long-term neuropathological consequences following repeated exposure to physically traumatic events such as chronic traumatic encephalopathy (CTE). With such a large number of returning Veterans sustaining TBI, understanding the molecular circuitry involved in the long-term sequalae resulting from TBI is critically important to the health and productivity of our Military and Veteran population.

Various animal models have been established to study TBI-related pathology, including direct exposure to live explosives and controlled blast waves from compressed air generators, with the use of these models increasing in recent years. In particular, our group has developed a model of blast overpressure in rats (Ahlers et al., 2012) to explore the pathology and molecular outcomes resulting from mild blast injury (Elder et al., 2012; Haghighi et al., 2015; Gama Sosa et al., 2019). High-level blast exposure is associated with hemorrhagic lesions as well as histological effects including axonal, glial, microglial, and myelin changes (Elder et al., 2010). Until recently, the animal models have mainly used powerful high-level blast exposures capable of causing extreme intracranial damage, but our collaborative efforts and other groups have now begun to investigate the effects of a lower-intensity blast model known as repeated blast overpressure (rBOP). The mild nature of this animal model seems to more closely resemble human blast exposure in current war zones and operational settings (Moochhala et al., 2004; Saljo et al., 2010; Park et al., 2011; Pun et al., 2011; Rubovitch et al., 2011). Our group previously found that chronic and persistent behavioral effects can be found in rats months after rBOP, including increased anxiety-like behavior consistent with the manifestation of PTSD-like symptoms (Elder et al., 2012).

Behavioral phenotypes following mTBI in both rodents and humans have been associated with changes in gene expression in the brain and periphery (Gill et al., 2017). Modulation of gene expression is one way the brain creates new homeostasis in response to experience, including response to injury, making transcriptomic analyses following mTBI a particularly interesting area of study. As previously described, the advent of animal models of mTBI, such as our rBOP model, has allowed us to query the rodent brain transcriptome following blast injury. Our group previously found changes to neuronal gene expression and DNA methylation in the rat frontal cortex following rBOP. Transcriptional changes are present following blast exposure in the rodent frontal cortex (Hayes et al., 1995; Haghighi et al., 2015) and hippocampus (Phillips and Belardo, 1992; Hayes et al., 1995; Hua Li et al., 2004; Tweedie et al., 2013; Luo et al., 2017), but transcriptional changes in other brain regions important in emotion and learning, such as the amygdala, have not yet been investigated.

The majority of work investigating rodent models of TBI has focused on more sub-acute changes to behavior or structural/functional changes in the brain (days to weeks following blast), but more recent studies from our group suggest that deleterious effects of mTBI are long-lasting or may emerge 8–10 months following the blast exposure (Perez-Garcia et al., 2016; Gama Sosa et al., 2019). The long-term outcomes of mTBI are of particular interest due to the high levels of neurodegenerative disorders in aging, mTBI-exposed Veterans (Elder, 2015).

In the current study, we sought to replicate and extend previous findings (Elder et al., 2012) by determining both the sub-acute and chronic effects of rBOP in a similar rodent model. Specifically, we chose to investigate anxiety-like and cognitive behavior induced by rBOP and aimed to correlate these changes to transcriptional changes in the rodent amygdala, which has been shown to exhibit molecular, functional, and structural alterations following TBI and mTBI in humans (Depue et al., 2014; Han et al., 2015) and animal models (Elder et al., 2012; Heldt et al., 2014; Palmer et al., 2016; Hall et al., 2017; Hubbard et al., 2018). We hypothesized that rBOP would produce increased anxiety-like behavior, enhanced fear learning, and significantly alter gene expression in the amygdala, with the most drastic changes in aged rats that experienced rBOP. Identifying aberrant regulation of gene expression and behavior immediately following rBOP or months following exposure is critical in revealing molecular mechanisms leading to the manifestation of psychopathology, and possibly neuropathology, later in life.

MATERIALS AND METHODS

Subjects

All study procedures were approved by Institutional Animal Care and Use Committees of the Naval Medical Research Center and the James J. Peters Veterans Administration (VA) Medical Center, and were conducted in conformance with Public Health Service policy regarding the humane care and use of laboratory animals and the National Institutes of Health (NIH) Guide for the Care and Use of Laboratory Animals. Specifically, male Long Evans rats weighing between 250–300 grams and approximately 10–12 weeks of age (Charles River Laboratories International, Inc., Wilmington, MA, USA) were utilized as subjects. NMRC's animal housing rooms were maintained at a temperature between 17.8–26°C, humidity level between 30–70%, and 12:12 light-dark cycle. JJPVAMC's animal housing rooms were maintained at a temperature between 21–22°C, humidity level between 30–70%, and 12:12 light-dark cycle. In

both facilities, animals were individually housed in standard clear plastic cages complete with Bed-O'Cobs (The Andersons, Inc., Maumee, OH, USA) bedding and EnviroDri nesting article (Sheppard Specialty Articles, Milford, NJ, USA) with food and water provided *ad libitum*.

Repeated Blast Overpressure Exposure (rBOP)

Rats were exposed to multiple BOP events with the Walter Reed Army Institute of Research (WRAIR) shock tube as described previously (Elder et al., 2012). Animals were handled for 2 min a day for the 2 days before the beginning of the blast procedure which itself requires handling for the 3 days of blast exposure. For the rBOP procedure, animal subjects were anesthetized with 5% isoflurane gas for at least 2 min, outfitted with plastic restraint cones, and positioned in the shock tube's animal holder. Animals were situated prone (dorsal side up), facing the direction of the blast wave emitted by the WRAIR shock tube. The head, upper torso, and lower torso areas of the subjects were further secured with three rubber tourniquets to restrict movement without hindering respiration. Subjects assigned to blast-exposed groups received a single 74.5 kPa (≈10.8 psi) BOP event every 24 h for 72 h. Control subjects were treated identically to blast-exposed subjects barring the BOP exposures. After sham or blast treatment, subjects were placed in boxes and transferred from NMRC to JJPVAMC within 10 days *via* approved commercial transport carrier. Upon arriving at JJPVAMC, the sub-acute cohort of animals was acclimated to the facility for seven days after which they were handled three times a week for 2 weeks before the onset of the behavioral assessment battery. The chronic cohort remained in the JJPVAMC facility for 12–14 months before being handled three times a week for 2 weeks before the onset of the behavioral assessment battery.

Behavioral Assessment Battery

For the characterization and assessment of behavioral changes that emerge after rBOP exposure, the study employed a condensed form of a previously described behavioral assessment battery that has been shown to possess utility in profiling the multi-faceted behavioral phenotypes associated with blast exposure (Elder et al., 2012). Rats were tested at both a sub-acute (1–1.5 months following rBOP) and chronic (12–14 months following rBOP) timepoints (**Figure 1A**). The streamlined battery of tests consisted of 4–6 of the nine tasks from the original behavioral assessment battery—including the open field test (OFT), novel object recognition, light/dark box, elevated zero maze (EZM), prepulse inhibition (PPI) and fear conditioning (see cohort-specific behavioral tests in **Figure 1A**). Note that novel object recognition and PPI were not performed in the chronic cohort because no blast-related effects were found in the acute cohort, and we opted to focus only on the anxiety-related traits for which we had prior robust findings chronically in this paradigm (Elder et al., 2012). Therefore, we do not report findings for novel object recognition or PPI in the current manuscript as they do not directly relate to anxiety-like phenotypes.

Open Field Test (OFT)

Locomotor function and anxiety-like behaviors were assessed in the OFT for 10 min for two consecutive days (only Day 1 reported). For the sub-acute cohort, the open field apparatus was a 48 × 48 cm square. Because of the significantly larger size of the aged rats in the chronic cohort (**Figure 1C**; no differences between treatment groups), we used a larger chamber. The apparatus comprised a white 120 × 120 cm square base and white 60 cm-high walls. The "center" of the open field arena measured 3,600 cm^2; the center region was determined by dividing the base into 16 identical 30 × 30 cm squares and selecting the four most central squares. Animals were acclimated to the testing room for 1 h before beginning the task. At the start of each trial, subjects were positioned in the corner of the apparatus facing away from the center of the open field. Data were automatically acquired by ANY-Maze software (Stoelting Co., Wood Dale, IL, USA). The apparatus was cleaned before and between trials first with Clidox, then with 70% ethanol.

Light/Dark Box

We also used the light/dark box as another measure of anxiety-like behavior. The arena was an opaque black Plexiglas box (40 × 40 cm) enclosing the right half of the interiors so that only the left side was illuminated. Animals were allowed a 60 min habituation period to the chamber on day 1, and on day 2 animals were placed in the dark compartment and allowed to freely explore for 10 min with access to the light side through an open doorway located in the center of the divider. Beam breaks at the ground level were used to detect motion in the dark vs. light side using Versamax activity monitor. We measured the time spent in the light side of the chamber as an index of anxiety-like behavior. The apparatus was cleaned before and between trials first with Clidox, then with 70% ethanol.

Elevated Zero Maze (EZM)

To further assess anxiety-like behaviors, subjects were tested on the EZM for 5 min for two consecutive days (only Day 1 reported). The EZM apparatus (San Diego Instruments, San Diego, CA, USA) was a 5.1 cm-wide, black, acrylic, annular platform that measures 61 cm in diameter placed 61 cm above floor level. The platform was equally divided into two pairs of walled (closed) and un-walled (open) quadrants such that the opposite quadrants were identical. Animals were acclimated to the testing room for 1 h before beginning the task. At the start of each trial, subjects were placed in the closed arm closest to the door facing away from the investigator. The number of animals tested for EZM was slightly smaller than other behavioral tasks in the chronic cohort because some animals from both blast and sham conditions were unable to complete this task due to body size (with no group difference in the completion rate). All trials were recorded with a video camera mounted overhead and data were automatically acquired by ANY-Maze. The maze was cleaned before and between trials first with Clidox, then with 70% ethanol.

Cued and Contextual Fear Conditioning

Cognitive functions related to associative fear learning were evaluated using cued and contextual fear conditioning as we

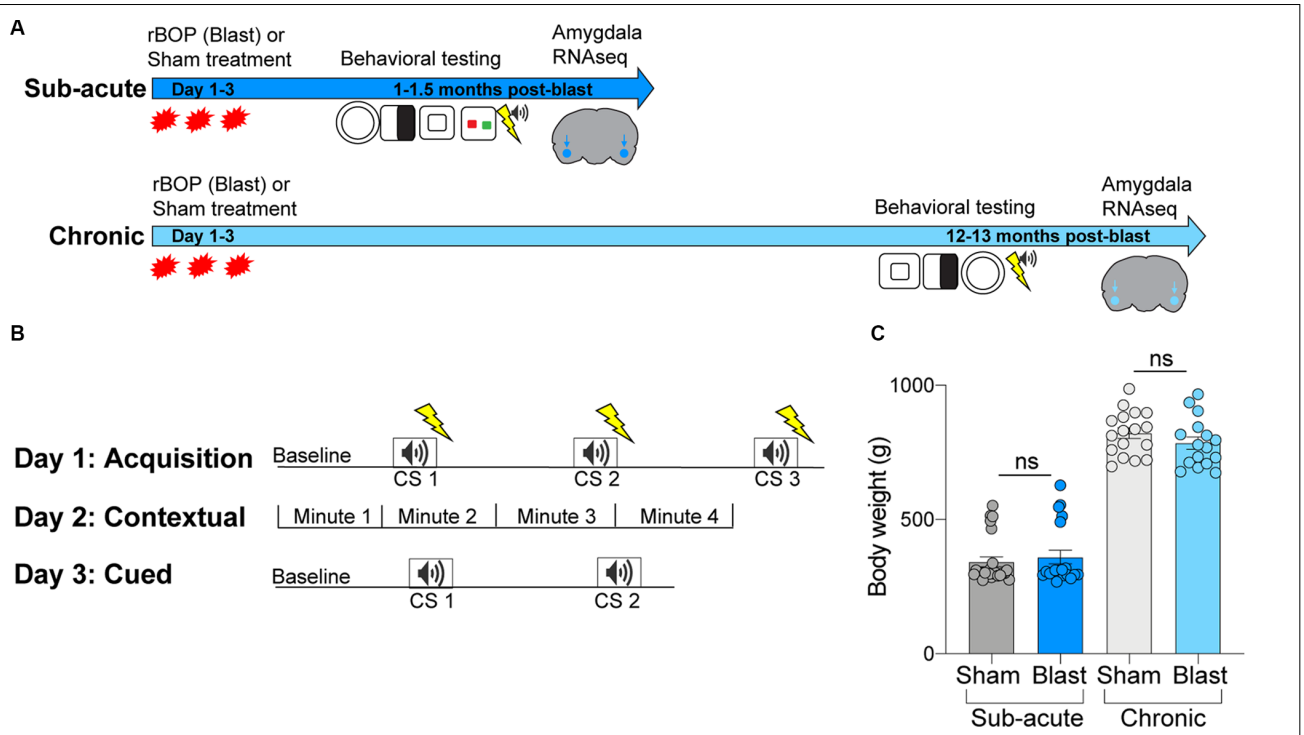

FIGURE 1 | Methodologies for blast exposure and behavioral testing. **(A)** Timeline for blast exposure, behavioral experiments, and tissue collection for the sub-acute and chronic cohorts. **(B)** Schematic of fear conditioning protocols, including acquisition, cued, and contextual fear conditioning. **(C)** Body weights of sub-acute and chronic cohorts at time of sacrifice (ns, not statistically significant; error bars represent SEM).

have described previously (Elder et al., 2012). In brief, the fear conditioning procedure consists of three parts and is conducted over 3 days (**Figure 1B**). The procedure utilized a rodent conditioning chamber (Coulbourn Instruments, Inc., Lehigh Valley, PA, USA) equipped with a grid floor shocker and positioned within a sound-attenuating cubicle. Our paradigm used a 2-s long foot shock (0.7 mA) as the unconditioned stimulus (US) and a 20-s long, 2 kHz, 80 dB tone as the conditioned stimulus (CS). On day 1, subjects underwent a training trial that paired the conditioned stimulus (CS) and the unconditioned stimulus (US). On day 2, contextual fear conditioning was evaluated by testing subjects in the same environment as the training trial without any presentation of CS and/or US. Finally, on day 3, cued fear conditioning was tested by placing animals in a novel environment with presentations of the CS but not US. Freezing responses were recorded and quantified using Freeze Frame video tracking software (Actimetrics, Coulbourn Instruments, Incorporation).

Tissue Collection and Processing

Subjects were sacrificed ∼1–2 weeks after the last behavioral test by rapid decapitation under light anesthesia (4% isoflurane). Whole brains were extracted and flash frozen in methyl butane chilled with dry ice. Frozen brains were subsequently coronally sectioned using a 1 mm brain matrix. Sections were gently brushed onto slides and stored at −80°C. Bihemispheric tissue samples of the central nucleus/ basolateral (CeA/BLA) amygdala were collected for each subject using 1.50-mm tissue punches and stored for downstream processing. Punches were taken between approximately −2.6 mm and −3.2 mm from Bregma (Campolongo et al., 2009).

RNA Isolation and Sequencing

Amygdala samples were homogenized in 400 µl of DNA/RNA Lysis Buffer as per the manufacturer's instructions (Zymo Research Incorporation). Purified total RNA samples were aliquoted and stored at −80°C until submission for RNA sequencing. RNA sequencing libraries were prepared using the KAPA Stranded RNA-Seq Kit with RiboErase (Kapa Biosystems) following the manufacturer's instructions and sequenced on an Illumina HiSeq2500 sequencer (v4 chemistry) using 2 × 50 bp cycles. The alignment was done with STAR 2.4.2a. STAR index was created using a splice junction annotation database for guidance and both genome sequence and annotation files of Ensembl Rnor 6.0. Quantification of gene expression was achieved through featureCounts 1.4.3-p1 with Ensembl Rnor 6.0 annotation. The RNA-seq data are available on the GEO database under the accession code GSE155393.

Statistical and Bioinformatics Analyses

Behavioral Assessment Analyses

Statistical analyses were performed with Graphpad Prism software. To compare group differences between sham and blast animals in the sub-acute and chronic cohorts, we used unpaired *t*-tests (OFT, EZM, and baseline freezing for fear conditioning).

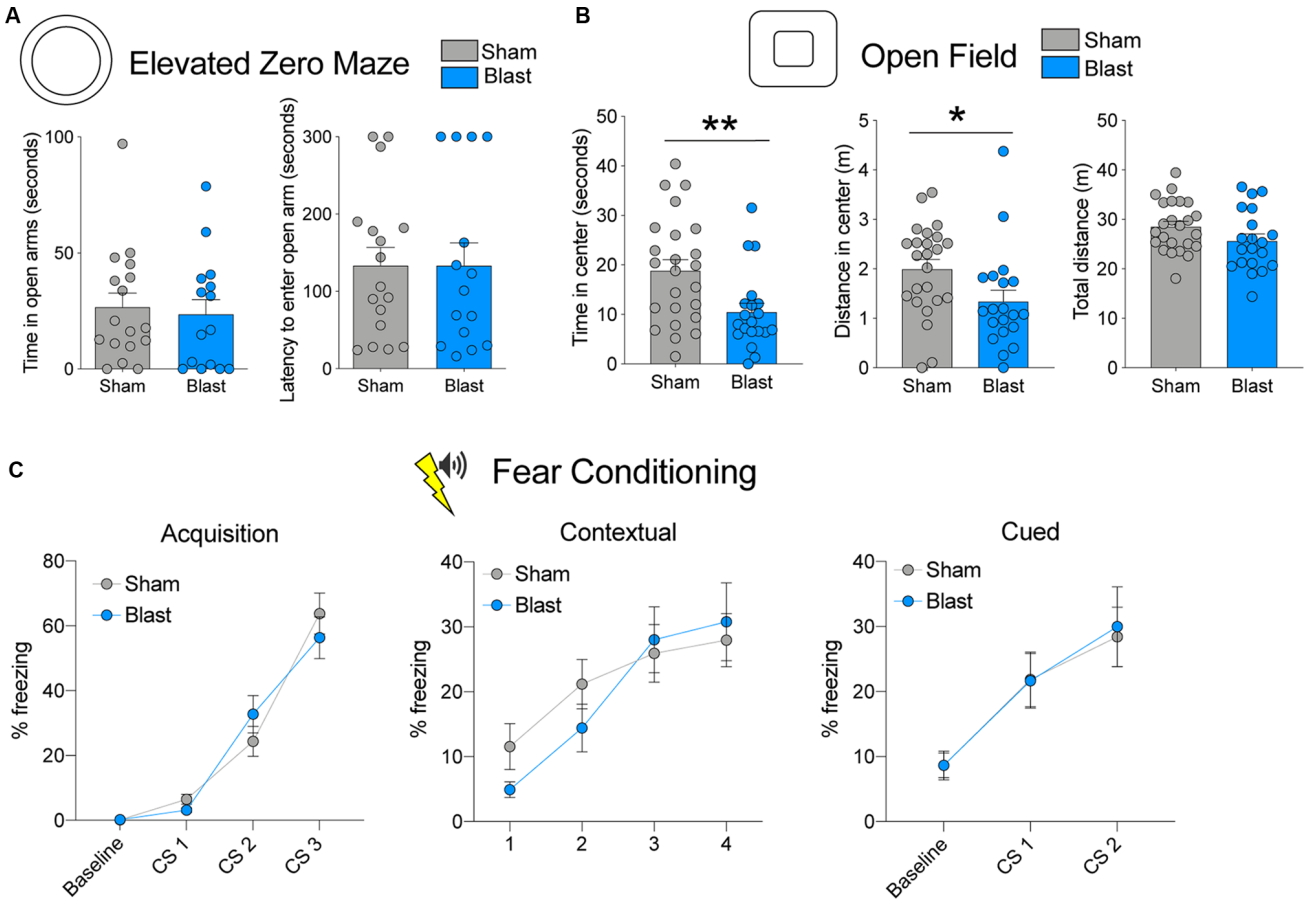

FIGURE 2 | Behavioral testing results for the sub-acute cohort. **(A)** Time spent in open arms and latency to enter open arms for the elevated zero maze (EZM). **(B)** Time spent in the center, distance traveled in the center, and total distance traveled in the open field test (OFT). **(C)** Percent freezing levels during acquisition, contextual fear testing, and cued fear testing (error bars represent SEM; $^{**}p < 0.01$, $^{*}p < 0.05$).

Because the aforementioned statistical tests require normal distribution and equal variance between groups, we performed an F-test of variance and a Kolmogorov-Smirnov test (to test normality) for each dataset and only performed the stated tests if $p > 0.05$ for variance and normality tests. If data was not normally distributed according to the Kolmogorov–Smirnov test, we used the Mann–Whitney test or Wilcoxon test to compare ranks. For fear conditioning data, we used two-way repeated-measures (RM) ANOVAs (acquisition, cued, and contextual fear conditioning) with the Geisser-Greenhouse correction to account for unequal variance and non-normal distribution of data. Statistical significance was denoted at $p < 0.05$, and nominal changes approaching significance were considered trending and denoted at $p < 0.1$.

RNA Sequencing Analyses

To analyze transcriptome-wide gene expression changes in rat amygdala, a simple linear model was used to compare different conditions (blast vs. sham exposure) or time (chronic vs. sub-acute time-point) using the voom method (Law et al., 2014) in the Bioconductor (Gentleman et al., 2004) package Limma (Ritchie et al., 2015). We identified differentially expressed genes with a logFC between −1.2 and + 1.2 and with raw or adjusted p-values < 0.05 (**Figure 4**). To assess differences in variability of amygdala gene expression between conditions as well as time, variance ratios were calculated and histograms were generated (**Figure 4**), and the Kolmogorov-Smirnov test was used to compare two distributions. Furthermore, interaction plots were created to depict the interaction between treatment and timepoint for candidate genes previously implicated in neurodegeneration and neurotrauma (**Figure 5**).

We also used Ingenuity Pathway Analysis (IPA[1]; Qiagen, Inc.) for the identification of canonical pathways and detection of significant gene networks. The causal network analysis identified functional enrichment of gene categories for our datasets, and each category was considered significantly activated (or inhibited) if overlap p-value < 0.05 (correcting for multiple testing *via* the Benjamini–Hochberg method (Benjamini and Hochberg, 1995)) and if the activation z-score was between −2 and + 2. Detailed descriptions of IPA analysis are available on the Qiagen website.

[1]www.ingenuity.com

RESULTS

rBOP Exposure Increases Anxiety-Like Behavior in a Sub-acute Manner but With Diminished Behavioral Effects in the Chronic Cohort

To measure anxiety-like behavior in rats that were exposed to rBOP or sham treatment, we used the EZM (n = 17 sham, 15 blast) and OFT (n = 24 sham, 20 blast), which are both well-characterized in detecting anxiety-like behavior in rodent models. In the sub-acute cohort of rats, which were tested 1–1.5 months following rBOP or sham treatment, we did not detect changes in anxiety-like behavior in the EZM (time in open arms: $t_{(30)} = 0.3594$, $p = 0.722$, latency: $t_{(30)} = 0.000$, $p = 0.999$; **Figure 2A**) or the light/dark box (**Supplementary Figure S1A**, Mann–Whitney $U = 230.5$, $p = 0.828$). In the OFT, however (**Figure 2B**), blast animals showed increased anxiety compared to sham controls, spending less time in the center (Mann–Whitney $U = 131$, $p = 0.009$) and traveling less distance in the center compared to sham animals (Mann–Whitney $U = 131$, $p = 0.009$), with no significant change in total distance traveled in the arena ($t_{(42)} = 1.697$, $p = 0.097$).

We also tested fear-related cognitive behavior in the same animals using cued and contextual fear conditioning (n = 24 sham, 20 blast; **Figure 1B**; **Figure 2C**). There were no differences between sham and blast conditions in baseline freezing levels (Mann–Whitney $U = 230$, $p = 0.776$). For the acquisition phase, a two-way repeated-measures ANOVA revealed an effect of CS presentation ($F_{(1.697,71.25)} = 74.77$, $p < 0.001$), showing that both groups were able to learn the association between tone and shock pairing, but there was no effect of blast treatment ($F_{(1,42)} = 0.037$, $P = 0.855$) or CS × blast treatment interaction ($F_{(2,84)} = 1.635$, $p = 0.201$). There were likewise no effects of blast treatment on freezing in contextual (two-way RM ANOVA treatment effect ($F_{(1,42)} = 0.209$, $p = 0.650$) or cued (two-way RM ANOVA treatment effect $F_{(1,42)} = 0.015$, $p = 0.904$) fear conditioning tests (**Figure 2C**). We ruled out the effects of blast-induced impairments of auditory functioning on fear conditioning due to auditory startle responses being intact during PPI testing for both sham and blast groups (data not shown).

To identify whether the same changes in anxiety-like behavior were present in a chronic manner following rBOP, we performed the same tests on a cohort of subjects that were left undisturbed for 12–13 months following rBOP (**Figure 3**). Attrition rates

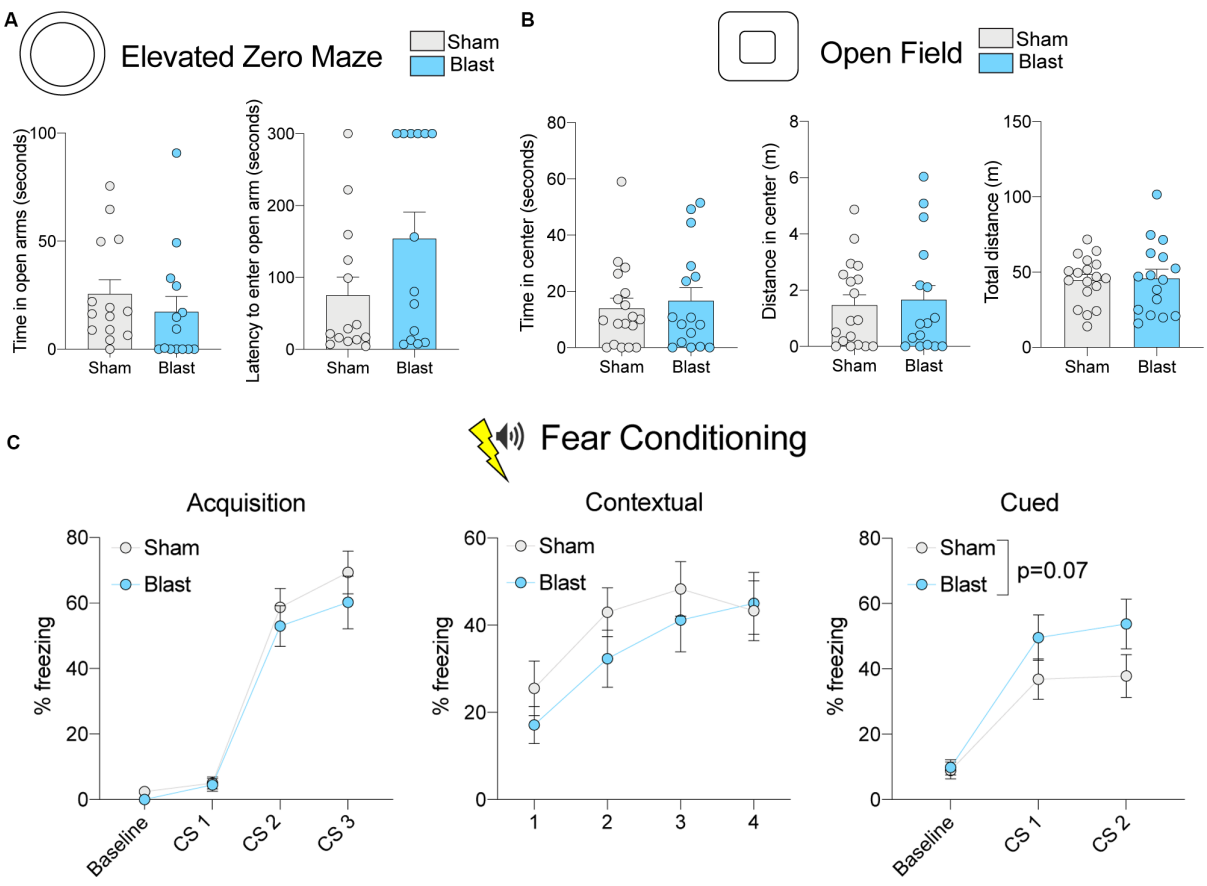

FIGURE 3 | Behavioral testing results for the chronic cohort. **(A)** Time spent in open arms and latency to enter open arms for the EZM. **(B)** Time spent in the center, distance traveled in the center, and total distance traveled in the OFT. **(C)** Percent freezing levels during acquisition, contextual fear testing, and cued fear testing. *P*-value corresponds to the main effect of blast treatment (error bars represent SEM).

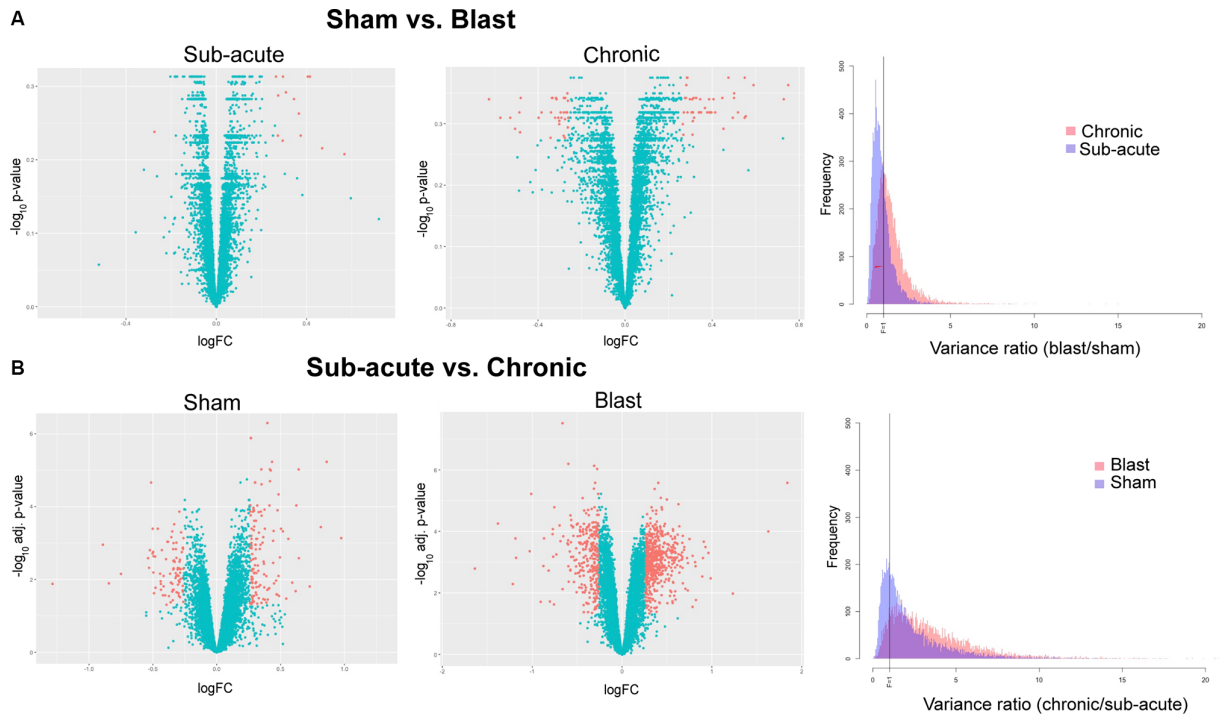

FIGURE 4 | Differentially expressed genes and variance ratios. Volcano plots depicting differentially expressed genes (orange; |logFC| ≥ 1.2 and raw or adjusted *p*-values ≤ 0.05) between **(A)** blast vs. sham animals within the sub-acute and chronic cohorts and **(B)** chronic vs. sub-acute time points with the sham and blast groups. Histograms depicting variance ratios to demonstrate variability within gene expression are also shown.

did not differ between the blast and sham animals (three sham and four blast animals died before chronic behavioral testing timepoint). In the EZM (n = 14 sham, 14 blast; **Figure 3A**), there was no effect of blast treatment on time in the open arms (Mann–Whitney U = 65, p = 0.134) or latency to enter an open arm (Mann–Whitney U = 70, p = 0.206). While there were no significant effects on the EZM, it should be noted that six out of 14 rats (43%) in the blast condition did not enter an open arm during the entire session while only 1 of the 14 sham rats (7%) did not enter an open arm during the session, suggesting a possible increase in anxiety-like behavior in the blast treatment chronic cohort. There were also no significant effects of treatment in the chronic cohort for any measures in the OFT (n = 18 sham, 16 blast; **Figure 3B**), including time in the center (Mann–Whitney U = 141, p = 0.925), distance traveled in the center (Mann–Whitney U = 142.5, p = 0.966), and total distance traveled in the arena ($t_{(32)}$ = 0.1797, p = 0.858). As noted previously in the "Materials and Methods" section, a larger open field chamber was used for the chronic cohort of animals due to a much larger body size after aging, although there were no differences in body weight between blast and sham in the sub-acute (Mann–Whitney U = 221, p = 0.662) or chronic ($t_{(31)}$ = 1.227, p = 0.229) cohort at the time of sacrifice (**Figure 1C**). We also found no effects of blast treatment on time in the center of the light-dark box (**Supplementary Figure S1**; Mann–Whitney U = 101, p = 0.195).

We likewise tested fear-related associative learning in the chronic cohort of animals using cued and contextual fear conditioning (n = 18 sham, 15 blast; **Figure 1B**; **Figure 3C**). During the acquisition phase, blast animals had a lower level of baseline freezing (Mann–Whitney U = 64.5, p = 0.002). Additionally, during the acquisition phase, a two-way RM ANOVA revealed an effect of CS presentation on freezing ($F_{(1.736,53.81)}$ = 78.70, $p < 0.001$), showing that both groups were able to learn the association between tone and shock pairing, but there was no effect of blast treatment ($F_{(1,31)}$ = 1.041, p = 0.316) or interaction between CS and blast treatment ($F_{(2,62)}$ = 0.3486, p = 0.707). There were also no significant differences in freezing between sham and blast groups in the contextual fear conditioning test (two-way RM ANOVA treatment effect $F_{(1,31)}$ = 0.7681, p = 0.388; **Figure 3C**). In the cued fear conditioning test, blast animals showed a trending increase in freezing upon exposure to the cue that was previously paired with shock ($F_{(1,31)}$ = 3.638, p = 0.066; **Figure 3C**).

Blast Exposure Alters Gene Expression in the Amygdala Both Sub-acutely and Chronically

Due to the increase in anxiety-like behavior for blast animals that were present in a time-dependent manner, we measured gene expression in the amygdala, a brain region highly implicated in anxiety-like behavior, at both sub-acute and chronic time-points in sham and blast animals. We used next-generation sequencing to assess levels of mRNA transcripts in amygdala tissue and data showed a multitude of changes in transcript abundance

between groups. First, we compared transcriptomes of blast vs. sham animals within the sub-acute timepoint and found that 14 genes were significantly altered (raw $p < 0.05$) in the blast group compared to sham animals (13 upregulated, 1 downregulated) with none of these changes survived multiple testing correction (**Figure 4A**; all adjusted $p > 0.05$). Within the chronic time-point, we also found transcriptional changes, with 78 genes significantly altered (raw $p < 0.05$) in the blast group compared to sham (44 upregulated, 34 downregulated), and again none of these comparisons survived multiple testing correction (**Figure 4A**; all adjusted $p > 0.05$). We further examined the relative variability in gene expression by treatment group. Examining the relative gene expression ratios in blast vs. sham animals within the sub-acute and chronic timepoints respectively, we observed greater variability in gene expression profiles comparing sham and blast in the chronic time point (**Figure 4A**; Kolmogorov–Smirnov test, p-value < 0.001).

As expected due to the typical effects of aging, a large number of genes (215 total) were differentially expressed (adjusted $p < 0.05$) when we compared chronic vs. sub-acute time-points within the sham group (**Figure 4B**; 129 upregulated, 86 downregulated). Most striking were the effects of time-point within the blast group, where we found 845 genes differentially expressed (adjusted $p < 0.05$) in the chronic vs. sub-acute time-point within the blast group (**Figure 4B**; 562 upregulated, 283 downregulated). To capture the relative variability associated with blast-exposure longitudinally, we examined the variability in gene expression in chronic vs. sub-acute time points in blast and sham groups separately. Specifically, we computed the variance ratios in the chronic vs. sub-acute animals in each treatment group and found that the distribution of the variance ratios was significantly different between the blast and sham groups with the blast group showing greater variability (**Figure 4B**; Kolmogorov–Smirnov test, p-value < 0.001).

Gene Expression Changes Associated With Chronicity of Blast Exposure

While we found changes between sham and blast groups within both the sub-acute and chronic time points, the most significant change was the abundance of genes differentially expressed within the blast group when we compared chronic vs. sub-acute time points, suggesting an interaction between treatment and chronicity of exposure post-blast. In an exploratory analysis, we examined the interaction between treatment (blast vs. sham) by time-point (chronic vs. sub-acute). The *Plpp3* gene showed significant interaction for treatment by time effect ($p = 0.007$ adjusted for multiple testing). In addition to *Plpp3*, we also identified other loci that have been previously implicated in neurotrauma and neurodegeneration, including *Apoe, Reln, Vegfb*, and *Bdnf*, which likewise show interaction effects in this model (raw $p < 0.05$; **Figure 5**).

Gene Networks Associated With Chronicity of Blast Exposure

We also used Ingenuity Pathway Analysis (IPA; Qiagen, Inc.) to investigate enrichment of genes in known biological pathways using the differentially expressed genes that showed significant fold changes (adjusted $p < 0.05$) in the chronic vs. sub-acute time points within each of the treatment groups (blast and sham respectively; **Figure 4B**). We first compared genes differentially expressed in the chronic vs. sub-acute time points within the sham group, which should represent normal aging processes. Of the top 10 canonical pathways enriched in our dataset (**Figure 6A**), the majority were enriched for genes that code for enzymes and ion channels for opioid, GP6, and dopamine signaling. We conducted the same assessment for the chronic vs. sub-acute timepoint within the blast group and found an altered set of canonical pathways (**Figure 6A**), with the top hit being the GABA receptor signaling pathway, a pathway that was not enriched significantly ($p > 0.05$) in the sham dataset. This gene category included *Adcy1, Adcy8, Cacna1d, Cacna*1 h*, Cacng4, Gabrg1, Gad1, Gad2, Gnas, Kcnh2, Slc32a1, Slc6a1, Slc6a11*.

Because of the altered set of functionally enriched genes between our sham and blast groups when comparing time points, we used a Comparison Analysis on IPA to compare the gene networks that are significantly altered in the sham (chronic vs. sub-acute) dataset and the blast (chronic vs. sub-acute) dataset. We identified the top gene network for each condition (blast and sham) and both were enriched for genes involved in neurological disorders and organismal injury and showed a large overlap between the blast and sham conditions (**Figure 6B**). The most notable difference between these conditions was an oppositional effect on *Bdnf*, which is the hub of this gene network, and we had previously identified this as an important gene showing the interaction of treatment and age.

DISCUSSION

The short and long-term neurological and psychological consequences of mTBI are of immense interest to the Veteran community. In the current study, we aimed to further define the behavioral and molecular effects of blast-related mTBI using a well-established rBOP model in rats. We exposed adult male rats to the rBOP procedure and conducted behavioral tests for anxiety and fear conditioning at 1–1.5 months (sub-acute) or 12–13 months (chronic) following blast exposure.

In the cohort of animals tested at the sub-acute timepoint, there was a robust increase in anxiety-like behavior in the OFT (although no changes detected in the EZM), but no change in acquisition of fear learning or cued and contextual fear memory. In the chronic cohort, blast animals showed only a trending increase in anxiety-like behavior in the EZM and no change in fear memory acquisition, but a trending increase in freezing to a tone CS after cued fear conditioning. An increase in anxiety-like behavior has been shown in multiple rodent models of TBI (Meyer et al., 2012; Almeida-Suhett et al., 2014; Heldt et al., 2014; Davies et al., 2016; Zuckerman et al., 2016), including our own (Elder et al., 2012), and our current data are in line with these findings. As discussed previously, the majority of studies in the field measure anxiety at a relatively short time interval post-blast, and our sub-acute timepoint likewise shows a significant increase in anxiety 1.5–2 months post-blast. Conversely, we did not find a statistically significant change in anxiety-like

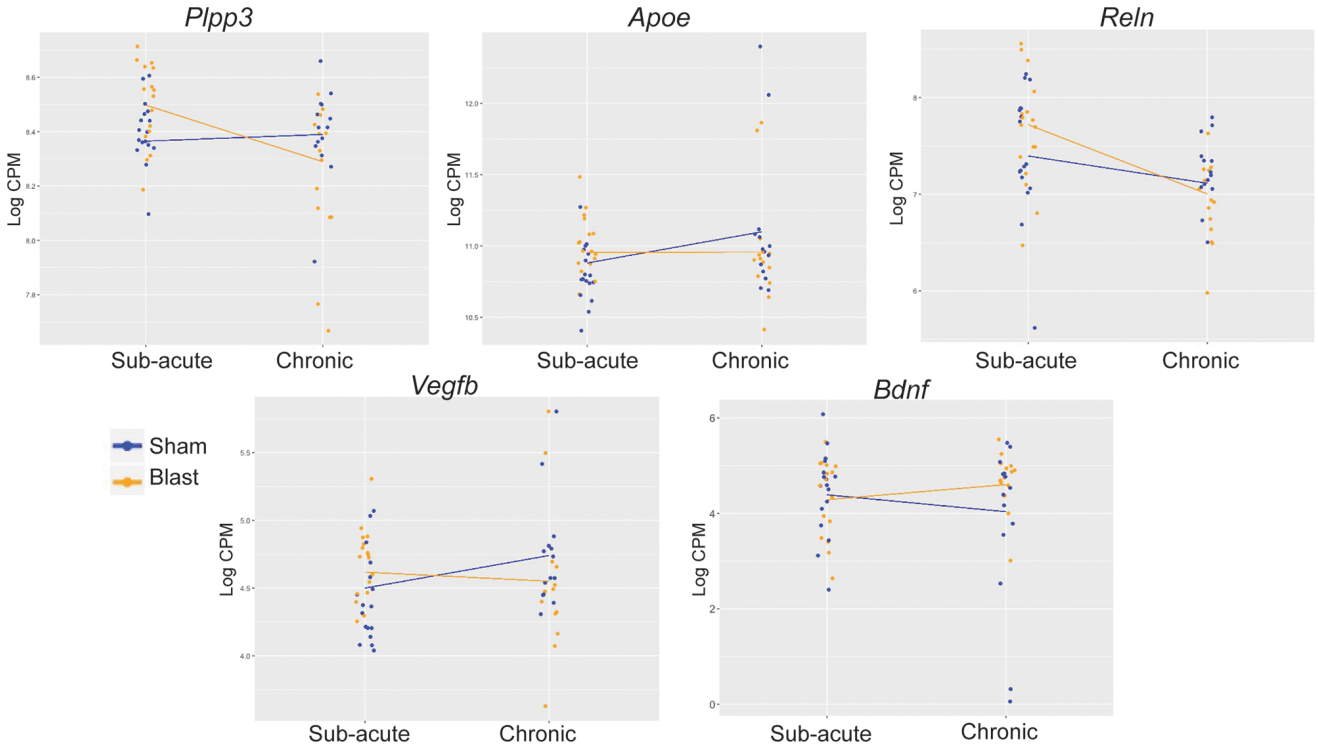

FIGURE 5 | Interaction plots for traumatic brain injury (TBI)- and neurodegeneration-associated candidate gene loci. Interaction analyses identified *Plpp3* as displaying a significant interaction between blast exposure and timepoint after correction for multiple testing (adj. p-value < 0.05). Of the other significant interactions (unadjusted $p < 0.05$), we chose to depict interaction plots for TBI- and neurodegeneration-related genes *Apoe, Vegfb, Reln*, and *Bdnf*.

behavior 12–13 months post-blast (chronic timepoint), which is in concordance with recent work showing that over time the anxiety-like phenotype is diminished over time, as shown by the EZM and other anxiety behavior tests (Popovitz et al., 2019). We also measured the acquisition of fear learning and both cued and contextual fear and found a trending effect of rBOP at chronic timepoint but no sub-acute effects. Some human studies (Glenn et al., 2017) and rodent models of the blast (Meyer et al., 2012; Davies et al., 2016) have found impaired fear acquisition following blast exposure, but there are still mixed findings of the effects of blast on cued and contextual fear recall (Elder et al., 2012; Meyer et al., 2012; Teutsch et al., 2018).

While an anxiety phenotype was not detected at the chronic time-point in our model, previous rodent studies from our lab (Perez-Garcia et al., 2016; Gama Sosa et al., 2019) and human studies (Glenn et al., 2017) suggest that long-term pathology exists following blast exposure that may contribute to the lasting deleterious effects of blast in the Veteran population. We chose to measure gene expression in the amygdala of rats that were exposed to rBOP because of the importance of this brain region in mTBI-related psychopathology, including anxiety and PTSD. An abundance of evidence exists that amygdala connectivity and structure is altered following exposure to TBI, leading to aberrant anxiety-like behavior (Han et al., 2015; Palmer et al., 2016; Tate et al., 2016; Popovitz et al., 2019). Changes in mRNA and protein levels for specific gene loci have also been identified in the rodent amygdala following TBI, including *Thy1* (Heldt et al., 2014), *Stathmin1* (Elder et al., 2012), and GABA-related proteins (Almeida-Suhett et al., 2014). We used a transcriptome-wide, unbiased approach to measure gene expression in the central/basolateral amygdala at a sub-acute and chronic time-point following rBOP. Within the sub-acute and chronic time points, we compared sham and blast conditions and found no differentially expressed genes that passed correction for multiple testing. Among the differentially expressed genes that had a p-value of <0.05 before correction, the chronic timepoint had a much larger abundance of differences, suggesting the amygdalar transcriptome is susceptible to more drastic changes after a significant delay post-injury.

Most notably we identified a strong interaction between blast condition and age. In comparison to the subtle effects between sham and blast at each time-point, when we compared the transcriptome of sham animals at the chronic vs. sub-acute time-points, we found an abundance of genes differentially expressed and surviving correction for multiple testing. These changes emphasize the large effect of aging on gene expression in the amygdala, and we identified significant alterations in expression levels of various genes that have previously been associated with normal aging and neurodegeneration, including *Gfap* (Rodríguez et al., 2014), *Vegfb* (Mahoney et al., 2019),

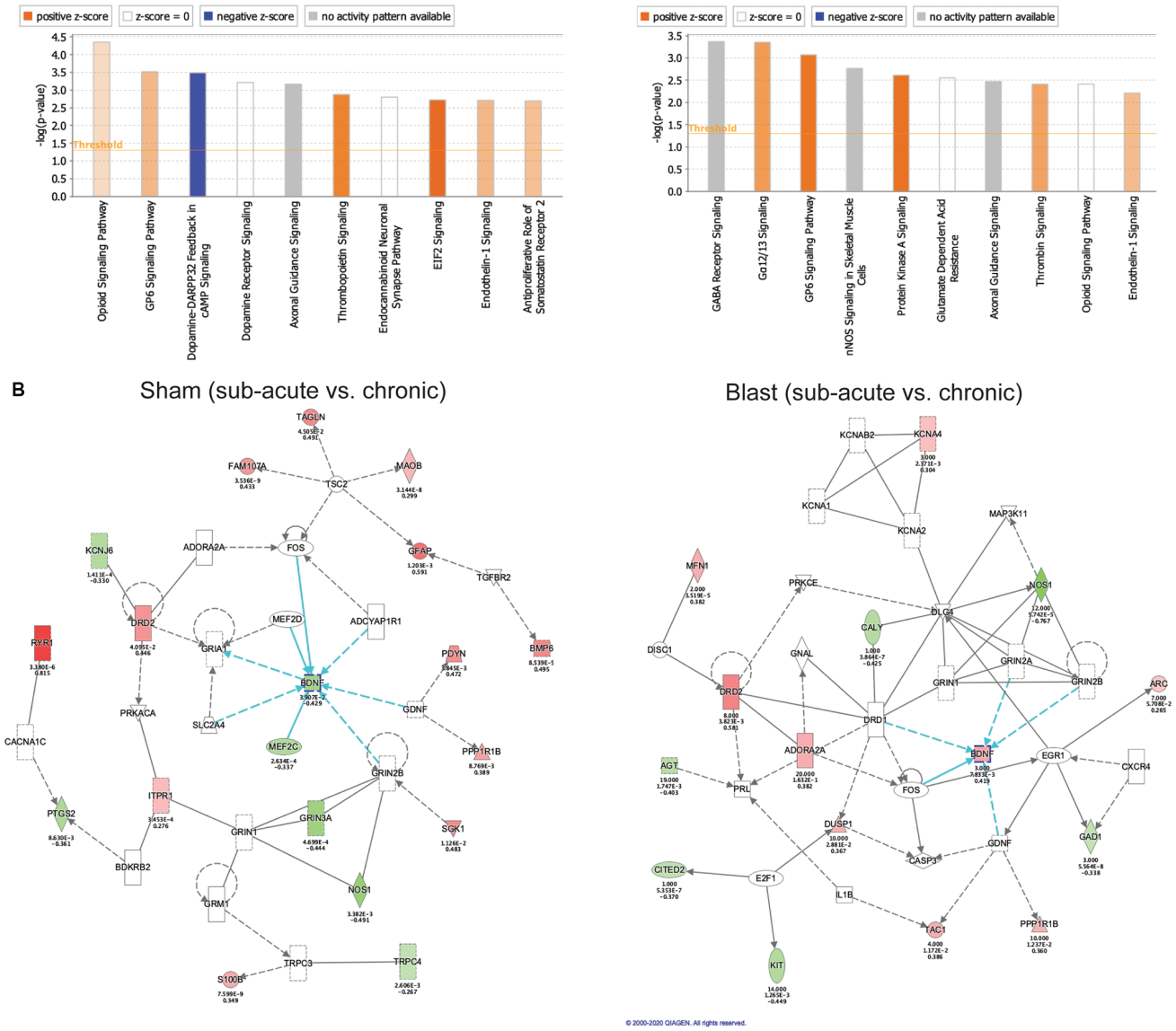

FIGURE 6 | Gene ontology enrichment using Ingenuity Pathway Analysis (IPA). **(A)** Top 10 gene categories. The y-axis gives the negative logarithm function of overlap *p*-value. Orange or blue bar represents a positive or negative activation z-score respectively, as calculated by IPA based on expected directionality of gene expression change within the gene category using the IPA knowledge base. White bars represent a z-score of 0 and gray bars signify that IPA was unable to calculate an activation z-score based on the unavailability of data in their knowledge base for that gene category. **(B)** Top gene network identified by IPA in the sham and blast cohorts comparing chronic vs. sub-acute time points. Green nodes within the network represent downregulated genes in our dataset and red nodes represent upregulated genes in our dataset. Nodes with no color represent IPA-generated genes using the IPA knowledge base. Blue arrows represent pathways interacting directly with *Bdnf* as a hub gene.

and *Bdnf* (Tapia-Arancibia et al., 2008; Guilloux et al., 2012). When we compared the chronic vs. sub-acute transcriptomes within the blast group, however, we identified the greatest number of differentially expressed genes, exemplifying the treatment by age interaction after mTBI, which we confirmed *via* interaction analyses. Significant interactions included *Plpp3*, which is enriched in the ventral midbrain and has been linked to dopaminergic functioning in the striatum but not yet linked to the amygdala function (Gómez-López et al., 2016). Of the abundant interactions that did not survive multiple testing correction, we chose to highlight four additional genes that have known roles in brain injury and/or amygdala functioning, including *Apoe* (Klein et al., 2014; Tang et al., 2015), *Reln* (Boyle et al., 2011; Frankowski et al., 2019), *Vegfb* (Wu et al., 2008; Savalli et al., 2014; Mahoney et al., 2019), and *Bdnf* (Wu et al., 2008; Guilloux et al., 2012; Sagarkar et al., 2017), which are all

crucial mediators of synaptic plasticity and neurotransmission as well as structure and function of brain vasculature. Interestingly, *Plpp3*, *Apoe*, *Reln*, and *Vegfb* show similar patterns of interaction, such that expression levels in blast animals are higher than sham animals at the sub-acute timepoint but lower than sham animals at the chronic time point. *Bdnf* however shows the opposite pattern, such that blast animals have lower *Bdnf* expression compared to shams at the sub-acute timepoint, but higher *Bdnf* expression compared to shams at the chronic time point.

Additionally, as evidenced by IPA analyses of canonical pathways enriched in both datasets, the differentially expressed genes in the aging amygdala within the blast group are enriched for GABA signaling pathways (including *Adcy1, Adcy8, Cacna1d, Cacna*1 h, *Cacng4, Gabrg1, Gad1, Gad2, Gnas, Kcnh2, Slc32a1, Slc6a1, Slc6a11*), while this pathway is absent from the sham group. Impaired GABA signaling in the amygdala following TBI has been established, including loss of GABAergic interneurons and decreased frequency of GABA receptor-mediated inhibitory postsynaptic currents (Almeida-Suhett et al., 2014). This decrease in inhibition leading to increased neuronal excitability in the amygdala may be a crucial mediator of anxiety-like behavior after brain injury. Previous work shows that decreased GABAergic functioning in the amygdala can directly lead to altered performance on the OFT, EPM, and fear conditioning (Babaev et al., 2018). Further, *Adcy8* codes for a protein kinase that has been repeatedly implicated in anxiety-like behavior, synaptic plasticity, and mood disorders (Schaefer et al., 2000; de Mooij-van Malsen et al., 2009; Bernabucci and Zhuo, 2016; Tanaka et al., 2019). A recent study found changes in anxiety-like behavior linked to a rodent PTSD-like model accompanied by aberrant *Adcy8* expression in the amygdala (Tanaka et al., 2019). Similar to our results, the stress-induced change in *Adcy8* expression was dependent on a time delay following the stressor, highlighting the importance of the treatment by timepoint interaction in regulating brain function and behavior after a stressor.

When we used IPA to identify gene networks involved in the interaction between blast exposure and timepoint, the top networks involved *Bdnf*, which we had already established displayed a statistically significant interaction (**Figure 5**). *Bdnf* codes for a protein that is crucial for neural plasticity and development and has been implicated widely in psychiatric disorders (Zagrebelsky and Korte, 2014). There is evidence in post-mortem human brain tissue from depressed subjects that *Bdnf* expression may correspond to GABA-related dysfunction in the amygdala (Guilloux et al., 2012), similar to our findings in aged mTBI rats. Additionally, many groups have demonstrated the importance of *Bdnf* expression following TBI in humans (Rostami et al., 2011; Failla et al., 2014; Korley et al., 2015) and animals (Griesbach et al., 2002; Wu et al., 2004, 2008; Feliciano et al., 2014) and have suggested alterations in *Bdnf via* pharmacology or experience as a potential therapeutic target following TBI (Griesbach et al., 2009; Wurzelmann et al., 2017). One group found that *Bdnf* levels were decreased after a short time interval post-TBI (Sagarkar et al., 2017), but did not investigate a later timepoint. Our findings here suggest that *Bdnf*, a known regulator of GABA-ergic transmission in the amygdala, may play a role in the aging-related phenotypic outcomes after blast exposure.

A potential limitation of the current study was the use of the same cohorts of animals for both behavioral and molecular assays, which may introduce the stress of behavioral testing as a confounding factor in transcriptomic results, especially when combined with aging and injury. We note however that all animals in both treatment groups (blast and sham) experienced the same testing procedures and therefore experienced the same levels of stress and conditions before molecular assays were performed, addressing this potential confound. Additionally, having additional groups (i.e., sub-acute and chronic × blast and sham) in parallel that did not undergo the behavioral battery increases the scope and costliness of the study, though certainly can be considered in future studies with the availability of greater funds. Another limitation of the current study was the lack of identification of mechanisms regulating gene expression. Exact mechanisms for gene expression regulation after blast exposure are still unknown, but DNA methylation and other epigenetic mechanisms may play a role in these outcomes. The *Bdnf* gene locus is heavily modified by epigenetic machinery which contributes to the experience- and activity-dependent nature of *Bdnf* expression (Boulle et al., 2012). We previously found changes in DNA methylation in the cortex after our rodent model of mTBI sub-acutely (Haghighi et al., 2015), and future studies will investigate DNA methylation at the chronic time point, which will likely uncover mechanistic insights into the abundant changes in gene expression we found here. Additionally, the current study focused solely on mRNA levels following blast exposure that may contribute to behavioral phenotypes, but in future investigations, we will identify protein levels for specific genes of interest to better link transcriptomics to behavioral outcomes. Future studies will also link gene expression in our animal models to changes observed in human cohorts using peripheral measures such as blood and saliva to allow a more translational approach.

Overall, the current study showed evidence for anxiety-like behavioral effects that may be related to amygdalar transcriptomic changes following blast exposure, and these changes occur in an age-dependent manner. Gene networks that we identified could provide crucial insights into the molecular underpinnings of mTBI and provide a link between experience and psychopathology resulting from blast exposure. Understanding the molecular circuitry involved in the long-term psychopathological outcomes resulting from mTBI is critically important to the health and productivity of our Military and Veteran population and will contribute to the development of targeted treatment interventions.

DATA AVAILABILITY STATEMENT

The original contributions presented in the study are publicly available. This data can be found here: GSE155393.

ETHICS STATEMENT

The animal study was reviewed and approved by Institutional Animal Care and Use Committees of the Naval Medical Research Center and the James J. Peters Veterans Administration (VA) Medical Center.

AUTHOR CONTRIBUTIONS

JB and FH wrote the manuscript. AT and SA generated blast-exposed animals. JB, IC, MU, NM, GE, and FH designed and performed animal behavior and animal molecular experiments. JB analyzed the behavioral data and performed IPA analyses on RNA seq data. ZW, YG, and FH analyzed RNA-seq data. All authors contributed to the article and approved the submitted version.

FUNDING

This work was supported in part by the Veterans Affairs Office of Research and Development. FH is the recipient of a Research Career Scientist Award (#1IK6CX002074) from the United States Department of Veterans Affairs. FH's research was supported by Veterans Affairs Merit Grants RX001705, CX001395, BX003794, and CX001728. GE was funded by merit grants I01RX002660-01 and 1I01BX0004067-01A from the United States Department of Veterans Affairs.

ACKNOWLEDGMENTS

We thank the New York Genome Center for performing the RNA sequencing assays.

SUPPLEMENTARY MATERIAL

The Supplementary Material for this article can be found online at: https://www.frontiersin.org/articles/10.3389/fnbeh.2020.00160/full#supplementary-material.

FIGURE S1 | Additional behavioral testing results. **(A)** Time spent in the light side of the light/dark box in the sub-acute cohort. **(B)** Time spent in the light side of the light/dark box in the chronic cohort (error bars represent SEM).

REFERENCES

Ahlers, S. T., Vasserman-Stokes, E., Shaughness, M. C., Hall, A. A., Shear, D. A., Chavko, M., et al. (2012). Assessment of the effects of acute and repeated exposure to blast overpressure in rodents: toward a greater understanding of blast and the potential ramifications for injury in humans exposed to blast. *Front. Neurol.* 3:32. doi: 10.3389/fneur.2012.00032

Almeida-Suhett, C. P., Prager, E. M., Pidoplichko, V., Figueiredo, T. H., Marini, A. M., Li, Z., et al. (2014). Reduced GABAergic inhibition in the basolateral amygdala and the development of anxiety-like behaviors after mild traumatic brain injury. *PLoS One* 9:e102627. doi: 10.1371/journal.pone.0102627

Babaev, O., Piletti Chatain, C., and Krueger-Burg, D. (2018). Inhibition in the amygdala anxiety circuitry. *Exp. Mol. Med.* 50:18. doi: 10.1038/s12276-018-0063-8

Benjamini, Y., and Hochberg, Y. (1995). Controlling the false discovery rate: a practical and powerful approach to multiple testing. *J. R. Stat. Soc. B* 57, 289–300. doi: 10.1111/j.2517-6161.1995.tb02031.x

Bernabucci, M., and Zhuo, M. (2016). Calcium activated adenylyl cyclase AC8 but not AC1 is required for prolonged behavioral anxiety. *Mol. Brain* 9:60. doi: 10.1186/s13041-016-0239-x

Boulle, F., van den Hove, D. L. A., Jakob, S. B., Rutten, B. P., Hamon, M., van Os, J., et al. (2012). Epigenetic regulation of the BDNF gene: implications for psychiatric disorders. *Mol. Psychiatry* 17, 584–596. doi: 10.1038/mp.2011.107

Boyle, M. P., Bernard, A., Thompson, C. L., Ng, L., Boe, A., Mortrud, M., et al. (2011). Cell-type-specific consequences of reelin deficiency in the mouse neocortex, hippocampus and amygdala. *J. Comp. Neurol.* 519, 2061–2089. doi: 10.1002/cne.22655

Campolongo, P., Roozendaal, B., Trezza, V., Hauer, D., Schelling, G., McGaugh, J. L., et al. (2009). Endocannabinoids in the rat basolateral amygdala enhance memory consolidation and enable glucocorticoid modulation of memory. *Proc. Natl. Acad. Sci. U S A* 106, 4888–4893. doi: 10.1073/pnas.0900835106

Chase, R. P., and Nevin, R. L. (2014). Population estimates of undocumented incident traumatic brain injuries among combat-deployed US military personnel. *J. Head Trauma Rehabil.* 30, E57–E64. doi: 10.1097/HTR.0000000000000061

Davies, D. R., Olson, D., Meyer, D. L., Scholl, J. L., Watt, M. J., Manzerra, P., et al. (2016). Mild traumatic brain injury with social defeat stress alters anxiety, contextual fear extinction and limbic monoamines in adult rats. *Front. Behav. Neurosci.* 10:71. doi: 10.3389/fnbeh.2016.00071

de Mooij-van Malsen, A., van Lith, H. A., Oppelaar, H., Hendriks, J., de Wit, M., Kostrzewa, E., et al. (2009). Interspecies trait genetics reveals association of adcy8 with mouse avoidance behavior and a human mood disorder. *Biol. Psychiatry* 66, 1123–1130. doi: 10.1016/j.biopsych.2009.06.016

Defense and Veterans Brain Injury Center (2019). Department of Defense numbers for traumatic brain injury worldwide.

Depue, B. E., Olson-Madden, J. H., Smolker, H. R., Rajamani, M., Brenner, L. A., and Banich, M. T. (2014). Reduced amygdala volume is associated with deficits in inhibitory control: a voxel- and surface-based morphometric analysis of comorbid PTSD/mild TBI. *Biomed Res. Int.* 2014:691505. doi: 10.1155/2014/691505

Elder, G. A. (2015). Update on TBI and cognitive impairment in military veterans. *Curr. Neurol. Neurosci. Rep.* 15:68. doi: 10.1007/s11910-015-0591-8

Elder, G. A., Dorr, N. P., De Gasperi, R., Gama Sosa, M. A., Shaughness, M. C., Maudlin-Jeronimo, E., et al. (2012). Blast exposure induces post-traumatic stress disorder-related traits in a rat model of mild traumatic brain injury. *J. Neurotrauma* 29, 2564–2575. doi: 10.1089/neu.2012.2510

Elder, G. A., Mitsis, E. M., Ahlers, S. T., and Cristian, A. (2010). Blast-induced mild traumatic brain injury. *Psychiatr. Clin. North Am.* 33, 757–781. doi: 10.1016/j.psc.2010.08.001

Failla, M. D., Kumar, R. G., Peitzman, A. B., Conley, Y. P., Ferrell, R. E., and Wagner, A. K. (2014). Variation in the BDNF gene interacts with age to predict mortality in a prospective, longitudinal cohort with severe TBI. *Neurorehabil. Neural Repair* 29, 234–246. doi: 10.1177/1545968314542617

Faul, M., Xu, L., Wald, M. M., and Coronado, V. G. (2010). *Traumatic Brain Injury in the United States: Emergency Department Visits, Hospitalizations and Deaths 2002–2006.* Atlanta, GA: Centers for Disease Control and Prevention, National Center for Injury Prevention and Control.

Feliciano, D. P., Sahbaie, P., Shi, X., Klukinov, M., Clark, J. D., and Yeomans, D. C. (2014). Nociceptive sensitization and BDNF up-regulation in a rat model of traumatic brain injury. *Neurosci. Lett.* 583, 55–59. doi: 10.1016/j.neulet.2014.09.030

Frankowski, J. C., Kim, Y. J., and Hunt, R. F. (2019). Selective vulnerability of hippocampal interneurons to graded traumatic brain injury. *Neurobiol. Dis.* 129, 208–216. doi: 10.1016/j.nbd.2018.07.022

Gómez-López, S., Martínez-Silva, A. V., Montiel, T., Osorio-Gómez, D., Bermúdez-Rattoni, F., Massieu, L., et al. (2016). Neural ablation of the

PARK10 candidate Plpp3 leads to dopaminergic transmission deficits without neurodegeneration. *Sci. Rep.* 6:24028. doi: 10.1038/srep24028

Gama Sosa, M. A., De Gasperi, R., Perez Garcia, G. S., Perez, G. M., Searcy, C., Vargas, D., et al. (2019). Low-level blast exposure disrupts gliovascular and neurovascular connections and induces a chronic vascular pathology in rat brain. *Acta Neuropathol. Commun.* 7:6. doi: 10.1186/s40478-018-0647-5

Gentleman, R. C., Carey, V. J., Bates, D. M., Bolstad, B., Dettling, M., Dudoit, S., et al. (2004). Bioconductor: open software development for computational biology and bioinformatics. *Genome Biol.* 5:R80. doi: 10.1186/gb-2004-5-10-r80

Gill, J., Cashion, A., Osier, N., Arcurio, L., Motamedi, V., Dell, K. C., et al. (2017). Moderate blast exposure alters gene expression and levels of amyloid precursor protein. *Neurol. Genet.* 3:e186. doi: 10.1212/NXG.0000000000000186

Glenn, D. E., Acheson, D. T., Geyer, M. A., Nievergelt, C. M., Baker, D. G., Risbrough, V. B., et al. (2017). Fear learning alterations after traumatic brain injury and their role in development of posttraumatic stress symptoms. *Depress. Anxiety* 34, 723–733. doi: 10.1002/da.22642

Griesbach, G. S., Hovda, D. A., and Gomez-Pinilla, F. (2009). Exercise-induced improvement in cognitive performance after traumatic brain injury in rats is dependent on BDNF activation. *Brain Res.* 1288, 105–115. doi: 10.1016/j.brainres.2009.06.045

Griesbach, G. S., Hovda, D. A., Molteni, R., and Gomez-Pinilla, F. (2002). Alterations in BDNF and synapsin I within the occipital cortex and hippocampus after mild traumatic brain injury in the developing rat: reflections of injury-induced neuroplasticity. *J. Neurotrauma* 19, 803–814. doi: 10.1089/08977150260190401

Guilloux, J. P., Douillard-Guilloux, G., Kota, R., Wang, X., Gardier, A. M., Martinowich, K., et al. (2012). Molecular evidence for BDNF- and GABA-related dysfunctions in the amygdala of female subjects with major depression. *Mol. Psychiatry* 17, 1130–1142. doi: 10.1038/mp.2011.113

Haghighi, F., Ge, Y., Chen, S., Xin, Y., Umali, M. U., De Gasperi, R., et al. (2015). Neuronal DNA methylation profiling of blast-related traumatic brain injury. *J. Neurotrauma* 32, 1200–1209. doi: 10.1089/neu.2014.3640

Hall, A. A., Mendoza, M. I., Zhou, H., Shaughness, M., Maudlin-Jeronimo, E., McCarron, R. M., et al. (2017). Repeated low intensity blast exposure is associated with damaged endothelial glycocalyx and downstream behavioral deficits. *Front. Behav. Neurosci.* 11:104. doi: 10.3389/fnbeh.2017.00104

Han, K., Chapman, S. B., and Krawczyk, D. C. (2015). Altered amygdala connectivity in individuals with chronic traumatic brain injury and comorbid depressive symptoms. *Front. Neurol.* 6:231. doi: 10.3389/fneur.2015.00231

Hayes, R. L., Yang, K., Raghupathi, R., and McIntosh, T. K. (1995). Changes in gene expression following traumatic brain injury in the rat. *J. Neurotrauma* 12, 779–790. doi: 10.1089/neu.1995.12.779

Heldt, S., Elberger, A., Deng, Y., Guley, N., Del Mar, N., Rogers, J., et al. (2014). A novel closed-head model of mild traumatic brain injury caused by primary overpressure blast to the cranium produces sustained emotional deficits in mice. *Front. Neurol.* 5:2. doi: 10.3389/fneur.2014.00002

Hua Li, H., Lee, S. M., Cai, Y., Sutton, R. L., and Hovda, D. A. (2004). Differential gene expression in hippocampus following experimental brain trauma reveals distinct features of moderate and severe injuries. *J. Neurotrauma* 21, 1141–1153. doi: 10.1089/neu.2004.21.1141

Hubbard, W. B., Lashof-Sullivan, M., Greenberg, S., Norris, C., Eck, J., Lavik, E., et al. (2018). Hemostatic nanoparticles increase survival, mitigate neuropathology and alleviate anxiety in a rodent blast trauma model. *Sci. Rep.* 8:10622. doi: 10.1038/s41598-018-28848-2

Klein, R. C., Acheson, S. K., Mace, B. E., Sullivan, P. M., and Moore, S. D. (2014). Altered neurotransmission in the lateral amygdala in aged human apoE4 targeted replacement mice. *Neurobiol. Aging* 35, 2046–2052. doi: 10.1016/j.neurobiolaging.2014.02.019

Korley, F. K., Diaz-Arrastia, R., Wu, A. H. B., Yue, J. K., Manley, G. T., Sair, H. I., et al. (2015). Circulating brain-derived neurotrophic factor has diagnostic and prognostic value in traumatic brain injury. *J. Neurotrauma* 33, 215–225. doi: 10.1089/neu.2015.3949

Law, C. W., Chen, Y., Shi, W., and Smyth, G. K. (2014). Voom: precision weights unlock linear model analysis tools for RNA-seq read counts. *Genome Biol.* 15:R29. doi: 10.1186/gb-2014-15-2-r29

Luo, Y., Zou, H., Wu, Y., Cai, F., Zhang, S., and Song, W. (2017). Mild traumatic brain injury induces memory deficits with alteration of gene expression profile. *Sci. Rep.* 7:10846. doi: 10.1038/s41598-017-11458-9

Mahoney, E. R., Dumitrescu, L., Moore, A. M., Cambronero, F. E., De Jager, P. L., Koran, M. E. I., et al. (2019). Brain expression of the vascular endothelial growth factor gene family in cognitive aging and Alzheimer's disease. *Mol. Psychiatry* 10.1038/s41380-019-0458-5. doi: 10.1038/s41380-019-0458-5

Meyer, D. L., Davies, D. R., Barr, J. L., Manzerra, P., and Forster, G. L. (2012). Mild traumatic brain injury in the rat alters neuronal number in the limbic system and increases conditioned fear and anxiety-like behaviors. *Exp. Neurol.* 235, 574–587. doi: 10.1016/j.expneurol.2012.03.012

Moochhala, S. M., Md, S., Lu, J., Teng, C. H., and Greengrass, C. (2004). Neuroprotective role of aminoguanidine in behavioral changes after blast injury. *J. Trauma* 56, 393–403. doi: 10.1097/01.TA.0000066181.50879.7A

Palmer, C. P., Metheny, H. E., Elkind, J. A., and Cohen, A. S. (2016). Diminished amygdala activation and behavioral threat response following traumatic brain injury. *Exp. Neurol.* 277, 215–226. doi: 10.1016/j.expneurol.2016.01.004

Park, E., Gottlieb, J. J., Cheung, B., Shek, P. N., and Baker, A. J. (2011). A model of low-level primary blast brain trauma results in cytoskeletal proteolysis and chronic functional impairment in the absence of lung barotrauma. *J. Neurotrauma* 28, 343–357. doi: 10.1089/neu.2009.1050

Perez-Garcia, G., Gama Sosa, M. A., De Gasperi, R., Lashof-Sullivan, M., Maudlin-Jeronimo, E., Stone, J. R., et al. (2016). Exposure to a predator scent induces chronic behavioral changes in rats previously exposed to low-level blast: implications for the relationship of blast-related TBI to PTSD. *Front. Neurol.* 7:176. doi: 10.3389/fneur.2016.00176

Phillips, L. L., and Belardo, E. T. (1992). Expression of c-fos in the hippocampus following mild and moderate fluid percussion brain injury. *J. Neurotrauma* 9, 323–333. doi: 10.1089/neu.1992.9.323

Popovitz, J., Mysore, S. P., and Adwanikar, H. (2019). Long-term effects of traumatic brain injury on anxiety-like behaviors in mice: behavioral and neural correlates. *Front. Behav. Neurosci.* 13:6. doi: 10.3389/fnbeh.2019.00006

Pun, P. B., Kan, E. M., Salim, A., Li, Z., Ng, K. C., Moochhala, S. M., et al. (2011). Low level primary blast injury in rodent brain. *Front. Neurol.* 2:19. doi: 10.3389/fneur.2011.00019

Ritchie, M. E., Phipson, B., Wu, D., Hu, Y., Law, C. W., Shi, W., et al. (2015). Limma powers differential expression analyses for RNA-sequencing and microarray studies. *Nucleic Acids Res.* 43:e47. doi: 10.1093/nar/gkv007

Rodríguez, J. J., Yeh, C.-Y., Terzieva, S., Olabarria, M., Kulijewicz-Nawrot, M., and Verkhratsky, A. (2014). Complex and region-specific changes in astroglial markers in the aging brain. *Neurobiol. Aging* 35, 15–23. doi: 10.1016/j.neurobiolaging.2013.07.002

Rostami, E., Krueger, F., Zoubak, S., Dal Monte, O., Raymont, V., Pardini, M., et al. (2011). BDNF polymorphism predicts general intelligence after penetrating traumatic brain injury. *PLoS One* 6:e27389. doi: 10.1371/journal.pone.0027389

Rubovitch, V., Ten-Bosch, M., Zohar, O., Harrison, C. R., Tempel-Brami, C., Stein, E., et al. (2011). A mouse model of blast-induced mild traumatic brain injury. *Exp. Neurol.* 232, 280–289. doi: 10.1016/j.expneurol.2011.09.018

Sagarkar, S., Bhamburkar, T., Shelkar, G., Choudhary, A., Kokare, D. M., and Sakharkar, A. J. (2017). Minimal traumatic brain injury causes persistent changes in DNA methylation at BDNF gene promoters in rat amygdala: a possible role in anxiety-like behaviors. *Neurobiol. Dis.* 106, 101–109. doi: 10.1016/j.nbd.2017.06.016

Saljo, A., Bolouri, H., Mayorga, M., Svensson, B., and Hamberger, A. (2010). Low-level blast raises intracranial pressure and impairs cognitive function in rats: prophylaxis with processed cereal feed. *J. Neurotrauma* 27, 383–389. doi: 10.1089/neu.2009.1053

Savalli, G., Diao, W., Schulz, S., Todtova, K., and Pollak, D. D. (2014). Diurnal oscillation of amygdala clock gene expression and loss of synchrony in a mouse model of depression. *Int. J. Neuropsychopharmacol.* 18:pyu095. doi: 10.1093/ijnp/pyu095

Schaefer, M. L., Wong, S. T., Wozniak, D. F., Muglia, L. M., Liauw, J. A., Zhuo, M., et al. (2000). Altered stress-induced anxiety in adenylyl cyclase type VIII-deficient mice. *J. Neurosci.* 20, 4809–4820. doi: 10.1523/JNEUROSCI.20-13-04809.2000

Tanaka, M., Li, H., Zhang, X., Singh, J., Dalgard, C. L., Wilkerson, M., et al. (2019). Region- and time-dependent gene regulation in the amygdala and

anterior cingulate cortex of a PTSD-like mouse model. *Mol. Brain* 12:25. doi: 10.1186/s13041-019-0449-0

Tang, X., Holland, D., Dale, A. M., and Miller, M. I. (2015). APOE affects the volume and shape of the amygdala and the hippocampus in mild cognitive impairment and Alzheimer's disease: age matters. *J. Alzheimers Dis.* 47, 645–660. doi: 10.3233/JAD-150262

Tapia-Arancibia, L., Aliaga, E., Silhol, M., and Arancibia, S. (2008). New insights into brain BDNF function in normal aging and Alzheimer disease. *Brain Res. Rev.* 59, 201–220. doi: 10.1016/j.brainresrev.2008.07.007

Tate, D. F., Wade, B. S. C., Velez, C. S., Drennon, A. M., Bolzenius, J., Gutman, B. A., et al. (2016). Volumetric and shape analyses of subcortical structures in united states service members with mild traumatic brain injury. *J. Neurol.* 263, 2065–2079. doi: 10.1007/s00415-016-8236-7

Teutsch, P., Jones, C. E., Kaiser, M. E., Avalon Gardner, N., and Lim, M. M. (2018). Gait and conditioned fear impairments in a mouse model of comorbid TBI and PTSD. *Behav. Neurol.* 2018:6037015. doi: 10.1155/2018/6037015

Tweedie, D., Rachmany, L., Rubovitch, V., Zhang, Y., Becker, K. G., Perez, E., et al. (2013). Changes in mouse cognition and hippocampal gene expression observed in a mild physical- and blast-traumatic brain injury. *Neurobiol. Dis.* 54, 1–11. doi: 10.1016/j.nbd.2013.02.006

Wu, A., Ying, Z., and Gomez-Pinilla, F. (2004). Dietary omega-3 fatty acids normalize bdnf levels, reduce oxidative damage and counteract learning disability after traumatic brain injury in Rats. *J. Neurotrauma* 21, 1457–1467. doi: 10.1089/neu.2004.21.1457

Wu, H., Lu, D., Jiang, H., Xiong, Y., Qu, C., Li, B., et al. (2008). Simvastatin-mediated upregulation of VEGF and BDNF, activation of the PI3K/Akt pathway and increase of neurogenesis are associated with therapeutic improvement after traumatic brain injury. *J. Neurotrauma* 25, 130–139. doi: 10.1089/neu.2007.0369

Wurzelmann, M., Romeika, J., and Sun, D. (2017). Therapeutic potential of brain-derived neurotrophic factor (BDNF) and a small molecular mimics of BDNF for traumatic brain injury. *Neural Regen. Res.* 12, 7–12. doi: 10.4103/1673-5374.198964

Zagrebelsky, M., and Korte, M. (2014). Form follows function: BDNF and its involvement in sculpting the function and structure of synapses. *Neuropharmacology* 76, 628–638. doi: 10.1016/j.neuropharm.2013.05.029

Zuckerman, A., Ram, O., Ifergane, G., Matar, M. A., Sagi, R., Ostfeld, I., et al. (2016). Controlled low-pressure blast-wave exposure causes distinct behavioral and morphological responses modelling mild traumatic brain injury, post-traumatic stress disorder and comorbid mild traumatic brain injury-post-traumatic stress disorder. *J. Neurotrauma* 34, 145–164. doi: 10.1089/neu.2015.4310

Conflict of Interest: The authors declare that the research was conducted in the absence of any commercial or financial relationships that could be construed as a potential conflict of interest.

Advantages of publishing in Frontiers

OPEN ACCESS
Articles are free to read for greatest visibility and readership

FAST PUBLICATION
Around 90 days from submission to decision

HIGH QUALITY PEER-REVIEW
Rigorous, collaborative, and constructive peer-review

TRANSPARENT PEER-REVIEW
Editors and reviewers acknowledged by name on published articles

Frontiers
Avenue du Tribunal-Fédéral 34
1005 Lausanne | Switzerland

Visit us: www.frontiersin.org
Contact us: frontiersin.org/about/contact

REPRODUCIBILITY OF RESEARCH
Support open data and methods to enhance research reproducibility

DIGITAL PUBLISHING
Articles designed for optimal readership across devices

FOLLOW US
@frontiersin

IMPACT METRICS
Advanced article metrics track visibility across digital media

EXTENSIVE PROMOTION
Marketing and promotion of impactful research

LOOP RESEARCH NETWORK
Our network increases your article's readership